

AD-A192 182

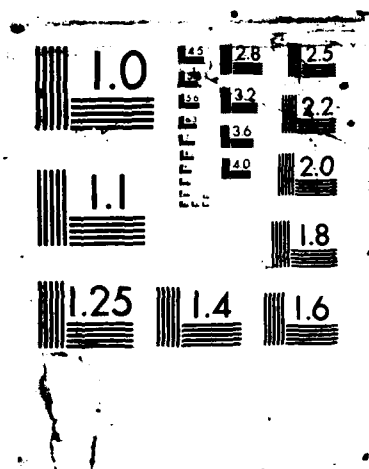
THE RAILGUN AND ITS POWER SOURCE(U) MATERIALS RESEARCH  
LABS ASCO, VALE (AUSTRALIA) D N SADEBIN ET AL. JUN 87  
HRL-R-1838 DOD-AR-885-133

1/4

UNCLASSIFIED

F/G 28/3

ML



DTIC FILE COPY

(4)

MRL-R-1058

AR-005-133



AD-A192 102

**DEPARTMENT OF DEFENCE**  
**DEFENCE SCIENCE AND TECHNOLOGY ORGANISATION**  
**MATERIALS RESEARCH LABORATORIES**  
**MELBOURNE, VICTORIA**

**REPORT**  
**MRL-R-1058**

**THE RAILGUN AND ITS POWER SOURCE**

**D.R. Sadedin and W.J. Bonwick\***

**\* Monash University, Clayton Victoria**

Approved for Public Release

**DTIC**  
**ELECTE**  
**S MAR 02 1988 D**

**DSTO**  
**MARIBYRNONG**

**C** Commonwealth of Australia  
**JUNE 1988**

**DISTRIBUTION STATEMENT A**

Approved for public release  
Distribution Unlimited

**88 3 01 103**

**DEPARTMENT OF DEFENCE  
MATERIALS RESEARCH LABORATORIES**

**REPORT**

**MRL-R-1058**

**THE RAILGUN AND ITS POWER SOURCE**

**D.R. Sadedin and W.J. Bonwick\***

**ABSTRACT**

Investigations into the propulsion mechanisms of railguns and into the power source requirements of railguns are reported. Power sources based upon rotating machines, capacitors and explosives are reviewed and a new method based upon batteries and pulse transformers is identified. The battery and pulse transformer method is studied in detail.

\* Associate Professor, Department of Electrical Engineering  
Monash University, Clayton Victoria

Approved for Public Release

© COMMONWEALTH OF AUSTRALIA 1987

---

**POSTAL ADDRESS:** Director, Materials Research Laboratories  
P.O. Box 80, Ascot Vale, Victoria 3032, Australia

---



# C O N T E N T S

Page No.

## INTRODUCTION

1

## CHAPTER 1      FORCE AND ENERGY IN THE RAILGUN

1.1	Force upon the projectile and the method of virtual work	3
1.2	Comparison of energy changes due to switching and sliding	6
1.3	Propulsion mechanism with a plasma arc	8

## CHAPTER 2      RAILGUN EFFICIENCY

11

2.1	Introduction	11
2.2	The "propelling" and "uncoupled" fluxes	12
2.3	Force factor and efficiency	14
2.4	Current flow in the railgun	15
2.5	Inductance in the projectile region is minimized	18
2.6	Initial resistance in the projectile region	19
2.7	The diffusion equation and depth of penetration	20
2.8	Inductance equations	23
2.8.1	Selection of current distributions	23
2.8.2	Inductance of a pair of parallel current sheets	26
2.8.3	Force due to current sheets on tops and bottoms of rails	29
2.8.4	Propelling inductance of uniform surface current upon rectangular rails	31
2.8.5	Propelling inductance for current uniformly distributed across the rail section	32
2.8.6	Total inductance for uniformly distributed surface current	33
2.8.7	Total inductance for uniform current across section	37
2.8.8	Kerrisk's equations for minimum inductance	37
2.9	Inductance equations - results and discussion	38



Availability Codes	
Dist	Avail and/or Special
A-1	

CONTENTS  
(Continued)

2.10	Efficiency equations for railguns	43
2.10.1	Loss mechanisms	43
2.10.2	Improved railguns	44
2.10.3	Simple condition for high efficiency	45
2.10.4	Current penetration model	46
2.10.5	Resistive loss in a portion of the rails	47
2.10.6	Rail loss comparisons - breech supplied gun	49
2.10.7	Rail loss comparisons - segmented gun	50
2.10.8	Rail losses - constant resistance per unit length	51
2.10.9	Other loss comparisons	53
2.10.10	Efficiency expressions	54
2.10.11	Example calculations and discussion	56
Appendix 1.	Inductance calculation by geometric mean distances	60
<u>CHAPTER 3</u>	<u>A REVIEW OF PULSED POWER SOURCES FOR ELECTROMAGNETIC PROPULSION</u>	 66
3.1	Features required of a power source	66
3.1.1	Quantity of energy required is 1MJ or more	66
3.1.2	Final component of power source must be an inductor	66
3.1.3	The ANU homopolar generator power source	67
3.1.4	Features of an ideal power source	69
3.1.5	Desirable power source pulse energy density	69
3.2	Capacitor based power source	71
3.2.1	Large mass and simple circuit	71
3.2.2	High voltage limitation	72
3.2.3	Low mass inductor	72
3.2.4	Limitations to the energy density of capacitors	72

CONTENTS  
(Continued)

3.3	Fly wheel based machines - inertial storage	74
3.3.1	Fly wheels	74
3.3.2	Homopolar generators	75
3.3.3	Ordinary large alternators	77
3.3.4	The compulsator	77
3.4	Explosive magnetic flux compression	80
3.5	Minimum mass of energy stores	82
3.5.1	Force is required to contain kinetic energy	82
3.5.2	Minimum mass of kinetic energy stores	82
3.5.3	Inferences concerning the ultimate energy density of capacitors	85
3.6	Battery and pulse transformer concept	86
CHAPTER 4	<u>GENERAL CONSIDERATION OF THE BATTERY AND PULSE TRANSFORMER POWER SOURCE</u>	88
4.1	Limitations of the pulse transformer scheme	88
4.1.1	High voltage across the primary	88
4.1.2	Coupling between primary and secondary must be tight	89
4.1.3	Open and closed circuit requirements of the secondary	90
4.2	Transformer versus inductor	90
4.2.1	Basic equivalence of battery/transformer and battery/inductor schemes	90
4.2.2	Inductor scheme requires means of disconnecting the battery	91
4.2.3	Transformer scheme does not require a rail switch	92
4.2.4	Batteries can be conveniently located in transformer scheme	93
4.3	Overall system energy density	93
4.3.1	Interaction of battery, coil and charging time	93
4.3.2	Examples based on Brooks Coil	93

CONTENTS  
(Continued)

4.4	Batteries	95
4.4.1	Safe, low mass prime energy store	96
4.4.2	The pulse power density of lead-acid batteries	97
4.4.3	Factors limiting the high rate discharge of lead-acid batteries	99
4.4.4	Design and performance of a high rate lead-acid cell	101
4.5	Motor-generator instead of batteries	103
4.5.1	Power density of motor-generator sets	103
4.5.2	Response time limitation of motor-generator	104
4.6	The primary opening switch	104
4.6.1	The mechanism of energy transfer	104
4.6.2	Opening time, energy, voltage and resistance of the switch	105
4.6.3	Fuses and vacuum arc switches	105
4.7	Previous use of pulse transformer method	107
4.8	Current transformer concept	107
<u>CHAPTER 5</u>	<u>ANALYSIS OF THE PULSE TRANSFORMER CIRCUIT</u>	109
5.1	Energy transfer (discharge) equations	109
5.1.1	Circuit parameters	109
5.1.2	Simple analysis	110
5.1.3	Rigorous Analysis	111
5.1.4	Discussion of Discharge Equations	115
5.2	Physical Explanation of Transfer of Energy	118
5.3	Coupling factors	122
5.3.1	Simplified model	122
5.3.2	Relationships between self inductances and coupling factors	124
5.4	Coaxial-toroidal transformer geometry	125
5.5	The charging of the primary	127
5.5.1	Secondary open	127
5.5.2	Secondary Closed	133

CONTENTS  
(Continued)

5.6	Physical explanation of closed secondary charging	140
5.7	Summary	143
 <u>CHAPTER 6</u> <u>ASSESSMENT OF VARIOUS TRANSFORMER GEOMETRIES</u>		145
6.1	Time constant and masses	145
6.1.1	Relationship between battery mass and circuit resistances	145
6.1.2	The Brooks Coil	148
6.1.3	The single layer solenoid compared with Brooks Coil	150
6.1.4	The external field toroid compared with Brooks Coil	152
6.1.5	The ordinary (or internal field) toroid	155
6.2	The degree of coupling of several forms of secondary	157
6.2.1	Basic theory	157
6.2.2	Short solenoid with various secondaries	164
6.2.3	The external field toroid with various secondaries	170
6.2.4	The internal field toroid with various secondaries	174
6.3	Forces and masses of windings in terms of stored energy	176
6.3.1	Mass of the short solenoid	176
6.3.2	Mass of the external field toroid	180
6.3.3	Mass of the internal field toroid	182
6.4	Discussion	184
6.4.1	Comparison of the single layer winding forms	184
6.4.2	Tension and compression components of coil mass	186
6.4.3	Multilayer coils	186
6.5	Flux distribution and inductance of real windings	187
6.5.1	The location of an equivalent current sheet	187
6.5.2	The flux distribution of N conductors compared to a current sheet	189
6.5.3	The inductance of a N conductor external field toroid	198
6.5.4	The transient current distribution of the secondary	202

CONTENTS  
(Continued)

<u>CHAPTER 7</u>	<u>THE FORCE REDUCED TORODIAL TRANSFORMER</u>	207
7.1	Problems caused by compressive forces	207
7.2	Magnetic force balancing	207
7.3	Basic force reduction relationships	210
7.3.1	Total inductance expression	210
7.3.2	Force reduction conditions	210
7.3.3	Magnetic energy of the force reduced coil	212
7.3.4	Use of a high permeability core	213
7.3.5	The mass of the force reduced toroid	214
7.3.6	Flux densities for force reduction	216
7.3.7	Reason for major radial force	217
7.4	Degree of coupling-coaxial cable force reduced transformer	218
<u>CHAPTER 8</u>	<u>DESIGN AND PERFORMANCE OF TOROIDAL TRANSFORMER/BATTERY POWER SOURCE</u>	221
8.1	Management of the variables	221
8.2	External field toroid - general relationships	222
8.2.1	Assumptions	222
8.2.2	Mass of the primary in terms of resistivity,	223
8.2.3	Mass of primary conductors in terms of tensile stress of stored energy	224
8.2.4	Power requirement	224
8.2.5	Primary Current	225
8.2.6	Battery Voltage	225
8.2.7	Number of primary turns	226
8.2.8	Primary circuit time constant	226
8.3	Disk supported external field toroid	226

CONTENTS  
(Continued)

8.4	Force reduced toroidal transformer	229
8.4.1	Assumptions	229
8.4.2	Cable diameters-winding space	230
8.4.3	Mass of the primary in terms of resistivity	231
8.4.4	Mass of the primary in terms of tensile stress of stored energy	231
8.4.5	Power requirement	231
8.4.6	Primary current	232
8.4.7	Battery voltage	232
8.4.8	Number of turns producing external flux	232
8.4.9	Primary circuit time constant	233
8.5	Discussion of parameters	233
8.5.1	Hierarchy of parameters	233
8.5.2	Conductor stress theory	233
8.5.3	Primary and secondary tensile stress and conductor materials	235
8.5.4	Resistivity	237
8.5.5	The $\frac{R}{a}$ ratio	237
8.6	Design graphs	237
8.7	Design examples	238
8.7.1	100 kJ example design; external field toroid, given tensile stress	238
8.7.2	100 kJ external field toroid with improved overall energy density	240
8.7.3	10MJ external field toroid transformers	243
8.7.4	100 MJ and 1GJ designs	245
8.7.5	Force reduced transformers	246
8.8	Discussion - overall pulse energy density	248
8.8.1	Values attained by the pulse transformer-battery systems	248
8.8.2	Expression for the overall pulse energy density	249
8.8.3	Resistivity - cooling of conductors	249
8.8.4	Power density of batteries	250

CONTENTS  
(Continued)

8.9	Alternative design approaches	251
8.10	Conclusions	252
<u>CHAPTER 9</u>	<u>EXPERIMENTS - PURPOSE AND DESCRIPTION</u>	261
9.1	Inductance measurements of rectangular rails	261
9.1.1	Purpose	261
9.1.2	Rails measured	261
9.1.3	Apparatus and methods	262
9.2	Degree of coupling	263
9.2.1	Purpose	263
9.2.2	Coils and secondaries used	263
9.2.3	Method of measuring degree of coupling	269
9.3	Force reduction	269
9.3.1	Purpose	269
9.3.2	Method	269
9.4	Pulse power density of lead-acid batteries	271
9.4.1	Purpose	271
9.4.2	Method of measuring pulse power density	271
9.4.3	Batteries tested	272
9.5	Model pulse transformer systems	276
9.5.1	Purposes of model pulse transformer systems	276
9.5.2	Transformers constructed	276
9.5.3	Fuses	285
9.5.4	Battery	287
9.5.5	Current shunts	288
9.6	Calculations and derivations	290
9.6.1	1.5 $\mu$ H test inductor	290
9.6.2	Phase plane plotting	291
9.6.3	Maximum length and frequency for rail measurements	295



CONTENTS  
(Continued)

9.6.4	Degree of coupling of external field toroid with bifilar winding	296
9.6.5	Derivation of degree of coupling expression	298
9.6.6	Force reduction models	299
9.6.7	Prime number of turns for primary of force reduced transformer	300
9.6.8	Fuse dimensions	304
 <u>CHAPTER 10</u> <u>EXPERIMENT RESULTS</u>		 306
10.1	Rail inductance measurements	306
10.1.1	Rectangular rails results	306
10.1.2	Ribbon cable rails	306
10.1.3	Test inductor	308
10.1.4	Phase plane method	308
10.2	Degree of coupling	310
10.2.1	Long solenoid with shorter layer secondaries	310
10.2.2	Short solenoids with thin sheet secondaries	311
10.2.3	Short solenoid with separate layer winding	312
10.2.4	Short solenoid with 100 turn bifilar windings	313
10.2.5	Short solenoid with co-axial cable winding	313
10.2.6	Bifilar external field toroid	314
10.2.7	Conclusions regarding degree of coupling experiments	314
10.3	Force experiments	314
10.4	Internal resistance of batteries	316
10.5	Pulse transformer tests	320

CONTENTS  
(Continued)

<u>CHAPTER 11</u>	<u>SUMMARY, CONCLUSIONS AND FURTHER WORK</u>	323
11.1	Summary and Conclusions	324
11.2	Applicability to the battery-inductor scheme	327
11.3	Further work	327
<u>ACKNOWLEDGEMENTS</u>		329
<u>REFERENCES</u>		330
<u>PRINCIPAL SYMBOLS</u>		
<u>PUBLISHED PAPERS</u>		

## THE RAILGUN AND ITS POWER SOURCES

### INTRODUCTION

The possibility of accelerating masses by the "railgun" principle has been proposed for military purposes a number of times in the past century. A source of very high electrical power is necessary, however. The lack of such a source was one of the chief reasons why attempts to put the principle into practice were unsuccessful until recently. The objectives of the work reported here to investigate the power source requirements of rail type electromagnetic launchers (or "railguns") and to investigate in detail a power source which seemed especially suited to them.

### **Background**

Figure 1 shows the principle of the railgun.

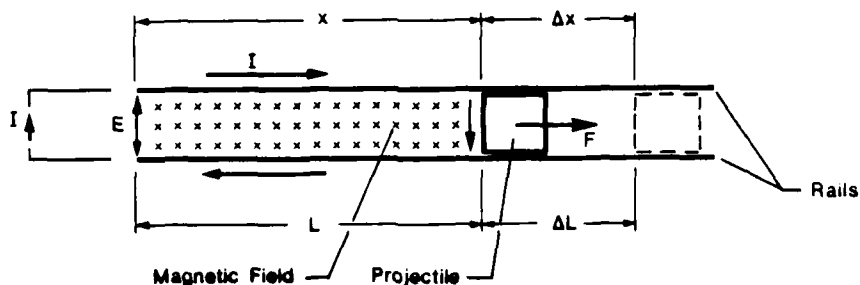


Fig. 1. Principle of the Railgun.

The force due to the current crossing its own magnetic field at the projectile causes the projectile to accelerate along the rails. The projectile does not

have to be a conductor because a plasma arc can be introduced behind it to carry the current [1]. To accelerate a mass of 5 grams to a velocity of 10 km/s in 1 millisecond requires a current of about 500,000A at a peak power of about 1 GW.

Using the Canberra Homopolar Generator, which is the largest such machine in the world with a peak power of 1 GW, J.P. Barber, working under R.A. Marshall at the Australian National University, in 1972 showed that the rail type electromagnetic launcher is feasible [2]. This revived military interest in it and also that of space launch and fusion researchers [3-5]. Since 1979, railguns have been built at a dozen or so places in the USA and at the Materials Research Laboratories in Melbourne, Australia [6].

Prior to the innovations of Barber and Marshall, railguns were thought of as adaptations of ordinary machines. The early inventors had no concept of the hypervelocity applications which are now the major reason for pursuing their development. The early patents show elaborate mechanical details of the gun construction, but very little about the power source. These inventors seem to have thought that generators or batteries could be readily arranged as power sources [7-9].

During World War II a serious attempt was made in Germany to develop electric guns as anti-aircraft guns, and as an alternative to the V2 rockets, based on the ideas of Fauchon-Villeplee [10]. When the calculations were done for an anti aircraft gun, it was found that the power source posed a formidable problem. It was found, for example, that the connections from the generators would require too much copper for the gun to be practical. Later attempts to build railguns were also foiled by the power source problem, until that by Barber.

#### Plan of the Report

The work in this Report falls into three broad categories.

Firstly, the railgun itself is studied in terms of its efficiency, which, when it is low, is a major factor in determining the size of the power source. As the power source and its load - the railgun - must be much more integrated than is the case with other electrical apparatus, familiarity with the railgun is a valuable basis for dealing with the power source problem.

The railgun study is presented in Chapters 1 and 2.

Secondly, in Chapter 3, the power sources that are being used and developed for railguns are reviewed. They are compared, especially in regard to their masses.

Chapters 4 to 10 of the Report deal in detail with a battery and pulse transformer scheme, which seems to naturally suit the railgun. The transformer design is most important, and its study takes up about a third of the whole Report.

## CHAPTER 1

### FORCE AND ENERGY IN THE RAILGUN

This Chapter deals with the force on the projectile in the railgun and the energy available to propel it. From these considerations we can proceed to a model for estimating the efficiency of the railgun.

#### 1.1 Force upon the projectile and the method of virtual work

The projectile acquires some of the energy that is supplied to the circuit of the railgun. It does so through the force exerted on current carriers that cross between the rails. In principle, the force may be found from the integral of  $\mathbf{J} \times \mathbf{B}$  through the volume where the current crosses between the rails, and where  $\mathbf{J}$  is the current density and  $\mathbf{B}$  is the magnetic flux density due to the current in the rails.

In practice it is very difficult to perform the above calculation and instead the expression:

$$F = \frac{1}{2} L' I^2 \quad (1.1)$$

is used. In this expression,  $F$  is the force,  $I$  is the railgun current and  $L'$  is loosely defined as the high frequency inductance per unit length of the rails, or the inductance gradient, and is often also denoted as  $\frac{dL}{dx}$ . The numerical value for  $L'$  is often obtained by measuring the inductance of the rails at a frequency reckoned to be typical of the rise time of the current as the projectile moves over new sections of the rails and then dividing that inductance value by the length of the rails.

Equation (1.1) is a very convenient means for estimating the force on the projectile. The velocities obtained from experimental railguns often indicate that the actual force on the projectile is much lower; sometimes only one third as much. The difference is often ascribed to friction or to leakage of the plasma arc past the projectile. However, it is worthwhile examining the background to Eqn. (1.1) to discover what other factors may affect its validity. Not only may this enable the force to be estimated more accurately, but the results may enable us to see how to improve the efficiency of the railgun.

Upon reference to text books, e.g. Seely [1], it is found that Eqn. (1.1) is obtained by applying the "method of virtual work" to circuits containing inductance. It is further found that the method of virtual work is actually concerned with energy changes associated with movements of current paths and not directly with forces. If the proper energy change to be associated with a movement can be determined, the force on the part that moved can be found by dividing the energy change by the amount of the movement. In symbols, therefore, the force is yielded by:

$$F_x = \frac{\partial W}{\partial x} \quad (1.2)$$

where W denotes energy and the partial derivative notation indicates that the portion of the energy change properly associated with an x direction movement is used to obtain the force in the x direction.

The proper identification of the energy changes is necessary for correct force calculation. This is possible when the movements are completely known and are so slight that the circuit geometry is practically unaltered (hence the term "virtual work").

Let us apply the general method used in the virtual work determination of force to the railgun but with consideration of processes that occur in addition to projectile movement. As in text book virtual work derivations, the energy supplied to the circuit must divide into three categories, viz. that which is stored in the inductance of the circuit, that which is dissipated by resistance and that which is "associated" with the movement of the projectile. With reference to Fig. 1, let:

I = constant current,  
 R = resistance of the rails and the projectile,  
 $\Delta x$  = movement of the projectile in time  $\Delta t$ ,  
 and  $\Delta L$  = increase in inductance in time  $\Delta t$ .

In considering the energy supplied to the system, we must take  $\Delta L$  to be the inductance change as seen at the points where voltage E is measured. Equating the energy supplied by the power source to the three categories within the railgun yields:

$$E I \Delta t = \frac{1}{2} I^2 \Delta L + I^2 R \Delta t + \Delta W_a \quad (1.3)$$

where  $\Delta W_a$  is the energy associated with projectile movement and includes, or is entirely composed of, the energy acquired by the projectile while it moves  $\Delta x$  in time  $\Delta t$ , and  $\frac{1}{2} I^2 \Delta L$  is the energy stored in the increased inductance.

Since the current is constant, the voltage E is:

$$E = I \frac{\Delta L}{\Delta t} + I R \quad (1.4)$$

(We strictly should consider R to vary by  $\Delta R$ , but the result is the same).

Substituting in (1.3) yields:

$$\Delta W_a = \frac{1}{2} I^2 \Delta L \quad (1.5)$$

Eqn. (1.5) shows that the source supplies a quantity of energy,  $\Delta W_a$ , above the amounts stored and dissipated, and the amount depends on the inductance change  $\Delta L$ . Because such a quantity of energy appears whenever the inductance of a circuit is altered, let us call  $\Delta W_a$  the "associated energy" of the inductance change. It is equivalent to the "free energy" in chemical reactions [2].

If we are sure that all the energy  $\Delta W_a$  is utilized in causing the projectile to move, then we may divide  $\Delta W_a$  by the movement  $\Delta x$  and so obtain the force,  $F'$ , on the projectile as:

$$F' = \frac{1}{2} I^2 \frac{\Delta L}{\Delta x} \quad (1.6)$$

Equation (1.5) shows that the increment  $\Delta W_a$  is equal to the increase in stored magnetic energy of the rails, assuming that the current is constant. In the event that all of  $\Delta W_a$  becomes increased kinetic energy and the resistance of the rails is negligible, the efficiency of the constant current railgun is at its maximum value, viz. 50%. (Higher efficiency may be obtained by allowing the current to decline, so that the stored energy of the rails drives the projectile. This is equivalent to utilizing a long barrel in a powder gun to extract as much energy as possible from the expanding gas.)

In an actual railgun there are several reasons why some of the associated energy,  $\Delta W_a$ , may be unable to cause projectile movement. For example, some of the total inductance change may be due to effects in other directions when the projectile is located a distance  $\Delta x$  further along the rails. Inductance is a function of the location of all the current filaments into which the current may be divided. Certain dimensions, e.g. the rail dimensions, may be characteristic measures. In general, we should write:

$$L = L(x, y, z), \quad (1.7)$$

where  $x, y$  and  $z$  are the characteristic dimensions, and from which:

$$\Delta L = \frac{\partial L}{\partial x} \Delta x + \frac{\partial L}{\partial y} \Delta y + \frac{\partial L}{\partial z} \Delta z \quad (1.8)$$

Only the term  $\frac{\partial L}{\partial x} \Delta x$  measures the energy change that takes place in the  $x$  direction and therefore the force in the  $x$  direction should be written as:

$$F'' = \frac{1}{2} I^2 \frac{\partial L}{\partial x} \quad (1.9)$$

If, while  $\Delta x$  changes,  $\Delta y$  and  $\Delta z$  are each zero, i.e. the  $y$  and  $z$  coordinates of every filament of current instantly assume the same values as at all other places and these values do not change, then  $\frac{\Delta L}{\Delta x}$  is the same as  $\frac{\partial L}{\partial x}$ . Only under these conditions is Eqn. (1.6) the same as Eqn. (1.9).

Because the current is actually diffusing, there are  $\Delta y$  and  $\Delta z$  components to the inductance change. The issue is whether they are significant changes compared to the  $\Delta x$  changes. By introducing diffusion we make  $y$  and  $z$  coordinates of the current filaments functions of time. Since the diffusion time at any location is the time after the projectile has passed that location, the  $y$  and  $z$  coordinates and the total inductance change are complicated functions of  $x$  and time (and of the rail dimensions).

Even if the  $\Delta y$  and  $\Delta z$  variations are eliminated for one reason or another, Eqn. (1.9) does not necessarily give the force on the projectile, for two further reasons.

Firstly, if the current has penetrated the rails, part of the inductance change in the  $x$  direction will be due to flux within the rails. This flux does not cross the current that passes behind the projectile and so cannot contribute to the force on it.

Secondly, when the projectile moves, there is disconnection and reconnection of current paths. With each disconnection and reconnection there is an inductance increment and an "associated energy". In switched inductor circuits it is known that energy is lost, presumably in the creation of sparks which carry the current until it has transferred to the new path. In the railgun, and especially in the case of the plasma arc driven railgun, we have to consider the possibility that some of the associated energy is lost in spark production and in other ways in the plasma.

Ideally, all the associated energy should become projectile energy, and the force should be given by Eqn. (1.6). If only a fraction,  $f$ , of the associated energy becomes projectile energy, we can express the force,  $F$ , on the projectile in terms of Eqn. (1.6) as:

$$F = \frac{1}{2} f I^2 \frac{\Delta L}{\Delta x} \quad (1.10)$$

Factor  $f$  may be defined to take into account all the loss mechanisms that we have considered.

In terms of the commonly used expression, Eqn. (1.1), we have:

$$L' = f \frac{\Delta L}{\Delta x}.$$

The interpretation of  $\Delta L$  is considered further in Chapter 2.

## 1.2 Comparison of energy changes due to switching and sliding

As stated in the previous section, it is known that when the inductance of a circuit is changed by switching, as in Fig. 2, there is a loss of energy. In the railgun the inductance is changed in small increments by sliding. It will now be shown that switching and sliding are the same in that



the "lost" energy of the switched circuit is the same in magnitude as the "associated energy" that arose in the energy balance analysis of the railgun.

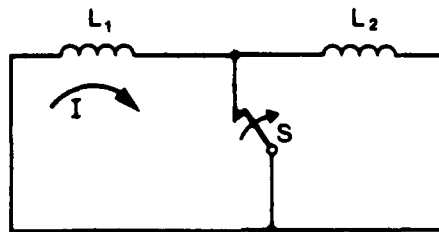


Fig. 2 Circuit with inductance changed by switching.

By applying the constant flux linkage theorem [3] to the circuit in Fig. 2, the current,  $I'$ , immediately after switch  $S$  is opened is found to be:

$$I' = I \frac{L_1}{L_1 + L_2}, \quad (1.11)$$

where  $I$  is the initial current in inductance  $L_1$ .

The difference between the initial and final stored energies gives the energy,  $\Delta W$ , lost in the switching:

$$\Delta W = \frac{1}{2} I^2 \frac{L_1 L_2}{L_1 + L_2}. \quad (1.12)$$

Now suppose that the inductance  $L_2$  is a small value,  $\Delta L$ , compared to  $L_1$ , so that the inductance change is similar to that considered in the sliding circuit of the railgun, and so that the current is practically constant. Substituting  $\Delta L$  into Eqn. (1.12) yields:

$$\Delta W = \frac{1}{2} I^2 \Delta L \quad (1.13)$$

Eqn. (1.13) has the same value as Eqn. (1.5); i.e. the "lost" energy of the switched inductor circuit is the same as the "associated" energy of the sliding circuit of the railgun.

The conclusion from this result is that some or all of the energy that would be lost in the sparks produced in the switched inductor circuit becomes the kinetic energy of the projectile when the inductance is changed by sliding in the railgun circuit.

Since arcing is deliberately introduced in the plasma arc railgun, the above result also leads to the question of how the associated energy becomes projectile energy. This is considered in the next section.

### 1.3 Propulsion mechanism with a plasma arc

The propulsion force on a solid conducting projectile is easy to explain. It is the same as on any metallic conductor - the  $J \times B$  forces which act on the electrons are transmitted as electrostatic forces of attraction to the positively charged bulk [4]. If the plasma arc behaves as an incompressible conducting fluid, direct transmission of the  $J \times B$  forces could take place as in solid conductors. If, instead, the plasma behaves like a gas, either direct transmission via electrostatic forces or indirect transmission via particle collisions could take place as set out in the following paragraphs.

Direct transmission of the  $J \times B$  forces via electrostatic forces could take place in a gaseous plasma as follows. The electrons, the principal current carriers in the plasma, are driven by the  $J \times B$  forces to the rear surface of the projectile, causing it to become negatively charged, as shown in Fig. 3. Electrons would continue to accumulate at the rear surface of the projectile until the force of repulsion, due to their field, equals the  $J \times B$  force which pushed the electrons. When this equilibrium condition is reached, the force of repulsion constitutes a "solid" connection between the  $J \times B$  force on the electrons and the projectile, causing both electrons and the projectile to move together. The positive bulk of the plasma follows the electrons by virtue of the attractive electrostatic forces, so the plasma accelerates with the projectile.

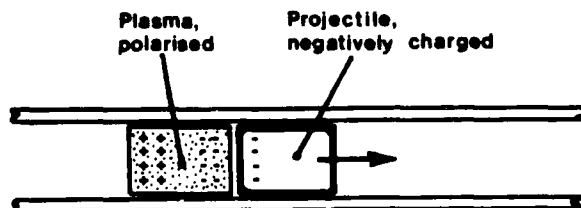


Fig. 3. Propulsion of projectile by repulsion force of negative charges.

In the above explanation, the bulk of the plasma particles are simply dragged along by their attraction to the electrons and play no part in the propulsion of the projectile. If the current could be carried behind the projectile by a beam of electrons the propulsion would still occur. Also, the conversion of the net associated energy to propulsion energy is 100% efficient because it occurs through the action of the  $J \times B$  forces upon the mass of the projectile.

Alternatively, it is conceivable that the  $J \times B$  forces upon the electrons may first accelerate the positive ions of the plasma, and the positive ions cause the propulsion of the projectile. The positive ions may cause the propulsion by charging the projectile as described above, or they may propel it by colliding with it. If the energy is first supplied to the positive ions, it may also be distributed via interparticle collisions amongst the degrees of freedom that are available.

Propulsion by collisions with the rear of the projectile is, in other words, propulsion by gas pressure, and, if this is the case, the arc driven railgun works like an ordinary gun, except that it uses electricity instead of explosives to provide a high pressure gas. An important consequence of the gas propulsion model is that the maximum velocity is determined by the speed of sound in the plasma, as opposed to a maximum equal to the speed of light for particles directly driven by  $J \times B$  forces.

By a simple application of the kinetic theory of gases, an estimate can be made of the efficiency of propulsion by particle collisions, and hence also an estimate of the factor "f" for use in Eqn. (1.10).

Again, it is convenient to consider a constant current railgun, because we may suppose that since the  $J \times B$  forces are then constant, the plasma that pushes the projectile is evolved at constant pressure. If the specific heat of the plasma at constant pressure is  $C_p$ , the heat supplied from the associated energy,  $\Delta Q$ , is:

$$\Delta Q = N C_p \Delta T \quad (1.14)$$

where  $N$  is the number of moles of the plasma and  $\Delta T$  is the temperature rise.

If the pressure is  $P$  and the volume increase due to projectile movement is  $\Delta V$ , the work done is:

$$P \Delta V = N R \Delta T \quad (1.15)$$

where  $R$  is the universal gas constant. But, from basic kinetic theory of gases,  $C_p = R + C_v$ , where  $C_v$  is the specific heat at constant volume.

$$\therefore P \Delta V = N (C_p - C_v) \Delta T \quad (1.16)$$

From (1.16) and (1.14), the efficiency,  $\eta$ , of the propulsion is:

$$\eta = \frac{\text{Work done at projectile}}{\text{Heat energy supplied}} = \frac{C_p - C_v}{C_p} \quad (1.17)$$

or,  $\eta = \frac{\gamma - 1}{\gamma},$  (1.18)

where  $\gamma$  is the ratio of the specific heats,  $\frac{C_p}{C_v}$ .

We now have to consider the value of  $\gamma$  for the plasma. From the kinetic theory of gases, we know that  $\gamma$  depends on the number of ways in which energy is free to divide (i.e. the number of degrees of freedom). If the plasma immediately behind the projectile consists only of ionized particles, all particles are influenced by the  $J \times B$  forces and their motion must be largely in the  $\pm x$  direction, i.e. along the line of motion of the projectile. In this case the gas is "one dimensional" and has the value  $\gamma = 3$ .

If on the other hand, there are a great number of neutral particles (produced for example by vapourization of the surface, with only a small fraction becoming ionized to provide current carriers), the energy from the  $J \times B$  forces will be distributed in all directions by numerous interparticle collisions before arriving at the rear surface of the projectile. In this case the value of  $\gamma$  would range between  $5/3$  and unity, depending upon whether the plasma particles were monatomic, with only 3 degrees of freedom, or polyatomic, with a large number of degrees of freedom.

Substituting  $\gamma = 3, 5/3$  and unity into Eq. (1.18) yields:

$$\eta = 0.67, 0.4 \text{ and zero.}$$

On the basis of this simple gas propulsion theory, at most 67% of the associated energy,  $\Delta W$ , could become projectile energy. Factor "f" would have a maximum value of 0.67.

In thermodynamic terms it is the free energy of the plasma which accelerates the projectile. The associated energy is, in these terms, the free energy of the electrical circuit and, depending on where the inductance changes occur, some or all of it is added to the plasma. The addition of this energy to the plasma causes it in turn to release free energy. The portion of the added energy which does not in effect become projectile energy raises the internal energy of the plasma and thereby raises its temperature.

In this discussion of the plasma arc several important factors have not been included. For example, there is ohmic heating of the plasma, which must raise its pressure and contribute to the projectile acceleration. Also, at the high temperatures (30,000 K) in the plasma, energy is radiated away rapidly. These factors are especially relevant to the gas pressure propulsion model.

Altogether, the points raised show that the plasma arc method may vary between very effective and very ineffective.

## CHAPTER 2

### RAILGUN EFFICIENCY

This Chapter has two major objectives.

One is to estimate the energy loss due to current distribution upon the rails.

The second objective is to develop efficiency expressions for railguns, including segmented and distributed energy stored railguns that have been proposed to reduce resistive losses. From such equations the reduction in size of the power source needed for the more complex guns can be balanced against the complexity of their construction.

#### **2.1 Introduction**

The overall efficiency of the simple railgun shown in Fig. 1 is a few percent. This is tolerable for small launchers, such as for experimental work, but limits the scale of their use. Spaceship launching, for example, might not be practicable because of the large size of the power source that would result from such a low efficiency.

It is important to quantify the various factors that affect efficiency because even small improvements are important when the efficiency is low. An improvement from 1% to 2% halves the size of the power source for example.

One reason for low efficiency of railguns is the  $I^2R$  loss in the circuit. The further that the projectile has moved from the breech in Fig. 1, the greater is the resistance through which the current must flow. The rail resistance is higher than the d.c. resistance because the current flows mostly near the rail surfaces.

Another cause of low efficiency is the energy stored in the magnetic field of the rails. As was found in Ch. 1, when the current is constant the quantity of energy stored in the rail field is the same as the associated energy,  $\Delta W$ , and in this case the maximum efficiency of the railgun is 50%. Some of the rail magnetic field energy may be recovered by using long rails and allowing the current to decline, or by the "distributed energy store" scheme (which will be discussed later)

Another possible loss, particularly relevant to plasma arc guns, may be due to gas particle propulsion of the projectile, as discussed in Ch. 1.

A more subtle cause of energy loss, also introduced in Ch. 1, is the inductance change in places other than immediately behind the projectile. These inductance changes are determined by the distribution of the current.

The work in the following Sections is particularly aimed at the effect of current distribution on inductance losses and the resistive losses as the current diffuses. The procedure is lengthy and complex and models have to be construed such that calculations are possible.

Firstly, the energy losses associated with current distribution that were introduced in Ch. 1 and embraced in factor "f" are expressed in terms of "propelling" and "uncoupled" fluxes.

Secondly, the factors that determine current distribution at various parts of the rails are discussed, leading to the selection of three current distributions for rail inductance loss estimates.

Thirdly, the "propelling" and total inductances are calculated for these current distributions, and, in turn, factor f is calculated.

Fourthly, rail resistive loss equations are derived for both diffusing current and fully penetrated current, for breech supplied, segmented and distributed energy store railguns.

Finally, various losses are combined to yield efficiency expressions. These are evaluated for a particular example and discussed.

## **2.2 The "propelling" and "uncoupled" fluxes**

If the railgun rails are thin, as indicated in Fig. 1, all the flux of the current passes into the space between them and is crossed by the current where it passes from one rail to the other. All the  $J \times B$  forces caused by current crossing flux act on the projectile. Alternatively, we can see that when the projectile moves distance  $\Delta x$  the flux increase is entirely located in the area swept out by the projectile. The inductance increase,  $\Delta L$ , and the corresponding associated energy,  $\Delta W$ , arise directly at the projectile and it is possible for all the associated energy to become projectile energy.

In Fig. 4 the rails are shown wider than in Fig. 1. Flux may now exist within the rails, as well as between them, depending on how the current is distributed.

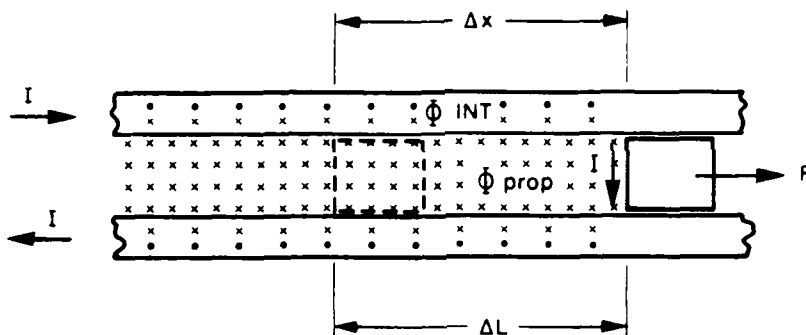


Fig. 4 Internal rail flux and the "propelling" flux.

The internal flux contributes to the inductance of the rails and to the associated energy  $\Delta W$ , but since it is not behind the projectile it cannot produce force on the projectile.

It will become clearer later that the term "internal flux" is not precise enough to describe the flux which does not cause force on the projectile. A better term is "uncoupled flux".

Only the flux which is behind the projectile in Fig. 4 can cause force upon the projectile. It is convenient to call this the "propelling flux". This flux is very nearly what is called the "external" flux of a conductor.

Since the total flux linkages are the sum of those of the propelling and uncoupled fluxes we can define the inductance change,  $\Delta L$ , in terms of propelling and uncoupled inductance changes i.e.

$$\Delta L = \Delta L_p + \Delta L_u, \quad (2.1)$$

where  $\Delta L_p$  is due to the flux linkages of the propelling flux,  $\Delta \Phi_p$ , and  $\Delta L_u$  is due to the flux linkages of the uncoupled flux,  $\Delta \Phi_u$ . The reader is reminded that the inductance change,  $\Delta L$ , is actually the change at the breech while the projectile moves distance  $\Delta x$ .

By comparison with Eqn. (1.8) it is apparent that  $\Delta L_p$  is some or all of the term  $\frac{\partial L}{\partial x} \Delta x$  while  $\Delta L_u$  is made up of the terms  $\frac{\partial L}{\partial y} \Delta y + \frac{\partial L}{\partial z} \Delta z$  and possibly a fraction of the  $\frac{\partial L}{\partial x} \Delta x$  term.

The associated energy change,  $\Delta W_a$ , in terms of  $\Delta L_p$  and  $\Delta L_u$  is:

$$\Delta W_a = \frac{1}{2} (\Delta L_p + \Delta L_u) I^2 \quad (2.2)$$

The energy which the projectile may acquire,  $\Delta W_p$ , is the portion due to  $\Delta L_p$ , i.e. the maximum value of  $\Delta W_p$  is:

$$\Delta W_p = \frac{1}{2} \Delta L_p I^2, \quad (2.3)$$

and the force on the projectile,  $F$ , is:

$$F = \frac{1}{2} \frac{\Delta L_p}{\Delta x} I^2 \quad (2.4)$$

In Ch. 1, a factor, "f", was introduced to account for the reduction of the associated energy available to the projectile with the result that the force could be expressed as:

$$F = \frac{1}{2} f \frac{\Delta L}{\Delta x} I^2. \quad (2.5)$$

From the foregoing equations it is apparent that a value of  $f$  is given by:

$$f = \frac{\Delta L_p}{\Delta L} \quad (2.6)$$

The portion of the associated energy that does not get distributed via the projectile force must be wasted. Because the energy must be distributed via the forces it causes, and these forces are where current crosses flux, the uncoupled flux portion of  $\Delta W_a$  must be dissipated in stretching and twisting the rails.

### 2.3 Force factor and efficiency

Let us now generalize the force factor,  $f$ , and relate it to efficiency. The application of this factor yields the actual energy available to the projectile, and hence the actual force upon it. Various effects contribute to  $f$ . We have discussed the effects of current distribution and the plasma arc. If the current distribution factor is 0.9 and the plasma arc factor is 0.67, the compound value of  $f$  is  $0.9 \times 0.67 = 0.603$ .

To get the actual kinetic energy that the projectile gains, further reductions in  $f$  must be made to allow for effects such as friction, plasma leakage past the projectile and air load ahead of the projectile.

Factor  $f$  is not constant throughout the acceleration, but, for practical application of the notion, we shall suppose that a realistic average value can be ascertained.



If  $\Delta W$  is the actual kinetic energy gained by the projectile, the associated energy change is  $\frac{\Delta W}{f}$ , where the value of  $f$  is the overall value. In the case of a constant current, resistanceless railgun, the source must supply twice the associated energy (because it must supply an equal amount of stored energy). The increment of energy supplied by the source,  $\Delta W_s$ , in this case is:

$$\Delta W_s = \frac{2\Delta W}{f} \quad (2.6)$$

and the efficiency,  $\eta = \frac{\Delta W}{\Delta W_s}$ , is:

$$\eta = \frac{f}{2} \quad (2.7)$$

Thus, if the value of  $f$  is 0.603, the maximum efficiency of the railgun is 30%. Because of resistance, the actual value will be lower.

#### 2.4 Current flow in the railgun

The manner in which the current is distributed within the rails and over their surfaces determines the proportions of the uncoupled and propelling inductances. The distribution near the projectile is of particular interest because it has most effect on the propelling inductance and hence on the propulsion force and factor  $f$ .

Although the current streamline flow has been discussed amongst railgun researchers, the only published diagram is an intuitive sketch by Marshall [1]. In this and the following Sections the physical and mathematical aspects of electromagnetics that seem pertinent to the current distribution will be reviewed. This work is a preparation for selecting current distributions for the calculation of propelling and total inductances.

At all times the general relationship between magnetic field intensity and current must hold, i.e.:

$$\nabla \times H = J + \frac{\partial D}{\partial t} \quad (2.8)$$

where  $H$  is the magnetic field intensity,  $J$  is the conduction current density and  $D$  is the electric displacement [2]. Taking the curl of Eqn. (2.8) and substituting  $J = \sigma E$  where  $\sigma$  is the conductivity and  $E$  is the electric field intensity, and substituting  $\nabla \times E = -\frac{\partial B}{\partial t}$ , leads to:

$$\nabla^2 H = \sigma \mu \frac{\partial H}{\partial t} + \epsilon \mu \frac{\partial^2 H}{\partial t^2} \quad (2.9)$$

where  $\mu$  is the magnetic permeability and  $\epsilon$  is the permittivity of the medium in which the current flows.

Eqns (2.8) and (2.9) may be separated into two simpler cases corresponding to non conducting and conducting mediums.

In a non conducting medium, such as the space surrounding a pair of parallel rails,  $\sigma = 0$  and Eqn. (2.9) becomes:

$$\nabla^2 H = \epsilon_{\mu} \frac{\partial^2 H}{\partial t^2} \quad (2.10a)$$

It is well known that the solution to this equation, for a pair of rails (i.e. a transmission line) having inductance, L, and capacitance, C, per unit length is a travelling electromagnetic wave which propagates energy with velocity  $1/\sqrt{LC} = 1/\sqrt{\mu\epsilon}$ , the velocity of light in the medium around the conducting rails (2).

In a conducting medium,  $J \gg \frac{\partial D}{\partial t}$ , and Eqn. (2.9) becomes:

$$\nabla^2 H = \sigma_{\mu} \frac{\partial H}{\partial t} \quad (2.10b)$$

This is well known as the "diffusion" equation [2,3,4]. It represents the physical process whereby concentrations spread out to eventually become uniform distributions, simply because a greater number of particles is likely to move from the more dense regions to the less dense regions than vice versa. In electromagnetics diffusion is complicated, compared to, say, heat diffusion, by the requirement to satisfy induction and circuit laws.

The rate of spreading out by diffusion is dependent on  $1/\sqrt{\sigma\mu}$  and is very much less than the velocity given by the analogous term,  $1/\sqrt{\epsilon\mu}$  in the wave propagation case. The rate of spreading by diffusion also varies as  $1/\sqrt{t}$ , where t is the time from the start of the process; hence it diminishes with time, in contrast to the constant velocity of pure wave propagation.

Another important aspect of diffusion is that the diffusion equation does not specify the initial distribution, but only the manner in which it changes from its initial state to a final state.

In regions where both J and  $\frac{\partial D}{\partial t}$  terms exist, Eqn. (2.9) applies and its solution may be regarded as containing both wave propagation and diffusion components.

Let us now consider how the current in the rails moves with the projectile. At first sight it seems that the railgun circuit must obey only Eqn. (2.10b) because it has no capacitance. In this case current and magnetic field variations would occur only because of diffusion. This cannot be the case at the projectile, though. Diffusion is too slow for the propulsion velocities attained and in any case is only a redistribution process and cannot account for the propagation of the total current values to the new portions of the rails. Note that diffusion includes  $J \times B$  forces on electrons

in the rails, so we cannot imagine the rail current to propagate in the same manner as the projectile.

Current must therefore propagate with the projectile by travelling wave means. Let us consider how this may come about given that the projectile (or plasma arc) may be a perfectly conducting short circuit.

The first point to note is that even though the projectile may be perfectly conducting, the flow of current at the rail/projectile interfaces is not a continuous process. The current flowing in and on the rails may be envisaged as many parallel filaments. When the projectile moves through its own length every filament of current in that region must cease flowing and be replaced by a new filament. The interruption causes high frequency induced e.m.f.s. in the projectile region. Because the inductance of the circuit is increased as the projectile moves, the new filaments must be established in a circuit of greater inductance. The sliding surfaces are thus equivalent to a great number of switched inductor circuits, such as Fig. 2, Ch. 1, in parallel. Filaments near the front may readily transfer to new contact points that arrive as the projectile moves forward. Filaments at the rear of the projectile, however have to overcome a greater inductance change.

The second point is that when the projectile moves distance  $\Delta x$  and increases the circuit inductance by  $\Delta L$ , it also increases the capacitance which the rails would have if they were of the same length and open circuited. It is tempting to suppose that the rear most current filaments may continue their conduction via this capacitance increment, due to induced e.m.f.s., and so constitute a displacement current component which, together with the  $\Delta L$  component, results in a travelling wave.

In short, the above two points suggest that the current follows the projectile because the projectile movement switches in  $L$  and  $C$  transmission line parameters and causes high frequency excitation.

If we imagine the projectile to be extremely thin, then when it moves forward it interrupts all the current. It is easy to appreciate in this case that the rails are then open circuited and the current must flow via the rail capacitance and reach the new projectile position by travelling wave means. With a longer projectile (or plasma arc) the displacement current and conduction current processes are probably intermingled and Eqn. (2.9) applies.

Even for perfectly steady D.C. conditions energy must be transmitted by electromagnetic waves. The apparent magnetostatic condition can be explained by a standing wave type of superposition [5].

The foregoing study leads to the same general picture of current distribution as that proposed by Marshall (see Fig. 5), viz. that there are three regions, A, B and C.

- A: Just behind the projectile, the current distribution is the high frequency electromagnetic wave distribution. It is essentially the "end effect" high frequency distribution of a short circuited

transmission line because electromagnetic waves move much faster than the projectile. Marshall includes the current distribution over the actual projectile in region A because it is velocity invariant also.

- B: Further behind the projectile, the end effect is negligible and the current filaments are established with the infinitely long transmission line distribution.
- C: Further yet behind the projectile, there are no displacement current components and only diffusion occurs, eventually resulting in uniform current distribution.

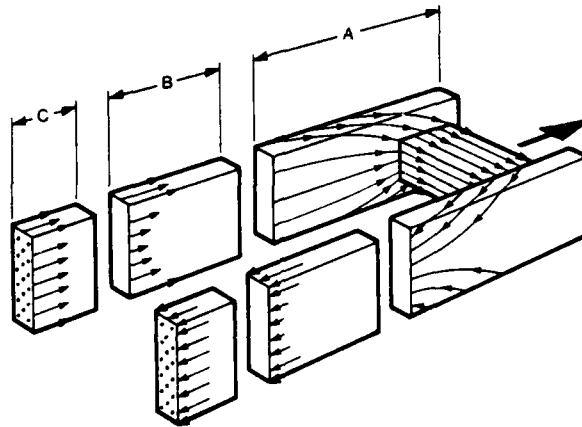


Fig. 5 Current flow pattern in railgun (Marshall)

## 2.5 Inductance in the projectile region is minimized

In the previous Section it was decided that the current is established near the projectile by high frequency propagation. The next step is to find the current distribution which relates to electromagnetic wave propagation.

Electromagnetic waves travel with velocity  $v = \frac{1}{\sqrt{LC}}$ . Since  $\frac{1}{\sqrt{LC}} = \frac{1}{\sqrt{\mu\epsilon}} = c$  the velocity of light, which is the maximum possible velocity in the medium, it follows that the product  $LC$  has the minimum possible value, i.e.

$$(LC)_{\min} = \frac{1}{c^2} \quad (2.11)$$

Electric charge, however is always distributed over conductors so as to produce the minimum capacitance [6]. The minimum value of LC therefore occurs when L is also least. The inductance in the projectile region is therefore, per unit length,

$$L = \frac{1}{c^2 C} \quad (2.12)$$

where c is the velocity of light and C is the capacitance per unit length, both for the medium surrounding the rails.

It follows that the current in the projectile region is distributed over the rails so as to minimize the inductance. It also follows that one way to find the current distribution would be to find the distribution which yields the minimum inductance.

There is another way in which we can deduce that the inductance near the projectile will be minimized. This is from the logical argument that the current in the railgun circuit will arise along the paths of least opposition, i.e. minimal inductive reactance.

Inductance is least when there is no magnetic field within the conductors. This is because the external flux is not affected by current distribution within the conductors as much as is the internal flux. The total inductance, i.e. the sum of the internal and external inductances, is therefore least when the current is distributed so that the internal flux is zero. The important conclusion that follows from this is that if the inductance is minimal, then all the flux is external, and hence is "propelling" flux.

## 2.6 Initial resistance in the projectile region

For there to be no internal flux, the current must be a surface current. This implies infinite resistive opposition unless the conductor has zero resistivity. The argument that current will distribute such that the opposition is least leads to the conclusion that there must be some penetration of real conductors and therefore some internal flux. We shall now develop this idea to obtain a simple estimate of the current penetration.

As the current penetrates, resistive opposition will diminish while the inductive opposition will increase owing to the internal inductance. This suggests that the minimum total of these two effects will occur when they are approximately equal i.e. when:

$$RI \approx \frac{d}{dt} (L_1 I), \quad (2.13)$$

where R is the effective resistance, I is constant current and  $L_1$  is the changing internal inductance. This can be seen by imagining the cross over region of the graphs of the two effects, remembering that since the external

flux links the whole cross section, it produces the same back emf, i.e. same opposition, in every filamentary circuit and so cannot affect the current distribution. Eqn. (2.13) is also, of course, Ohm's Law, but the minimization interpretation seems more appropriate in the present context.

Suppose that the current is spread over a length  $\ell$ , where it passes from the rails to the projectile. When the projectile moves a distance  $\ell_a$ , the current experiences the associated inductance change. If  $L'_1$  is the internal inductance per unit length in this region, due to current penetration, and if  $\Delta t$  is the time to move distance  $\ell_a$ , Eqn. (2.13) becomes:

$$R \approx \frac{L'_1 \ell_a}{\Delta t} \quad (2.14)$$

where  $R$  is the effective resistance of length  $\ell_a$ .

$$\text{i.e.} \quad R \approx L'_1 v \quad (2.15)$$

where  $v$  is the projectile velocity. Since we have defined  $f = \frac{L_p}{L_p + L_1}$ , Eqn. (2.15) can be expressed in terms of the total inductance per unit length and the fraction of external inductance as:

$$R \approx (1-f) L' v \quad (2.16)$$

where  $L'$  is the total inductance per unit length in the projectile region.

As an example, consider a pair of rails, 1 cm x 1 cm in section spaced 1 cm apart with a total inductance of 0.5  $\mu$ H/m, of which 90% is external inductance. If a projectile travels at 1 km/s between these rails, the rail resistance in the projectile region is given by Eqn. (2.16) as 50  $\mu\Omega$ . Depth of penetration can be calculated if some assumptions are made about the current distribution. Thus if the projectile is a 1 cm metal cube, we may take  $\ell_a = 1$  cm and we may calculate an equivalent depth of penetration as if the current all flows on the inner sides of the rails. For copper rails, the result in this case is an equivalent depth of penetration equal to 0.68 mm. If we imagine that current to be distributed over all four sides of the rails, the skin depth is 0.17 mm. Although we have picked figures for the sake of example and the parameters in Eqn. (2.16) are actually interdependent and not able to be separately selected, the resultant values for depth of penetration are similar to those obtained from the usual expressions, such as Eqn. (2.22), and hence suggest that  $f = 0.9$  is a realistic value.

## 2.7 The diffusion equation and depth of penetration

Diffusion is the only electromagnetic process affecting the current distribution some distance behind the projectile. As was discussed in Section 2.4 it obeys the expression:

$$\nabla^2 H = \sigma \frac{\partial H}{\partial t} \quad (2.10b)$$

The resistive losses decrease as the current diffuses. An equivalent depth of penetration of current is commonly used to estimate the resistive losses. We shall require such an expression to calculate the rail losses. The depth of penetration is also a guide to the internal inductance, and hence to factor  $f$  type of losses.

We shall now demonstrate that a simple derivation of depth of penetration consistent with Eqn. (2.10b), follows from the ideas in the previous Section.

Based upon the idea of minimization of force opposing current flow, it was suggested that current penetrates the rails such that  $RI \approx \frac{d}{dt}(L_1 I)$ , where  $L_1$  is the internal inductance of the rails. This expression can be shown to be a form of the diffusion equation.

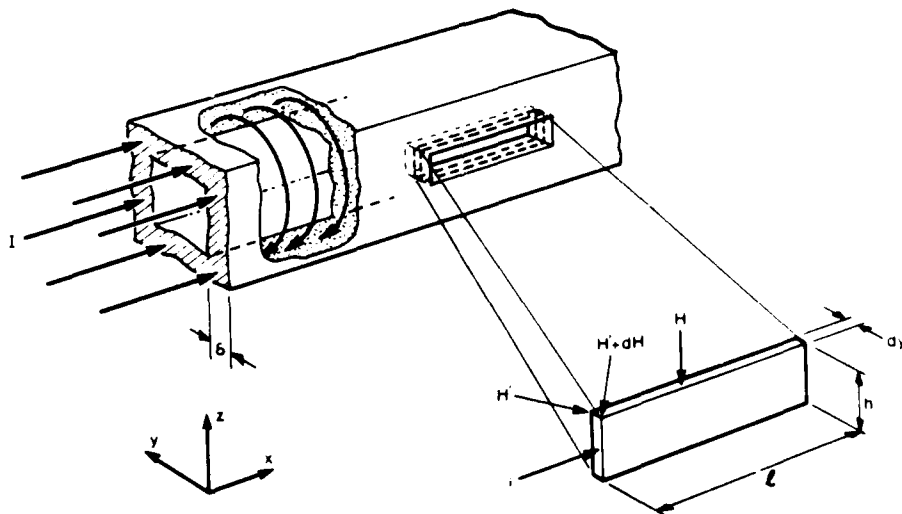


Fig. 6. Current and flux penetration of rail.

Consider the expression

$$RI = \frac{d}{dt} (L_1 I) \quad (2.17)$$

for the small element of the rail shown in Figure 6, in which current and flux exist in the shaded area of the rail. Replacing  $R$  by  $\frac{t}{\sigma h dy}$  and  $\frac{d}{dt} (L_1 i)$  by  $\frac{d\phi}{dt}$ , Eqn. (2.17) becomes:

$$\frac{t i}{\sigma h dy} = \frac{d\phi}{dt} \quad (2.18)$$

Application of the general law  $\int H dr = I$  to the element yields:

$$dH = i/h, \quad (2.19)$$

while  $\phi$  may be written as  $\int \mu H r dy$ . Equation (2.19) becomes:

$$\frac{t}{\sigma} \frac{dH}{dy} = \frac{d}{dt} \int \mu H r dy. \quad (2.20)$$

Differentiating (2.20) with respect to  $y$  yields:

$$\frac{d^2 H}{dy^2} = \sigma \mu \frac{dH}{dt}, \quad (2.21)$$

which is a one dimensional form of the diffusion equation.

The depth of penetration,  $\delta$ , is the equivalent depth of conductor, measured from the surface as indicated in Figure 6, in which the current, uniformly distributed, experiences the same resistance as is calculated from  $R_1 = \frac{t}{\sigma \delta}$  ( $L_1 i$ ). Because  $\delta$  is an equivalent depth, its value depends on its exact definition, however it is always of the form:

$$\delta = \alpha \sqrt{\frac{t}{\sigma \mu}}, \quad (2.22)$$

where  $t$  is the time for which current has been flowing and  $\alpha$  is a factor which depends on the definition and on the time function of the current waveform [7]. The usual way of evaluating  $\delta$  is by substituting the waveform time function into the diffusion equation, together with boundary conditions. The procedure is lengthy. Equation (2.22) can, however, be derived in a simplistic manner from the general one dimensional form of the diffusion equation. Thus, Eqn. (2.21) can be written as:

$$\frac{1}{\sigma} \frac{dH}{dy} = \int \mu \left( \frac{dH}{dt} \right) dy. \quad (2.23)$$

Let us now make the assumption that  $\frac{dH}{dt}$  is constant. This enables Eqn. (2.23) to be rearranged as:

$$\frac{1}{\sigma} \int_0^t dt = \int_0^\delta \left( \int \mu dy \right) dy. \quad (2.24)$$



$$\text{i.e.} \quad \frac{L}{\sigma} = \mu \frac{\delta^2}{2} \quad (2.25)$$

$$\text{or} \quad \delta = 1.414 \sqrt{\frac{L}{\sigma \mu}} ; \quad (2.26)$$

which is of the same form as the well known expression (2.22) given above.

Equations (2.22) and (2.26) yield  $\alpha = 1.414$ . A more rigorous derivation, referred to in Sect. 2.10.11, yields  $\alpha = 1.772$ .

It must be emphasized that depth  $\delta$  does not prescribe where the current and flux exist. It is simply a dimension which is compatible with changing flux and current assumed to exist in the location where it is calculated.

## 2.8 Inductance equations

In this Section expressions for the propelling and total inductances for three conceivable current distributions are set out. Inductance expressions for rectangular rails are tedious to derive and are cumbersome. A few specialists have derived expressions for rectangular sections for particular purposes [8,9], but it is necessary to especially derive most of the expressions of interest for the railgun, in particular for the propelling inductance.

### 2.8.1 Selection of current distributions

To calculate inductance it is necessary to know how the current is distributed.

In the preceding Sections three factors that bear upon current distribution were discussed, viz. that current is initially distributed such that the inductance is a minimum, that with time it redistributes and that it cannot flow in an infinitely thin sheet on the surface because the resistance would be infinite. Three current distributions follow from these factors.

Firstly there is the distribution for minimum inductance. We have deduced that electromagnetic wave propagation involves the minimum inductance. It also involves the capacitance of the rails and this enables the current filaments that yield the minimum inductance to be located by the "electrostatic analogy" [10]. By this it is meant that current initially flows in the same places as where charge accumulates on the rails when they are considered to be the plates of a capacitor. The physical reason for this is that the electric field component of the wave places the mobile charges in position on the surface and it is these charges which also move along the surface as current. Kerrisk [11] has used a numerical procedure to calculate the inductance of pairs of rectangular rails based upon a method for finding the electrostatic charge density distribution. He has fitted an empirical equation to the inductance values of a range of rail cross sections and spacings, thereby enabling the minimum inductance to be readily calculated.

Since electric charges are distributed on conductors so as to produce no internal electric field, there can be no internal magnetic field either. (Time varying fields must have both magnetic and electrical components.) The magnetic field is thus entirely external to the conductors, as was previously argued for the minimum inductance case, and the minimum inductance is also entirely propelling inductance.

It also follows that the minimum inductance is approached at high frequency, since it is known that high frequency currents do not diffuse substantially into conductors.

The next current distribution of interest is a uniform surface current over each of the sides of the rails. The reason for considering this distribution is that the minimum inductance distribution is a non uniform surface current that has infinitely dense current at the corners of the rails, as shown in Fig. 7. Because of very high resistive opposition, it may be that the current takes up a more uniform distribution, although still very near the surface.

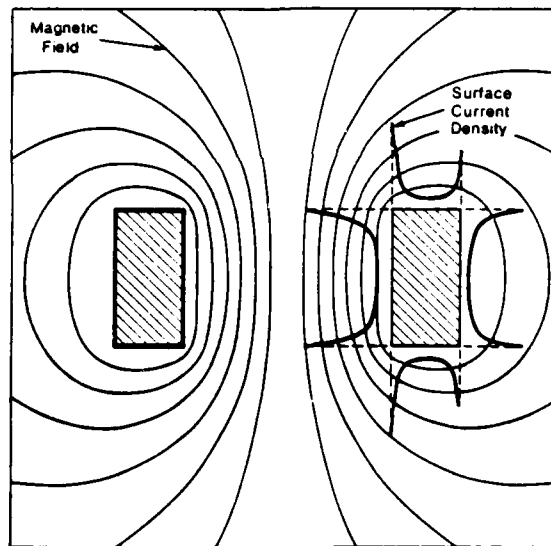


Fig. 7 Flux and current distribution for initial inductance, redrawn from Kerrisk's work.

It might seem that uniform surface current is actually more likely because it would minimize the resistive opposition whilst the flux is all external. All the flux, though, would not be totally external. Part of it passes within the conductor, as shown in Fig. 8(b). These lines cause greater

back e.m.f. in the filaments that they link than if the flux is completely external and hence, except at D.C., must reduce the current in that region. These flux lines, therefore, behave as "internal" flux, since truly external flux induces the same back e.m.f. in every filamentary circuit within the conductors.

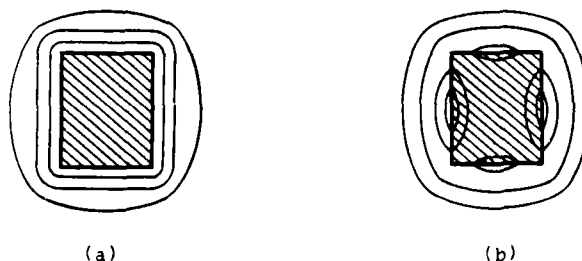


Fig 8. Flux lines around rail (a) with current distributed so as to produce minimum inductance (b) with uniformly distributed surface current.

Nevertheless, if the inductance for uniform surface current is not much greater than the minimum inductance, then the decrease in resistive opposition may outweigh the increase in inductance so that current takes up a more uniform distribution. The high currents and the randomly located arcing contacts may increase the extent to which this happens in railguns.

The other current distribution is that for full penetration of current, which gives a measure of the greatest effect possible due to the distribution of the inductance into propelling and uncoupled parts. It could only occur in railguns with thin rails, or slow or very long railguns.

Mention should be made of a current distribution which is taken to exist by some authors, viz. that the current is distributed over the inner sides of the rails [12,19]. Near the projectile it is taken as a current sheet on the inner surfaces and further back it penetrates the rails from those surfaces.

The reason for considering such a distribution is that high frequency currents flow on the inner sides of parallel plate transmission lines. The spacing of such transmission lines is small compared to the height, though, and they are only a rough approximation to the railgun geometry. This can be seen from the current profiles in Fig. 7, drawn from data given by Kerrisk [11]. For the typical railgun geometry in Fig. 7, about half as much current flows on the outer rail surface as flows on the inner surface.

Of the three distributions that we have selected it is necessary to derive the propelling inductances for the uniform surface current and fully penetrated current and the total inductance for the uniform surface current. For the total inductance of fully penetrated current we shall use an expression given by Arnold [13] and for the minimum inductance we shall use Kerrisk's expressions.

### 2.8.2 Propelling inductance of a pair of parallel current sheets

We begin by calculating the propelling inductance of a thin rectangular sheet circuit as shown in Fig. 9. The method is to calculate the

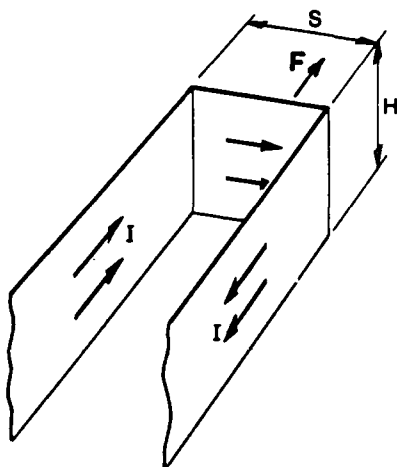


Fig. 9. Rectangular current sheet circuit.

force,  $F$ , exerted on the current sheet crossing the rails and to calculate the inductance from:

$$L'_p = \frac{2F}{I^2}. \quad (2.27)$$

Equation (2.27) is the virtual work equation rearranged to give the "propelling" inductance.

Before proceeding, it is convenient at this point to discuss the differences between internal and uncoupled, and external and propelling inductances. The terms internal and external inductance imply that flux lines are entirely inside or entirely outside the conductor. If there are lines that are partly internal and partly external, as shown in Fig. 8(b), then some of these lines will interact with the cross sheet current and so increase the propelling inductance and the internal inductance. The difference due to

these lines is small, but for accuracy we use the terms "propelling" and "uncoupled" rather than "external" and "internal".

The uniform current sheet rails provide a test of this theory; the flux lines which are not entirely external in this case link the same proportion of rail sheet current as the proportion of cross sheet current. Calculation should show that the total and propelling inductances are the same in this case even though there is some internal inductance.

Let us consider the sheets in Fig. 9 to be an assembly of filamentary currents, such as in Fig. 10. To find the force on a cross

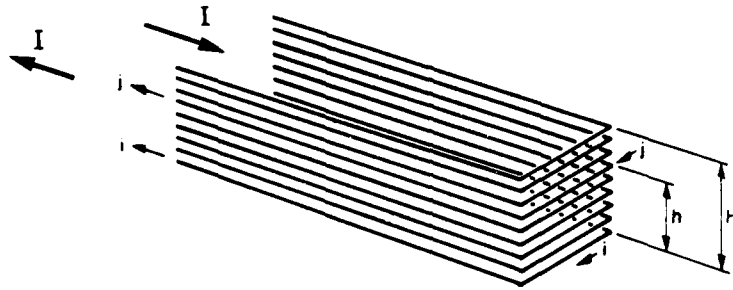


Fig. 10. Filamentary model.

filament, such that carrying current  $j$ , due to the current  $i$  in the bottom filament, we require the vertical component of the flux density at points along  $j$ , due to  $i$ . From Fig. 11, it can be seen that if the flux density at  $P$  on  $j$  is  $B$ , the vertical component is  $B \frac{s}{w}$ .

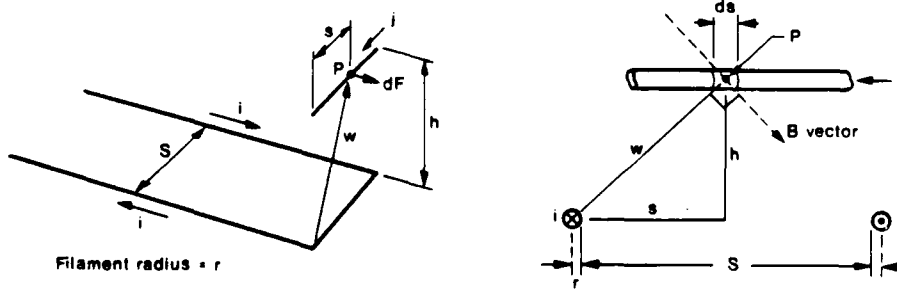


Fig. 11. Field at a point on filament  $j$  due to filament  $i$ .

The magnitude of the field at a point opposite the end of a filament of current is half that which it would be if the filament continued indefinitely, because of symmetry (Fig. 12). The magnitude of B at P is therefore  $\frac{\mu_0 i}{4\pi w}$ .

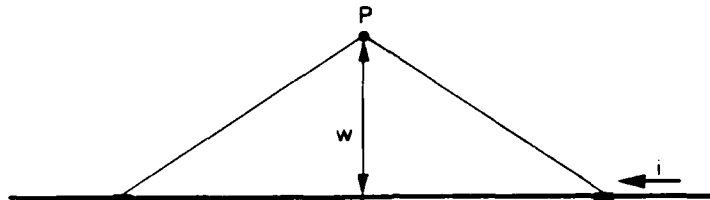


Fig. 12. Field at P is due to equal contributions from symmetrically located current elements on either side.

The elemental force at P is, from the general law, force =  $B i d\ell$ ,

$$dF = \frac{\mu_0 i j}{4\pi w} \frac{s}{w} ds. \quad (2.28)$$

Substituting  $s^2 + h^2 = w^2$  and noting that the force on the current  $j$  is doubled because of the go and return of current  $i$ , we obtain for the total force,  $F$ , on  $j$ :

$$F = \frac{\mu_0 i j}{2\pi} \int_r^{S+r} \frac{s}{s^2 + h^2} ds, \quad (2.29)$$

where  $r$  is the radius of the filament of current  $i$ . We next extend the integration to obtain the total normal force, due to the current  $i$ , on the whole current sheet. To do this replace  $j$  by  $\frac{I}{H} dh$ , where  $I$  is the total current uniformly distributed over height  $H$ , and integrate. This gives:

$$F = \frac{\mu_0 i I}{2\pi H} \int_0^H \int_r^{S+r} \left( \frac{s}{s^2 + h^2} \right) ds dh \quad (2.30)$$

or:

$$F = \frac{\mu_0 i I}{4\pi H} \left[ h \ln((S+r)^2 + h^2) - h \ln(r^2 + h^2) + 2(S+r) \arctan\left(\frac{h}{S+r}\right) - 2r \arctan\left(\frac{h}{r}\right) \right]_{h=0}^{h=H} \quad (2.31)$$

Finally, we sum the forces on the cross sheet due to all the filaments such as 1, by writing  $i = \frac{I}{H} dh$  and integrating Eqn. (2.31). Since a filament at height  $h$  produces force on cross sheets of height  $h$  below it and height  $(H-h)$

above it, it turns out that the integral must be doubled to get the total force,  $F$ , i.e.

$$F = \frac{\mu_0 I^2}{2\pi H^2} \int_0^H \{ h \ln((S+r)^2 + h^2) - h \ln(r^2 + h^2) + 2(S+r) \arctan(\frac{h}{S+r}) - 2r \arctan(\frac{h}{r}) \} dh \quad (2.32)$$

Evaluating (2.32) yields:

$$\begin{aligned} F = \frac{\mu_0 I^2}{4\pi} & \left[ \left(1 - \frac{(S+r)^2}{H^2}\right) \ln(H^2 + (S+r)^2) \right. \\ & - \left(1 - (r/H)^2\right) \ln(H^2 + r^2) + \frac{(S+r)^2}{H^2} \ln(S+r)^2 \\ & - (r/H)^2 \ln r^2 + 4 \frac{(S+r)}{H} \arctan(\frac{H}{S+r}) \\ & \left. - 4(r/H) \arctan(H/r) \right]. \quad (2.33) \end{aligned}$$

Allowing the filamental radius to diminish, and converting to inductance by expression (2.27) yields:

$$L'_p = \frac{\mu_0}{2\pi} \{ 4(S/H) \arctan(H/S) + \ln(1 + (S/H)^2) - (S/H)^2 \ln(1 + (H/S)^2) \} \quad (2.34)$$

Equation (2.34) is therefore the propelling inductance per metre for the uniformly distributed current sheets shown in Fig. 9.

At the beginning of this section it was deduced that the propelling inductance and the total inductance should be the same in this case. In the Appendix the method of geometric mean distances is used to obtain the total inductance for a pair of parallel current sheets. The result, (Eqn. (23) of the Appendix), is the same as Eqn. (2.34) and shows the deduction to be correct.

### 2.8.3 Force due to current sheets on tops and bottoms of rails

To obtain the propelling inductance for current uniformly distributed over the surface of a pair of rectangular rails, we require the sum of the forces on the cross sheet due to current sheets on each of the 8 sides of the rails. Equation (2.33) will do for 4 sides; setting  $r = 0$  gives

the force for the inner sides and setting  $r = W$ , the width of the rails, gives the force for the outer sides (Fig. 13).

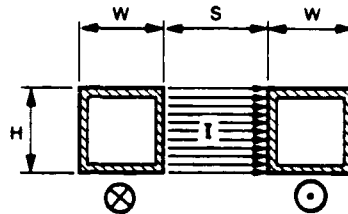


Fig. 13. Rectangular rails with uniform surface current.

To obtain the force on the cross sheet due to the top and bottom current sheets on the rails it is necessary to use Eqn. (2.31) and integrate in the direction of the width  $W$ , with  $r$  as the variable (Fig. 14).

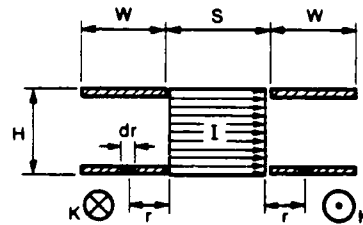


Fig. 14. Top and bottom current sheets.

Let the current distributed over the lower surface be  $K$ , i.e.  $i = \frac{K}{W} dr$ ; we then have from Eqn. (2.31) the force,  $F$ , on the cross sheet:

$$F = \frac{\mu_0 I K}{4\pi W} \int_0^W \left[ \ln(H^2 + (S+r)^2) - \ln(H^2 + r^2) + 2 \frac{(S+r)}{H} \arctan\left(\frac{H}{S+r}\right) - 2 \frac{r}{H} \arctan\left(\frac{H}{r}\right) \right] dr, \quad (2.35)$$

where  $I$  is the total cross sheet current. When evaluated, this yields:

$$F = \frac{\mu_0 I K}{4\pi} \left( \ln\left(\frac{H^2 + (S+W)^2}{H^2 + W^2}\right) + \frac{S}{W} \ln\left(\frac{H^2 + (S+W)^2}{H^2 + S^2}\right) + \frac{(S+W)^2}{WH} \arctan\left(\frac{H}{S+W}\right) \right)$$



$$\begin{aligned}
& + \frac{H}{W} \arctan\left(\frac{S+W}{H}\right) - \frac{H}{W} \arctan\left(\frac{W}{H}\right) - \frac{W}{H} \arctan\left(\frac{H}{W}\right) \\
& - \frac{S^2}{WH} \arctan\left(\frac{H}{S}\right) - \frac{H}{W} \arctan\left(\frac{S}{H}\right) \quad (2.36)
\end{aligned}$$

#### 2.8.4 Propelling inductance of uniform surface current upon rectangular rails

Using correctly proportioned values for the side and top/bottom rail currents, Eqns. (2.31) and (2.36) can be combined to give the total force on the cross sheet and hence, by Eqn. (2.27), the propelling inductance of a uniform surface current upon rectangular rails. In this case it is appropriate to refer to the inductance as the propelling inductance since not all the flux that passes externally crosses the space between the rails. In Fig. 8(b) it can be seen that the partial flux linkages on three sides are such flux lines. The equation for the propelling inductance becomes:

$$\begin{aligned}
L'_p &= \frac{\mu_0}{2\pi} \frac{W}{H+W} \left[ \ln\left(\frac{H^2 + (S+W)^2}{H^2 + S^2}\right) + \frac{S}{W} \ln\left(\frac{H^2 + (S+W)^2}{H^2 + S^2}\right) \right. \\
& + \frac{(S+W)^2}{WH} \arctan\left(\frac{H}{S+W}\right) + \frac{H}{W} \arctan\left(\frac{S+W}{H}\right) - \frac{H}{W} \arctan\left(\frac{W}{H}\right) \\
& - \frac{W}{H} \arctan\left(\frac{H}{W}\right) - \frac{S^2}{WH} \arctan\left(\frac{H}{S}\right) - \frac{H}{W} \arctan\left(\frac{S}{H}\right) \left. \right] \\
& + \frac{\mu_0}{2\pi} \frac{H}{H+W} \left[ \left(1 - \left(\frac{S+W}{H}\right)^2\right) \ln(H^2 + (S+W)^2) - \left(\frac{W}{H}\right)^2 \ln W^2 \right. \\
& - \left(1 - \left(\frac{W}{H}\right)^2\right) \ln(H^2 + W^2) + \frac{(S+W)^2}{H^2} \ln(S+W)^2 \\
& + 4 \left(\frac{S+W}{H}\right) \arctan\left(\frac{H}{S+W}\right) - 4 \frac{W}{H} \arctan \frac{H}{W} \\
& \left. + 4 \frac{S}{H} \arctan\left(\frac{H}{S}\right) + \ln\left(1 + \left(\frac{S}{H}\right)^2\right) - \left(\frac{S}{H}\right)^2 \ln\left(1 + \left(\frac{H}{S}\right)^2\right) \right] \quad (2.37)
\end{aligned}$$

where  $H$  is the rail height,  $W$  the rail width and  $S$  is the separation between the rails and where the current on the top and bottom of the rails is  $\frac{W}{H+W}$  and the current on the inner and outer sides is  $\frac{H}{H+W}$ , as proportions of the total current.

### 2.8.5 Propelling inductance for current uniformly distributed across the whole rail cross section

The propelling inductance for this case is obtained by integrating the current sheet expression, Eqn. (2.33) over the width,  $W$ , of the rails (Fig. 15). The term  $I^2$  in Eqn. (2.33) is due to the product  $I \times I$ , one  $I$

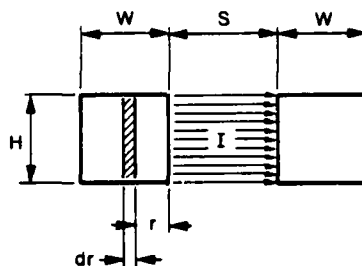


Fig. 15. Integration to obtain propelling inductance for current uniformly distributed across rail cross section.

referring to the cross sheet current and the other to the sheet current. We now replace the latter term by  $\frac{I}{W} dr$  to obtain the force of an elemental current strip of width  $dr$ . The total force is thus:

$$\begin{aligned}
 F = & \frac{\mu_0 I^2}{4\pi W} \int_0^W \left[ \left(1 - \frac{(S+r)^2}{H^2}\right) \ln(H^2 + (S+r)^2) \right. \\
 & - \left(1 - \left(\frac{r}{H}\right)^2\right) \ln(H^2 + r^2) + \frac{(S+r)^2}{H^2} \ln(S+r)^2 - \left(\frac{r}{H}\right)^2 \ln r^2 \\
 & \left. + 4 \frac{(S+r)}{H} \arctan\left(\frac{H}{S+r}\right) - 4 \left(\frac{r}{H}\right) \arctan\left(\frac{H}{r}\right) \right] dr \quad (2.38)
 \end{aligned}$$

Evaluation of Eqn. (2.38) yields, after laborious integration by parts, for the inductance:

$$\begin{aligned}
 L'_p = & \frac{\mu_0}{2\pi} \left[ \ln\left(\frac{H^2 + (S+W)^2}{H^2 + W^2}\right) + \frac{S}{W} \ln(H^2 + (S+W)^2) \right. \\
 & \left. - \frac{(S+W)^3}{3H^2 W} \ln\left(1 + \left(\frac{H}{S+W}\right)^2\right) + \frac{W^2}{3H^2} \ln\left(1 + \left(\frac{H}{W}\right)^2\right) \right]
 \end{aligned}$$

$$\begin{aligned}
& + \frac{2}{3} \frac{H}{W} \left( \arctan\left(\frac{S+W}{H}\right) - \arctan\left(\frac{W}{H}\right) \right) \\
& + \frac{2}{WH} \left( (S+W)^2 \arctan\left(\frac{H}{S+W}\right) - W^2 \arctan\left(\frac{H}{W}\right) \right) - \frac{S}{W} \ln(H^2 + S^2) \\
& + \frac{S^3}{3WH^2} \ln\left(1 + \left(\frac{H}{S}\right)^2\right) - \frac{2}{3} \frac{H}{W} \arctan\left(\frac{S}{H}\right) - 2 \frac{S^2}{WH} \arctan\left(\frac{H}{S}\right) \quad (2.39)
\end{aligned}$$

#### 2.8.6 Total inductance for uniformly distributed surface current

Firstly, it is necessary to select a method for calculating the total inductance. By calculating the work done when two filamentary circuits, such as shown in Figure 16, approach each other, it is shown in text books [14] that their inductance is given by:

$$L = \frac{\mu_0}{4\pi} \int_{C_1} \int_{C_2} \frac{d\vec{s}_1 \cdot d\vec{s}_2}{r} \quad (2.40)$$

which is called the Neumann integral. We can consider a circuit with a real conductor to be made up of filamentary circuits parallel to each other. The magnetic energy of the circuit is the total work done in bringing all the filamentary circuits together and the corresponding total inductance is obtained by evaluating Eqn. (2.40) for every pair of filamentary circuits. In general it is only practical to evaluate Eqn. (2.40) by numerical methods.

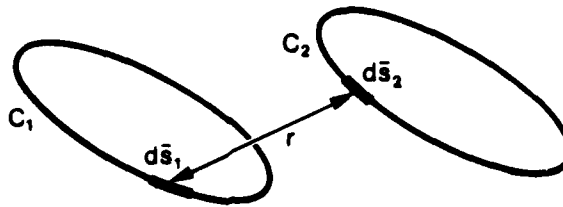


Fig. 16. Filamentary circuits - Neumann integral.

If the filamentary circuits are long compared to any distance  $r$  between them, as for pairs of parallel conductors, the "geometric mean distance" method, due to Maxwell, transforms the integration to a routine process. As is shown in Appendix 1, the inductance expression for two equal conductors becomes:

$$L = \frac{\mu_0}{\pi} [\ln R_{12} - \ln R_{11}] \quad (2.41)$$

where  $R_{12}$  is the geometric mean distance between the conductors and  $R_{11}$  is the geometric mean distance of each conductor from itself. This is the method that we shall use.

The task is to calculate  $R_{12}$  and  $R_{11}$  for rectangular rails with current uniformly distributed over their surfaces i.e. as if the rails were very thin wall sections. This is done by combining the basic equations for the geometric mean distances (GMD) of each side of one rectangle, from the other to obtain  $R_{12}$ , and from its own sides to obtain  $R_{11}$ . There are, thus, 16 contributions to each of  $R_{12}$  and  $R_{11}$  (Fig. 17), viz.:

for $R_{11}$ :	GMD of each line from itself	4 cases
	GMD of parallel lines	4 cases
	GMD of lines at right angles	8 cases
for $R_{12}$ :	GMD of parallel lines	4 cases
	GMD of lines in the same straightline	2 cases
	GMD of lines diagonally displaced	2 cases
	GMD of lines at right angles	8 cases

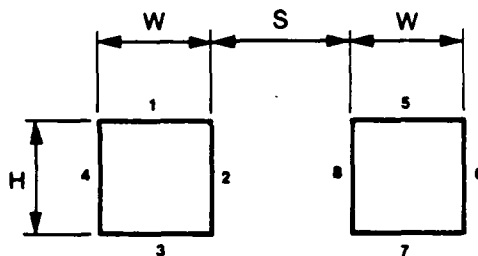


Fig. 17. Thin wall rectangular section for total inductance calculation with uniform surface current, geometric mean distance method

#### Calculation of $R_{11}$

- (i) The GMD,  $R$ , of a line of length  $a$  from itself is given by Rosa and Grover [15] as  $\ln R = \ln a - 3/2$ . The rectangular section  $H \times W$  has two lines of length  $W$  and two of length  $H$ , for which the basic equations are:

$$\ln R = \ln W - 3/2 \quad (2.42)$$

$$\ln R = \ln H - 3/2 \quad (2.43)$$

- (ii) For parallel equal length lines Rosa and Grover give an expression, which for the lines 4 from 2, 2 from 4, separated by  $W$  and of length  $H$  yields:

$$\ln R = \left(\frac{W}{H}\right)^2 \ln W + \frac{1}{2} \left(1 - \left(\frac{W}{H}\right)^2\right) \ln(H^2 + W^2) + 2 \frac{W}{H} \arctan\left(\frac{H}{W}\right) - 3/2. \quad (2.44)$$

For the GMD's of lines 1 from 3 and 3 from 1, W and H reverse their roles in Eqn. (2.44).

- (iii) The GMD of lines at right angles to each other does not appear to have been published and is derived in the Appendix. It is (putting  $S = 0$ ):

$$\ln R = \frac{1}{2WH} [WH \ln(H^2 + W^2) - 3WH + W^2 \arctan \frac{H}{W} + H^2 \arctan \frac{W}{H}] \quad (2.45)$$

The symmetry of this equation makes it applicable to all eight combinations 1,2; 2,1 etc.

When these equations are combined according to the rule [16]

$$\ln R = \frac{AB \ln R_{AB} + CD \ln R_{CD} +}{AB + CD +}$$

where R is the composite GMD of a system comprised of lines of lengths A and B with a GMD of  $R_{AB}$ , lengths C and D with a GMD of  $R_{CD}$  etc., we obtain:

$$\ln R_{11} = \frac{1}{(W+H)^2} [W^2 \ln W + H^2 \ln H + WH \ln(H^2 + W^2) - \frac{3}{2} (W+H)^2 + (W+H) (H \arctan(\frac{W}{H}) + W \arctan(\frac{H}{W}))] \quad (2.46)$$

#### Calculation of $R_{12}$

- (i) Equation (2.44) applies to the parallel lines of the two rectangles but with W replaced by S for lines 2,8 and by S+W for lines 4,8 and 2,6 and by S+2W for lines 4,6 (Fig. 17).
- (ii) For lines in the same straight line i.e. 1,5 and 3,7 the equation given by Rosa and Grover [15] is used, viz.,

$$\ln R = \ln nW - \frac{1}{12n^2} - \frac{1}{60n^4} \quad (2.47)$$

in which  $n = \frac{S+W}{W}$ .

- (iii) For lines that are parallel but diagonally displaced, i.e. lines 1,7 and 3,5 the following equation, derived in the Appendix, is used.

$$\ln R = \frac{1}{2W^2} \left[ \frac{(S+2W)^2 - H^2}{2} \ln(H^2 + (S+2W)^2) - 3W^2 + 2HS \arctan\left(\frac{S}{H}\right) \right]$$

$$\begin{aligned}
& + 2H (S+2W) \arctan\left(\frac{S+2W}{H}\right) - 4H (S+W) \arctan\left(\frac{S+W}{H}\right) - \left(\frac{H^2 - S^2}{2}\right) \ln(H^2 + S^2) \\
& + (H^2 - (S+W)^2) \ln(H^2 + (S+W)^2) \quad (2.48)
\end{aligned}$$

(iv) The lines at right angles in this case are separated by distances S and S+W and there are 4 cases of each separation. The following equation applies to separation S and is derived in the Appendix:

$$\begin{aligned}
\ln R &= \frac{1}{2WH} [H(S+W) \ln((S+W)^2 + H^2) - 3WH \\
& + H^2 \arctan\left(\frac{S+W}{H}\right) + (S+W)^2 \arctan\left(\frac{H}{S+W}\right) - HS \ln(S^2 + H^2) \\
& - H^2 \arctan\left(\frac{S}{H}\right) - S^2 \arctan\left(\frac{H}{S}\right)] \quad (2.49)
\end{aligned}$$

Many terms cancel when combined to give the composite value for  $\ln R_{12}$ . Substituting the composite values for  $\ln R_{12}$  and  $\ln R_{11}$  into Eqn. (2.41) yields:

$$\begin{aligned}
L &= \frac{\mu_0}{4\pi(W+H)^2} [S^2 \ln S + 2(H-S) (S \arctan\left(\frac{H}{S}\right) - H \arctan\left(\frac{S}{H}\right)) \\
& - 6H^2 + 2(S+W)^2 \ln(S+W) + 2(H^2 - (S+W)^2) \ln(H^2 + (S+W)^2) \\
& + 4(S+W) H (\arctan\left(\frac{H}{S+W}\right) - \arctan\left(\frac{S+W}{H}\right)) + (S+2W)^2 \ln(S+2W) \\
& + 2W^2 (\ln(S+W) - \frac{1}{12} \left(\frac{W}{S+W}\right)^2 - \frac{1}{60} \left(\frac{W}{S+W}\right)^4) - 3W^2 - 12HW \\
& - 2HS \ln(S^2 + H^2) + 2H(S+2W) \ln((S+2W)^2 + H^2) \\
& + 2H^2 \arctan\left(\frac{S+2W}{H}\right) + 2(S+2W)^2 \arctan\left(\frac{H}{S+2W}\right) \\
& - 4(W^2 \ln W + H^2 \ln H + WH \ln(H^2 + W^2)) - \frac{3}{2}(W+H)^2 \\
& + (W+H) (H \arctan\left(\frac{W}{H}\right) + W \arctan\left(\frac{H}{W}\right))]
\end{aligned}$$

$$+ 2(S+2W) H \left( \arctan\left(\frac{S+2W}{H}\right) + \arctan\left(\frac{H}{S+2W}\right) \right), \quad (2.50)$$

where L is the inductance in Henries/metre.

### 2.8.7 Total inductance for uniform current across section

The inductance of rectangular sections with the current uniformly distributed across the section has been derived by Gray [16]. The equation is more complicated than Eqn. (2.50). Arnold [13] developed the following approximate equation, which is generally accurate to within  $1/2\%$ .

$$L = \frac{\mu_0}{\pi} \ln[4.48(\alpha + \beta) + \frac{(1 - 2.41\alpha + \alpha^{2.3})}{(1 + 1.34\beta + .6\beta^{1.5})}] \quad (2.51)$$

where  $\alpha = \frac{W}{W+H}$  and  $\beta = \frac{S}{W+H}$

### 2.8.8 Kerrisk's equations for minimum inductance

Kerrisk's equations for the minimum inductance of rectangular rails are [11]:

$$L = [A + B \ln(F_1)] \ln(F_2) \mu H/m, \quad (2.52)$$

where  $F_1 = 1 + a_1 \left(\frac{W}{H}\right) + a_2 \left(\frac{W}{H}\right) \left(\frac{S}{H}\right)$

$$F_2 = b_1 + b_2 \left(\frac{S}{H}\right) + b_3 \left(\frac{W}{H}\right) + b_4 \left(\frac{S}{H}\right) \left(\frac{W}{H}\right)$$

$$A = 0.4406410$$

$$B = -0.0777133$$

$$a_1 = 3.397143$$

$$a_2 = -0.0660307$$

$$b_1 = 1.007719$$

$$b_2 = 2.743651$$

$$b_3 = 0.0220931$$

$$b_4 = 0.2637392$$

## 2.9 Inductance equations - results and discussion

The inductance equations given in the previous section are tabulated and graphed on the following pages. These results enable several ideas that have been put forward to be assessed, viz.,

- (i) that the initial inductance is the minimum total inductance,
- (ii) the range of "f" values that occur owing to internal inductance,
- (iii) the possibility of the current taking up a different distribution to that which gives minimum initial inductance.

The tables and graphs (Fig. 18) show that Kerrisk's equation does give initial inductance values lower than the total inductance values of either the uniform surface or fully penetrated currents. (Kerrisk states that his equation is not applicable to the case  $W/H = 0$  and is generally accurate within 7% (iii)).

The values of "f", defined as  $\frac{\text{propelling inductance}}{\text{total inductance}}$  are plotted in Fig. 19 for uniform surface and fully penetrated currents. Railguns generally have rails with  $W/H$  in the range 0.2 to 1 with an approximately square bore, i.e.  $S \approx H$ . The graphs show that for such geometries f is in the range 0.8 to 0.95 for uniform surface current and 0.65 to 0.9 for fully penetrated rails. Full penetration of rails with  $H = W$  would only occur in very slow railguns, though, i.e.  $f = 0.65$  would be the worst case.

Two factors have been raised as influencing the current distribution - the minimum opposition principle and the initial location of surface charge. According to the minimum opposition principle, current will arise, as the projectile sweeps over new sections of rail, such that the opposition due to both resistance and inductance is least. The rail surfaces ahead of the projectile, however, are charged by the voltage drop across the projectile (or plasma arc) so that initial current flow is determined by the location of the surface charges. One way to combine the factors, as noted before, is to consider the initial charge locations as the boundary condition for the location of current in the solution of the diffusion equation, which is compatible with the minimum opposition principle. According to this scheme, current would diffuse inwards with the same pattern as on the surface, gradually overlapping from all sides until the distribution becomes uniform. Resistance opposition, though, will all the time be favouring uniform distribution in all directions. The issue is how much penetration will occur before the current becomes substantially uniformly distributed at the surface. In the railgun, other factors may have a role also. The transfer of current to the projectile or plasma arc is a violent process, something of an electrical storm. This may stir up the initial distribution so that at least on the inner surfaces of the rails, the current is uniformly distributed. The writer has examined railgun rails to see if there is evidence of preferential arcing towards the edges of the rails in accordance with the minimum inductance distribution. The examination showed only a uniform feathery



Inductance tabulation, Rectangular rails, $\mu H/m$ .						
	W/H	S/H				
		.1	.2	.5	1	2
Minimum	.1	.105	.187	.365	.556	.787
Inductance	.2	.103	.181	.353	.536	.758
Kerrisk	.5	.097	.170	.327	.496	.699
Equation (2.52)	1	.093	.159	.303	.456	.640
	2	.090	.150	.279	.413	.575
	0	.110	.202	.407	.628	.885
Propelling	.1	.097	.179	.367	.576	.824
Inductance	.2	.088	.163	.339	.537	.778
Uniform Surface	.5	.072	.134	.284	.460	.682
Current	1	.058	.109	.234	.387	.586
Equation (2.37)	2	.044	.083	.182	.305	.474
	0	.110	.202	.407	.628	.885
Propelling	.1	.100	.184	.377	.588	.837
Inductance	.2	.092	.170	.352	.554	.797
Fully Penetrated	.5	.075	.141	.297	.477	.700
Current	1	.059	.111	.238	.392	.591
Equation (2.39)	2	.042	.080	.175	.296	.462
	0	.111	.202	.407	.628	.885
Total	.1	.140	.211	.385	.583	.823
Inductance	.2	.156	.222	.376	.556	.782
Uniform Surface	.5	.206	.253	.371	.517	.712
Current	1	.259	.293	.380	.494	.656
Equation (2.50)	2	.323	.345	.404	.485	.608
	0	.110	.201	.408	.629	.885
Total	.1	.163	.242	.423	.625	.866
Inductance	.2	.204	.273	.436	.621	.849
Fully Penetrated	.5	.286	.337	.461	.611	.808
Current	1	.360	.395	.485	.600	.762
Equation (2.51)	2	.430	.452	.500	.588	.708

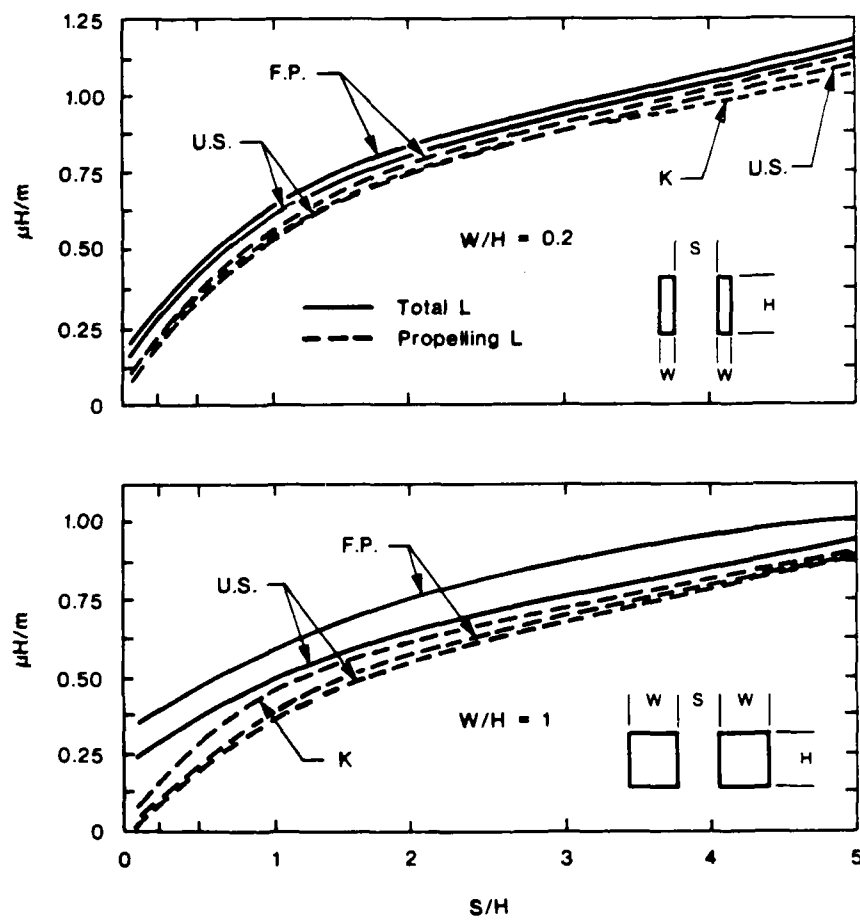


Fig. 18. Inductance of rails,  $\mu H/m$ , plotted from expressions given in Section 2.8.

U.S. = uniform surface current  
 F.P. = fully penetrated current  
 K = minimum total inductance

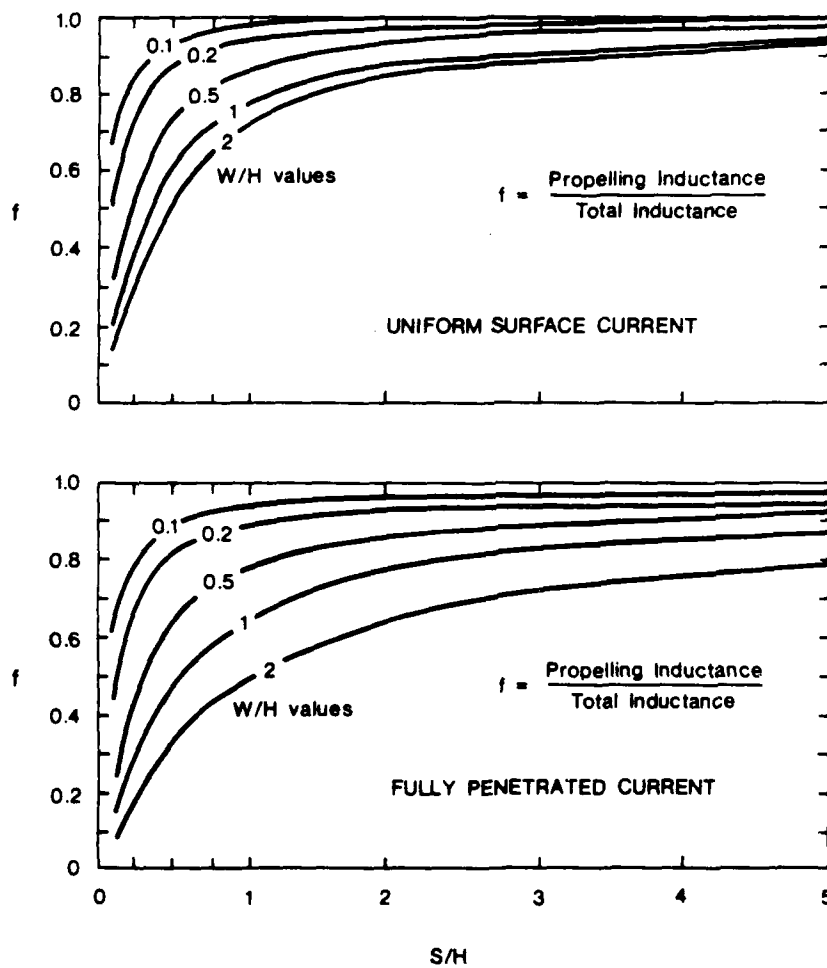


Fig. 19. Graphs of factor  $f$ , computed from inductance tabulations.

pattern across the width of the rails exposed to the plasma, i.e. supporting the uniform surface current theory.

The extent to which the above factors cause initial departure from the minimum inductance distribution and hence affect the force on the projectile depends on the increase in inductance that is incurred. If the inductance increase for uniform current distribution is slight, the resistance and arcing influences may cause this distribution to be favoured. By examining the ratio of the minimum to total inductances we can gain an idea of the relative ease of current flow under minimum inductance conditions and hence the likelihood of more uniform current distributions.

Ratio of minimum inductance to total inductance

(i) Uniform surface current

W/H				S/H		
	.1	.2	.5	1	2	5
.1	.75	.89	.95	.95	.96	.97
.2	.66	.82	.94	.96	.97	.98
.5	.47	.67	.88	.96	.98	.98
1	.36	.54	.80	.92	.98	.99

(ii) Fully penetrated current

W/H				S/H		
	.1	.2	.5	1	2	5
.1	.64	.77	.86	.89	.91	.93
.2	.50	.66	.81	.86	.89	.92
.5	.34	.50	.71	.81	.87	.90
1	.26	.40	.62	.76	.84	.89

The ratio tabulation shows that for railgun geometries (W/H in the range 0.2 to 1 and S/H  $\approx$  1) the minimum inductance is 96% to 90% of the total inductance of a uniform surface current, i.e. the inductive opposition of a uniform surface current is 4% to 10% greater than the minimum.

It follows that if a more uniform current distribution reduces the resistive opposition by more than 4% to 10%, the total opposition will be reduced and the more uniform distribution will occur. Examination of the current distribution for minimum inductance (Fig. 7) suggests that redistribution of the current peaks at the corners would reduce the resistive opposition by about 10%. Bearing in mind the arcing and high current densities in the railgun it is therefore suggested that the current is initially established with a distribution that is somewhere between that for minimum inductance and a uniform surface current.

## Conclusions

We have used the uniform surface current distribution as a convenient model from which to estimate the effect of a more realistic current distribution than the ideal surface current distribution that gives the minimum inductance.

Relatively small inductance differences were found between the surface current distributions, for railgun geometries. On the assumption that current flows such that total opposition is minimized, it is concluded that current is initially distributed more uniformly than for the minimum inductance. The factor  $f$  is likely to be in the range 0.8 to 0.95, depending on rail geometry.

The values of  $f$  referred to above are those in the immediate projectile region. Current penetration increases with distance behind the projectile and the rail inductance increases. The associated energy of the inductance increase behind the projectile is lost, as discussed when this work was commenced, and hence the value of  $f$  due to current distribution effects during the whole acceleration period is lower than the above values.

Even if the current initially has very nearly the minimum inductance distribution, so that  $f = 1$  at the projectile, the diffusion of current behind the projectile will cause a lower value of  $f$ .

The effect of current distribution is least for thin rails; therefore railgun rails should be as thin as other factors, such as heating and strength, allow.

## 2.10 Efficiency equations for railgun configurations

### 2.10.1 Loss mechanisms

The losses in the railgun itself (i.e. not including the power source) may be put into six categories:

- (i) the magnetic energy stored by the rails, which limits the efficiency of the simple constant current railgun to 50%;
- (ii) the magnetic energy of flux that is not coupled to the projectile and
- (iii) an equal amount of associated energy (included in factor  $f$ );
- (iv) the resistive heating of the rails;
- (v) the voltage drop across the projectile (or plasma), measured as the muzzle voltage of the railgun;
- (vi) friction and windage, which may also be included in the factor  $f$ .

The energy required to accelerate the plasma is also generally lost, but this loss is not included in the above list, i.e. the plasma is taken to be negligible in mass compared to the projectile.

### 2.10.2 Improved railguns

To improve the efficiency of the simple railgun shown in Fig. 1, two variations have been proposed. The first, due to Hawke [17], reduces the resistive losses by breaking the long rails into a series of short rails, each with its own power source, as in Fig. 20. This is called "segmentation". Clearly, the resistive losses in all except the short section of rail containing the projectile are eliminated. The other variation, due to Marshall and Weldon [18], uses power from sources distributed along the length of the rails, each source being switched on when the projectile passes it (Figs. 21, 22). In this scheme, called the "distributed energy store" scheme, the currents from the individual sources are not constant, but decay to zero. The currents from all the sources, however, sum to an approximately constant current in the region of the projectile, so giving the desirable constant acceleration. As well as greatly diminishing the resistance loss, this scheme, by allowing the current to collapse to zero, automatically recovers the field energy of the rails. Marshall and Weldon suggest that this scheme would have an efficiency of 70% in space launch applications. Both these variations also improve the factor  $f$ , because there will be less time for current to penetrate and give rise to internal inductance at any section of the rails.

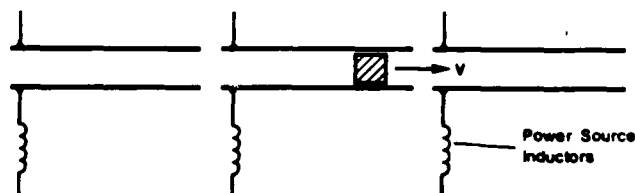


Fig. 20. Segmentation of rails (Hawke).

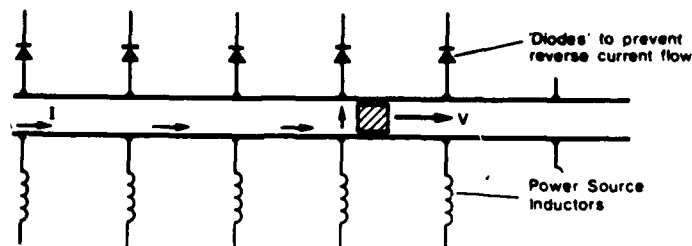


Fig. 21. Distributed Energy Stores (Marshall, Weldon)

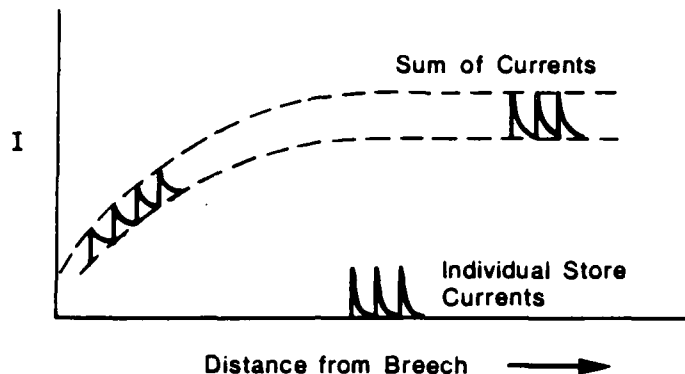


Fig. 22. Currents in distributed energy store scheme.

In the following Sections, equations will be derived for the efficiency of the simple and improved railguns, taking into account the losses listed above. Constant current is assumed for mathematical simplicity.

### 2.10.3 Simple condition for high efficiency

The extent to which resistance is a problem in attaining high efficiency can be determined in a simple manner. As far as the power source is concerned, the electrical energy that becomes kinetic energy of the projectile, is dissipated. If the projectile is accelerated by force  $F$  and has velocity  $v$ , then:

$$Fv = R_{EQ} I^2 \quad (2.53)$$

where  $R_{EQ}$  is a resistance which dissipates the same power as the projectile gains and  $I$  is the railgun current. Since  $F = \frac{1}{2} L' I^2$ , where  $L'$  is the propelling inductance per unit length, we obtain:

$$R_{EQ} = \frac{1}{2} L' v \quad (2.54)$$

This equation can be used to deduce the permissible resistance of the rails and power source, since for an efficient gun, these should be much less than  $R_{EQ}$ . If a 5 gram mass were to be launched at 10 km/s from rails with  $L' = 0.5 \mu\text{H/m}$ ,  $R_{EQ}$  would have a maximum value of  $2.5 \times 10^{-3}$  ohms. The

resistance of the rails and power source should be much less than  $2.5 \times 10^{-3}$  ohms for high efficiency. Owing to the current flowing near the surfaces, it is difficult to make the rail resistance low except by using short rails. From this we can conclude that for high efficiency the acceleration must be high. Note that the equivalent resistance relationship holds whether the current is constant or not.\*

#### 2.10.4 Current penetration model

In Section 2.7 it was shown that the resistance may be deduced by equating the resistive and inductive opposition forces and that this is a solution of the diffusion equation. Depth of penetration of the current, for resistance calculation, can be an equivalent depth of a convenient current distribution. For the railgun it is convenient to suppose that the current penetrates from the inner rail surfaces as a uniform layer of cross-section  $d \times H$  where  $d$  is the depth of penetration and  $H$  is the height of the rails (Fig. 23). Hawke [19] and Barber [12] have used such a model previously. Actually, as has been discussed, the current is distributed all around the rails and the assumed distribution cannot be used for calculating rail inductance.

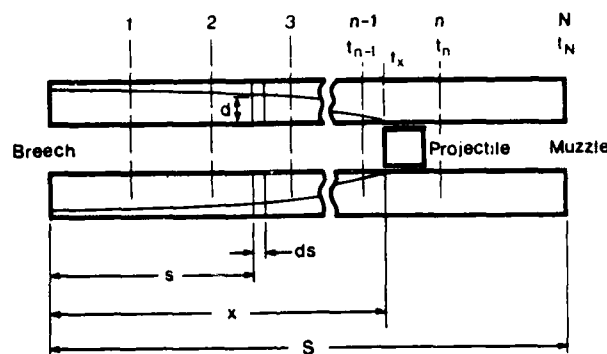


Fig. 23. Parameters used in equations.

\* The ratio of the inductance to the equivalent projectile resistance at any instant has the curious property of being equal to the time for which the circuit has been switched on, in a constant current railgun. If the projectile has moved distance  $x$  from the breech, the inductance is  $L'x$  and

$$\frac{L'x}{R_{EQ}} = \frac{L'x}{\frac{1}{2} L'v}$$

but with constant current the force is constant and hence the acceleration is constant and

$$x = \frac{1}{2} vt$$

where  $t$  is the time for which the acceleration has proceeded. Hence,  $\frac{L'}{R_{EQ}} = t$ .



### 2.10.5 Resistive loss in a portion of the rails

Consider a portion of the rails between distances  $s$  and  $x$ , as in Fig. 23. The current has penetrated depth  $d$  at distance  $s$  from the breech and the resistance of the elemental slice of width  $ds$  is given by:

$$dR = \frac{\rho ds}{Hd} \quad (2.55)$$

where  $\rho$  is the resistivity and  $H$  is the height of the rails. In Sect. 2.7 it was shown that the depth of penetration,  $d$ , is given by an expression of the form  $d = a \sqrt{\frac{t}{\sigma \mu}}$  where  $t$  is the time for which current has flowed,  $\sigma = \frac{1}{\rho}$  is the conductivity and  $\mu$  is the permeability.

The time for which current has flowed at a slice is the time elapsed since the projectile passed it. Let this time be denoted by  $\tau$  i.e.

$$\tau = t_x - t_s \quad (2.56)$$

The energy loss in the slice at distance  $s$ ,  $\Delta W_s$ , is therefore:

$$\Delta W_s = \frac{I^2}{H\sigma} (\rho\mu)^{1/2} \left[ \int_0^{t_x - t_s} (t_x - t_s - \tau)^{-1/2} d\tau \right] ds \quad (2.57)$$

Since the current is constant, the acceleration is nominally constant and we may put  $ds = a t_s dt_s$ , where  $a$  is the acceleration. The total energy loss between distances  $s$  and  $x$  is the sum of the losses of all the elemental slices in both rails and is given by:

$$\Delta W_{s,x} = \frac{2I^2 a}{H\sigma} (\rho\mu)^{1/2} \int_{t_s}^{t_x} \left[ \int_{t_s}^{t_x - t_s} (t_x - t_s - \tau)^{-1/2} d\tau \right] t_s dt_s \quad (2.58)$$

$$= \frac{16 I^2 a}{15 H\sigma} (\rho\mu)^{1/2} t_x^{5/2} \left[ \frac{5}{2} \frac{t_s}{t_x} \left( 1 - \frac{t_s}{t_x} \right)^{3/2} + \left( 1 - \frac{t_s}{t_x} \right)^{5/2} \right] \quad (2.59)$$

Putting  $t_s = 0$  we obtain the total resistive loss,  $W_R$ , in both rails up to the time that the projectile reaches distance  $x$ :

$$W_R = \frac{16 I^2 a}{15 H\sigma} (\rho\mu)^{1/2} t_x^{5/2} \quad (2.60)$$

Equations (2.59) and (2.60) enable us to obtain the loss in the portion of the rails from distance  $s$  to  $x$  as a fraction of the total loss from the breech to  $x$ :

$$\frac{\text{Rail loss from } s \text{ to } x}{\text{Rail loss from breech to } x} = \frac{\Delta W_R}{W_R}$$

$$= \frac{5}{2} \frac{t_s}{t_x} \left(1 - \frac{t_s}{t_x}\right)^{3/2} + \left(1 - \frac{t_s}{t_x}\right)^{5/2} \quad (2.61)$$

Eqn. (2.61) becomes much more useful when expressed in terms of the distances reached at times  $t_s$  and  $t_x$ . Consider the rails to be divided into  $N$  equal length sections by marks as indicated in Fig. 23. The energy lost in the  $n$ th section is obtained by putting

$$s = \frac{(n-1)S}{N}, \quad x = \frac{nS}{N}$$

where  $S$  is the total rail length, from which, since the acceleration is constant, we have

$$\frac{t_s}{t_x} = \frac{t_{n-1}}{t_n} = \left(1 - \frac{1}{n}\right)^{1/2} \quad (2.62)$$

Eqn. (2.61) becomes, on substituting Eqn. (2.62):

$$\frac{\Delta W_R}{W_R} = \frac{\text{Rail loss in } n\text{th section as it is traversed by projectile}}{\text{Rail loss in all sections to end of } n\text{th}}$$

$$= \frac{5}{2} \left(1 - \frac{1}{n}\right)^{1/2} \left(1 - \left(1 - \frac{1}{n}\right)^{1/2}\right)^{3/2} + \left(1 - \left(1 - \frac{1}{n}\right)^{1/2}\right)^{5/2} \quad (2.63)$$

$$\text{or, } \frac{\Delta W_R}{W_R} \approx \frac{5}{4\sqrt{2}} (n)^{-3/2}, \quad (2.64)$$

using  $\left(1 - \frac{1}{n}\right)^{1/2} \approx 1 - \frac{1}{2n}$ , for  $n > 1$ .

As an example of the use of Eqn. (2.64) let us find the loss in the final 10% of the rails of a simple railgun, compared to the total resistive loss from the time that the projectile was at the breech. To do this, put  $n = 10$  in Eqn. (2.64). The result is that 2.8% of the total resistive loss occurs in the last 10% of the rails.

As the projectile accelerates the depth of penetration of the current decreases in the portion of the rails containing the projectile. It

is important to know whether the resistive loss increases or decreases compared to the energy gained by the projectile. Using factor  $f$  to denote the effective force on the projectile due to flux distribution and factors such as friction and air load ahead of the projectile, the energy gained by the projectile in the  $n$ th portion of the rails,  $\Delta W_p$ , is:

$$\Delta W_p = \frac{1}{4} f L' I^2 a (t_n^2 - t_{n-1}^2) \quad (2.65)$$

where  $L'$  is the average total inductance per unit length and  $t_{n-1}$  and  $t_n$  are the times at which the projectile enters and leaves the  $n$ th portion of the rails. Eqns. (2.60), (2.62), (2.64) and (2.65), together with

$$t_n = \frac{v_n}{a} = \frac{2Mv_n}{fL'I^2} \quad (2.66)$$

where  $v_n$  is the velocity at the end of the  $n$ th portion, enable us to obtain:

$$\begin{aligned} \frac{\Delta W_R}{\Delta W_p} &= \frac{\text{Rail loss in } n\text{th portion as it is traversed by projectile}}{\text{Energy gained by projectile in } n\text{th portion}} \\ &= \frac{16}{3Ha f L' I} \left( \frac{Mv_n \rho_s}{fL'n} \right)^{1/2} \end{aligned} \quad (2.67)$$

or, alternatively:

$$\frac{\Delta W_R}{\Delta W_p} = \frac{16(\rho_s)^{1/2}}{3 H a} I^{-1/2} (fL')^{-5/4} \left( \frac{SM}{Nn} \right)^{1/4} \quad (2.68)$$

Eqns. (2.67) and (2.68) show that the energy lost in resistive heating in the portion of the rails containing the projectile diminishes as  $n$ , i.e. as distance from the breech, increases. This means that the shorter time spent by the projectile in traversing equal length portions outweighs the effect of shallower current penetration.

#### 2.10.6 Rail loss comparisons - breech supplied railgun

In formulating an efficiency equation for the breech supplied railgun the following relationship is required:

$$\frac{W_R}{W_p} = \frac{\text{Rail loss from breech to distance } x}{\text{Projectile energy at distance } x}$$

Eqn. (2.60) together with  $W_p = \frac{1}{2} \ell L I^2 x$  yields:

$$\frac{W_R}{W_p} = \frac{64}{15 H a I} (2 M V_{x p s})^{1/2} (\ell L')^{-3/2} \quad (2.69)$$

Another relationship of interest for the breech supplied gun is:

$$\frac{\Delta W_R}{W_R(t_{n-1}, t_n)} = \frac{\text{Rail loss in nth portion as it is traversed by projectile}}{\text{Rail loss in all portions during same time}}$$

This is obtainable from Eqns. (2.60) and (2.64); the result is:

$$\frac{\Delta W_R}{W_R(t_{n-1}, t_n)} = (2n)^{-1/2} \quad (2.70)$$

According to Eqn. (2.70) the resistive loss in the tenth equal length section is 22% of the loss in the whole of the rails during the time that the projectile traverses the tenth section, for example.

#### 2.10.7 Rail loss comparison - segmented railgun

Equation (2.64) shows that if the power source could always be connected to just the 10% of the length of the rails that contains the projectile, the rail losses would be reduced to 2.8% of those in a gun powered from the breech. Such segmentation would require very short segments near the breech. The total rail loss for a gun constructed with  $N$  equal length, separately supplied, segments can be obtained by summing Eqn. (2.59) for all segments. Together with Eqns. (2.60) and (2.64) this enables the reduction in rail loss due to segmentation compared to a breech supplied gun to be calculated.

$$\begin{aligned} \frac{W_R(N)}{W_R} &= \frac{\text{Rail loss, segmented railgun, } N \text{ equal segments}}{\text{Rail loss, breech supplied gun}} \\ &\approx \sum_{n=1}^N \left( \frac{t_n}{t_N} \right)^{5/2} \frac{5}{4\sqrt{2}} (n)^{-3/2} \\ &\approx \frac{5}{4\sqrt{2}} (N)^{-5/4} \sum_{n=1}^N (n)^{-1/4} \end{aligned} \quad (2.71)$$

Substituting  $\sum_{n=1}^N (n)^{-1/4} \approx (N)^{4/5}$  Eqn. (2.71) becomes:

$$\frac{W_R(N)}{W_R} \approx \frac{5}{4\sqrt{2}} (N)^{-9/20} \quad (2.72)$$

Eqn. (2.71) predicts that for a railgun with 20 equal length, separately powered, constant current segments the rail loss would be 23% of that of a breech supplied gun. For 100 and 1000 segments, the losses reduce to 11% and 4% respectively.

For efficiency calculations we require the ratio:

$$\frac{W_R(N)}{W_P} = \frac{\text{Rail loss, Segmented railgun, } N \text{ equal segments}}{\text{Projectile energy}}$$

This is obtained by multiplying Eqn. (2.72) by Eqn. (2.69).

The result is:

$$\frac{W_R(N)}{W_P} = \frac{16}{3H\alpha I} (fL')^{-3/2} (Mv_{N\mu})^{1/2} (N)^{-9/20} \quad (2.73)$$

#### 2.10.8 Rail losses - constant resistance per unit length

If the rails are thin, or the acceleration is slow enough, the current will be uniformly distributed across the rail cross section and the resistance per unit length will approach the d-c value. It is also of interest to know whether uniform resistance per unit length would be advantageous, if it could be attained by some special rail construction. Let the resistance of the rails be  $R'$  ohms/m. When the projectile is distance  $x$  from the breech, the rail resistance measured from the breech is  $\frac{1}{2} R a t_x^2$ , since we are assuming constant current and hence constant acceleration. The energy dissipated in the rails up to time  $t_x$  is therefore:

$$W_R = \frac{R'}{6} I^2 a t_x^3 \quad (2.74)$$

If we consider the rails to be divided into  $N$  equal sections as in Fig. 23, the energy dissipated while the projectile moves over the  $n$ th section is:

$$\Delta W_R = \frac{R'}{2} a \int_{t_{n-1}}^{t_n} (t^2 - t_{n-1}^2) dt, \quad (2.75)$$

or

$$\Delta W_R = \frac{R'}{6} I^2 a t_n^3 \left[ 1 - 3\left(1 - \frac{1}{n}\right) + 2\left(1 - \frac{1}{n}\right)^{3/2} \right], \quad (2.76)$$

where  $t_n$  is the time at which the projectile reaches the end of the  $n$ th section. Since  $\frac{R}{I^2}$  a  $t_n$  is the energy lost in the whole of the rails up to the end of the  $n$ th section, we have:

$$\frac{\Delta W_R}{W_R} = \frac{\text{Rail loss in } n\text{th section as it is traversed by projectile}}{\text{Rail loss in all sections up to end of } n\text{th}}$$

$$= 1 - 3\left(1 - \frac{1}{n}\right) + 2\left(1 - \frac{1}{n}\right)^{3/2}, \quad (2.77)$$

or 
$$\frac{\Delta W_R}{W_R} \approx \frac{3}{4} \left(\frac{1}{n}\right)^2. \quad (2.78)$$

Eqn. (2.78) predicts that the resistive loss in the final 10% of the rails is 0.75% of the total rail loss, compared to 2.8% in the case of diffusion proportional to  $t^{1/2}$ .

Eqns. (2.72) and (2.77) and  $W_p = \frac{1}{2} fL'I^2x$  lead to:

$$(i) \quad \frac{W_R}{W_p} = \frac{\text{Rail loss from breech to distance } x}{\text{Projectile energy at distance } x}$$

$$= \frac{4}{3} R' M v_x (fL'I)^{-2} \quad (2.79)$$

$$(ii) \quad \frac{\Delta W_R}{\Delta W_p} = \frac{\text{Rail loss in } n\text{th section as it is traversed by projectile}}{\text{Energy gained by projectile in } n\text{th section}}$$

$$= \frac{R' M v_n}{n} (fL'I)^{-2} \quad (2.80)$$

$$= \frac{R'}{I} \left(\frac{SM}{Nn}\right)^{1/2} (fL')^{-3/2} \quad (2.81)$$

(using Eqns. (2.65) and (2.66) also).

$$(iii) \quad \frac{\text{Rail loss in } n\text{th section as it is traversed by projectile}}{\text{Rail loss in all sections in the same time}}$$

$$= \frac{\Delta W_R}{W_R(t_{n-1}, t_n)} \approx \frac{1}{2n} \quad (2.82)$$

According to Eqn. (2.82) the loss in the final 10% of the rails is only 5% of the loss in the rest of the rails during the same time, if the resistance per unit length is constant. For the diffusing current case, Eqn. (2.70), the result was 22% i.e. the loss in the final 10% was relatively much greater.

Summing Eqn. (2.76) to obtain the losses in  $N$  equal length segments and using Eqn. (2.74) we obtain for a segmented railgun:

$$\frac{W_R(N)}{W_R} = \frac{\text{Rail loss, Segmented railgun, } N \text{ equal segments}}{\text{Rail loss, breech supplied gun}}$$

$$\approx \frac{3}{4} \left(\frac{1}{N}\right)^{3/2} \sum_{n=1}^N \left(\frac{1}{n}\right)^{1/2} \quad (2.83)$$

which becomes, substituting  $2 N^{1/2}$  for the sum of the series for large  $N$ ,

$$\frac{W_R(N)}{W_R} \approx \frac{3}{2N} \quad (2.84)$$

For  $N = 20$  the sum of the series is  $1.70 N^{1/2}$  and Eqn. (2.83) predicts that the rail loss would be 6.4% of that of a breech supplied gun (compared to 23% obtained for current diffusion proportional to  $t^{1/2}$ ).

For the ratio

$$\frac{W_R(N)}{W_P} = \frac{\text{Rail loss, Segmented railgun, } N \text{ equal segments}}{\text{Projectile energy}},$$

we obtain:

$$\frac{W_R(N)}{W_P} = \frac{2R'Mv_N}{N} (fLi)^{-2}, \quad (2.85)$$

by multiplying Eqn. (2.84) by Eqn. (2.79).

#### 2.10.9 Other loss comparisons

In Section 2.10.1 five losses were listed in addition to the resistive losses discussed in the previous Sections - the stored magnetic energy that is coupled with the projectile movement and that which is not, the associated energy which is not coupled with the projectile and friction and windage, and muzzle voltage losses.

The total magnetic energy,  $W_M$ , at distance  $x$  from the breech of a simple railgun is:

$$W_M = \frac{1}{2} L' I^2 x \quad (2.86)$$

This includes both the energy of the flux that couples the projectile and that which does not. Since the projectile energy is  $W_p = \frac{1}{2} f L' I^2 x$ ,

$$\frac{W_M}{W_p} = \frac{1}{f} \quad (2.87)$$

As was discussed in Chapter 1, the associated energy,  $W_a$ , equals the total magnetic energy  $W_M$ . We have supposed that only fraction  $f$  of the associated energy becomes projectile energy, therefore the total wasted, including that which is dissipated in friction and windage, is  $(1-f) W_a$  and

$$\frac{(1-f)W_a}{W_p} = \frac{(1-f)}{\frac{1}{2} f L' I^2} \frac{1}{2} L' I^2 = \frac{1}{f} - 1 \quad (2.88)$$

The muzzle voltage in guns with conducting projectiles is usually negligible (less than 10V). In arc driven guns the voltage is in the range 200V to 300V for typical currents, i.e. 200kA to 500kA. The resistance of the arc is therefore around 1 mΩ, which means that the energy dissipated in the arc is comparable to the energy gained by the projectile, especially at low velocities. If the arc voltage is  $V_A$ , the ratio of arc energy to projectile energy is:

$$\frac{W_A}{W_p} = \frac{4V_A}{fL'vI} \quad (2.89)$$

where  $v$  is the velocity at any point in the gun. The expression applies to breech supplied or segmented guns.

#### 2.10.10 Efficiency expressions

The efficiency,  $\eta$ , is:

$$\eta = \frac{\text{Projectile energy}}{\text{Projectile energy} + \text{losses}}$$

$$\text{i.e. } \eta = \frac{1}{1 + \frac{W_M}{W_p} + \frac{(1-f)W_a}{W_p} + \frac{W_R}{W_p} + \frac{W_A}{W_p}}$$

which becomes, substituting Eqns. (2.87) and (2.88)

$$\eta = \frac{f}{2 + \frac{f W_R}{W_p} + \frac{f W_A}{W_p}} \quad (2.90)$$



Equation (2.90) is applicable to breech supplied and segmented railguns, upon substitution of relevant expressions for  $\frac{W_R}{W_p}$  and  $\frac{W_A}{W_p}$ .

The chief difference between segmented and distributed energy store railguns, so far as efficiency is concerned, is that the magnetic field energy is recovered, i.e. there is no loss  $W_M$  to be included. Putting  $W_M = 0$  yields:

$$\eta = \frac{f}{1 + \frac{f W_R}{W_p} + \frac{f W_A}{W_p}} \quad (2.91)$$

Equation (2.91) may be applied to the distributed energy store railgun with a "segment" defined in terms of the number of energy stores which contribute to the region of substantially constant current behind the projectile.

Throughout the development of these equations we have taken  $f$  as constant. As was discussed before,  $f$  must have a variable part because it includes the effect of flux penetration of the rails, which has the same  $t^{1/2}$  dependence as resistance. To allow  $f$  to be a variable would make the derivations too difficult. We therefore take  $f$  to be an effective value, found by experiment.

Substituting for  $\frac{W_R}{W_p}$  and  $\frac{W_A}{W_p}$  in Eqn. (2.90) yields:

- (a) for current diffusion proportional to  $\sqrt{\text{time}}$ :  
 $\eta$  (Breech supplied) =

$$\frac{f}{2 + \frac{64}{15H\pi I} \left( \frac{2MV_{pe}}{f} \right)^{1/2} (L')^{-3/2} + \frac{4V_A}{L'v_I}} \quad (2.92)$$

where  $v$  is the exit velocity.

$\eta$  (N segments) =

$$\frac{f}{2 + \frac{16}{3H\pi I} \left( \frac{MV_N^{pp}}{f} \right)^{1/2} (L')^{-3/2} (N)^{-9/20} + \frac{4V_A}{L'v_N I}} \quad (2.93)$$

where  $v_N$  is the exit velocity at the Nth segment.

- (b) for constant resistance,  $R'$ , per unit length of gun:  
 $\eta$  (Breech supplied) =

$$\frac{f}{2 + \frac{4}{3} \frac{R' MV}{f} (L'I)^{-2} + \frac{4V_A}{L'v_I}} \quad (2.94)$$

$\eta$  (N segments) =

$$\frac{f}{2 + \frac{2 R' M V_N}{N f} (L' I)^{-2} + \frac{4 V_A}{L' V_N I}} \quad (2.95)$$

- (c) for distributed energy store railguns, the equations are the same as (2.93) and (2.95) but with the 2 at the left hand end of the denominator replaced by 1, and N is the number of equivalent segments, i.e. the total number of energy stores divided by the number of stores connected to the region behind the projectile where the current is substantially constant.

#### 2.10.11 Example calculations and discussion

To evaluate Eqns. (2.92) and (2.93) the value of  $\alpha$  is required, where  $\alpha$  is the factor which adjusts the general skin depth relationship  $d = \alpha \sqrt{\frac{\rho t}{\pi}}$  for the particular case. As noted before, the skin depth is an equivalent depth and need not represent the actual distribution of current. Instead, the current may be considered all to flow on the inner surfaces. Barber (12,22) considers this applicable to the railgun and gives

$$d = \sqrt{\frac{\pi \rho t}{\pi}} \quad (2.96)$$

from which  $\alpha = \sqrt{\pi} = 1.772$ , compared to  $\alpha = 1.414$  by the simple evaluation in Sect. 2.7. As the current redistributes, the value of  $\alpha$  will change, but as with factor  $f$ , it would be too complicated to allow  $\alpha$  to be a function of time and location along the rails.

Suppose that a mass of 5 grams is to be launched at 10 km/s from a railgun with the average total inductance per unit length,  $L' \approx 0.5 \mu\text{H/m}$ ; copper rails for which  $\rho = 1.72 \times 10^{-8}$  at room temperature; rail height = 1.25 cm and arc voltage = 200V. Eqns. (2.92)-(2.95) give the tabulated results.  $R' = 1.502 \text{ m}\Omega/\text{m}$  is used for the constant resistance per unit length equations because that is the value which gives the same efficiency at 500 kA and  $f = 1$  as in the equations for current penetration proportional to  $\sqrt{t}$  and so gives a common reference condition.

In the tabulation, figures are substituted into Eqns. (2.92)-(2.95) in the same order as given above in those equations to enable their relative proportions to be seen. Two efficiency figures are given, (i) for systems in which the rail field energy is not recovered and (ii) for systems in which it is recovered. In the tabulations for segmented guns, these values could be taken as the upper limit for distributed energy stores guns with an appropriate number of energy stores (eg. 4 or 5 per "segment"). In the last two tabulations, the temperature is considered to have risen near to the melting point and the resistivity is taken as 4 times that of the room temperature copper.

Inspection of the tabulations shows a wide range of efficiencies; from less than 1% to 69%. Five factors stand out.

- (i) The dominance of the factor  $f$ . By virtue of its definition, the efficiency cannot be higher than  $f$ . The value of  $f$  must be greater than 0.5 for high efficiency. In small railguns, e.g. 1 cm x 1 cm bore  $f$  is  $\approx 0.25$ . The figure improves with bore size, presumably because friction forces diminish relatively.
- (ii) 20 segments is a sufficient number to reduce the resistance loss term to a magnitude similar to the sum of the other loss terms. A greater number of segments would not increase the efficiencies greatly. Ways of reducing the arc loss, for example, then become necessary in order to make further gains in efficiency.
- (iii) Constant resistance per unit length does not generally result in much higher or much lower efficiency than diffusing current; except in the case of breech supplied rails that are very hot, where diffusing current has lower losses.
- (iv) The higher the current, the higher the efficiency. This is because the acceleration is higher and the time for losses to accumulate in the rails and arc is less, for a given final velocity.
- (v) By taking the ratio of efficiency for segmented railguns to that for breech supplied railguns, the reduction in total energy and hence in total power source size can be estimated. From the tabulation, for diffusing current (i.e. the practical situation), the power source size is in the range  $1/3$  to  $2/3$  that required for breech supply. To attain this reduction, however, requires 20 power sources in the case of segmented designs and perhaps 100 in the case of distributed energy stores (allowing 5 stores per "segment"). The complication of so many stores, including the means of switching them into circuit at the right moments, makes the reduction in required energy a questionable achievement.

Since segmentation and distributed energy stores reduce the rail losses, they will be of most value where the rail losses would otherwise be the dominating losses. An example might be where, as a breech supplied gun, efficiency would be 1% and segmentation or distributed energy stores might raise it to 10%, thereby reducing the power source size to  $1/10$  and justifying the complexity.

Lower acceleration designs would also benefit, since they would require longer rails and a longer time in order to obtain a given velocity. Space launch applications might be such an application; several seconds rather than 1 ms being required to attain say 8 km/s, on account of the limited launch forces which the cargo could withstand.

It must be observed that the diffusion efficiency equation cannot be used when the current has diffused to greater than the rail width. After that time the resistance per unit length becomes constant, i.e. Eqns. (2.94) and (2.95) apply. The relatively slow acceleration space launch is again an

Efficiency Tabulation: 5g accelerated to 10 km/s Room Temperature

f	Diffusion $\propto \sqrt{t}$	$\eta$ (i)	$\eta$ (ii)	Const R/m	$\eta$ (i)	$\eta$ (ii)
I = 500 kA, Breech Supplied, $\rho = 1.72 \times 10^{-8}$ ohm-m						
1	$\frac{1}{2 + 1.602 + .32}$	.25	.34	$\frac{1}{2 + 1.602 + .32}$	.25	.34
.5	$\frac{.5}{2 + 2.266 + .32}$	.11	.14	$\frac{.5}{2 + 3.204 + .32}$	.09	.11
.25	$\frac{.25}{2 + 3.204 + .32}$	.05	.06	$\frac{.25}{2 + 6.408 + .32}$	.03	.03
I = 500 kA, 20 Segments, $\rho = 1.72 \times 10^{-8}$ ohm-m						
1	$\frac{1}{2 + .368 + .32}$	.37	.59	$\frac{1}{2 + .120 + .32}$	.41	.69
.5	$\frac{.5}{2 + .520 + .32}$	.18	.27	$\frac{.5}{2 + .240 + .32}$	.20	.32
.25	$\frac{.25}{2 + .736 + .32}$	.08	.12	$\frac{.25}{2 + .481 + .32}$	.09	.14
I = 250 kA, Breech Supplied, $\rho = 1.72 \times 10^{-8}$ ohm-m						
1	$\frac{1}{2 + 3.204 + .64}$	.17	.21	$\frac{1}{2 + 6.408 + .64}$	.11	.12
.5	$\frac{.5}{2 + 4.531 + .64}$	.07	.08	$\frac{.5}{2 + 12.816 + .64}$	.03	.03
.25	$\frac{.25}{2 + 6.408 + .64}$	.03	.03	$\frac{.25}{2 + 25.632 + .64}$	.009	.009
I = 250 kA, 20 Segments, $\rho = 1.72 \times 10^{-8}$ ohm-m						
1	$\frac{1}{2 + .736 + .64}$	.30	.42	$\frac{1}{2 + .240 + .64}$	.35	.53
.5	$\frac{.5}{2 + 1.041 + .64}$	.14	.19	$\frac{.5}{2 + .481 + .64}$	.16	.24
.25	$\frac{.25}{2 + 1.472 + .64}$	.06	.08	$\frac{.25}{2 + .962 + .64}$	.07	.10

Efficiency Tabulation: 5g accelerated to 10 km/s - Hot Rails

f	Diffusion $\propto \sqrt{t}$	$\eta$ (i)	$\eta$ (ii)	Const R/m	$\eta$ (i)	$\eta$ (ii)
I = 500 kA, Breech Supplied, $\rho = 4 \times 1.72 \times 10^{-8}$ ohm-m.						
1	$\frac{1}{2 + 3.204 + .32}$	.18	.22	$\frac{1}{2 + 6.408 + .32}$	.11	.13
.5	$\frac{.5}{2 + 4.531 + .32}$	.07	.09	$\frac{.5}{2 + 12.816 + .32}$	.03	.04
.25	$\frac{.25}{2 + 6.408 + .32}$	.03	.03	$\frac{.25}{2 + 25.632 + .32}$	.009	.009
I = 500 kA, 20 Segments, $\rho = 4.172 \times 10^{-8}$ ohm-m						
1	$\frac{1}{2 + .736 + .32}$	.33	.49	$\frac{1}{2 + .240 + .32}$	.39	.64
.5	$\frac{.5}{2 + 1.041 + .32}$	.15	.21	$\frac{.5}{2 + .481 + .32}$	.18	.27
.25	$\frac{.25}{2 + 1.472 + .32}$	.07	.09	$\frac{.25}{2 + .962 + .32}$	.08	.11

example. In long, slow acceleration guns, segmentation and distributed energy stores could be used to improve factor f, by preventing current diffusion, but this would be a marginal benefit since f includes other effects as well.

Finally, it can also be seen that if the efficiency of the gun with a breech supply is a high proportion of the maximum allowed by factor f, then little would be gained by segmentation or distributed energy stores.

As was indicated at the beginning of this Section, the losses related to the power source have not been included in the above treatment. In particular, the energy remaining in the storage inductor of the power source will be dissipated when the projectile leaves the gun unless there is a recovery means. Without a means to conserve this energy the efficiency of the gun plus power source system may be only a fraction (e.g. 1/3) of the values calculated above.

Since the distributed energy store scheme allows the energy of its storage inductors to fully discharge into the gun, it is much less affected in this regard.

## APPENDIX 1 TO CHAPTER 2

### INDUCTANCE CALCULATION BY GEOMETRIC MEAN DISTANCES

The geometric mean distance method is useful for calculating the inductance of parallel conductors when the filaments of current are known to be uniformly distributed over the whole cross section, i.e. strictly speaking it applies only to D.C. Although the method is referred to in the works of specialists such as Grover, Rosa and Grover and Higgins [20,15,21], they do not explain it from fundamentals. The best explanation that the writers have found is that by Gray [16] in 1893, upon which the following development is based.

Consider two long, parallel conductors, A and B, whose cross sections have areas  $S_1$  and  $S_2$  as shown in Fig. 24.

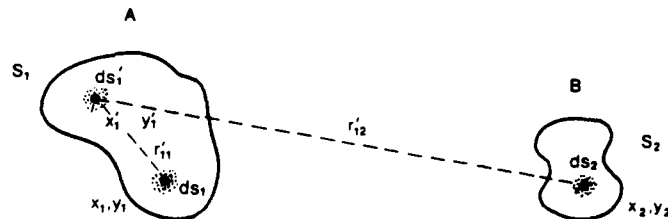


Fig. 24 Cross sections of long parallel conductors.

The conductors form a circuit in which current  $\gamma$  flows. Consider filamentary areas located at  $x_1, y_1$  in A and  $x_2, y_2$  in B to form a circuit. We now calculate the flux that links this circuit due to another filamentary current located in A at  $x_1', y_1'$  and having an area  $ds_1'$ . The flux density, at a distance  $r$  from a straight filament of current  $I$  is  $\frac{\mu_0 I}{2\pi r}$ . Therefore the flux linking the filament at  $x_1, y_1$  is:

$$\frac{\mu_0 \gamma}{2\pi} \frac{ds_1'}{S_1} \int_{r_{11}}^{\infty} \frac{dr}{r} \text{ per unit length,} \quad (1)$$

where  $r_{11}$  is the distance between  $x_1', y_1'$  and  $x_1, y_1$ . The flux from the filament at  $x_1', y_1'$  that links the filament at  $x_2, y_2$  is:

$$\frac{\mu_0 \gamma}{2\pi} \frac{ds_1'}{S_1} \int_{r_{12}}^{\infty} \frac{dr}{r} \text{ per unit length,} \quad (2)$$

where  $r_{12}$  is the distance between  $x_1', y_1'$  and  $x_2, y_2$ . The flux that passes through the area between the two filaments that form the circuit is:

$$\frac{\mu_0 \gamma}{2\pi S_1} ds_1' \left( \int_{r_{11}}^{\infty} \frac{dr}{r} - \int_{r_{12}}^{\infty} \frac{dr}{r} \right) \quad (3)$$

$$\text{i.e.} = \frac{\mu_0 \gamma ds'_1}{2\pi s_1} (\ln r'_{12} - \ln r'_{11}) \quad (4)$$

The total flux linking this filamentary circuit due to all the filaments in A,  $d\phi_A$ , is:

$$d\phi_A = \frac{\mu_0 \gamma}{2\pi s_1} \int_A (\ln r'_{12} - \ln r'_{11}) ds'_1 \quad (5)$$

A similar equation is obtained by considering the flux that links this filamentary circuit due to the current in B, viz.,

$$d\phi_B = \frac{\mu_0 \gamma}{2\pi s_2} \int_B (\ln r'_{21} - \ln r'_{22}) ds'_2 \quad (6)$$

We next calculate the stored energy of the circuit, using the fact that inductive energy is given by  $\frac{1}{2} I \phi$  where  $I$  is the current and  $\phi$  the flux. Since the current in every filamentary circuit is the same in a filament in A and its return filament in B,  $\frac{\gamma}{s_1} ds_1 = \frac{\gamma}{s_2} ds_2$ . The energy,  $dW$ , of a filamentary circuit can be written as:

$$\begin{aligned} dW = \frac{1}{2} \gamma \left( \frac{\mu_0 \gamma}{2\pi} \right) & \left( \frac{ds_2}{s_1 s_2} \int_A \ln r'_{12} ds'_1 - \frac{ds_1}{s_1^2} \int_A \ln r'_{11} ds'_1 \right. \\ & \left. + \frac{ds_1}{s_1 s_2} \int_B \ln r'_{21} ds'_2 - \frac{ds_2}{s_2^2} \int_B \ln r'_{22} ds'_2 \right) \end{aligned} \quad (7)$$

To get the total inductive energy,  $W$ , we integrate:

$$\begin{aligned} W = \frac{\mu_0 \gamma^2}{4\pi} & \left( \frac{2}{s_1 s_2} \int_B \int_A \ln r_{12} ds_1 ds_2 - \frac{1}{s_1^2} \int_A \int_A \ln r'_{11} ds'_1 ds_1 \right. \\ & \left. - \frac{1}{s_2^2} \int_B \int_B \ln r'_{22} ds'_2 ds_2 \right) \end{aligned} \quad (8)$$

$$\text{Now write: } s_1 s_2 \ln R_{12} = \int_B \int_A \ln r_{12} ds_1 ds_2 \quad (9)$$

$$s_1^2 \ln R_{11} = \int_A \int_A \ln r'_{11} ds'_1 ds_1 \quad (10)$$

$$s_2^2 \ln R_{22} = \int_B \int_B \ln r'_{22} ds'_2 ds_2 \quad (11)$$

Substituting (9), (10) and (11) in (8) yields:

$$W = \frac{\mu_0 \gamma^2}{4\pi} [2 \ln R_{12} - \ln R_{11} - \ln R_{22}] \quad (12)$$

from which, since  $L = \frac{2W}{\gamma}$ , we obtain:

$$L = \frac{\mu_0}{2\pi} [2 \ln R_{12} - \ln R_{11} - \ln R_{22}] \quad (13)$$

The integration of  $\ln r_{ij}$  type of terms in (9) - (11) is the same as the logarithm of the product of all  $r_{ij}$  values,

$$\begin{aligned} \text{i.e.} \quad \iint \ln r_{ij} &= \iint \ln r_{ij} \\ &= \ln (r_{11} \cdot r_{12} \cdot r_{13} \dots r_{NN}) \end{aligned}$$

The latter term can be written  $\ln R^{(N^2)}$  where

$$R = (r_{11} \cdot r_{12} \cdot r_{13} \dots r_{NN})^{\frac{1}{N^2}}$$

i.e.  $R$  is the geometric mean distance of all the points in an area from every point either within the area that it is itself part of, or from an outside area. These cases correspond to  $R_{11}$  and  $R_{22}$ , and  $R_{12}$  respectively.

If the conductors have the same cross section,  $R_{11} = R_{22}$  and Eqn. (13) becomes:

$$L = \frac{\mu_0}{\pi} [\ln R_{12} - \ln R_{11}] \quad (14)$$

Since (13) and (14) give the inductances of parallel thin tubular conductors or radii  $R_{11}$  and  $R_{22}$  separated by distance  $R_{12}$  between their centres, it can be deduced that the geometric mean distance is a transformation from other shapes to equivalent tubular geometry.

As three examples, the geometric mean distances of lines at right angles and of lines of equal length that are parallel but diagonally displaced are derived, and the inductance of a pair of parallel thin strip conductors is found.



Lines at right angles (Fig. 25)

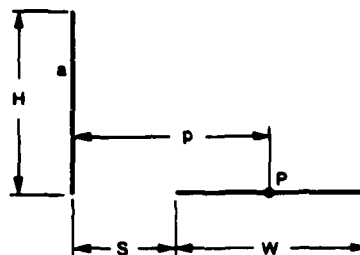


Fig. 25 Lines at right angles, separated.

Gray [16] gives the GMD of a line of length  $a$  from a point  $P$ , distant  $p$  from one end as:

$$\ln R = \frac{1}{2a} [a \ln(p^2 + a^2) - 2a + 2p \arctan(\frac{a}{p})] \quad (15)$$

which, substituting  $H$  for  $a$  becomes:

$$\ln R = \frac{1}{2H} [H \ln(p^2 + H^2) - 2H + 2p \arctan(\frac{H}{p})] \quad (16)$$

To extend this equation we integrate with respect to  $p$

$$\begin{aligned} \text{i.e.} \quad \ln R &= \frac{1}{2WH} \int_S^{S+W} [H \ln(p^2 + H^2) - 2H + 2p \arctan(\frac{H}{p})] dp \quad (17) \\ &= \frac{1}{2WH} [Hp \ln(p^2 + H^2) - 3Hp + H^2 \arctan(\frac{H}{p}) + p^2 \arctan(\frac{H}{p})]_S^{S+W} \\ &= \frac{1}{2WH} [H(S+W) \ln((S+W)^2 + H^2) - 3H(S+W) + H^2 \arctan(\frac{S+W}{H}) \\ &\quad + (S+W)^2 \arctan(\frac{H}{S+W}) - HS \ln(S^2 + H^2) + 3HS - H^2 \arctan(\frac{S}{H}) \\ &\quad - S^2 \arctan(\frac{H}{S})] \quad (18) \end{aligned}$$

Equal parallel diagonally displaced lines (Fig. 26)

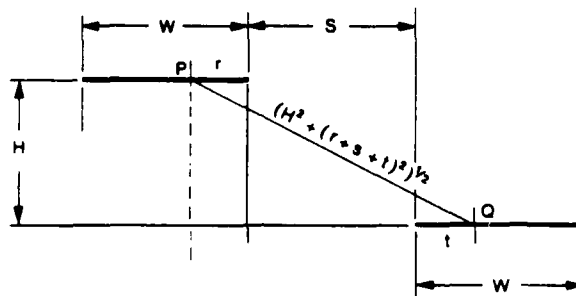


Fig. 26 Equal parallel diagonally displaced lines.

We require the sum of the logarithms of distances between points such as P, Q, on the lines of length W, displaced H vertically and S horizontally.

The GMD is given by:

$$\ln R = \frac{1}{2W^2} \int_0^W \int_0^W \ln [H^2 + (r + s + t)^2] dt dr \quad (19)$$

Integrating with respect to t yields:

$$\begin{aligned} \ln R = & \frac{1}{2W^2} \int_0^S \{ (r + s + W) \ln(H^2 + (W + s + r)^2) - 2W \\ & + 2H \arctan \frac{(r + s + W)}{H} - (r + s) \ln(H^2 + (r + s)^2) \\ & - 2H \arctan(\frac{r+s}{H}) \} dr \end{aligned} \quad (20)$$

which when integrated with respect to r yields:

$$\ln R = \frac{1}{2W^2} \{ (\frac{(S+2W)^2 - H^2}{2}) \ln(H^2 + (S+2W)^2) - 3W^2 + 2HS \arctan(\frac{S}{H}) \}$$

$$\begin{aligned}
& + 2H(S+2W)\arctan \frac{(S+2W)}{H} - 4H(S+W)\arctan\left(\frac{S+W}{H}\right) - \left(\frac{H^2 - S^2}{2}\right)\ln(H^2 + S^2) \\
& + (H^2 - (S+W)^2)\ln(H^2 + (S+W)^2) \quad (21)
\end{aligned}$$

#### Inductance of parallel strips (Fig. 27)

Let the strips have height  $H$  and be separated by distance  $S$ , i.e. as in Fig. 9. Eqn. (2.44) in Sect. 2.8.6 for parallel equal length lines gives the value for  $\ln R_{12}$  to be used in Eqn. (14), by putting  $S$  for  $W$ , i.e.

$$\ln R_{12} = \left(\frac{S}{H}\right)^2 \ln S + \frac{1}{2} \left(1 - \left(\frac{S}{H}\right)^2\right) \ln(H^2 + S^2) + 2 \frac{S}{H} \arctan \left(\frac{H}{S}\right) - 3/2 \quad (22)$$

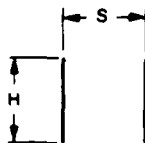


Fig. 27 Parallel strip conductors (or current sheets).

For  $\ln R_{11}$  we use the equation for the GMD of a line from itself (Eqn. (2.43) Sect. 2.8.6) i.e.  $\ln R_{11} = \ln H - 3/2$ . Substituting for  $\ln R_{12}$  and  $\ln R_{11}$  in Eqn. (14) yields:

$$L = \frac{\mu_0}{4\pi} \left[ \left(\frac{S}{H}\right)^2 \ln S + \frac{1}{2} \left(1 - \left(\frac{S}{H}\right)^2\right) \ln(H^2 + S^2) + 2 \frac{S}{H} \arctan \left(\frac{H}{S}\right) - \ln H \right]$$

i.e.

$$L = \frac{\mu_0}{2\pi} \left[ \frac{4S}{H} \arctan\left(\frac{H}{S}\right) + \ln\left(1 + \left(\frac{S}{H}\right)^2\right) - \left(\frac{S}{H}\right)^2 \ln\left(1 + \left(\frac{H}{S}\right)^2\right) \right] \quad (23)$$

which is the same as Eqn. (2.34) of Sect. 2.8.2. This shows that the total inductance and the propelling inductance are the same for this case.

## CHAPTER 3

### A REVIEW OF PULSED POWER SOURCES FOR ELECTROMAGNETIC PROPULSION

The power sources being used and proposed for railguns are described and discussed in this Chapter, especially in terms of the energy delivered per unit mass. An overall pulse energy density of at least 1 kJ/kg is considered to be necessary for railguns to be at all comparable with powder guns.

It is shown that the mass of a system that stores kinetic energy in some form can be simply estimated and that about 10 kJ/kg is an upper limit for metal structures.

The battery and pulse transformer scheme is introduced and shown to have potential advantages.

#### **3.1 Features required of a power source**

##### **3.1.1 Quantity of energy required is 1MJ or more**

For masses up to a few grams the chief reason for electromagnetic propulsion is to obtain velocities greater than those possible with light gas guns i.e. greater than about 8 km/s. For masses in the kilogram range there is military interest in attaining velocities of about 3km/s, about twice the present artillery velocities. There is also interest in accelerating masses of the order of tonnes to about 10 km/s for space launching.

For the reasons discussed in the previous chapters, the maximum efficiency of actual guns is likely to be in the range 10% to 30%. Allowing 50% efficiency for the transfer of energy from the power source to the gun indicates that the power source (an inductor) that finally operates the gun must be supplied with 7 to 20 times the kinetic energy that the projectile acquires. For the three applications mentioned, the energies required at the final stage of the power supply system typically become 1MJ, 100 MJ and hundreds of thousands of megajoules.

##### **3.1.2 Final component of power source must be an inductor**

The important contributions which Barber made were the realizations that railguns should be operated with a constant current and that the final component of the power source should be an inductor. A constant current produces a constant acceleration force and lowest overall stresses for a given final velocity. An inductor current source automatically provides the e.m.f. necessary to maintain the current against the rising resistance and back e.m.f. presented to it by the gun. Voltage sources such as capacitors would give extremely high (and destructive) currents initially, but the current would fall rapidly and the acceleration would fall even more rapidly.

### 3.1.3 The ANU homopolar generator power source

Having identified the inductor as the final component, the power source problem is how to charge the inductor and connect it to the railgun. The homopolar generator scheme devised by Marshall and Barber at the Australian National University [Fig. 28] shows that this can be a complicated task.

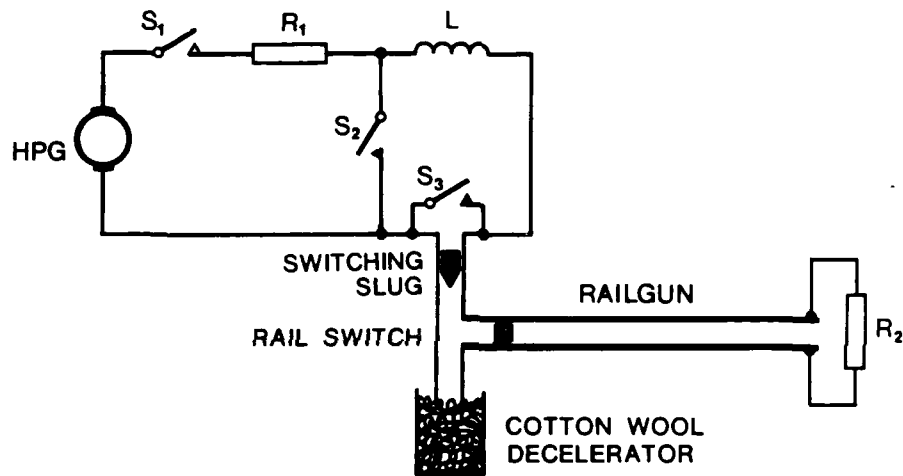


Fig. 28 ANU Railgun power source.

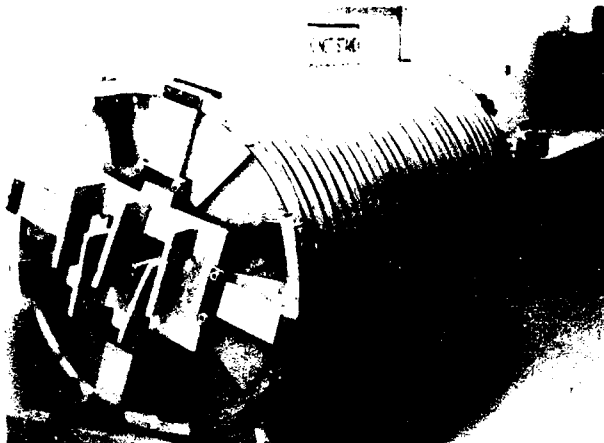


Fig. 29 The inductor used in the ANU railgun. The inductor, which is now located at the Materials Research Laboratories in Melbourne, has an inductance of approximately  $20 \mu\text{H}$ . It is approximately 2m long x 1 m dia and is constructed from 4.3 x 4.3 cm hollow aluminium with 7 turns effectively, each "turn" consisting of 4 turns in parallel. At the maximum operating current of 500,000A it stores 2.5 MJ.

The homopolar generator (HPG) charges the inductor,  $L$ , via switch  $S_1$  and the "rail switch" which is itself a short, large bore railgun. The "switching slug" in the rail switch is restrained mechanically (e.g. by pins) while the current builds up. The HPG is equivalent to a large capacitor and its energy transfers to the inductor in a quarter of a cycle of the resonant period of the inductor and the equivalent capacitance of the HPG. When the current reaches the desired value the switching slug is released and switch  $S_2$  is closed. The switching slug accelerates along the rail switch and, when it crosses the gap, current flows via the rails and projectile. At a pre determined time, before the projectile reaches the muzzle, switch  $S_3$  is closed so that the inductor is short circuited and dissipates the remaining energy in itself. Resistor  $R_1$  is to limit the short circuit current of the HPG while  $S_2$  is closed until  $S_1$  is opened. Resistor  $R_2$  absorbs the energy of the rail field, thereby preventing muzzle damage from the arc that would otherwise arise.

The system can be simplified if the remaining energy of the inductor and the HPG is allowed to dissipate in the muzzle resistor  $R_2$ .  $R_1$ ,  $S_2$  and  $S_3$

can then be omitted, together with the associated synchronizing requirements of the switches. This simplification applies particularly to the case of a homopolar generator that stores only enough energy for one shot. If a large HPG is used, as for a rapid multishot gun, the more complex arrangement is necessary.

In principle it is possible to return the energy of the inductor and rail field to the HPG, since the inductor and HPG form a resonant pair. To do this, R1 and S2 would be omitted. The rail field would be recovered by replacing R2 with a shorting switch and omitting S3.

The HPG must be brought up to speed, either by running it as a motor or by means of another motor. If electricity is used for the purpose, a powerful source of electricity is necessary to bring the HPG up to speed within a few minutes. A powerful source of electricity is also needed to supply the field of the HPG particularly if it is to be run up to speed as an electric motor. The full "power train" is therefore long and much more complicated than the railgun itself.

#### **3.1.4 Features of an ideal power source**

In contrast to the practical system just discussed, we can list the features of an ideal system. Ideally a power source should:

- (i) have simple switching with no need for synchronization i.e. one switch only and that a closing switch;
- (ii) contain its own prime energy store, e.g. chemical fuel;
- (iii) have high power and energy densities so as to be low in mass and volume;
- (iv) be reliable and safe, so that despite high power density the risk of destructive release of the energy is low (a fuel made up of a two part mixture with the parts well separated and brought together in just the required amounts when required, for example);
- (v) be low cost.

Bearing in mind the above points and the practical HPG system we can say that the power source problem is how to charge the inductor and connect it to the railgun in the simplest and most compact manner.

#### **3.1.5 Desirable power source pulse energy density**

Although the advantages of railguns, such as high velocity, may justify them even if they are considerably more massive than powder guns, it is obviously desirable that their total mass be as low as possible. In particular, the power source mass should be as low as possible.

By examining the performance of powder guns an estimate can be made of the desirable minimum quantity of energy per unit of mass which a railgun power source should deliver in a single pulse. The tabulation below lists the projectile energies (muzzle energies) compared to masses for the smallest to the largest powder guns [1,2].

Powder gun	Muzzle energy J	Mass kg	Muzzle energy/Mass J/kg
Colt 45	477	1.13	422
Winchester 270	3905	3.63	1080
M14 7.62 mm	3562	4.1	869
155 mm Artillery	$8.25 \times 10^6$	12,372	715
16" Seacoast	$364.5 \times 10^6$	454,000	802

The tabulation shows that the greatest muzzle energy to mass ratio is about 1 kJ/kg. Assuming the gun propulsion to be about 30% efficient, the energy released by the powder is about 3 kJ per kilogram of gun mass. We can use this value as an indication of the energy to mass ratio, i.e. energy density, which railgun power sources should attain to be comparable with powder guns. Assuming further that the railgun itself has a muzzle energy to mass ratio of 1kJ/kg, the following values are obtained for the muzzle energy to mass ratio of the system comprising the railgun and power source.

Railgun Efficiency	Power Source Energy Density	Railgun Energy Density	Muzzle energy/Mass (Total system)
25%	1 kJ/kg	1 kJ/kg	200 J/kg
	3 kJ/kg	1 kJ/kg	429 J/kg
50%	1 kJ/kg	1 kJ/kg	333 J/kg
	3 kJ/kg	1 kJ/kg	600 J/kg

The railgun tabulation shows that for railguns to approach the performance of powder guns, power source pulse energy densities in the range 1 to 3 kJ/kg are required together with railgun efficiencies in the range 25% to 50%. As the study in Ch. 2 shows, such efficiencies are very optimistic.



We can conclude that the power source should deliver at least 1 kJ/kg for the total railgun mass to come within a factor of 2 of that of a revolver with the same muzzle energy.

### 3.2 Capacitor based power source

A capacitor based power source can have two important advantages, viz. a simple circuit and a low mass inductor. The capacitors themselves, however, are massive.

#### 3.2.1 Large mass and simple circuit

Capacitor banks can power railguns because they can discharge energy at the rate of megajoules in tens of microseconds. Whilst their power density is extremely high ( $10^5$  W/kg) their energy density, between 100 and 200 J/kg, is an order of magnitude less than is desirable. Even for the lowest energy applications of railguns, the capacitor bank must have a mass of several tonnes. Nevertheless capacitors are useful for small scale launchers because they can transfer their energy quickly to an inductor via the railgun and thereby permit particularly simple switching (Fig. 30).

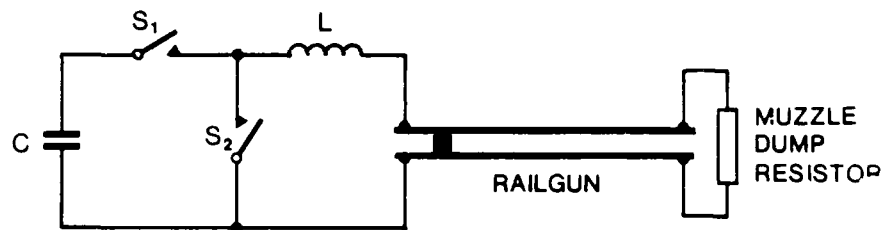


Fig. 30 Railgun with capacitor power source

The capacitor in Fig. 30 is selected so that its quarter cycle resonance period is a small fraction of the time to accelerate the projectile. The capacitor is charged to a voltage that stores the energy desired in the inductor and switch  $S_1$  is closed. Current immediately flows via the inductor and the railgun and reaches its quarter cycle peak before the projectile has moved far. At this time all the energy has transferred to the inductor and the voltage across the capacitor is zero. Switch  $S_2$  is then closed to isolate the inductor, which thereafter drives the projectile with the desirable approximately constant current. Both  $S_1$  and  $S_2$  are active only as closing switches and hence triggered spark gaps and ignitrons can be used. Only the closing switch  $S_2$  needs to be synchronized, but the timing is not critical.

There must of course be a prime energy source from which to charge the capacitor in the first place. If the charging is to be done quickly this source must be powerful and hence massive, as was mentioned in regard to HPG systems.

### 3.2.2 High voltage limitation

To launch a 5 gram mass at 10 km/s in one millisecond from a railgun with an inductance of 0.5  $\mu$ H/m would require an inductor of about 16  $\mu$ H charged with about 2MJ of energy at a current of 500 kA. If we allow 100  $\mu$ s for the quarter period transfer time of the capacitor energy to the inductor, a capacitor of 250  $\mu$ F would be needed, charged to 125 kV. This example shows that the simple capacitor scheme may require impractically high voltages. A voltage of 125 kV is close to the limit for which capacitors can be constructed and poses great safety and technical problems, such as in protective fusing and charging.

In the railgun application the capacitor is infrequently used and since it is clamped when the voltage reaches zero it is not subject to reverse voltage. Under these conditions it could be constructed to store energy at about 200 J/kg and so to store 2MJ the capacitor bank would have a mass of about 10 tonnes.

The problem of the high voltage required on the capacitor could be overcome by using a larger capacitance to store the energy. This, however, means that the inductor must be charged before it is connected to the railgun. That makes the capacitor similar to the HPG and brings us back to a scheme similar to Fig. 28.

### 3.2.3 Low mass inductor

The higher the voltage from which an inductor is charged, the smaller can be its mass for a given loss in the conductors. Smaller conductors can be used because, although their resistance loss is higher, the higher voltage charges the inductor in a shorter time. Since capacitors operate at very high voltages compared to HPGs (which typically have voltages of 100V), the inductors for capacitive power sources are much less massive than for HPG power sources. The massiveness of the capacitors themselves nullifies this advantage, though.

### 3.2.4 Limitations to the energy density of capacitors

If capacitors are to be used for other than low energy railguns their energy density needs to be increased to at least 1 kJ/kg i.e. a factor of 10 improvement is necessary.

In considering the energy density of capacitors it must be realized that their energy density is not an absolute value but is the value compatible with a certain lifetime under certain conditions. In railgun service the lifetime is the number of discharges and the chief conditions are the voltage,

the time for which the capacitors are required to hold voltage before being discharged and the degree of voltage reversal before clamping is accomplished.

- (i) Since capacitor life varies with voltage according to  $(\text{voltage})^{-K}$  where  $K$  is in the range 5 to 7, the decrease in life with voltage is rapid [3]. Increasing the voltage by 25% beyond the rated value, and so increasing the energy density by 50%, may reduce the life to 25% of the rated life.
- (ii) The life of a capacitor depends upon the time for which it must withstand electric field stress and this includes the charging and holding time as well as the conditions during discharge [4]. The capacitor should be charged quickly and immediately discharged to obtain the rated number of discharges. In railgun service it may be desired to hold the capacitors charged for several minutes prior to discharge, which would directly reduce the number of discharges prior to failure.
- (iii) Another factor to be borne in mind is that the likelihood of dielectric breakdown due to randomly distributed faults increases with area, and therefore with the capacitance. This is important in regard to capacitor banks as well as to individual capacitors, since the whole bank fails if one capacitor fails. As an example, the maximum energy stored in a single capacitor appears to be 10 kJ with a 90% survival rate after  $10^5$  shots with zero voltage reversal [5]. 100 of these capacitors would be required in parallel to obtain 1MJ and 10 of them could be expected to fail before the  $10^5$  shots were obtained. On average there would be a failure every  $10^4$  shots. Since capacitors fail by internal short circuit, the energy of the rest of the bank may discharge into the failed capacitor, with destructive effects on busbars and other capacitors, unless protective fusing is carefully devised and installed.

From the preceding discussion it is evident that no further trade off of life can be made to increase energy density of capacitors for railgun service\*. Increased energy density must come about through improvements in one or both of two basic factors, viz. increased electric stress for the same life as at present and increased dielectric constant.

There are two limitations to the electric stress in capacitors; the dielectric strengths of the insulating materials and corona. These factors presently limit the average dielectric stress in capacitors to 100 to 200 V/ $\mu$ m [6]. To increase the energy density by a factor of 10 would require the average electric stress to approach 600 V/ $\mu$ m. Such electric stresses are

---

\* Such trade offs can be made for capacitors in other service. Defibrillator capacitors store 400 J/kg. They have the highest energy density of any capacitors. They are rated at 5000 shots with 95% survival. The maximum storage time is 60 seconds and they are small (approx 1 kg).

presently only attained as the intrinsic dielectric strengths over small areas.

Corona occurs in two ways - through the degradation of the dielectric materials (especially at sites where there are impurities or faults) [7] and, more importantly, at the edges of the foil electrodes [8].

To obtain an energy density of 1 kJ/kg through increased electric stress evidently requires practically perfect dielectric films in large areas and practically perfect impregnants to eliminate all water and air and new construction techniques that will reduce electric stress concentrations at the foil edges. Perfluorocarbon impregnants have been recently claimed to be near perfect impregnating liquids [9].

The paper, plastic and oil combinations presently used for energy storage capacitors have dielectric constants in the range 2-5. If the dielectric constants could be increased for the same dielectric strengths as the present materials have, higher energy densities could be obtained. There is a difficulty with this option, though, because high dielectric constant goes with ease of polarization, and the easier it is to polarize a molecule the easier it is to remove electrons, i.e. to cause ionization and corona. [10].

Taking into account the facts that multi megajoule capacitor banks require hundreds of individual capacitors and that for operational reasons a large part of the capacitor life must be used up in charging and holding voltage, the 90% survival life of each capacitor needs to be  $10^6$  discharges to ensure  $10^4$  trouble free railgun shots. Ennis [11], after considering the best existing materials and design strategies, concludes that the attainment of even 200 J/lb (440 J/kg) with a  $10^6$  shot life is unlikely.

Overall, we must conclude that unless unforeseen breakthroughs in materials occur, capacitors can be considered only for small, infrequently fired, railguns.

### 3.3 Flywheel based machines - inertial storage

#### 3.3.1 Flywheels

Flywheels can easily store energy at densities in excess of the 1 kJ/kg rate which we have nominated as the minimum for a railgun power source. The tensile strength of a flywheel determines the amount of kinetic energy that it can store. Using carbon fibre/epoxy composites, flywheels can store energy at 300 kJ/kg i.e. thousands of times more densely than capacitors [12]. Metal flywheels cannot store energy as densely as can the new composites because their density is much higher but their tensile strength is much the same. (Steel or beryllium copper flywheels can store up to 66 kJ/kg [13].)

To make use of a flywheel it must be incorporated within an electrical generator and there must be a means of bringing it to speed. The

need to place windings on it or to use brushes reduces the speed at which it can be used. These necessary features cause the energy density of the overall system to be far less than that of the basic flywheel.

### 3.3.2 Homopolar generators

For about 20 years the homopolar generator has been recognised as equivalent to a large capacitor which is able to store energy with the same density as does a flywheel. Intensive development of these machines has been undertaken at several places in the last 10 years, especially at the Center for Electromechanics, University of Texas [14]. The principle of the machine and one of the developmental models at the University of Texas are shown in Fig. 31.

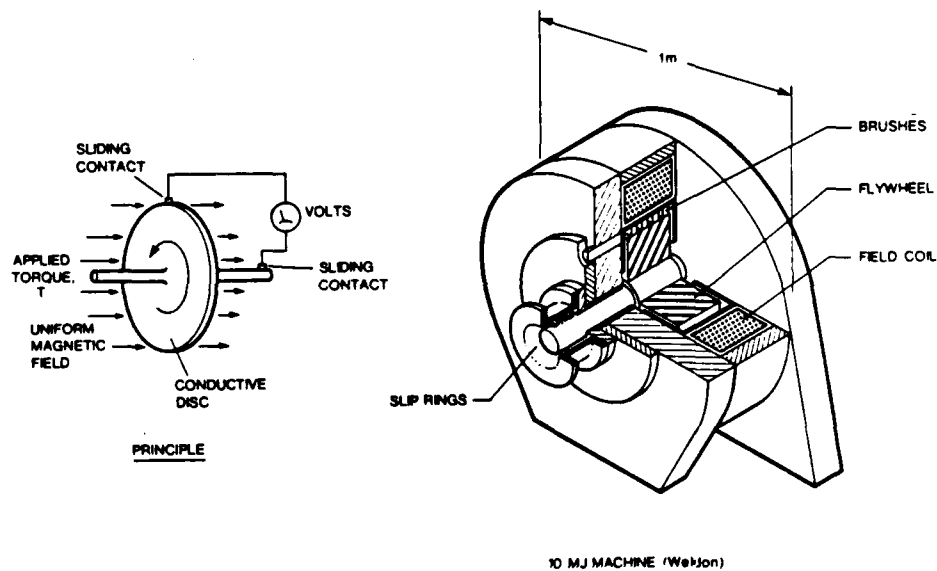


Fig. 31 Homopolar generator.

From the diagram of the principle, the two major features of the machine can be seen. Firstly, since it has only one turn the output voltage is low. Secondly, the machine can deliver high current, fast rising pulses because it has only one low resistance, low inductance turn and because the armature reaction is small (the field lines of the radial current paths on the flywheel with brushes all around the rim are concentric circles at right angles to the exciting field). The field of homopolar generators may be separately excited or self excited. If self excitation is used the machine

and its load are interdependent and a critical speed must be reached before the machine will generate [15]. The output characteristic is no longer like that of a discharging capacitor.

The rotors of the machines cannot take advantage of the energy storage potential of modern composites since they must be made of metal to conduct electricity and furthermore their peripheral speeds must be lower than about 500 m/s because of brush limitations.

A most difficult aspect of homopolar generator development has been that of collecting the high current which they can produce. Mercury and liquid sodium-potassium jets appeared to have the ability to collect current from the whole rim surface, but have many problems [16]. Marshall has shown that copper graphite brushes, similar to those used in car starter motors, work satisfactorily for rubbing speeds up to 200 m/s, even though they may run red hot for the second or so that current is collected [17]. According to Marshall, the important point is that sparking be prevented by maintaining sufficient pressure on the brushes. For the highest current, fastest discharges, the flywheel rim should be covered with brushes. The need to mechanically actuate the brushes and hold them with the correct pressure adds to the complexity of the machine and to the operation sequence of Fig. 28.

Taken together, the rotor and brush properties enable currents in the range  $10^5 - 10^6$  A to be obtained from machines in the 5-10 MJ range. Mega joules of energy may be discharged into a low inductance, low resistance load in tens of milliseconds [18].

The most serious limitation of the homopolar generator in the railgun application is that its output voltage is ordinarily less than about 100V. This low voltage (or alternatively the large capacitance of the machine) means that the time to transfer the energy to the railgun inductor is long, and unless the inductor is wound with massive conductors, most of the generator energy will be wasted in  $I^2 R$  losses. Attempts to overcome the low voltage include transformers [19], superconducting windings to raise the exciting field to 6 Tesla [20] and multiple rotors connected in series [21].

The incentive for building flywheel type machines is that they appear to have the potential for much higher energy density than capacitors. Unfortunately, when all the necessary parts are considered, the improvement, although significant, is disappointing. For a start, it is necessary to supply a magnetic-field, and as can be seen from the machine in Fig. 31, the flywheel becomes a small part compared to the iron and copper that surrounds it. The flywheel of the machine in Fig. 31 has a mass of approximately 1 tonne [22], hence, when it stores 10MJ its energy density is 10 kJ/kg. From the drawing of the machine we can estimate its total mass at about 10 tonnes; hence its overall energy density is only about 1 kJ/kg i.e. about five times that of capacitors. When we take into account the fact that it may deliver only half its energy into an inductor which is many times the mass of an inductor into which a high voltage capacitor would deliver most of its energy, and the mass of the apparatus needed to bring the machine to speed, the advantage over capacitors diminishes to a factor of only two, with a great deal of operational complexity added.

Another example is a relatively high technology design [20]. The machine in this case stores 10MJ at about 14 kJ/kg in two counter-rotating aluminium rotors and uses superconducting coils fed with liquid helium to establish a field of 6 Tesla. From the dimensions given we can estimate its mass at about 40 tonnes and consequently its energy density at 250 J/kg.

The degrading effect of the iron and copper that does not rotate prompted Marshall to devise a machine in which the field coils are set into the flywheel and very little iron is needed in the frame for the flux return path [23]. The rest of the frame can be of aluminium instead of iron. Such a machine, the AIR (all iron rotating) or compact homopolar generator, has been recently completed at the University of Texas and stores 6.2 MJ with an overall density of 4 kJ/kg. This development has led to other concepts which in theory could treble this figure [24].

Even if these new machines eventuate, the energy density of the total system may still not exceed 1 kJ/kg. The low voltage (50V) of the compact HPG results in an inductor with a mass of 1.5 tonne (the same mass as the machine) that must be cooled with liquid nitrogen in order to store the energy of the HPG with 50% efficiency [25]. Thus, for the inductor and HPG the stored energy is 3.1 MJ from a total mass of 3 tonnes, or 1 kJ/kg. When we include the mass of the power source required for the field and auxiliaries, such as a 200 HP electric motor, the energy density is less again.

### 3.3.3 Ordinary large alternators

Ordinary or modified alternators have been used under virtually short circuit conditions to produce up to 20 times the normal rating of the frame size. Manufacturers of large circuit breakers use machines in this way for testing their products. Up to 3 gigawatts can be produced for a few cycles [26]. The energy densities are less than those of homopolar machines, though, because their rotors cannot be run to store the same energy densities owing to the windings and slots. Also, if DC is wanted expensive rectification is necessary.

### 3.3.4 The compulsator

The "compulsator" is a machine recently invented at the University of Texas especially for pulse production [27]. It combines in the one machine the flywheel storage principle and an inductor to which the flywheel energy is transferred. The transfer from the flywheel to the inductor takes place by "magnetic flux compression".

Consider a conducting loop with inductance  $L_1$  and current  $I_1$ , as in Fig. 32 (a). Suppose that a uniform pressure is applied around the



Fig. 32 Magnetic flux compression.

circumference of the loop so that it decreases in diameter. The small loop has a smaller inductance,  $L_2$ , than the large loop. If the compression is quick so that  $I^2R$  losses are negligible, the flux linkage remains constant. Thus we have  $L_1 I_1 = L_2 I_2$ , and since  $L_2 < L_1$ ,  $I_2$  is greater than  $I_1$  and in particular the stored energy of the small loop,  $\frac{1}{2} L_2 I_2^2$  is greater than that originally present in the larger loop. The quick compression has resulted in an energy magnification in the ratio  $\frac{L_1}{L_2}$ ; the increase coming from the work done by compressing the loop against the  $\mathbf{J} \times \mathbf{B}$  force present on it. (Analogous to whirling a stone on a string and pulling it towards the centre against the centrifugal force - the kinetic energy and the angular velocity of the stone increase).

The way that the compulsator employs this principle is shown in Fig. 33.

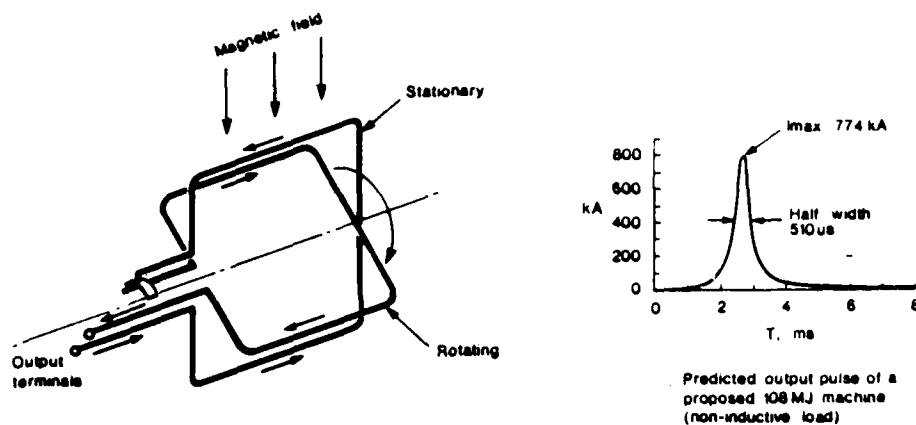


Fig. 33 The principle of the Compulsator (Weldon 1978).



The machine has identical rotor and stator windings which are connected in series via a slip ring. The output is obtained from the other ends of these windings. When the turns are parallel, with the current in the same direction in each, the circuit has maximum inductance. If the rotor moves to the other parallel position in a time that is very short compared to the initial  $\frac{L}{R}$  value for the circuit, the flux linkages will be conserved. In this position the currents are in opposite directions and the inductance decreases to about 2.5% of its value at the first position. The current and the energy of the windings could therefore increase by a factor of 40, in principle, during the rotation from one position to the other. The mechanical energy of the rotor is converted to magnetic energy through the work it does in moving the rotating winding against the  $J \times B$  forces. At this stage, the machine is equivalent at its output terminals to an inductance charged with perhaps megajoules of energy at hundreds of thousands of amperes. The machine, however, continues to rotate, the inductance increases and the magnetic energy returns to the rotor and the current pulse is "switched off", and so on. In Fig. 33 there is shown the current pulse calculated for a machine which stores 108 MJ in its rotor.

During the millisecond or so that the machine is equivalent to a charged inductor it could conceivably power a railgun. In particular it could do so, in principle, at least once per revolution and a repetition rate of tens of shots per second appears possible. With the machine rotating, one closing switch to power its field would be all that is necessary for the whole power train.

A fundamental difficulty exists in the application of this idea though. In order for the flux compression principle to work the machine must generate an initial current, via the railgun, as a normal generator. Since the railgun is virtually a short circuit early in the acceleration this seems possible. However, during the flux compression stage, the rate at which energy is extracted should be much less than that at which it is stored. If high power is supplied to the railgun during the compression stage, the flux compression will be degraded. The degradation will increase with the velocity of the projectile because the equivalent resistance of the railgun increases with velocity. From the flux compression view point, the best way to operate the machine is to use a switch to short circuit it until the compression is complete and then to open the switch so that the current flows via the load. That, however, would defeat one of the attractions of using the compulsator to power the railgun. Another possibility is to ensure that the railgun power is small compared to the compression power, but that means using an otherwise over sized machine and hence degrading its energy density. If the compulsator and the railgun are designed together a resolution of the conflict is apparently possible [28]; although, from the sinusoidal current versus-time plot given in the reference indicated, it seems that not much flux compression takes place.

The energy density of the compulsator in terms of the energy which it can deliver in a pulse is low. The mass of a machine which would store 108 MJ in its rotor is given as 87.6 tonnes [29] i.e. 1.23 kJ/kg. But less than 10% of the rotor energy could be delivered in a single pulse, which gives an effective single pulse density of 123 J/kg, about the same as for capacitors. The justification for the compulsator as a railgun power source therefore has to be its potential for rapid, repetitive shots.

### 3.4 Explosive magnetic flux compression

For about 30 years magnetic flux compression by means of explosives has been used to generate megagauss magnetic fields and megamp currents. Explosive magnetic flux compression has also been used to power railguns [30]. In the simplest form the explosive destroys the generator and so the generator is one shot. Reusable types have been proposed [31].

Explosives are attractive as pulse energy sources because they release megajoules of energy per kilogram in microseconds. The energy is firstly released as heat. The heat must be converted into kinetic energy of the current carrying medium which compresses the flux.

A simple example of the technique is the strip generator (Fig. 34). The chamber, which is formed into a single turn coil at one end, is

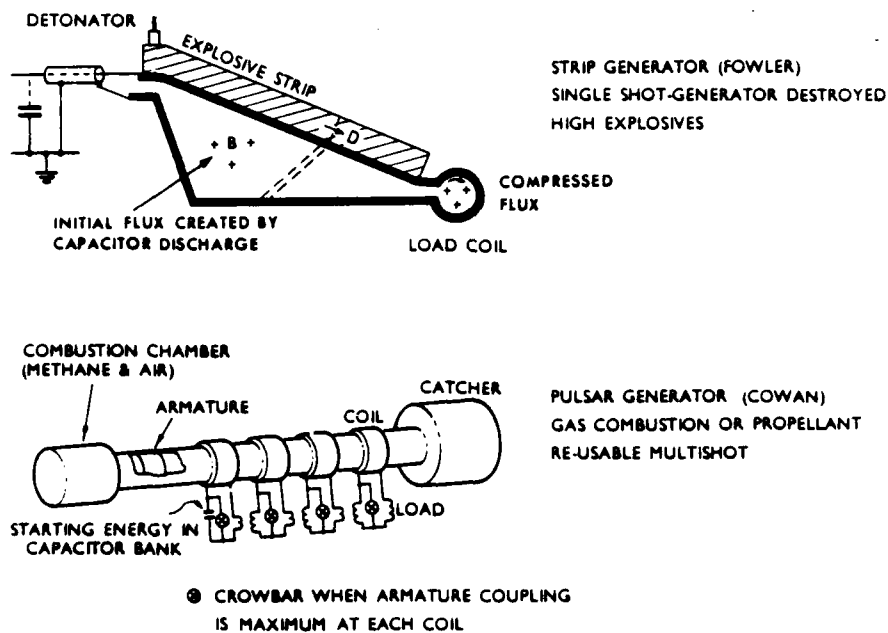


Fig. 34 Pulse generation by flux compression.

initially charged with current by discharging a capacitor bank into it at the other end [32]. The explosive strip is detonated and it shorts together the open end of the chamber so that the current circulates. The explosion

progressively compresses the chamber as indicated by the dashed section. The compression process is rapid compared to the  $\frac{L}{R}$  value of the chamber at any stage (in theory) and therefore flux linkages are conserved. The force of the explosive, in moving the chamber walls against the magnetic field force, causes a portion of the energy released by the explosive to become magnetic energy in the single turn load coil. A variety of configurations has been tried. Helical designs [33] for example enable the ratio of initial to final inductance to be large (100:1) and hence should produce a greater energy conversion.

The "Pulsar" device shown in Fig. 34 is an attempt to produce a reusable explosive flux compressor [31]. It uses a piston (also called an armature), which may be metal or plasma, to increase the mutual inductance between itself and a conducting coil. A circulating current is induced into the piston and magnetic energy is created by the action of forcing together the like poles of magnets. A variety of fuels (diesel, natural gas, petrol) may be used to drive the piston. A capacitor bank is required to create a magnetic field in the first section, but thereafter the sections induce currents into the succeeding sections and create the required magnetic field. The "Pulsar" is claimed to be suitable for producing pulse energies of 10 MJ and above, and as a power source for railguns.

The proportion of the heat energy of the explosive that becomes electrical energy is only about 5% in devices constructed so far [34]. From the literature on flux compression it seems that there are three main reasons for the low conversion efficiency. The first is that the conversion of the heat energy to kinetic energy is at best only about 40% [35] (although the temperatures are high enough to give a Carnot efficiency of about 90%). Secondly, although in principle the extremely rapid compression obtained with explosives reduces the time for  $I^2R$  losses, it also means that the generated current is confined to the conductor surfaces and the resistive losses are high. Since most of the current increase occurs towards the end of the compression, the  $I^2R$  losses increase rapidly as the compression proceeds (temperature rise of the metal surface, including melting or even vapourization is reported [36]). Thirdly, a fundamental conflict exists between the need for compression to be quick enough to reduce  $I^2R$  losses and the conversion of all the kinetic energy of the moving part [37], because as the kinetic energy is extracted the moving part slows down. The compression process must have a slow ending in the presence of high currents if the majority of the kinetic energy is to be converted. Owing to  $I^2R$  losses the maximum magnetic energy must occur while there is still considerable kinetic energy. In the case of the "Pulsar" the excess kinetic energy can pass out of the system, but in one shot devices it shortly destroys the generator itself.

Since about 5% of the heat energy becomes magnetic energy, the explosives energy density is effectively about 100 kJ/kg (hydrocarbon fuels must have the correct amount of air supplied e.g. as compressed air). The containment structure however, greatly degrades the overall density. In the self destructive types only the final portion of the apparatus must be strong enough to contain the delivered energy. On simple pressure vessel calculations it is unlikely that the energy density for this portion can exceed about 20 kJ/kg. The capacitor bank needed to charge the generator with an initial current must be included too. If the energy gained from the explosive is 100 times that supplied by the capacitors, since capacitors at

best store about 200 J/kg, the overall energy density cannot be greater than 20 kJ/kg. Considering the other masses necessarily present also, the overall energy density even of the self destructive explosive magnetic flux compressor cannot exceed about 5 kJ/kg. The nondestructive "Pulsar", because its entire structure must survive the explosion, must have much greater associated masses and hence a lower overall energy density.

Marshall has recently [38] investigated a reusable flux compressor in which a sliding armature progressively reduces the number of turns in an inductor. The compression is carried out relatively slowly (15 ms) but this allows the current to fully penetrate the conductors and the resistive losses turn out to be only about 10% of the stored energy of 50 MJ. The overall energy density is only about 3 kJ/kg even in this almost lossless flux compression process.

### 3.5 Minimum mass of energy stores

#### 3.5.1 Force is required to contain kinetic energy

To introduce this Section let us discuss the fundamental necessity for there to be containment forces associated with stored kinetic energy.

According to Newton's 1st law, force is present whenever the motion of a mass is altered in magnitude or direction. If a set of moving particles is constrained to remain within a fixed volume, forces must be exerted on the particles to change their direction of motion at the boundaries of the volume. Since the moving particles have kinetic energy, we can say that a force is necessary to store their kinetic energy within the volume.

The description above is the basis of the kinetic theory of gas pressure, but let us apply it more widely. A flywheel, for instance, stores kinetic energy within its spinning volume. In this case the direction of the particles is changed gradually all the time by the centripetal force, and we can say that it is the centripetal force that constrains the kinetic energy of the flywheel to remain within the spinning volume. The expression for stored magnetic energy, viz.  $\frac{1}{2}LI^2$ , has the same form as that for the stored energy of a flywheel, viz.  $\frac{1}{2}I\omega^2$ . This suggests that magnetic energy is a form of kinetic energy, stored as if by a flywheel, and that the  $\mathbf{J} \times \mathbf{B}$  force on current crossing its own magnetic field is, like centrifugal force, the result of "particles" being constrained to move around curved paths [39].

#### 3.5.2 Minimum mass of kinetic energy stores

The power sources that we have considered make use of kinetic energy in some form. The notion that kinetic energy can be contained within a finite volume i.e. can be stored only if there are forces which change the direction of the moving masses, enables the minimum mass of the container to be calculated. The minimum mass and stored energy relationship has been attributed in the literature [40] to the Virial Theorem by Clausius, but, as we shall show, the results are directly obtainable from the boundary force notion.

(i) Consider a volume of gas at pressure  $P$  in a container of length  $l$  and cross section  $A_w$  (Fig. 35 (a)).

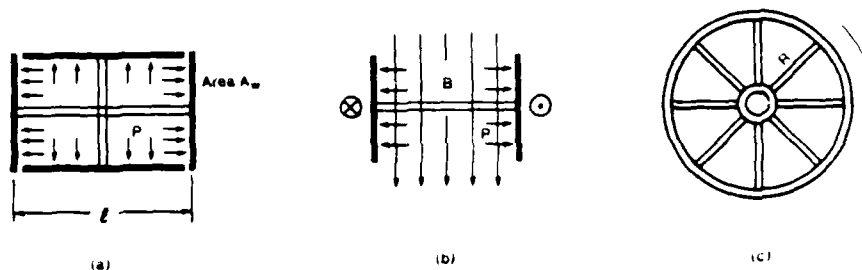


Fig. 35 Kinetic energy stores. (a) gas, (b) magnetic (c) flywheel.

Suppose that the walls are rigid so that they do not bend but are held in place by three struts at right angles to each other. The mass of the strut of length  $l$  is given by:

$$M = \rho l A_s, \quad (3.1)$$

where  $\rho$  is the density of the strut and  $A_s$  is its cross sectional area. But the cross sectional area of the strut equals the force on the wall divided by the tensile stress,  $\sigma_s$ , in the strut, which leads to:

$$M = \frac{\rho PV}{\sigma_s}, \quad (3.2)$$

where  $V = l A_w$  is the volume of the container of gas. From the kinetic theory of gases, the kinetic energy associated with one direction in a gas is  $\frac{1}{2} PV$ ; therefore (3.2) can be written:

$$M = \frac{2\rho W}{\sigma_s}, \quad (3.3)$$

where  $W$  is the kinetic energy of the gas in one direction. Since the same result is obtained in each direction, equation (3.3) also yields the mass of the three struts where  $W$  is the total kinetic energy ( $\frac{3}{2} PV$ ), assuming the struts all have the same density and tensile stress.

(ii) For the case of a magnetic field contained by surface currents as indicated in Fig. 35 (b), the magnetic energy is  $PV$ , since the pressure,  $\frac{B^2}{2\mu_0}$ , is the same as the energy stored per unit volume. We obtain in this case:

$$M = \frac{\rho W}{\sigma_s}, \quad (3.4)$$

where  $W$  is the stored magnetic energy ( $\frac{1}{2} LI^2$ ).

(iii) Let the portion of the thin rimmed flywheel associated with each spoke have mass  $M$  (Fig. 35 (c)). The kinetic energy,  $W$ , of mass  $M$  is:

$$W = \frac{1}{2} MR^2 \omega^2,$$

which may be written as:

$$W = \frac{1}{2} FR, \quad (3.5)$$

where  $F$  is the centripetal force on the spoke. The mass of the spoke is given by

$$M = \rho R A_s, \quad (3.6)$$

where  $\rho$  is the density of the spoke and  $A_s$  its cross section, which may be written:

$$M = \frac{\rho R F}{\sigma_s}, \quad (3.7)$$

where  $\sigma_s$  is the tensile stress in the spoke. Using (3.5), we finally obtain:

$$M = \frac{2 \rho W}{\sigma_s}, \quad (3.8)$$

where  $M$  is the total mass of all the spokes,  $W$  the total kinetic energy of the rim and  $\sigma_s$  the tension in the spokes.

The above results give the minimum masses for the conditions stated. The mass may be halved if the struts become plates and support biaxial tension instead of uniaxial [41]. If compressive forces are also caused by the spokes, as in a solenoid by the flux lines as they bend over at the ends, additional mass is required [42].

For general estimates it can be stated that the minimum mass of a system that stores kinetic energy is given by  $M = \frac{2W}{\sigma_s}$ , where  $\rho$  is the density of the containment structure,  $\sigma_s$  is the tensile stress and  $W$  is the kinetic energy.

As an example, high tensile steel, stressed to  $1000 \text{ MPa}$ , has a mass of  $1 \text{ kg}$  per  $1000 \text{ kJ/kg}$ . If there are compression forces as well as tension, the mass required is greater.

AD-A192 102

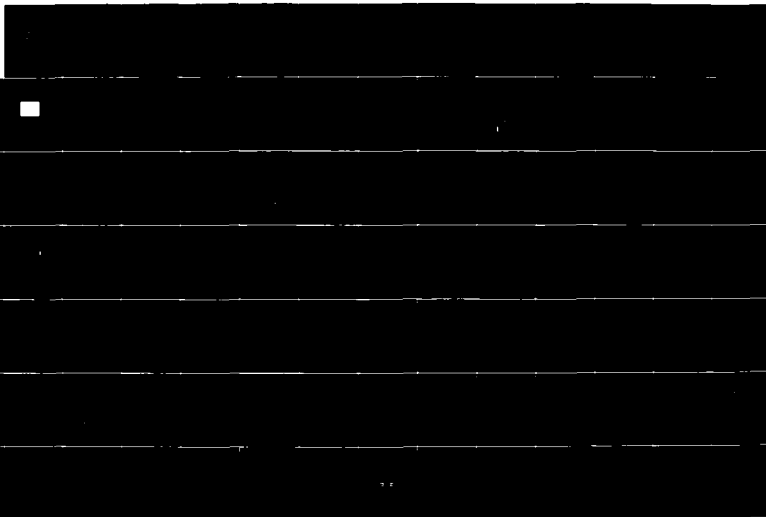
THE RAILGUN AND ITS POWER SOURCE(U) MATERIALS RESEARCH  
LABS ASCOT VALE (AUSTRALIA) D N SADEIN ET AL. JUN 87  
NRL-R-1036 DODM-AR-005-133

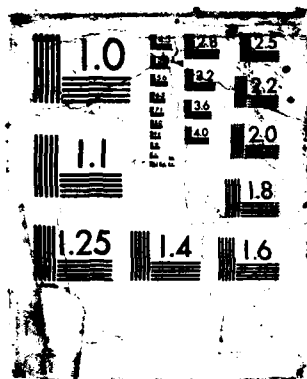
2/4

UNCLASSIFIED

F/G 20/3

NE







masses not directly working to hold the energy, the energy density of the assembly is degraded. As these factors are invariably present, it can be seen that it is hard to attain an overall energy density greater than 10 kJ/kg. Knowing this, and the basic cost of raw materials, the minimum cost of a system can be estimated from the total stored energy [43].

Note that we are referring to the energy contained in the volume enclosed by the structural mass and not its own elastic energy, which is very small. Steel, for example, at 300 Mpa has a strain energy of only 30 J/kg.

### 3.5.3 Inferences concerning the ultimate energy density of capacitors

Energy storage in the dielectric of a capacitor is simple in concept - the energy is stored by the work that the applied field does in displacing electrons and polar atoms and molecules within the material. In principle the limitation to capacitive storage is the ability of the atomic nuclei to hold electrons as the applied field is increased. This simple model predicts dielectric breakdown at electric fields which would give peripheral electrons their ionization energies within interatomic distances. Since ionization energies are of the order of 10eV for good insulators and the distances are about  $10^{-10}$  m, it predicts breakdown field strength of the order of  $10^{11}$  V/m. If this were the case, then by working capacitors to 1/10 of the dielectric breakdown, energy densities of 1 MJ/kg would appear to be possible, based upon materials with a dielectric constant of 2 (electron polarization only at such high field strengths) and a density of  $1 \text{ g/cm}^3$ .

In fact the intrinsic breakdown fields of dielectrics have maximum values of around  $10^9$  V/m at which the stored energy density is about 10 kJ/kg. For the reasons discussed in Section 3.2.4 even this value far exceeds energy densities attained in practice.

Dielectric constants very much greater than 2 at fields of  $10^9$  V/m are probably unlikely because high dielectric constants require materials with highly polar molecules, and such materials tend to have lower breakdown strengths than non-polar, low dielectric constant materials.

The reason why intrinsic breakdown fields are such a small fraction of those required to directly ionize an atom is considered by von Hippel, Frohlich and Whitehead [44] to be that a few conduction electrons are inevitably present due to a variety of causes. Calculations by Frohlich show that if such electrons are present, then at fields of about  $10^9$  V/m they will gain sufficient energy in between collisions to eventually ionize the dielectric atoms and produce a gas discharge type of breakdown.

Capacitive storage involves forces upon the charges and in turn upon the electrodes and the dielectric and mechanical strength must be considered as well as dielectric breakdown. In a similar manner to the derivations at the beginning of this Section it can be deduced that the mass, M, of the dielectric of a simple parallel plate capacitor is:

$$M = \frac{\rho W}{\epsilon_0 C} \quad (3.9)$$

where  $\rho$  is the density of the dielectric material,  $W$  is the stored energy and  $\sigma_c$  is the compressive stress in the dielectric.

Equation (3.9) is the same as Eqn. (3.4) for the containment of magnetic energy, except that the stress is compressive. Stresses upon the metal electrodes and their masses must also be taken into account in obtaining the overall energy density. The result is that mechanical strength considerations probably set an upper limit of 10 kJ/kg for capacitive storage, regardless of the limit due to dielectric breakdown.

### 3.6 Battery and pulse transformer concept

Except for capacitors, all the power sources discussed in the previous sections are still being developed and except for the homopolar generator the development has a long way to go. At best the overall energy density of these systems may be 5 times (HPGs) to 20 times (explosives) greater than for capacitor systems, but are much more complicated. The compulsator and the reusable flux compressors have yet to be proven in real railgun firings. Explosives are a very compact primary energy store but pose handling and storage problems which detract from one of the possible advantages of the electric gun, viz. that it can eliminate explosives.

A method of supplying power to a railgun that does not seem to have been investigated is one based on batteries and a pulse transformer, as shown in Fig. 36.

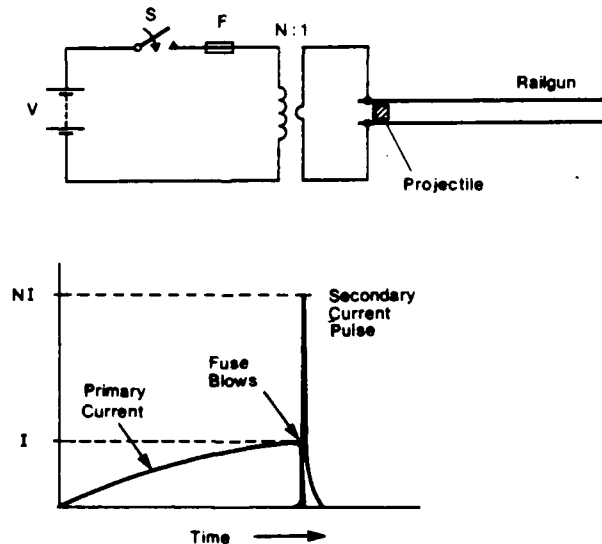


Fig. 36 Battery and pulse transformer power source.

In the battery and pulse transformer scheme the switch  $S$  is closed and the current in the primary rises to a pre selected value, at which time

the fuse, F, blows and rapidly interrupts the primary current. A current that is N times the primary current arises in the secondary during the rupture time of the fuse. The secondary current passes through the conducting material of the projectile and the secondary becomes the charged inductor that is needed to power the railgun.

Provided that the system works as described, it comes nearer to the ideal system described in section 3.1.4 than do the other systems. Firstly its switching is simpler; there is nothing more to the power train than is shown in the diagram. No switching is involved on the high current side. Whilst it involves an opening switch in addition to a closing switch, no other switches are necessary. The opening switch design is simplified (a fuse) by the low current to be carried and interrupted on the primary side. The energy necessarily dissipated in the opening switch can in principle be reduced to zero by tight primary to secondary coupling.

Secondly, batteries are a compact means of storing energy. Lead acid batteries have one of the lowest energy densities yet in 1 tonne they store 100 MJ. Batteries can therefore be used to store sufficient energy for many shots and so can be regarded as the prime energy store.

Thirdly, use of the transformer reduces the mass of the batteries so that the scheme is competitive with the other systems. This is because the primary charging time is much longer than the secondary discharge time. For example, to accelerate the 5 gram particle mentioned in Section 3.2.2 to 10 km/s in one millisecond, using a lead acid battery connected directly to the rails, would require at least 1000 tonnes of batteries. Using a pulse transformer with a primary charging time of one tenth of a second, the battery mass is reduced to 10 tonnes, the same mass as was calculated for a high voltage capacitor system. If the charging time was one second, the battery mass would become 1 tonne, which would be comparable to that of one shot destructive explosives systems.

Fourthly, the energy is contained safely in chemical form in the batteries, which may be subdivided into many small units so that an internal short circuit does not produce destructive release of the total energy, much more easily than for capacitors. The transformer is inherently much safer than machines with rapidly rotating flywheels.

Finally, the cost of the system should be low because the batteries, fuse and transformer, once they are understood and developed for the particular purpose, are very simple devices.

Because the battery and pulse transformer scheme has not received any attention for electromagnetic launching, and because it has some attractive possibilities, it is investigated in detail in this Report.

## CHAPTER 4

### GENERAL CONSIDERATION OF THE BATTERY AND PULSE TRANSFORMER POWER SOURCE

This Chapter is the beginning of the investigation into the battery and pulse transformer power source for the railgun. The requirements and advantages of the scheme are examined, for the scheme as a whole and in terms of the main components, viz. the transformer, the battery and the fuse (or opening switch).

The scheme is compared with a battery-inductor scheme that is free of problems that are due to the transformer, but the low current of the transformer is thought to be a more important advantage.

The Brooks Coil is used to estimate the overall pulse energy densities that may be achieved. It is found that 1 kJ/kg can be approached provided the battery can supply 1 kW/kg and the transformer is cooled to the temperature of liquid nitrogen.

Because of the major influence of the power density of the battery upon the total mass, the maximum power density of lead-acid batteries is estimated in a detailed study.

#### **4.1 Limitations of the pulse transformer scheme**

In Ch. 3 a number of advantages of the battery and pulse transformer power source were listed. There are, however, limitations. The transformer itself introduces three parameters which must have acceptable values for the scheme to work, viz. the high voltage that is induced in the primary, the coupling of the primary and secondary and open and short circuit conditions required for the secondary.

##### **4.1.1 High voltage across the primary**

The voltage which is across the secondary while it discharges into the railgun also appears across the primary, stepped up according to the turns ratio. The voltage across a railgun with an inductance of  $0.5 \mu\text{H/m}$  and a current of 500 kA is at least 2.5 kV when the projectile reaches 10 km/s, so if the transformer has a turns ratio of 100, the primary voltage is at least 250 kV.

Dielectrics such as those used for capacitors can withstand 100 V/ $\mu\text{m}$ , so in principle about 0.25 cm thickness of such material would suffice for insulation. Polythene has been reported to withstand 1MV RMS/cm for 40 minutes without breakdown [1]. The short time (milliseconds) for which the high voltage pulses would be present in the pulse transformer decreases the likelihood of breakdown.

Breakdown of air around the primary, unless it actually damages the insulation, would not affect the pulse transformer performance because the great majority of the secondary energy would discharge into its own circuit.

The high voltage across the primary though ultimately limits the number of primary turns, which otherwise could be as many as desired to reduce the primary current. Where there is danger of high voltage breakdown, protective spark gaps might be installed across the primary to prevent damage to insulation.

#### 4.1.2 Coupling between primary and secondary must be tight

It is well known that it is difficult to open a switch in an inductive circuit carrying high current because of the arcing which occurs. The reason for the arcing is that the magnetic energy of the circuit must be disposed of before current flow can cease. If the circuit contains a high power source of electricity there is danger of current continuing to flow via the arc, which in effect has short circuited the switch, until sufficient destruction occurs to interrupt the current.

In the pulse transformer the short circuited secondary ideally absorbs all the magnetic energy of the primary, thus eliminating the opening switch problem because the opening switch (the fuse) does not have to dissipate any of the stored magnetic energy. This situation would only occur, though, if the primary and secondary were perfectly coupled i.e. all the flux of one winding linked the other winding.

In Chapter 5 it is shown that the energy,  $W_{sw}$ , which is not transferred to the secondary, and hence which must be disposed of on the primary side when the fuse opens, is:

$$W_{sw} = (1 - k^2) W_1,$$

where  $k$  is the degree of coupling of the windings and  $W_1$  is the stored energy of the primary. Exploding type fuses can be reliably designed to dissipate energies in the tens of kilojoules range [2]. If a fuse which could dissipate 10 kJ were to be used to transfer 1 MJ from primary to secondary, the above equation shows that  $k$  would have to be at least .995, which is extremely tight coupling.

The upper limit to the energy which the scheme can handle is thus determined by the degree of coupling attainable and the ability of fuses (or other opening means) to dissipate the energy which cannot be transferred.

It is also evident that the design of the transformer so as to attain a high degree of coupling is a most important consideration.

#### 4.1.3 Open and closed circuit requirements of the secondary

Whilst the primary is being charged with the secondary closed, as indicated in Fig. 36, current will flow in the secondary by normal transformer induction. In fact, if the secondary were perfectly coupled to the primary and if the secondary also had zero resistance, the primary would be rendered non inductive and would not store energy at all. Ideally, during charging of the primary, the secondary should be open. At the moment when the fuse opens, though, it is vital that the secondary be closed otherwise all the primary energy will dissipate in the arc, possibly with destructive consequences, especially should the arc be maintained and the entire energy of the battery be discharged through it.

Since the secondary current that is induced during the charging of the primary flows in the opposite direction to that which flows when the primary circuit is opened, a diode may be used to automatically provide the open and closed functions. In plasma driven guns this diode might be a small expendable device placed across the railgun breech instead of a short circuiting foil. The destruction of the diode would then be the means of initiating the plasma arc. Synchronized mechanical switching of the secondary can also be imagined but would have to be incorporated without introducing stray inductance, which would degrade the coupling of the secondary circuit to the primary.

In Chapter 5 it is shown that the problem is in fact not too severe. So long as the secondary has a time constant which is short compared to that of the primary, the primary can be charged with very little effect from the closed secondary, and with relatively little induced current in the secondary. In the railgun application the secondary does have a short time constant compared to the primary, because its operating time is only milliseconds, whereas the primary must have a time constant of a second or so. Thus, it is possible to have the circuit operate as in Fig. 36.

#### 4.2 Transformer versus inductor

##### 4.2.1 Basic equivalence of battery/transformer and battery/inductor schemes.

The pulse transformer enables the current from the battery to be reduced to a small fraction of that needed to power the railgun. This requires the battery to be of series connected units which produce a relatively high voltage. Instead, the units could be connected in parallel and used to charge the secondary directly with the high current, as shown in Fig. 37. This is the battery-inductor scheme and would be free of the limitations of the transformer discussed above.

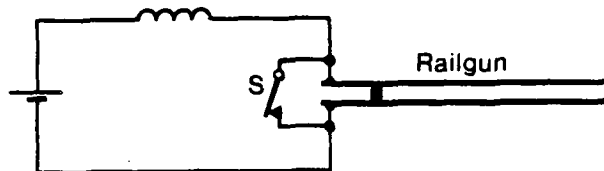


Fig. 37 simple battery-inductor power source

To compare the two schemes we note the following two points.

- (i) By cutting the primary of the transformer into  $N$  equal parts and connecting the parts in parallel with the secondary, the transformer could be converted into an inductor with the same mass as the transformer, the same inductance as the secondary and with virtually the same time constant as the transformer primary.
- (ii) By dividing the battery into  $N$  units connected in parallel its voltage is reduced to  $\frac{1}{N}$  of the battery voltage in the transformer scheme.

Because the inductor resistance is reduced to  $(\frac{1}{N})^2$  times that of the original primary, the maximum current from the rearranged battery and coil is  $N$  times the original primary current. The battery and transformer scheme could thus be rearranged as the battery-inductor scheme and charged in the same time as could the transformer primary and therefore would have the same ability to reduce the battery mass. There is no fundamental advantage of one over the other. The transformer system has the practical restrictions discussed in the previous section. The requirement for high degree of coupling means that the transformer design and construction is much more difficult than that of the inductor.

There are several requirements of the practical implementation of the inductor scheme though, of which the pulse transformer is free, and these may be more troublesome than the pulse transformer requirements. These are discussed in the following sections.

#### 4.2.2 Inductor scheme requires means of disconnecting the battery

The inductor scheme cannot actually be as simple as shown in Fig. 37; it requires a switching system similar to that in Fig. 28, so that it is possible to disconnect the battery. The battery, so far as stored energy is concerned, is like a homopolar generator which stores far more

energy than is extracted for a single shot. (It does not of course behave like the HPG in the sense that the HPG is similar to a capacitor.) The need for a switching system that enables the battery to be disconnected can be appreciated by considering the simplest battery/inductor system, shown in Fig. 37.

In Fig. 37, the battery charges the inductor to the required current, whereupon the switch S is opened and the current is diverted into the railgun. When the projectile leaves the muzzle of the railgun the energy remaining in the inductor and rails of the gun will cause an arc. Since the separation of the railgun rails is of the order of centimetres, it is possible that the arc will not cease to conduct simply by dissipating the energy remaining in the inductor. If the arc causes virtually a short circuit across the rails, the inductor may become recharged (which would only take a second or so) and so fuel the arc. The discharge could conceivably continue until the battery had exhausted its energy, dissipating hundreds of times the energy of a single shot in the system and probably destroying it.

The design and operation of shunt switch S2 and the series switch S1 and resistor R1 shown in Fig. 28 are not simple; they must carry currents of hundreds of kA and be synchronized with each other and the railgun operations. S1 and S2 must be certain to work because of the destruction which might ensue if they fail.

To minimize the ability of the battery to sustain an arc its voltage should be as low as possible (e.g. 10V). Low voltage means that it would take longer to charge an inductor and the inductor mass must be increased to give it a correspondingly longer time constant.

#### 4.2.3 Transformer scheme does not require a rail switch

The switch across the railgun in the battery/inductor scheme has the same requirements as in the HPG scheme, i.e. it must shunt the railgun for the time required to charge the inductor and then must divert the current into the railgun. Marshall and Barber's rail switch would therefore be suitable. In contrast, the secondary of the pulse transformer is rapidly charged during the explosion of the fuse and so can be charged via a short circuiting foil across the railgun breech in a similar manner to the high voltage capacitor powered railgun.

Although the rail switch is a proven practical means [3] of diverting the inductor current into the railgun it must suffer some damage at its trailing edge each time it is used. This is because there must be an arc between one rail and the conducting leaves at the trailing end of the switching slug as they break contact and switch extra inductance into the circuit at the railgun gap (see Fig. 28). Maintenance or replacement of the switching slug is therefore necessary. Even if the rail switch were to work for a large number of shots without attention it is a considerable complication to the breech region of the railgun.



#### **4.2.4 Batteries can be conveniently located in transformer scheme**

In the inductor scheme the leads from the battery to the inductor must have resistances in the micro-ohms region to carry currents of hundreds of kA without excessive voltage drop. Consequently the leads must be massive busbars and the battery must be adjacent to the inductor so that they are as short as possible. The magnetic forces on them must also be considered as the forces could be of similar magnitude to those in the railgun.

The greatly reduced current in the transformer scheme enables the leads to be much less massive (e.g. 1/10) and enables the batteries at the same time to be located further away (e.g. 10 times as far). These are important practical advantages; it should be remembered that the massive busbars required was one of the reasons why the attempt to build an electric gun in Germany was abandoned.

### **4.3 Overall system energy density**

#### **4.3.1 Interaction of battery, coil and charging time**

Although batteries store energy very compactly, (e.g. 100 kJ/kg for lead-acid batteries), the energy can be released only slowly. The slow release of the energy means that batteries must be regarded as sources of power and their effective pulse energy density in a pulse type of application depends on the duration of the pulse. A battery which can deliver power at 100W/kg, if used in 1 second pulses, has an effective pulse energy density of 100 J/kg. If it is used in 10 second pulses it has an effective energy density of 1kJ/kg. Since the mass of a system must be greater than that of the battery alone, the overall system pulse energy density cannot exceed that obtained from the battery.

The greater the length of time for which the primary of the pulse transformer can be charged, the greater will be the effective pulse energy density of the battery. The length of time which can be selected for the charging is limited by the coil time constant; very little energy is stored after about 3 time constants. Long charging times require correspondingly long coil time constants, i.e. a low coil resistance and therefore a more massive coil. Long charging times are undesirable from the operational viewpoint because they limit both the response time and the firing rate of the railgun.

From the previous two paragraphs it is apparent that there is a maximum energy density that is attainable, because the coil mass must be increased in order to reduce the battery mass.

#### **4.3.2 Examples based on Brooks Coil**

To convert the above ideas into figures we can suppose that a Brooks Coil is charged from a battery. The Brooks Coil is not suitable as the primary of the pulse transformer, but as it has the longest time constant for a given mass it will yield the maximum values for overall pulse energy

density. If suitable values cannot be obtained with the Brooks Coil they will not be obtainable with any other winding form. (The Brooks Coil is further described in Ch. 6).

Gröver [4] gives the mass of the Brooks Coil in terms of its time constant as:

$$w = 0.05027 \tau^{3/2} \text{ kg (copper, at room temp.)}$$

where  $w$  is the coil mass and  $\tau$  is the time constant in milliseconds. If we select the time constant as 1 second, the above equation yields a coil mass of 1.6 tonnes. To store 1MJ in this coil in 1 second using a battery capable of charging the coil at an average rate of 1 kW/kg would require 1 tonne of battery. Thus we would have 1 MJ stored in the coil from 2.6 tonnes of battery and coil, or an overall energy density of 384 J/kg. This energy density is intermediate between that of capacitors and the advanced homopolar generator (remembering that the HPG uses a liquid nitrogen cooled coil). If the battery also stores 100 kJ/kg and the efficiency of charging is 50%, about 50 shots could be fired before it was necessary to recharge the battery.

Commonly, lead acid batteries are reckoned to deliver only about 100W/kg; 10 tonnes of such batteries would be needed to charge the coil with 1 MJ in 1 second and the overall energy density would drop to 86 J/kg i.e. somewhat less than that of capacitor systems. Alternatively, 1 tonne of batteries capable of 100 W/kg could deliver 1 MJ to the coil if its time constant was increased to 10 seconds. In this case the coil would have a mass of 50 tonnes and the overall energy density would be only 19 J/kg. Obviously, it would be preferable to increase the mass of the batteries, because, as well as yielding a greater overall energy density, a greater number of shots (500) could be fired and with a more rapid response (1 second instead of 10 seconds).

Instead of increasing the coil time constant by increasing its mass, the time constant could be increased by a factor of 7, compared to room temperature, by cooling the coil with liquid nitrogen. Thus, cooling the 1.6 tonne coil would increase its time constant to 7 seconds. In this case 1.4 tonnes of batteries capable of 100 W/kg would be needed to charge the coil in one time constant, yielding an overall energy density of 330 J/kg. The improvement in energy density must be balanced against the complexity of the cooling. Using liquid nitrogen cooling, a coil with a time constant of 1 second would have a mass of 90 kg. Together with a battery capable of charging it at an average rate of 1 kW/kg for 1 second, a 1 MJ system would have an overall mass of 1.09 tonnes and hence an energy density of about 900 J/kg, i.e. about the same as the advanced H.P.G. system.

The energy density of the 1.6 tonne coil used to store 1 MJ is 600J/kg. Based on a typical strength of copper, the theory in Chapter 3 predicts that 10 kJ/kg is possible. The mechanical strength of the coil is therefore under utilized. For the 90 kg liquid nitrogen cooled coil, the energy density is about 11 kJ/kg i.e. the mechanical strength is well utilized.

In the table below, the various options are summarized.

Summary of 1MJ Brooks Coil and battery combinations

Charge time = Coil Time Const.	Coil		Battery : 100 W/kg			Battery : 1 kW/kg		
	Mass	Energy Density	Batt. Mass	Overall Energy Density	No of 1 MJ Shots	Batt. Mass	Overall Energy Density	No of 1 MJ Shots
1 sec. Room Temp.	1.6t	600 J/kg	10t	86 J/kg	500	1t	384 J/kg	50
1 sec LN <sub>2</sub> cooled	90 kg	11 kJ/kg	10t	99 J/kg	500	1t	900 J/kg	50
7 sec. LN <sub>2</sub> cooled	1.6t	600 J/kg	1.4t	330 J/kg	70	140 kg	575 J/kg	7
10 sec Room Temp.	50t	20 J/kg	1t	20 J/kg	50	100 kg	20 J/kg	5

The discussion in this Section leads to the conclusion that batteries capable of at least 1 kW/kg together with liquid nitrogen cooled coils are necessary to yield pulse energy densities that approach 1 kJ/kg and are comparable to those of advanced HPG systems. With batteries capable of 100W/kg, the charging times must be ten times longer and the overall pulse energy densities are comparable to those of capacitor systems.

#### 4.4 Batteries

It is evident from the previous Section that the battery has a great bearing on the performance of the pulse transformer system in two ways, viz. as a prime energy store which determines the number of shots and as a source of high power electricity that suits the transformer.

We shall now examine these aspects in relation to lead-acid batteries, especially power density.

#### 4.4.1 Safe, low mass prime energy store

The railgun power source problem includes the provision of sufficient energy for a large number of shots, i.e. it includes consideration of the prime energy store. Except where the prime source of electricity is also provided for other purposes, e.g. the electricity grid, its mass must be included in the overall mass of the railgun system.

There are three forms of energy storage which may be utilized for the railgun; these are fuels, explosives and batteries. They all store energy in chemical form, which is to say by means of the inner forces of molecules, and this is much more compact than storage in flywheels and capacitors.

The most compact storage is in hydrocarbon fuels, which, provided they are burned in air breathing engines, can be reckoned to store energy at 40 MJ/kg. Taking into account the efficiency of diesel motor generator sets (20 - 25% [5]) about 8 MJ of electrical energy can be obtained from each kilogram of hydrocarbon fuel.

Explosives store several megajoules per kilogram, which may be converted to electricity by flux compression devices as discussed in Ch. 3 or by explosive MHD generators [6] (which appear not to have been examined for railguns). The low conversion efficiency of these methods ( $\approx 5\%$ ) means that only about 100 kJ of electrical energy can be obtained per kilogram of explosive.

Batteries (and fuel cells which are presently impractical) are in principle ideal devices for storing energy for electrical systems because they convert chemical energy directly into electrical form without additional apparatus and with 100% efficiency. Lead-acid batteries store about 100 kJ/kg, which is one of the lowest energy densities of all the various types of batteries.

On the above figures, it requires the same mass of explosives as of lead-acid batteries to obtain a given electrical output. Since the safety problems associated with the storage of say 1 tonne of explosives are vastly greater than with 1 tonne of batteries, to say nothing of the complexity of the conversion system associated with the explosives, batteries are preferable. The batteries must eventually be charged, but this can be done at a low rate over a long time, and hence by means of a small motor generator set, from hydrocarbon fuel at the rate of 8 MJ/kg.

Unfortunately, ordinary motor generator sets cannot provide the power to charge railgun inductors in a short enough time. This is the whole reason for the developments discussed in Ch. 3, and is further examined in Sect. 4.5. The conclusion from this discussion is, therefore, that a mass of batteries sufficient to provide enough energy for a burst of shots and a tank of hydrocarbon fuel, together with a small motor generator, comprise a prime energy source of high power electricity which is safe and as compact as possible.

#### 4.4.2 The pulse power density of lead-acid batteries

Although batteries, together with a small motor generator and a fuel tank, yield a safe and low mass prime energy store and the pulse transformer system has simple switching, the most important measure is the energy which the pulse transformer system can deliver per shot from its total mass, i.e. the pulse energy density.

The work in Section 4.3 shows that for a battery based power source to attain an energy density of 1 kJ/kg the battery must have a power density of at least 1 kW/kg. This calls for "high rate" discharge batteries. Such batteries have been developed, for military purposes in particular [7]. The silver oxide-zinc battery is a notable example; it has energy and power densities at least four times those of lead-acid batteries [8]. The most practical battery to consider in this study is the lead-acid battery because of its availability and low cost and because it appears to have the potential for high rate performance.

From elementary theory the maximum power delivered by a battery occurs when the load resistance equals the battery internal resistance. This is complicated by the effects of the chemical reaction which cause the battery voltage to decrease rapidly when it is heavily discharged.

Information about the power produced by commercial lead-acid batteries loaded to the above condition is not generally available and often is not known by the manufacturers. A value of 100 W/kg is spoken of, based upon the most common high rate application, viz. cranking of engines, for which a typical specification is 350A for 30 seconds and a terminal voltage not less than 7.6 V at -18C. A battery which meets this specification has a mass of about 24 kg.

There is also little in the literature concerning the maximum power density of batteries. The present interest in electric vehicles is raising the matter because a power density of 100-200 W/kg is required to give electric vehicles adequate acceleration and hill climbing ability [9]. In the case of electric vehicle batteries, these figures must be achieved in conjunction with high energy density (200 kJ/kg) and long cycle life (1000 cycles). These requirements, long cycle life in particular, could be sacrificed in the case of a railgun battery. The writer (DRS) found four instances where high rate power densities of lead-acid batteries are reported in the literature.

- (i) The "Cyclon" cell, 600 W/kg maximum power density. Duration not given [10].
- (ii) Aircraft starting battery, 24V, "Chloride", 400 W/kg for 50 seconds at 1.42 volts per cell [11], which implies 470 W/kg maximum power density.
- (iii) Experimental electric vehicle battery, 650 W/kg maximum power density, duration not specified [12].

- (iv) Experimental electric vehicle battery, 440 W/kg maximum power density, duration not specified [9].

To determine the power density of batteries for periods of seconds, the writer short circuited various types of automotive starting batteries and recorded the battery voltage and battery current. Fig. 38 is a typical record, although the results vary greatly from one battery to another. (More results and discussion are given in Chapter 10).

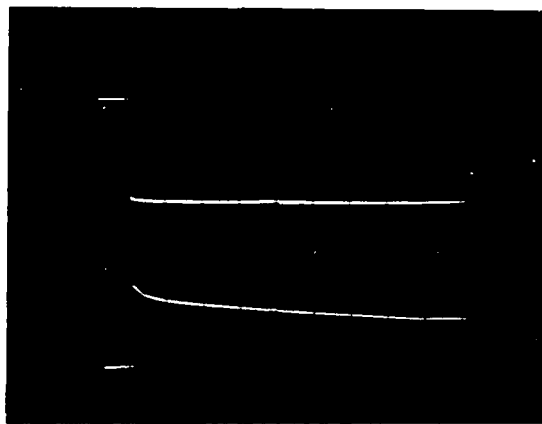


Fig. 38 9 seconds short circuit test on Exide "Torque-Starter" battery. Lower trace is the battery current (800A/div), upper trace is the battery voltage (4V/div). Time is 1 second/div. Battery voltage prior to test is shown for the first second of the trace. Battery mass = 14 kg.

From Fig. 38 it can be seen that the current diminished to about half its initial value after 9 seconds. The average current during the first second was about 1500A, and since the battery voltage fell 10.5V the internal resistance was about 7 mΩ. The maximum power from the battery for the first second would therefore be about  $(6.25)^2 / 7 \times 10^{-3} = 5.58 \text{ kW}$ , or about 399 W/kg, since the battery mass was 14 kg. The average power density during the 9 second discharge would be about 300 W/kg.

The tests carried out showed that automotive type batteries can deliver energy into matched loads at rates in the range 270W/kg for 10 seconds to 1 kW/kg for 1 second. These batteries are the products of designers in pursuit of high cranking power at low temperature for the automotive market and the short circuit currents at room temperature are more or less accidental results from that effort.

The above tests carried out by the writers upon the newest types of automotive starting batteries and the published values up to 650 W/kg suggest that a lead-acid battery could be constructed to have a maximum power density of 1 kW/kg for several seconds.

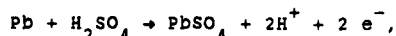
#### 4.4.3 Factors limiting the high rate discharge of lead-acid batteries

We shall now review the theory relevant to high rate discharge of the lead-acid battery and then apply it to estimate its maximum feasible power density.

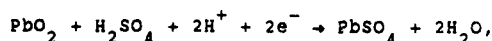
Electrical energy is released at the rate of 600 kJ/kg from the substances that actually react in the lead-acid battery. The overall energy density of the battery is about 100 kJ/kg because the active substances are not fully used due to polarization and because of the need for electrodes with which to collect the current and the need for a container. If all the molecules of the reacting substances could contact each other simultaneously their entire mass would react simultaneously with the production of a pulse of electrical energy at the rate of 100 kJ/kg. If this condition could be attained, 100 kJ/kg electrical pulses could be produced in times similar to those for explosive reactions.

Let us now consider the reactions in the lead-acid battery and identify the factors which prevent such a rate.

When the external circuit of the battery is closed, electricity is produced by the complementary need in the chemical reaction for electrons and  $H^+$  ions to be given up at the lead plate and supplied to the lead dioxide plate. The reactions are [13]:



at the lead, or negative, plate; and



at the lead dioxide, or positive, plate (via intermediate reactions).

The electrons reach the positive plate through the external circuit and the  $H^+$  ions reach it by passing, as current, through the electrolyte.

There are two basic restrictions to the rate at which the above reactions may proceed. One is the rate at which electrons and  $H^+$  ions are able to reach the positive electrode. The resistance of the circuit, including the resistance of the lead, lead dioxide and electrolyte, determines this limit. The other restriction is the rate at which lead and electrolyte ions arrive by diffusion at the electrode - solution interfaces of both plates from the bulk to replace those that have been used up, or in other terms, the

rate is determined by the equilibrium concentrations at the electrode "double layers" [13].

The lead sulphate, which is produced in solution at both electrodes and is immediately deposited as crystals, impedes the diffusion of lead and electrolyte ions from the distant regions to the interface region and also increases the electrical resistance. Until the proportion of lead sulphate is relatively high (60-70% of the active materials converted), which is towards the end of the battery's useful discharge capacity, the lead sulphate does not greatly increase the ohmic resistance [14]. When the battery is nearly fully charged it has a negligible contribution to ohmic resistance.

The effect of lead sulphate on diffusion is more serious. In particular it inhibits the passage of lead ions ( $Pb^{++}$ ) from the active materials and into solution [15]. The degree to which this limitation occurs depends upon the nature of the electrodes; fine pores become blocked. The lead sulphate is deposited with many cracks and imperfections rather than as a uniform layer and it is not until the active masses are largely converted that it virtually prevents the passage of lead ions.

Water is produced at the positive electrode, as well as lead sulphate. The water dilutes the acid, which must have a specific gravity greater than about 1.1 for the reaction to proceed. The water also increases the electrical resistance of the electrolyte, approximately doubling it if the battery is deeply discharged. As with the lead sulphate, the water has the greatest effect in fine pores. Calculation shows that the volume of electrolyte required is about 18 times that of the lead dioxide. Long, narrow pores would be depleted of acid before the active material at the pore surfaces had been used up, and furthermore, diffusion between the liquid within such pores and the fresh electrolyte outside them would be slow.

We now have to consider the relative importance of the above factors in the context of maximum rate discharge for periods of seconds, with such time between the discharges that diffusion reestablishes the acid concentrations.

The limiting effect of the lead sulphate upon the diffusion of lead ions can be distinguished from that upon the diffusion of the electrolyte. The release of divalent lead ions ( $Pb^{++}$ ) from the tetravalent lead ions ( $Pb^{++++}$ ) of the lead dioxide electrode requires the supply of electrons and thus can only occur when the battery is delivering current. Electrolyte diffusion, however, can take place when the battery is allowed to rest. Therefore, if lead ion diffusion is the limiting factor the battery will not recover when it is allowed to rest, even though the electrolyte specific gravity is adequate.

The above discussion leads to the conclusion that while a battery has useful capacity, electrolyte depletion must be the factor that causes the current to decline from its initial, ohmically determined, value. At the positive electrode, not only is the electrolyte used up, but water is formed as well. We therefore conclude that for maximum rate discharges for periods of seconds (e.g. up to ten seconds), the positive electrode needs particular attention.



The current waveform in Fig. 38 can now be explained. While the battery was at rest before the test, the ion concentrations in the electrode interface regions reached their maximum values. The initial current peak is limited only by the ohmic resistance of the circuit, and exceeds the rate at which the ion concentrations can be replenished. The current declines for about a third of a second towards an equilibrium value. The generation of water, and, to a lesser extent, lead sulphate, continues to reduce the diffusion rates and the current continues to decline, but at a slower rate.

The water also causes the electrolyte resistance to increase, but for short duration discharges the resistance increase is too small to cause the current to decline.

#### 4.4.4 Design and performance of a high rate lead-acid cell

We shall now estimate the power density of a lead-acid battery constructed to minimize the rate reducing factors that we have just discussed.

Firstly, the ohmic resistance must be low enough that the power density can attain desirable values. Most of the resistance is due to the electrolyte, so the electrodes should be as close together as possible and of as great a surface area as possible. The increase in resistance due to dilution by water can be prevented by providing enough acid to prevent the S.G. falling below about 1.2, starting with an S.G. of 1.3.

Secondly, diffusion must be maximized, i.e. the electrolyte must have easy access to the active materials, especially at the lead dioxide electrode. Since pores restrict the access, we shall suppose that the electrodes are thin foils upon which the active materials are formed as thin films. This means that large areas are needed for capacity, but large areas are consistent with low electrolyte resistance. Porous structures are used to give high capacity in a small volume, so to gain high diffusion rates we sacrifice energy density. A compromise might be to use a surface with a short bristle like structure.

According to Vinal, each AH of charge (i.e. each 3600 Coulombs) produced by a lead-acid cell consumes [16]:

Pb	3.866 grams, having volume	0.341 c.c. (S.G. = 11.34)
PbO <sub>2</sub>	4.463 grams	0.476 c.c. (S.G. = 9.4)
H <sub>2</sub> SO <sub>4</sub>	3.660 grams	2.815 c.c. (S.G. = 1.3)

from which it yields:

PbSO <sub>4</sub>	11.32 grams	1.797 c.c. (S.G. = 6.3)
H <sub>2</sub> O	0.672 grams	0.672 c.c. (S.G. = 1)

Additional H<sub>2</sub>SO<sub>4</sub> must be provided to prevent its S.G. falling below 1.2. Calculation shows that 18.4 c.c. are required to be provided instead of just the 2.815 c.c. actually consumed [17].

Dividing the above volumes by 3,600 yields the average thicknesses of the substances per coulomb per  $\text{cm}^2$  (i.e. per  $2 \text{ J/cm}^2$  from a 2V cell):

Pb	1.0 $\mu$
PbO <sub>2</sub>	1.3 $\mu$
Electrolyte	51 $\mu$
PbSO <sub>4</sub>	2.5 $\mu$ (each electrode)
H <sub>2</sub> O	1.9 $\mu$ (PbO <sub>2</sub> electrode)

The thinness of these average layers confirms the feasibility of thin foil construction with formed active surfaces.

A cell with electrodes of  $1 \text{ m}^2$  and the above thickness of active materials could produce an electrical pulse of 20 kJ, in principle. If there was 1mm of electrolyte between the electrodes and the Pb and PbO<sub>2</sub> layers were increased to 20  $\mu$  and 26  $\mu$  respectively, 400 kJ could be obtained from about 1.8 kg of active materials. Let us now check the performance of such a cell in terms of ohmic resistance and diffusion.

The resistance will be approximately that of the electrolyte, taking the electrolyte resistivity as  $1.3 \Omega\text{-cm}$  yields  $13 \mu\Omega$  for the cell resistance, which could dissipate 308 kW from the 2V cell and in principle could discharge the cell in 1.3 seconds. The ultimate power density as set by ohmic resistance is thus about 75 kW/kg, allowing 2.2 kg for electrodes, extra active material and a container, and thus a total mass of 4 kg.

Diffusion will greatly reduce the above power density. With the large area thin film electrodes that we are assuming the high rate limitation is chiefly due to electrolyte depletion at the positive electrode, which has a greater need for electrolyte than the negative electrode [16] and at which the electrolyte is diluted by the production of water. An estimate of the rate of diffusion from the bulk electrolyte to the water layer can be obtained from the following expression [16]:

$$Q = D AC (a/r)$$

in which Q is the quantity of electrolyte diffusing per unit time; D is the diffusion coefficient (at least  $1 \times 10^{-5} \text{ cm}^2/\text{sec}$ ); AC is the difference in concentration between the water and the bulk electrolyte ( $0.3 \text{ gm/c.c.}$ ); a is the aggregate area into which the electrolyte is diffusing ( $10^4 \text{ cm}^2$ ) and r is the depth of the pores through which the diffusion occurs. The thickness of the PbO<sub>2</sub> layer, if solid would be 26  $\mu$ ; allowing for extra material and that the PbO<sub>2</sub> is in fact a porous thin layer let us suppose r to be effectively 50  $\mu$ . Substituting in the above expression yields  $Q = 6 \text{ gms/second}$ . Since the positive plate consumes nominally  $3.660/2 = 1.83 \text{ gms}$  per 7.2 kJ of electrical energy, diffusion to the positive plate could support a discharge of 23.6 kJ per second.

In this calculation we assume that the water produced at the positive electrode is the single most important rate limitation; allowing for

other factors let us derate the above figure to 20 kJ/second i.e. 20 kW. Allowing the resistance of connections to be such that half the power is dissipated before reaching the terminals, the maximum delivered power is 10 kW.

Since the useful mass of the active materials is 1.8 kg, the total energy produced is 400 kJ. Assuming a total mass of 4 kg for the cell, we finally obtain an energy density of 100 kJ/kg and a maximum power density of 2.5 kW/kg, which diffusion could support until the 1.8 kg of active materials had been used up, i.e. for 20 seconds.

The diffusion calculation upon which the above result depends refers to still liquids. Other factors may improve the transport process by agitating the liquids, e.g. convection due to heating by the high rate discharge. It may be possible to assist diffusion, e.g. by vibrating the electrodes.

From the foregoing study it appears that it is possible to construct a lead-acid battery with a maximum power density of 2.5 kW/kg when dilution by water at the positive electrode is the chief limitation i.e. for several seconds before there is significant production of lead sulphate. If the lead sulphate can be deposited so that it does not greatly interfere until the active materials are mostly used up and the quantity of acid is sufficient that its resistance does not alter greatly, 2.5 kW/kg may be attained for 20 seconds. This performance may be at the expense of other desirable properties, cycle life in particular.

#### **4.5 Motor-generator instead of batteries**

##### **4.5.1 Power density of motor-generator sets**

If motor-generator sets had power densities greater than those of batteries, it would be preferable to use a motor-generator set to charge the transformer primary. Investigation of this possibility showed that motor-generator sets are unlikely to exceed 250 W/kg for 1 second times and therefore cannot compete with batteries.

The above figure is obtained as follows. The maximum power from a tuned up ordinary car engine is around 1 kW/kg [18]. From suppliers catalogs a "ball park" figure of 100 W/kg applies to generators, continuously loaded. If such a generator under maximum power condition could be overloaded for 1 second to deliver 500 W/kg, which is unlikely, since the study in Ch. 3 indicates that specially constructed flywheel machines are necessary for such an output, the overall power density when coupled to the engine mentioned, would be 250 W/kg.

That 250 W/kg is a generous assessment of motor-generator sets can be seen from the figures for an actual motor generator set, rated for 30 kVA continuously, and which has a mass of 1100 kg. The 1.5 second rating for this set is 45 kVA, or 40 W/kg, and is only 50% above the continuous rating. The designers of this set stated that they would not dream of applying a load to it equal to its internal resistance [19]. Whilst the generator might stand

such a test, the mechanical shock transmitted to the engine might break the connecting shaft or the crankshaft. The engine would have to be fitted with a large flywheel in which the desired amount of energy was stored, and decoupled from the engine when the electrical pulse was required. That, of course, brings us back to flywheel machines, discussed in Ch. 3.

#### 4.5.2 Response time limitation of motor-generator

Since a motor cannot go from off to full load at full speed in a fraction of a second, it must be running at the full speed prior to the demand for full power by the generator. If the time of the firing demand is unknown, the motor must run continuously at full speed with a fuel injection system, able to instantly supply the fuel for full power, synchronized with the firing demand. This is especially important if the system is not provided with a flywheel in which the energy for a shot is stored.

Batteries, however, can remain idle for long periods (e.g. a year) with no consumption of fuel and yet instantly supply full load power.

#### 4.6 The primary opening switch

##### 4.6.1 The mechanism of energy transfer

The purpose of the fuse, or other means of causing the primary current to cease, is to transfer the magnetic energy of the primary to the secondary. The energy transfer actually takes place through a chain of events. When the fuse commences to operate its resistance rapidly increases and the energy dissipated in it diminishes the stored energy. The primary current and the primary flux fall and the portion of the falling flux that links the turns of the secondary induces within the secondary an e.m.f. The secondary is charged by this induced e.m.f. and acquires energy from the field of the primary with which it is mutually linked.

Since the secondary will dissipate in its own resistance the energy that it receives, the secondary resistance must be small enough that the energy is not dissipated as fast as it is received. This means that the primary current must fall in a time that is short compared to the secondary time constant.

From the foregoing it can be appreciated that the important action of the fuse is to cause a rapid enough fall of primary current. The energy will be transferred to the secondary whatever means is used to bring about such a fall of primary current. Opening a switch across a capacitor in series with the primary would suffice, provided the capacitor and the effective inductance of the primary during transfer has a high enough resonant frequency. An advantage of this method over fuses is that the capacitor would not have to be replaced every shot, as does a fuse. Another method that has been proposed to replace fuses is to use liquid nitrogen cooled wires [20]. The wires are rapidly heated to a sufficient resistance, but not exploded, and so can be used repetitively. Carbon filled polymers are another possible reusable fuse material [21].

#### 4.6.2 Opening time, energy, voltage and resistance of the switch

Since the acceleration time in typical railguns is about a millisecond, the energy of the primary should be transferred in about 100  $\mu$ s and the time constant of the secondary should be several milliseconds. The resistance introduced into the primary should therefore cause the primary current to fall to zero in 100  $\mu$ s.

We have previously discussed the fact that the energy which does not transfer to the secondary must be dissipated in the opening switch, and that the amount of energy is determined by the coupling between the primary and secondary. If the current is assumed to fall linearly with time during the opening of the primary, and we know the energy to be dissipated, we can estimate the average voltage across the switch. Thus, if the primary current,  $I$ , is 5000A and is reduced to zero in  $t = 100 \mu$ s together with the dissipation  $W_{sw} = 10$  kJ in the switch, then

$$W_{sw} = V \frac{I}{2} t,$$

from which the voltage,  $V$ , across the opening switch is 40 kV.

From the above expression, we see that the shorter the opening time, the greater the voltage which the switch must withstand during opening. Opening times which are unnecessarily short compared to the secondary circuit requirement should be avoided because of the high voltage across the switch.

With 40 kV across the fuse at 5000A, its resistance would be 8 ohms. When the resistance has reached 80 ohms all but 1% of the energy would have transferred to the secondary. This shows that it is not necessary for the fuse to attain what is normally considered an open circuit.

During the transfer of energy from the primary to the secondary, the turns per volt are not the same for each winding. If the primary energy transferred to the secondary in 100  $\mu$ s was 2 MJ, and if the secondary current was 500 kA, the secondary voltage would be about 80 kV. If the turns ratio was 100 and the same rate of change of flux affected each winding, the primary voltage would be 8MV. The rising current in the secondary, however, induces a counter e.m.f. in the primary which reduces the primary back e.m.f. to 40 kV.

#### 4.6.3 Fuses and vacuum arc switches

The major challenge in the design of the opening switch is to absorb the energy that cannot be transferred without the switch breaking down and reclosing the circuit. Fuses are an effective means of doing this because the energy is got rid of by using it to destroy the switch.

The actual mechanism by which the fuse works is that the energy to be dissipated converts the metal of the fuse to a vapour at temperature and pressure conditions such that the vapour is a poor conductor. The vapour is

condensed in a medium (e.g. sand) so that it is too dispersed to conduct. The basis of design is to select the mass of metal such that its vapourization energy equals the energy to be dissipated. If there is too much metal, it will not be properly vapourized and if there is too little, the excess energy will ionize the vapour [22].

Fuses, in the form of exploding wires or foils, have been developed over the past 30 years for the transfer of energy from one inductor to another in thermonuclear fusion experiments. Designs which can absorb 70 kJ have been reported [23]. Wires exploded in water have been reported to withstand 1.3 kV/cm for milliseconds [24] and 16 kV/cm for microseconds [25].

Unless an opening switch is placed across the fuse to divert current into it, the fuse design must be such that it does not commence to rupture until the desired current is reached. This requirement seems to be able to be met, in general, because the fuse action culminates in a rapid positive feedback process. The more the fuse heats, the higher its resistance becomes.

A switch which could function upon an electrical command as either a closing switch or an opening switch would be preferable to the closing switch and fuse in Fig. 36. Because there is a general need for reusable opening/closing switches in inductive-circuits, attempts are being made to devise such switches. The vacuum arc switch being developed by Gilmour [26] is an example (Fig. 39).

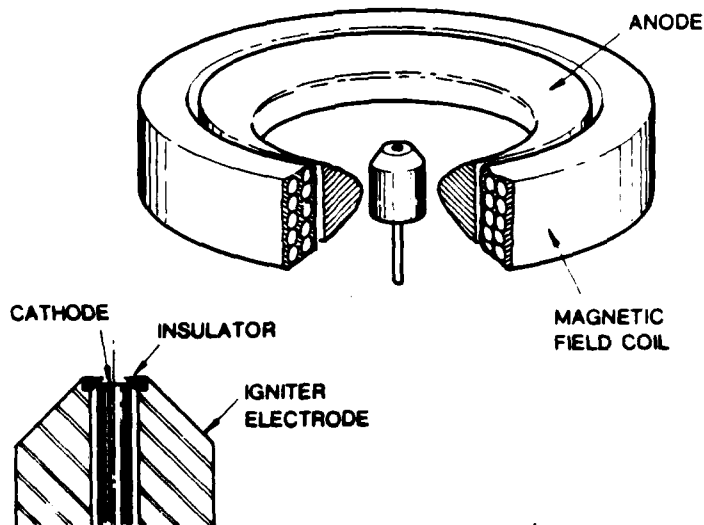


Fig. 39 High voltage arc interrupter (Gilmour)

To turn the switch on, a pulse is applied to the igniter electrode. The igniter electrode has a metallic film deposited on it which enables it to generate a plasma and conduct between cathode and anode. As an opening switch, it works by the magnetic blow-out principle. A pulse applied to the field coil sets up a magnetic field which causes forces on the current carriers travelling between anode and cathode. These carriers must in effect climb a hill, in the process causing a large voltage between anode and cathode and absorbing the circuit switching energy. Eventually the carriers (presumably mostly electrons) strike the anode. The anode thus is the structure in which the energy is ultimately given up, as heat.

#### 4.7 Previous use of pulse transformer method

Although the pulse transformer concept for generating a high pulsed current is simple, it appears to have been investigated only a few times. The writer has found only three accounts in the literature.

The first attempt was by Peter Kapitza at the Cavendish Laboratory in 1924 [27]. He wanted to use the high current from the secondary to produce a high magnetic field in another coil. He did not analyse the factors involved and evidently tried to use mechanical switching. He found it impossible to prevent sparking and the loss of all the energy and abandoned the idea.

The next use of the idea seems to have been by Walker and Early at the University of Michigan in 1957, 58 [28]. They did not analyse the factors involved in detail, but successfully produced a 117:1 current step up transformer to transfer 105 kilojoules to a load at 525 kA. Walker and Early's papers [28,29] are frequently cited, hence the pulse transformer concept must be widely known. The reason for their papers being frequently cited is probably that they established several basic practical features of inductive storage, e.g. the economic advantages with coil size, the use of flywheel machines to store the energy with which to charge the coils and the use of mechanical switches in parallel with exploding wire fuses to transfer energy.

The third account of the idea was given [30] in 1979. The objective in this case was to generate megavolt pulses at powers of  $10^{11}$  watts by dumping the stepped up current in the secondary into a resistive load. The pulse transformer is not suited to this because of the stepped up voltage across the primary, and the idea was not actually put into practice.

None of these attempts, it seems, was based on a detailed study of the power supply, switch and transformer interactions.

#### 4.8 Current transformer concept

We have discussed a number of problems and advantages of the transformer scheme and similarly of the inductor scheme. A method of obtaining the advantages of each is shown in Fig. 40, in principle.

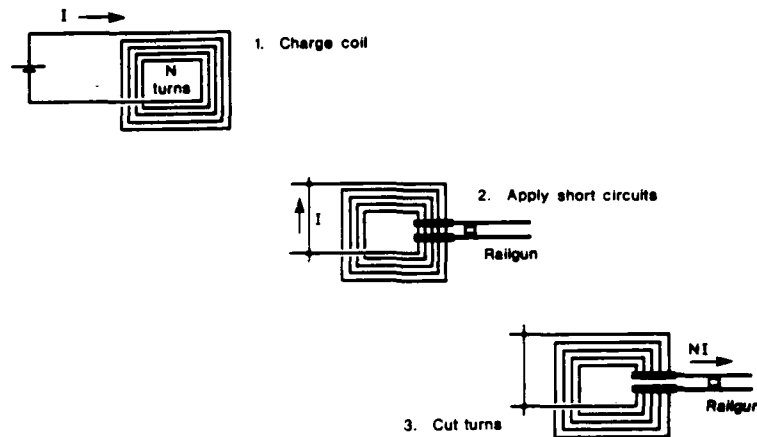


Fig. 40 Current transformation using one winding.

Firstly, the coil is charged with current,  $I$ . Secondly, the busbars of the railgun are shorted across the turns as shown in the second diagram. The coil has a very low resistance so that the circulating current is not affected by the busbars. Finally, the turns between the shorting busbars are severed. The current in each of the turns diverts via the busbars and redistributes via the turns on the other side and continues its flow around the  $N$  turn circuit. The current through the railgun, however, is  $NI$ .

The effect is that the turns are charged with current when in series and discharged in parallel, corresponding to the way in which capacitors are charged in parallel and discharged in series to obtain high voltages.

If the coil connections could be remade and the busbars removed, the current would resume its path through the coil alone. In this way the energy of the coil could be tapped.

The method retains the low current charging of the transformer. Since the same winding is used for both low current charging and high current discharging, it has in effect perfect coupling. There is no primary into which a high voltage is induced during the discharge into the load. Because there is no need to consider degree of coupling, the coil can have convenient geometry; in particular so as to be as compact as possible and to not produce external magnetic field.

The difficulty with the idea is in the switching. A set of make before break contacts can be imagined. The problem is the same as for the inductor scheme where the rail switch is used, except that the current is subdivided into perhaps 100 parallel paths which must be separately switched. The disconnection of the battery is not as difficult as with the inductor scheme because it is done at low current.



## CHAPTER 5

### ANALYSIS OF THE PULSE TRANSFORMER CIRCUIT

In Chapter 4 an overall view of the pulse transformer system was presented; in particular it appears competitive with advanced H.P.G. systems in terms of energy density per shot, given a not unreasonable improvement in the pulse energy density of batteries. The finer details of the scheme are now studied. Firstly, in this Chapter, the discharging and charging processes are analysed mathematically, irrespective of the actual form of the transformer. Secondly, in Chapters 6 and 7, the geometry of the transformer is considered.

#### 5.1 Energy transfer (discharge) equations

##### 5.1.1 Circuit parameters

The equivalent circuit of the pulse transformer system is shown in Fig. 41.

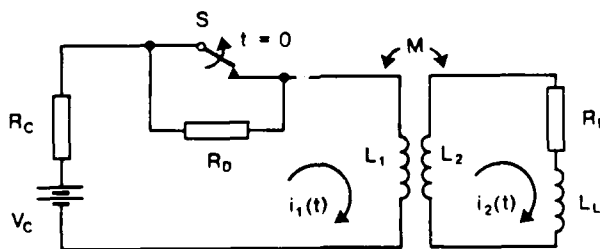


Fig. 41 Circuit for analysis of pulse transformer scheme.

The primary and secondary self inductances are  $L_1$  and  $L_2$  and  $M$  is the mutual inductance.  $R_C$  is the resistance of the primary circuit, including that of the voltage source  $V_C$ , when switch  $S$  is closed.  $R_L$  includes the secondary and load resistances and  $L_L$  includes the busbar and load inductances.

The fuse, or other means of opening the primary circuit, is represented by the switch  $S$  and parallel resistance  $R_D$ . It is impossible to define  $R_D$  mathematically, as it depends on the switching means and may have a strong interaction with the other circuit parameters. We shall suppose that from the manner in which a fixed value of  $R_D$  affects the discharge, the role played by the switch resistance can be adequately inferred.

In the following Sections the circuit will be analyzed, firstly, in a simple manner, and then rigorously by network analysis. The complex expressions from the rigorous analysis are then simplified and their physical meaning is discussed.

### 5.1.2 Simple analysis

For the simple analysis we assume that  $R_p$  has a large enough value that, when the switch is opened, the primary current falls to zero virtually instantly compared to the time required for appreciable energy to dissipate in the secondary circuit. In this case the flux linkages with the secondary are conserved while the primary current falls to zero. Let the current in the primary be  $i_1(t) = i_1(0)$  just prior to the opening of the switch. Then:

$$M i_1(0) = - L_2 i_2(0) \quad (5.1)$$

$$\text{i.e.} \quad i_2(0) = - \frac{M}{L_2} i_1(0) \quad (5.2)$$

where the flux linkages with the secondary prior to switching are given by  $M i_1(0)$  and  $i_2(0)$  is the secondary current immediately after switching.

$$\text{Since } M = k \sqrt{L_1 L_2} \quad (5.3)$$

where  $k$  is the degree of coupling between the primary and the secondary,

$$i_2(0) = - i_1(0) k \sqrt{\frac{L_1}{L_2}} \quad (5.4)$$

If the transformer windings are geometrically similar, then:

$$\sqrt{\frac{L_1}{L_2}} = \frac{N_1}{N_2} \quad (5.5)$$

where  $N_1$  and  $N_2$  are the primary and secondary turns, and so:

$$i_2(0) = - k \frac{N_1}{N_2} i_1(0) \quad (5.6)$$

The energy transferred to the secondary,  $W_2$ , is:

$$W_2 = \frac{1}{2} L_2 (i_2(0))^2 = \frac{1}{2} k^2 L_1 (i_1(0))^2 = k^2 W_1 \quad (5.7)$$

where  $W_1$  is the primary stored energy just prior to  $t = 0$ . The energy lost during the switching,  $W_{sw}$ , is:

$$W_{sw} = W_1 - W_2 = (1 - k^2) W_1 \quad (5.8)$$

The energy lost is dissipated in the resistance  $R_D$  since  $R_D$  was assumed to have a relatively high value compared to  $R_C$ .

Equations (5.7) and (5.8) show that the coupling factor determines the energy transferred to the secondary and the energy which the switch must dissipate, as was discussed in Chapter 4.

### 5.1.3 Rigorous Analysis

The simple analysis is independent of the value of the circuit resistances and gives no measure of how quickly the primary should be opened. These are the reasons for carrying out a rigorous analysis of the circuit. The analysis is in terms of the circuit time constants and thereby includes the circuit resistances.

Applying Kirchoff's voltage law to the primary and secondary at time  $t = 0^+$ , i.e. immediately after the switch is opened, we obtain:

$$V_C = (R_C + R_D)i_1 + L_1 \frac{di_1}{dt} - M \frac{di_2}{dt} \quad (5.9)$$

$$0 = R_L i_2 + (L_L + L_2) \frac{di_2}{dt} - M \frac{di_1}{dt} \quad (5.10)$$

Taking Laplace Transforms and using the initial conditions

$i_1(0^+) = i_1(0)$ ,  $i_2(0^+) = 0$ , and letting  $i_1(0) = \frac{V_C}{R_C}$ , i.e. the final value of the current which would flow if the primary were charged for a long time prior to  $t = 0$ , we obtain:

$$I_1(s) = \frac{V_C \left\{ \left( \frac{1}{s} + \frac{L_1}{R_C} \right) [s(L_L + L_2) + R_L] - \frac{SM^2}{R_C} \right\}}{[sL_1 + (R_C + R_D)][s(L_L + L_2) + R_L] - s^2 M^2} \quad (5.11)$$

$$I_2(s) = \frac{SM \left\{ V_C \left( \frac{1}{s} + \frac{L_1}{R_C} \right) - \frac{MV_C}{R_C} [sL_1 + (R_C + R_D)] \right\}}{[sL_1 + (R_C + R_D)][s(L_L + L_2) + R_L] - s^2 M^2} \quad (5.12)$$

Let  $T_1 = \frac{L_1}{R_C + R_D}$ ,  $T_2 = \frac{L_2 + L_1}{R_L}$ ,  $T_0 = \frac{L_1}{R_C}$  where  $T_0$  and  $T_1$  are the primary circuit time constants prior to, and after,  $t = 0$  and  $T_2$  is the secondary time constant. Let  $k^2 = \frac{M^2}{L_1(L_1 + L_2)}$  i.e. the coefficient of coupling between the primary and secondary circuits rather than of the transformer alone. With these substitutions we obtain:

$$I_1(s) = I_1(o) \frac{(s + \frac{1}{T_0})(s + \frac{1}{T_2}) - s^2 k^2}{s[(s + \frac{1}{T_1})(s + \frac{1}{T_2}) - s^2 k^2]} \quad (5.13)$$

$$I_2(s) = I_1(o) \frac{M}{L_L + L_2} \frac{\frac{1}{T_0} - \frac{1}{T_1}}{[(s + \frac{1}{T_1})(s + \frac{1}{T_2}) - s^2 k^2]} \quad (5.14)$$

Since  $k^2 \leq 1$  the roots of the quadratic expressions are real. We obtain next, factorizing the expressions:

$$I_1(s) = I_1(o) \frac{(s + \gamma)(s + \delta)}{s(s + \alpha)(s + \beta)} \quad (5.15)$$

$$I_2(s) = I_1(o) \frac{M}{(L_L + L_2)} \frac{\frac{1}{T_0} - \frac{1}{T_1}}{(s + \alpha)(s + \beta)} \quad (5.16)$$

$$\text{where} \quad \alpha, \beta = - \frac{[(\frac{1}{T_1} + \frac{1}{T_2}) \pm \sqrt{(\frac{1}{T_1} + \frac{1}{T_2})^2 - \frac{4(1 - k^2)}{T_1 T_2}}]}{2(1 - k^2)} \quad (5.17)$$

and  $\gamma, \delta$  are given by the same expression except that  $T_1$  is replaced by  $T_0$ . Using partial fractions and taking the inverse transforms we finally obtain:

$$i_1(t) = i_1(o) [\frac{\gamma \delta}{\alpha \beta} + \frac{(\gamma - \delta)(\delta - \alpha)}{-\alpha(\beta - \alpha)} e^{-\alpha t} + \frac{(\gamma - \delta)(\delta - \beta)}{-\beta(\alpha - \beta)} e^{-\beta t}] \quad (5.18)$$

$$i_2(t) = i_1(o) \frac{M}{(L_L + L_2)} \frac{(\frac{1}{T_0} - \frac{1}{T_1})}{(\beta - \alpha)} [e^{-\alpha t} - e^{-\beta t}] \quad (5.19)$$

Owing to the need to evaluate  $\alpha$ ,  $\beta$ ,  $\gamma$ ,  $\delta$  using (5.17) it is not possible to deduce much by inspection of equations (5.18) and (5.19). They can be readily evaluated by computer and the results presented in tables or graphs. A compact mathematical expression that is easy to evaluate and interpret is more useful than tables or graphs. In addition, we really need the expressions to directly use the values of  $T_0$ ,  $T_1$ ,  $T_2$  and  $k$  rather than an obscure function of these variables.

By noting some relationships between the roots of quadratic expressions we can obtain reasonably good approximations to (5.18) and (5.19) in terms of the desirable variables. The relationships are:

$$\alpha \beta = \frac{1}{(1 - k^2) T_1 T_2}, \quad (5.20)$$

$$\gamma \delta = \frac{1}{(1 - k^2) T_0 T_2}, \quad (5.21)$$

$$\text{and; if } \left(\frac{1}{T_1} + \frac{1}{T_2}\right)^2 \gg \frac{4(1 - k^2)}{T_1 T_2} \quad (5.22)$$

$$\text{and } \left(\frac{1}{T_0} + \frac{1}{T_2}\right)^2 \gg \frac{4(1 - k^2)}{T_0 T_2}, \quad (5.23)$$

$$\text{then, } \alpha \approx \frac{\frac{1}{T_1} + \frac{1}{T_2}}{1 - k^2}, \quad (5.24)$$

$$\beta \approx \frac{1}{T_1 + T_2}, \quad (5.25)$$

$$\gamma \approx \frac{\frac{1}{T_0} + \frac{1}{T_2}}{1 - k^2}, \quad (5.26)$$

$$\delta \approx \frac{1}{T_0 + T_2} \quad (5.27)$$

Before utilizing these approximations let us investigate their degree of accuracy. Suppose we desire the error in  $\alpha$ ,  $\beta$ ,  $\gamma$ ,  $\delta$  to be less than 5%. Taking into account the effect of the square root on errors we deduce that if

$$\left(\frac{1}{T_1} + \frac{1}{T_2}\right)^2 \geq 20 \frac{(1 - k^2)}{T_1 T_2}, \quad (5.28)$$

$$\text{i.e. if } k^2 \geq 0.9 - \frac{T_2^2 + T_1^2}{20 T_1 T_2}, \quad (5.29)$$

then  $\alpha$ ,  $\beta$  will be estimated by (5.24), (5.25) to within 5% (Likewise for  $\gamma$ ,  $\delta$  except that  $T_0$  replaces  $T_1$ .)

Let  $T_2 = m T_1$  in (5.29). Then, (5.29) becomes:

$$k^2 \geq 0.9 - \frac{m + \frac{1}{m}}{20}. \quad (5.30)$$

From this last equation we can deduce that for  $m \geq 18$  or  $m \leq \frac{1}{18}$ ,  $\alpha$  and  $\beta$  will be estimated by (5.24) and (5.25) for any value of  $k^2$ .

This means that if  $T_2/T_1$  and  $T_0/T_2$  are greater than 18 then no matter what the value of  $k^2$  we can substitute the simpler relations for  $\alpha$ ,  $\beta$ ,  $\gamma$ ,  $\delta$  within 5% error bounds.

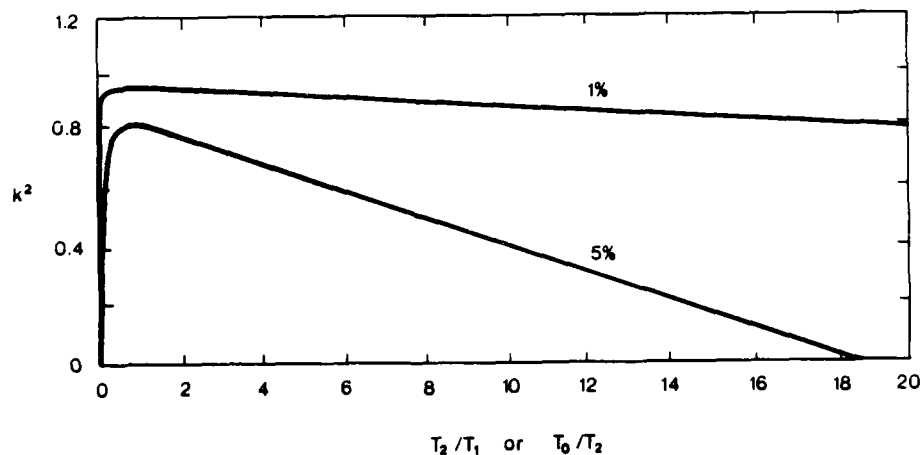


Fig. 42 Values which  $k^2$  must exceed for errors in estimates of  $\alpha$ ,  $\beta$ ,  $\gamma$ ,  $\delta$  to be less than 5% or 1%.

Fig. 42 shows graphs of the values which  $k^2$  must exceed for 5% and 1% error bounds, as functions of the time constant ratios.

To estimate the errors that might apply to the pulse transformer analysis it is necessary to know  $k^2$  and the ratios  $T_2/T_1$  and  $T_0/T_2$ . In Ch. 4 it was found that  $k^2$  should be at least 0.99 for ease of switching; Figure 42 shows that in this case the errors in  $\alpha$ ,  $\beta$ ,  $\gamma$  and  $\delta$  will be less than 1% irrespective of the time constant ratios. Since the switching must be completed in a time that is short compared to the secondary time constant ( $T_2/T_1 \approx 100$ , e.g.  $T_2 = 10$  ms,  $T_1 = 100$   $\mu$ s) and since the time to charge the primary is long compared to the secondary time constant ( $T_0/T_2 \approx 100$ , e.g.  $T_0 = 1$  s,  $T_2 = 10$  ms) it can be seen from Figure 42 that  $\alpha$ ,  $\beta$ ,  $\gamma$  and  $\delta$  will be accurate to within a few percent for even very low values of  $k^2$ .

Using Eqns. (5.20) to (5.27) together with the assumption that  $T_2/T_1$  and  $T_0/T_2$  are very much greater than unity, Eqns. (5.18) and (5.19) can be written as:

$$i_1(t) \approx i_1(0) \left[ \frac{T_1}{T_0} + e^{-\frac{t}{T_1(1-k^2)}} + k^2 \frac{T_1}{T_2} e^{-\frac{t}{T_2}} \right] \quad (5.31)$$

$$i_2(t) \approx i_1(0) k \sqrt{\frac{L_1}{L_L + L_2}} \left( e^{-\frac{t}{T_1(1-k^2)}} - e^{-\frac{t}{T_2}} \right) \quad (5.32)$$

Eqns. (5.31) and (5.32) are plotted in Fig. 43, taking the primary discharge time to have a normalized value of unity, and  $T_2/T_1$  and  $T_0/T_2$  each equal to 100, and  $\sqrt{\frac{L_1}{L_L + L_2}} \approx \frac{N_1}{N_2} = 10$  (the ratio of primary to secondary turns).

For the time ratios stated,  $i_1(t)$  and  $i_2(t)$  will always be accurate to within a few percent.

#### 5.1.4 Discussion of discharge equations

As was made clear before, the derivations in this Chapter are based upon  $R_D$  being constant whereas in fact  $R_D$  varies greatly with time. The equations cannot, therefore, give accurately the values of the currents. Their principal features, however, should be a good indication of the influence of circuit parameters. By inspection of the above equations and the graphs, we can draw the following conclusions.

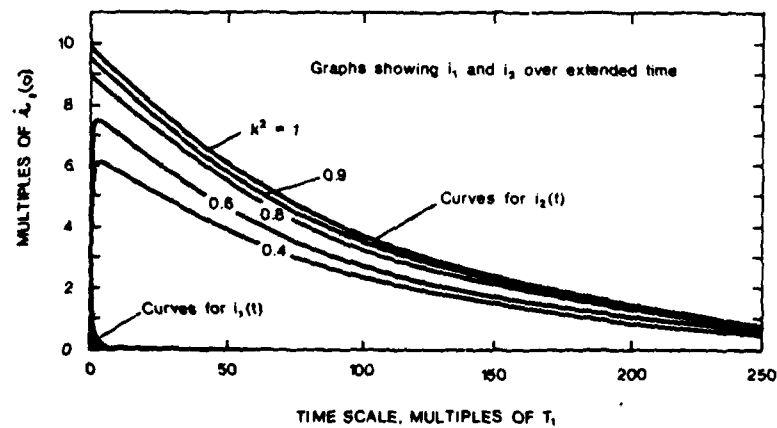
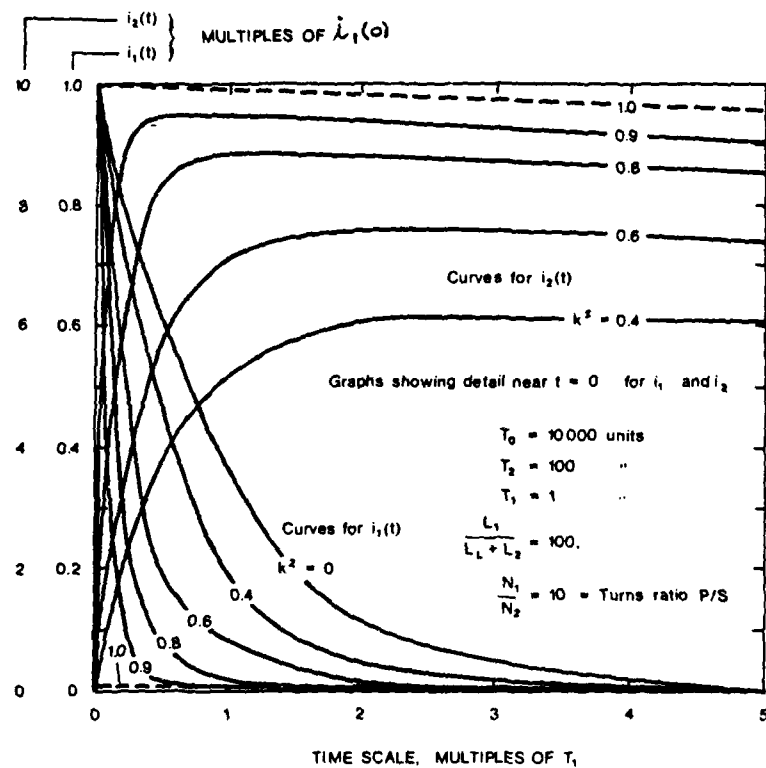


Figure 43. Primary and secondary discharge currents of the pulse transformer.



- (i) The primary current has three components. The first component,  $i_1(o) \frac{T_1}{T_0}$ , is very small because the switch resistance soon becomes much larger than the circuit resistance. The component is simply due to the fact that when the switch is opened the current supplied by the battery becomes  $\frac{C}{R_C + R_D}$  eventually.

The second component is the dominating one for most of the discharge. It shows that the time constant of the primary during discharge is diminished by the factor  $(1 - k^2)$ . A high coefficient of coupling therefore speeds up the transfer of energy in a manner which is not obvious without this analysis.

The third term shows the influence of the secondary discharge. Its effect is negligible during the actual transfer of energy to the secondary because  $T_1/T_2 \ll 1$ . In the case of a fuse,  $R_D$  would become virtually infinite at the end of transfer of current to the secondary and therefore the effect of the third term on the primary current is virtually zero.

In view of the above discussion we can further approximate the primary current by the expression:

$$i_1(t) \approx i_1(o) e^{-\frac{t}{T_1(1-k^2)}} \quad (5.33)$$

- (ii) Equation (5.33) can be further approximated by:

$$i_1(t) \approx i_1(o) \left(1 - \frac{t}{T_1(1-k^2)}\right) \quad (5.34)$$

This is because an exponential waveform is approximately linear with time for the first time constant.

The significance of this approximation is that it enables us to easily estimate the voltage induced across the primary, while the fuse is opening, as was done in Section 4.6.2.

- (iii) The energy dissipated in the primary during switching can be found using Eqn. (5.33);

$$\begin{aligned} \text{i.e. } W_{sw} &= \int_0^\infty (R_C + R_D) i_1^2(t) dt \\ &= (R_C + R_D) i_1^2(o) \int_0^\infty e^{-\frac{2t}{T_1(1-k^2)}} dt \end{aligned}$$

$$= (R_C + R_D) i_1^2(o) \frac{T_1(1 - k^2)}{2}$$

$$= (R_C + R_D) i_1^2(o) \frac{L_1}{2(R_C + R_D)} (1 - k^2)$$

i.e.  $W_{sw} = \frac{1}{2} (1 - k^2) L_1 i_1^2(o) = (1 - k^2) W_1.$

This is exactly the same as obtained previously (Eqn. (5.8)) and testifies to the validity of the approximations involved in obtaining Eqn. (5.33).

(iv) The equation for the secondary current can be written:

$$i_2(t) \approx i_1(o) \times \frac{N_1}{N_2} \left[ e^{-\frac{t}{T_1(1 - k^2)}} - e^{-\frac{t}{T_2}} \right], \quad (5.35)$$

since  $\sqrt{\frac{L_1}{L_L + L_2}} \approx \frac{N_1}{N_2}$  if  $L_L \ll L_2$  and the geometry is the same for both primary and secondary (i.e. so that primary and secondary differ only in the numbers of turns).

Owing to the rapid decay of the first exponential term, shortly after  $t = 0$  the secondary current becomes  $\frac{N_1}{N_2} \times i_1(o)$ , which is the same as obtained by the constant flux linkage method.

The rise of the current is controlled by the first term with the effective time constant  $T_1(1 - k^2)$ . The second term represents the discharge of the secondary energy in the load and is of no consequence during switching, so long as  $T_2 \gg T_1(1 - k^2)$ .

## 5.2 Physical Explanation of Transfer of Energy

The mathematical methods used so far enable the transfer of energy to the secondary to be plotted instant by instant. They do not, however, explain why it occurs. The following discussion shows how the mutual induced voltages control the exchange of energy. In this treatment the coefficients of coupling of the primary and secondary are individually designated. This enables changes in current, voltage and energy to be identified with primary or secondary flux changes. In the preceding analyses it was only possible to use the composite coefficient and therefore the individual effects of the windings could not be identified.

Fig. 44 shows the equivalent circuit for this discussion. Current  $i_1(o)$  circulates in a zero resistance primary which is coupled to a shorted

zero resistance secondary. The permeance of the flux path of the primary is  $P_1$  and that of the secondary is  $P_2$ , as used by Fitzgerald and Kingsley [1].

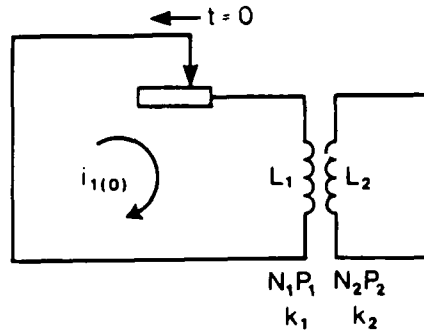


Fig. 44 Circuit for analysis based upon physical events.

The fraction of the flux of  $L_1$  that effectively links all the turns of  $L_2$  is  $k_1$  and the fraction of the flux of  $L_2$  that links  $L_1$  is  $k_2$ .  $N_1$  and  $N_2$  are the primary and secondary turns, respectively.

The variable resistor represents the fuse or other circuit opening means. When some resistance is introduced the inductor  $L_1$  loses energy and current  $i_1$  diminishes. Consider the effect of a decrease  $\Delta i_1$  in the primary current. The accompanying change of primary flux causes an induced voltage in the secondary and hence a current  $\Delta i_2$  in the secondary. Due to the combined effects of  $\Delta i_1$  and  $\Delta i_2$  the flux linking the primary decreases by  $\Delta \phi_1$ , where

$$\Delta \phi_1 = - N_1 \Delta i_1 P_1 + k_2 N_2 \Delta i_2 P_2. \quad (5.36)$$

The voltage induced in the secondary is:

$$e = - \frac{N_2 \Delta \phi_{1m}}{\Delta t}, \quad (5.37)$$

where  $\Delta \phi_{1m} = - k_1 N_1 \Delta i_1 P_1$  is the mutual portion of the flux change arising from  $\Delta i_1$  in time  $\Delta t$ . Noting also that for inductors  $i = \frac{Vt}{L}$  in general, we obtain:

$$\Delta i_2 = \frac{e \Delta t}{L_2} = \frac{N_2 k_1 \Delta i_1 P_1}{L_2}, \quad (5.38)$$

which becomes, by substituting  $L_2 = N_2^2 P_2$ ,

$$\Delta i_2 = \frac{k_1 N_1 \Delta i_1 P_1}{N_2 P_2} \quad (5.39)$$

Equation (5.39) can now be substituted in (5.36). The result is:

$$\Delta \phi_1 = - N_1 \Delta i_1 P_1 (1 - k_1 k_2). \quad (5.40)$$

Since  $L = \frac{N \phi}{i}$  in general, this expression can be written as:

$$L' = N_1^2 P_1 (1 - k_1 k_2) = L_1 (1 - k_1 k_2). \quad (5.41)$$

This is the incremental inductance during the transfer of energy to the secondary. If the primary time constant is  $T_1$  then the effective time constant during switching is  $T_1(1 - k_1 k_2)$  which is the same result as obtained previously, since  $k_1 k_2 = k^2$ . The implication of (5.41) is that if  $k_1 = k_2 = 1$  then the inductance of the primary would be zero during energy transfer and so no matter what the rate of change of current there would be no induced voltage in the primary and hence a switch could be opened without any arcing.

Equation (5.39) will now be developed into an expression for the secondary current. From elementary electromagnetics,  $k_1 P_1 = k_2 P_2$

$$\therefore \Delta i_2 = k_2 \frac{N_1}{N_2} \Delta i_1 \quad (5.42)$$

Putting  $\Delta i_2 = \frac{di_2(t)}{dt} \Delta t$ , etc and allowing  $\Delta t \rightarrow 0$  and integrating gives:

$$\int_0^t \frac{di_2}{dt} dt = k_2 \frac{N_1}{N_2} \int_0^t \frac{di_1}{dt} dt$$

Integrating and inserting the initial conditions  $i_2(t) = 0$ ,  $i_1(t) = i_1(0)$  gives:

$$i_2(t) = k_2 \frac{N_1}{N_2} (i_1(t) - i_1(0)) \quad (5.43)$$

As  $t \rightarrow \infty$  all the energy in the primary is dissipated or transferred to the secondary and so  $i_1 \rightarrow 0$ . Finally, therefore:

$$i_2 = -k_2 \frac{N_1}{N_2} i_1(o). \quad (5.44)$$

This is the same equation as obtained by the previous methods except for one thing, viz., the coefficient of coupling that is effective is that due to the secondary, and has nothing to do with that of the primary. As was implied, this method has the advantage of being able to reveal this. If the coefficients of coupling are equal, as is usual, then the result is of no practical significance. Configurations will be described for which they are not the same and then Eqn. (5.44) does have a practical application.

By comparing the terms of Eqn. (5.43) and (5.35) an expression for the primary current can be deduced, viz;

$$k_2 \frac{N_1}{N_2} i_1(t) = i_1(o) k \frac{N_1}{N_2} e^{-\frac{t}{T_1(1-k^2)}}.$$

Since we have deduced above that  $k = k_2$ , we have:

$$i_1(t) = i_1(o) e^{-\frac{t}{T_1(1-k^2)}}$$

This is precisely Eqn. (5.33) and is a valuable check of both the physical and mathematical analyses.

Equation (5.44) shows that the secondary current is independent of the degree of coupling which the primary has with the secondary. Even if  $k_1$  were zero, current would be induced in the secondary, according to (5.44). It seems contradictory that current, and energy, could be transferred to a winding to which it is not coupled. Let us, therefore, calculate the energy in the secondary, using Eqn. (5.44).

$$\frac{1}{2} L_2 i_2^2 = \frac{1}{2} L_2 k_2^2 \left(\frac{N_1}{N_2}\right)^2 i_1^2(o)$$

$$\text{But, } L_2 = N_2^2 P_2$$

$$\therefore \frac{1}{2} L_2 i_2^2 = \frac{1}{2} N_2^2 P_2 N_1^2 i_1^2(o),$$

and, since  $k_2 P_2 = k_1 P_1$ ,

$$\frac{1}{2} L_2 i_2^2 = k_1 k_2 \frac{1}{2} N_1^2 P_1 i_1^2(0).$$

Also,  $N_1^2 P_1 = L_1$ .

$$\therefore \frac{1}{2} L_2 i_2^2 = k_1 k_2 \frac{1}{2} L_1 i_1^2(0), \quad (5.45)$$

i.e. the energy transferred to the secondary is  $\frac{1}{2} k^2 L_1 i_1^2(0)$ , where  $k^2 = k_1 k_2$ , which is the usual result. No energy could in fact be transferred if  $k_1$  is zero, but, according to (5.44) current would still flow in the secondary. The somewhat artificial nature of  $k_1$  and  $k_2$  and the resolution of the above difficulty will be discussed in Section 5.3.

The preceding paragraphs show that by the process of induction the primary energy does actually transfer to the secondary. In addition we can see that:

- (i) As stated previously, the role of the switched in resistance is to cause flux change. Other ways of causing the flux to change would also transfer energy. For example, capacitors, reverse voltage, change of permeability and change of coupling factor might be used.
- (ii) The secondary current is not completely accumulated until the primary current has decayed to zero. There is no way of transferring the  $k_1 k_2$  portion of the primary energy and keeping a current flowing in the primary of such a value as to save the portion of primary energy which is not transferred.
- (iii) The accumulation of the secondary current depends upon the secondary resistance being low enough that the first induced increments of secondary current have not diminished significantly before the primary current decays to zero.
- (iv) The energy transferred is not the same as the energy in the mutual field of the primary. The initial mutual field energy is  $k_1 \frac{1}{2} L_1 i_1^2(0)$  whereas the energy transferred is  $k_1 k_2 \frac{1}{2} L_1 i_1^2(0)$ .

### 5.3 Coupling factors

#### 5.3.1 Simplified model

The coupling between the primary and secondary of the pulse transformer is such an important parameter that it is necessary to be able to

evaluate it numerically for various transformer designs. To do this rigorously is extremely difficult except for certain idealized cases.

The model upon which the treatment in the previous section is based is one in which the flux of each winding is considered to consist of a portion which links all the turns of both primary and secondary (the "mutual" flux) and a portion which links only the winding from which it arises (the "leakage" flux). Such a model is set out in detail by Fitzgerald and Kingsley [1] in connection with iron cored transformers and enables the degree of coupling between one winding and another to be expressed as the ratio of the mutual flux to the total flux. The situation is actually more complicated, especially in air cored coils, because each turn of each winding produces flux which links the other turns of its own winding in varying degrees and the turns of the other winding in varying degrees.

The simple model is still applicable, though, because it gives the correct induced e.m.f.s., which are the overall effect of the flux linkages, however they are actually distributed. This can be shown as follows. Let the back e.m.f. of a primary of  $N_1$  turns be  $E_1$  and the induced voltage in a secondary of  $N_2$  turns be  $E_2$ . The ratio of the average e.m.f. per turn in each winding, e.g.

$$\frac{E_2/N_2}{E_1/N_1}$$

for the secondary to primary ratio, can be written as:

$$\frac{\frac{d \phi_{1m}}{dt}}{\frac{d \phi_1}{dt}},$$

which, since the time changes are the same for each e.m.f., has the value:

$$\frac{\phi_{1m}}{\phi_1},$$

which is the usual definition of coupling factor  $k_1$ . The flux  $\phi_{1m}$  may be conveniently be regarded as the mutual flux in the simple model and flux  $\phi_1$  may be conveniently regarded as made up of the mutual flux and the so called "leakage" flux.

For the toroidal transformers proposed in the following Chapters the simple model is in fact applicable because the fluxes can be clearly separated into mutual and leakage portions.

### 5.3.2 Relationships between self inductances and coupling factors

In Sect. 5.2 the use of idealized coupling factors  $k_1$  and  $k_2$  led to the conclusion that it was possible to induce current into a coil from another coil even though none of the flux of the inducing coil links the second coil (Eqn. 5.44), although no energy could be transferred. The difficulty is resolved by showing that the self inductances and coupling factors are related, as follows.

Firstly, let us define the coupling factors in the usual (idealized) fashion:

$$k_1 = \frac{\phi_{1m}}{\phi_1} \quad (5.46)$$

and similarly for  $k_2$ , where  $\phi_1$  denotes the average flux per turn of the primary and  $\phi_{1m}$  denotes the average flux per turn which the primary induces into the secondary.

Let  $M_{12}$  be the mutual inductance of the secondary, due to current  $i_1$  in the primary (and similarly for  $M_{21}$ ),

$$\text{i.e.} \quad M_{12} = \frac{N_2 \phi_{1m}}{i_1} = \frac{N_2 k_1 \phi_1}{i_1}$$

$$\text{i.e.} \quad M_{12} = \frac{N_2}{N_1} k_1 L_1. \quad (5.47)$$

Similarly,

$$M_{21} = \frac{N_1}{N_2} k_2 L_2. \quad (5.48)$$

Now  $M_{12} = M_{21}$  always. This must be so to satisfy conservation of energy (21).

$$\therefore \frac{L_2}{L_1} = \left(\frac{N_2}{N_1}\right)^2 \frac{k_1}{k_2} \quad (5.49)$$

Equation (5.49) resolves the difficulty in Sect. 5.2 because it shows that if  $k_1$  is zero while  $k_2$  is not zero, then either  $L_2$  is zero or  $L_1$  is infinite. If  $L_2$  is zero the secondary does not exist and if  $L_1$  is infinite the primary can never be charged i.e. either way there can be no energy in the secondary.



Further conclusions can be drawn from Eqn. (5.49).

- (i) The ratio of the coupling coefficients must be constant no matter what the separation or orientation of the coils may be. This is because the self inductances,  $L_1$  and  $L_2$ , are not affected by the placement of the coils, i.e.  $L_1$ ,  $L_2$ ,  $N_1$  and  $N_2$  remain constant in Eqn. (5.49).
- (ii) The maximum proportion of the energy stored in one coil that can be transferred to the other is given by  $\frac{1}{k_2}$  or  $\frac{1}{k_1}$ , selected such that the denominator has the largest value. This is because the maximum value that  $k_1$  or  $k_2$  may have is 1 and because, as shown above,  $\frac{1}{k_1 k_2}$  must remain constant. Hence, the maximum value of  $k_1 k_2$  is  $1 \times \frac{1}{k_2}$  or  $\frac{1}{k_1} \times 1$ .
- (iii) For maximum energy transfer, the windings must have the same shape factors. This follows from the fact that  $L_1$  and  $L_2$  may be expressed as  $L_1 = N_1^2 A$  and  $L_2 = N_2^2 B$ , where  $A$  and  $B$  are shape factors (or the permeances) which have the dimensions of length. We thus have:

$$\frac{L_2}{L_1} = \left(\frac{N_2}{N_1}\right)^2 \frac{B}{A}, \quad (5.50)$$

which, using Eqn. (5.49), yields:

$$\frac{k_1}{k_2} = \frac{B}{A} \quad (5.51)$$

From (ii) it follows that for maximum energy transfer,  $B = A$ . (Further consideration shows that the shapes must be identical in size and form and coincident in space.)

#### 5.4 Coaxial-toroidal transformer geometry

Coaxial cable with a tubular inner has a flux distribution which can be clearly separated into parts in accordance with the theory just presented (Fig. 45(a)). Since no flux can exist within a hollow cylinder carrying a uniformly distributed current, the flux of each conductor is entirely external to that conductor. The flux of the inner is clearly divided into two portions; that which is between the inner and the outer and which therefore links the inner only and is therefore leakage flux, and that which surrounds both the outer and the inner and is therefore mutual flux. All the flux of the outer, however, surrounds both outer and inner and therefore there is no leakage flux of the outer.

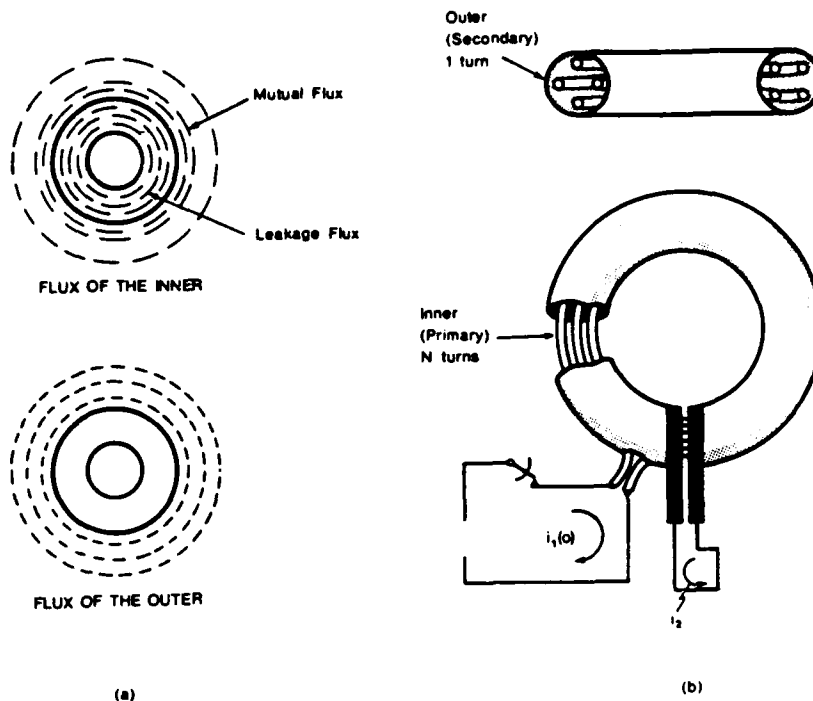


Fig. 45 Coaxial toroidal transformer.  
 (a) Fluxes of coaxial tubes. (b) Transformer with similar flux distribution.

A transformer which incorporates the coaxial cable flux distribution is shown in Fig. 45 (b). Assuming that the primary turns function as a cylinder with uniformly distributed current and that the ratio of the major to minor diameters is large enough that the flux at any section is the same as that due to long, straight conductors, the transformer flux distribution is the same as that of the coaxial tubes. In particular, the coupling coefficient of the secondary,  $k_2$ , is unity. Using Eqn. (5.44) we obtain

$$i_2 = -\frac{N_1}{N_2} i_1(o) \quad (5.52)$$

in the shorted secondary when the primary is opened, i.e. exact transformation in the ratio of the turns.

## 5.5 The charging of the primary

From a theoretical point of view the primary should be charged with the secondary open to prevent secondary current during the charging. From a practical point of view it would be simpler to charge the primary while the secondary is shorted. In the following Section various measures of the efficiency of charging the primary while the secondary is open are developed. In the Section after that the possibility of introducing resistance into the secondary to permit charging with a closed secondary is examined.

### 5.5.1 Secondary open

When an inductor is charged all the energy initially supplied is stored, i.e. the charging is 100% efficient. As the charging proceeds, energy is dissipated in the resistance of the inductor and by the time the inductor is 90% charged most of the energy supplied has been dissipated in the resistance. We seek an optimum charging time which combines high efficiency of charging with the storage of a large fraction of the total energy which the coil could store if charged for a long time.

During charging with the secondary open the charging current can be written as:

$$i_1(t) = \frac{V_C}{R_C} (1 - e^{-\frac{t}{T_0}}) = i_1(\text{INF}) (1 - e^{-n}) \quad (5.53)$$

where

$$i_1(\text{INF}) = \frac{V_C}{R_C}, \text{ i.e. the final value of } i_1(t)$$

and,  $n$  = number of time constants for which charging has proceeded  
i.e.  $n = \frac{t}{T_0}$  where  $T_0 = \frac{L}{R_C}$ . (See Fig. 41).

Let  $W_0$  be the energy supplied by the voltage source,  $V_C$ , up to any instant. Then,

$$\begin{aligned} W_0 &= \int_0^t V_C i_1(t) dt \\ &= L i_1^2(\text{INF}) (n - 1 + e^{-n}) \end{aligned} \quad (5.54)$$

If  $W_1$  is the stored energy at any instant, then the efficiency of charging is:

$$\frac{W_1}{W_0} = \frac{(1 - e^{-n})^2}{2(n - 1 + e^{-n})} \quad (5.55)$$

The fraction of the maximum energy,  $W_{(INF)}$ , that the inductor can store for a given voltage, is at any instant given by:

$$\frac{W_1}{W_{(INF)}} = 1 + e^{-2n} - 2e^{-n} \quad (5.56)$$

The ratio of the energy supplied to the maximum stored energy is:

$$\frac{W_0}{W_{(INF)}} = 2(n - 1 + e^{-n}) \quad (5.57)$$

These expressions are plotted in Figs 46 and 47. Fig. 46 shows how the energy supplied,  $W_0$ , rapidly exceeds the stored energy if the charging persists beyond one time constant. Fig 47 shows the efficiency of charging and the fraction of maximum possible stored energy as functions of charging time. The fraction of final current is also shown.

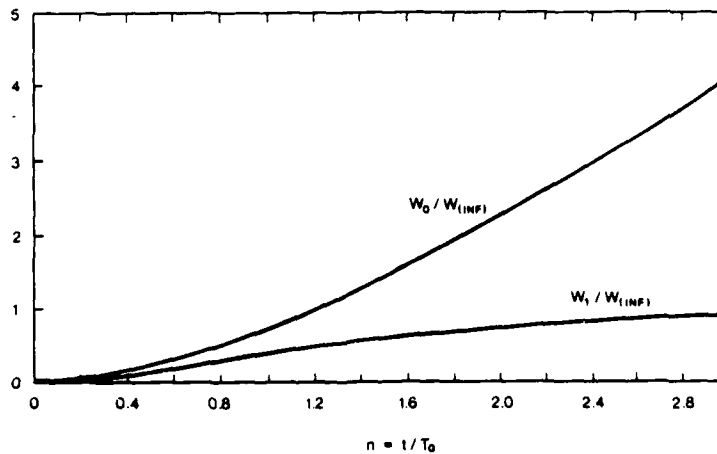


Fig. 46. Effectiveness of charging an inductor.  $W_0$  is the total energy supplied after  $n$  time constants,  $W_{INF}$  is the maximum possible stored energy,  $W_1$  is the energy stored after  $n$  time constants.

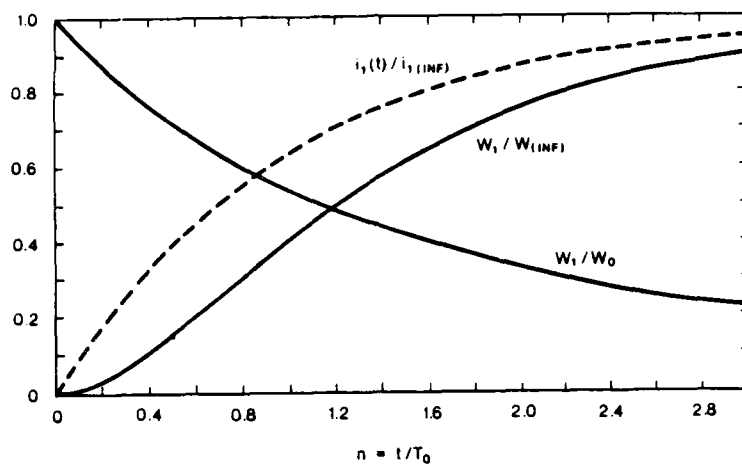


Fig. 47 Effectiveness of charging an inductor,  $\frac{W_1}{W_0}$  is the efficiency of charging.

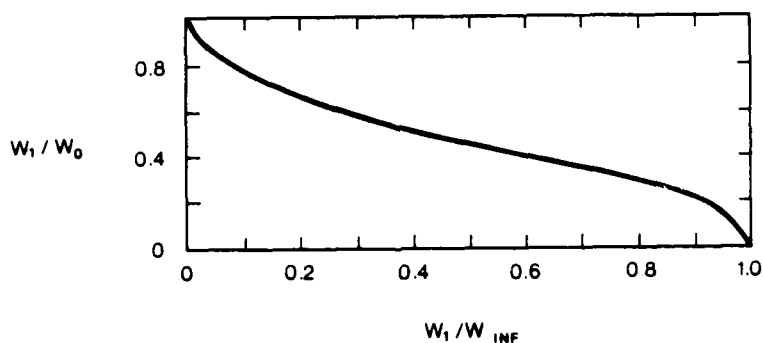


Fig. 48 Effectiveness of charging on inductor, showing rate of change of efficiency against fraction of maximum possible stored energy.

The crossover point in Fig. 47, at approximately 1.2 time constants, is the point of simultaneous maximum of efficiency of storage and of the fraction of maximum possible stored energy. At this point the current is

approximately 70% of its maximum possible value and the efficiency of storage and the utilization of the coil's storage capacity are each about 50%. This is not necessarily the optimum charging period, however, because  $W_1/W_0$  and  $W_1/W_{(INF)}$  vary nearly linearly over a broad range of  $t/T_0$  values. Fig. 48 shows that initially the losses increase more rapidly than the stored energy but that from about 0.7 of a time constant to 2.5 time constants the rate of losses is smaller and remains approximately constant. This is because the stored energy immediately increases with the square of the current but the losses require time to accumulate. From about 3 time constants onwards the rate of the losses rapidly exceeds the storage rate. This is because the current and hence the stored energy remain almost constant with time whereas the losses continually increase.

It is desirable to have a single factor which measures both the efficiency of charging and the utilization of the coil's energy storage capacity. The product of the two factors,  $\frac{W_1}{W_0}$  and  $\frac{W_1}{W_{(INF)}}$ , is proportional to a measure of the energy density of the charging source and the transformer. Firstly, we note that the mass of the charging source is proportional to the power it must deliver and also to the total energy required. The basic pulse transformer scheme minimizes the mass on account of the power requirement. We now seek to minimize the mass by reducing the losses as much as possible, and hence reducing the amount of energy which must be stored. Since  $W_0$  is the total energy supplied by the charging source per pulse, we have:

$$W_0 = C_1 M_C,$$

where  $C_1$  is a constant and  $M_C$  is the mass of the charging source.

Secondly, as discussed in Chapter 3, the maximum energy which the transformer can store is a function of its mass, therefore:

$$W_{(INF)} = C_2 M_T,$$

where  $C_2$  is a constant and  $M_T$  is the transformer mass.

Let us now consider the product:

$$\frac{W_1}{W_0} \times \frac{W_1}{W_{(INF)}} = \frac{W_1^2}{C_1 C_2 M_C M_T}.$$

If we define an equivalent mass,  $M_{EQ}$ , as:

$$M_{EQ} = \sqrt{M_C M_T}, \quad (5.58)$$

then:

$$\frac{W_1}{M_{EQ}} = \sqrt{\left(\frac{W_1}{W_0} \times \frac{W_1}{W_{(INF)}}\right)} \quad (5.59)$$

since  $C_1$  and  $C_2$  are constants.

Thus, from the product of the factors  $\frac{W_1}{W_0}$  and  $\frac{W_1}{W_{(INF)}}$ , we can obtain a composite factor for the energy density of the charging source and the transformer. Fig. 49 shows how this factor varies with charging time.

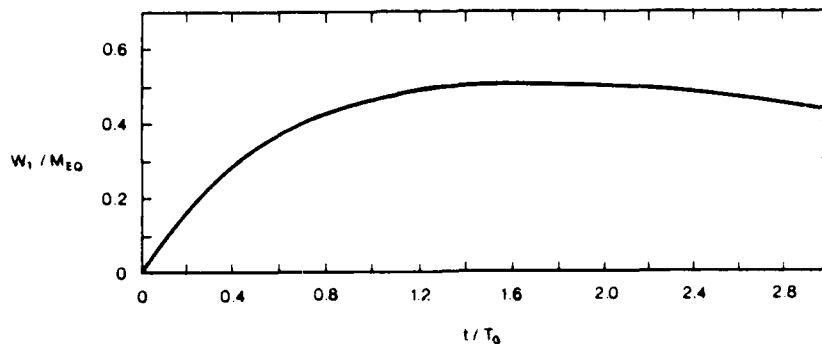


Fig. 49 Plot of stored energy density factor,  $\frac{W_1}{M_{EQ}}$ , scaled to  $\sqrt{C_1 C_2} = 1$ .

Figure 49 indicates that to fully utilize the mass of the system, the charging should proceed for at least one time constant. Further charging does not degrade the utilization of the mass until the resistive losses greatly exceed the rate of storage of energy, after more than 3 time constants.

Another way of measuring the optimum charging time is by considering the average useful power during charging. In order for the voltage source to be capable of charging the primary in the exponential manner assumed, it must be capable of maintaining its terminal voltage until it delivers current  $i_1(INF)$ . If the supply voltage is constant the power versus time graph will have the same shape of graph as the current (Fig. 47). The fraction of the energy that is stored is the useful energy and we may consider a ratio defined as

$$\frac{W_1/t}{V C_1 i_1(INF)} = PU \quad (5.60)$$

to be a "power utilization" factor. It measures the average power of the stored energy compared to the necessary power capability of the voltage source.

The maximum storage capacity of the coil can be expressed as:

$$\begin{aligned} W_{(INF)} &= \frac{1}{2} L_1 i_1^2(INF) \\ &= \frac{1}{2} L_1 \left( \frac{V_C}{R_C} \right)^2 ; \end{aligned}$$

$$\text{i.e.} \quad W_{(INF)} = \frac{1}{2} T_0 V_C^2 i_1(INF) \quad (5.61)$$

Using (5.60) we obtain:

$$PU = \frac{W_1}{2n W_{(INF)}} \quad (5.62)$$

Fig. 50 is a plot of (5.61). The curve reaches its maximum value of 0.2036 at 1.25 time constants, and to make the maximum use of the necessarily installed power capacity of the voltage source charging should continue for at least this time. (For comparison, if the voltage source was used to deliver power to a resistive load instead of the inductor, the power utilization value would be 0.5, i.e. when the load was matched to the internal resistance of the voltage source.)

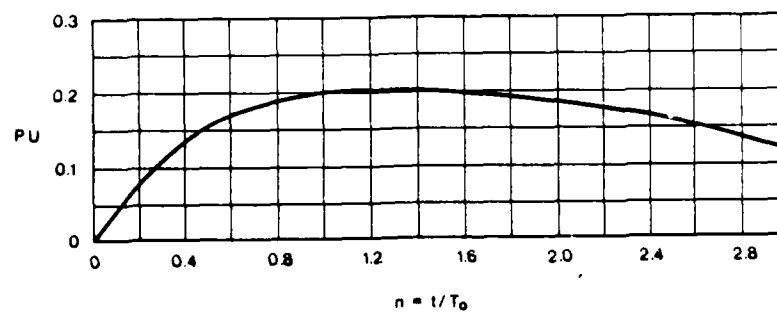


Fig. 50 Plot of power utilization factor, P.U.



On the basis of Figs 47, 49 and 50 we can conclude that charging for about 1.2 time constants is optimum, because it is a long enough time for the energy density and power factors to approach their high values while maintaining the energy efficiency high also (approx 50%).

Three points are worth noticing, in conclusion.

- (i) The discussion assumes that the voltage of the power source remains constant during charging. This means that the internal resistance of the voltage source must be included in the value of  $R_C$  used in the equations. However, if the internal resistance increases during the charging, e.g. due to polarization in the batteries, the current curve will flatten earlier and the optimum charging times will shorten.
- (ii) The problem of finding an optimum charging time is fundamental and would not be eliminated if the coil resistance could be greatly reduced, e.g. by using superconductors. Because  $R_C$  includes the resistance of the voltage source and the busbars, reduction of the coil resistance to much less than these other resistances has little effect. Also, if the voltage source resistance was negligible, the voltage source could power the railgun directly, without the pulse transformer.
- (iii) When an exploding wire fuse is used to interrupt the primary the resistance will increase during the charging and the optimum charging time will be shortened, as in (i). If the effect of the fuse were too limiting, it would be necessary to short it with a parallel switch until the desired current was reached, an undesirable complication.

#### 5.5.2 Secondary Closed

The study of charging with the secondary closed requires the solution of the circuit equations for Fig. 51.

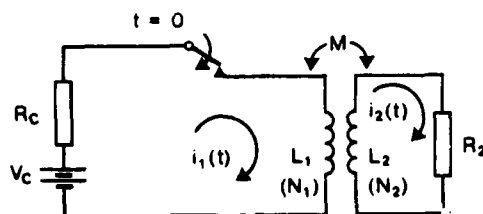


Fig. 51 Circuit for closed secondary charging.

$$V_C = i_1(t) R_C + L_1 \frac{di_1(t)}{dt} - M \frac{di_2(t)}{dt} \quad (5.63)$$

$$0 = i_2(t) R_2 + L_2 \frac{di_2(t)}{dt} - M \frac{di_1(t)}{dt} \quad (5.64)$$

Taking Laplace Transforms and using the facts that initially  $i_1$  and  $i_2$  are zero, one eventually obtains:

$$i_1(t) = \frac{V_C}{L_1(1-k^2)} \left[ \frac{1}{T_2\gamma\delta} + \frac{\frac{1}{T_2} - \gamma}{\gamma(\gamma - \delta)} e^{-\gamma t} - \frac{\frac{1}{T_2} - \delta}{\delta(\gamma - \delta)} e^{-\delta t} \right] \quad (5.65)$$

and

$$i_2(t) = \frac{V_C k}{(1-k^2)(\gamma - \delta) \sqrt{L_1 L_2}} [e^{-\gamma t} - e^{-\delta t}] \quad (5.66)$$

where  $k^2 = \frac{M^2}{L_1 L_2}$ , and  $\gamma$  and  $\delta$  are, as before, given by:

$$\gamma, \delta = \frac{-\left(\frac{1}{T_0} + \frac{1}{T_2}\right) \pm \sqrt{\left(\frac{1}{T_0} + \frac{1}{T_2}\right)^2 - \frac{4(1-k^2)}{T_0 T_2}}}{2(1-k^2)}, \quad (5.17)$$

and  $T_0 = \frac{L_1}{R_C}$  and  $T_2 = \frac{L_2}{R_2}$ .

By applying the approximation technique in Sect. 5.1.3 we can obtain:

$$i_1(t) \approx i_{1(INF)} \left[ 1 - \frac{T_2}{T_0 + T_2} e^{-\frac{(\frac{1}{T_0} + \frac{1}{T_2})t}{(1-k^2)}} - \frac{T_0}{T_0 - T_2} e^{-\frac{t}{T_0 + T_2}} \right], \quad (5.67)$$

and

$$i_2(t) \approx i_1(\text{INF}) \frac{k \frac{N_1}{N_2}}{1 + \frac{T_0}{T_2}} \left[ e^{-\frac{t}{T_0 + T_2}} - e^{-\frac{1}{\frac{T_0}{1-k^2} + \frac{1}{T_2}} t} \right] \quad (5.68)$$

As before, the accuracy of these approximations depends upon the  $\frac{T_0}{T_2}$  ratios. The content of these equations parallels that of the equations obtained for discharge of the primary energy. The primary current consists of a steady state term and two transient terms. The secondary current consists only of two transient terms. One of the transient terms contains the factor  $(1 - k^2)$  which, for high  $k$ , causes it to rapidly decay. For  $k \approx 1$  we can therefore approximate the currents by:

$$i_1(t) \approx i_1(\text{INF}) \left[ 1 - \frac{1}{1 + \frac{T_0}{T_2}} e^{-\frac{t}{T_0 + T_2}} \right] \quad (5.69)$$

and

$$i_2(t) \approx \frac{i_1(\text{INF}) \frac{N_1}{N_2}}{1 + \frac{T_0}{T_2}} e^{-\frac{t}{T_0 + T_2}} \quad (5.70)$$

In the proposed pulse transformer system the ratio  $\frac{T_0}{T_2}$  will be large, at least 10. (The charging time, and hence  $T_0$ , will be at least 100 ms and the discharge time will be typically 1 ms. If the short circuit resistance of the secondary is about 1/10 of the rail plus projectile effective resistance then  $T_2 \approx 10$  ms) If the turns ratio is 100 then from (5.70) we obtain:

$$i_2(t) \approx 9 i_1(\text{INF}) e^{-\frac{t}{T_0}}$$

Since  $i_1(\text{INF})$  would be in the region of 5,000 A (in order to give a current of approximately 350,000 A in the secondary, which is typically required for electromagnetic launching) the peak induced secondary current, due to charging, would be about 45,000 A. This is not large compared to the working current of 350,000 A and may be tolerable. Typically, the charging time would be about 1 s and  $\frac{T_0}{T_2} \approx 100$ . In this case the secondary current would be only 5,000A, i.e. the same as the primary current.

To assess more accurately the effect of the shorted secondary upon charging it is necessary to calculate efficiency factors as was done for charging with the secondary open. Since the effect is most pronounced for  $\frac{T_0}{T_2}$  values less than 10 the full expressions given by equations (5.65), (5.66) and (5.17) are used.

The quantities to be calculated are:

$$(i) \quad \frac{W_1}{W_{(INF)}} = \frac{\text{Stored energy of primary}}{\text{Max. possible stored energy}}$$

$$= \frac{\int V_C i_1 dt - \int R_C i_1^2 dt - \int R_2 i_2^2 dt}{\frac{1}{2} L_1 i_1^2 (INF)},$$

$$(ii) \quad \frac{W_1}{W_0} = \text{Efficiency of charging}$$

$$= \frac{\int V_C i_1 dt - \int R_C i_1^2 dt - \int R_2 i_2^2 dt}{\int V_C i_1 dt}$$

$$(iii) \quad \frac{W_1}{M_{EQ}} = \text{Energy density factor}$$

$$= \sqrt{\frac{W_1}{W_{(INF)}}} \times \frac{W_1}{W_0},$$

and (iv) P.U. = Power Utilization Factor

$$= \frac{W_1}{2n W_{(INF)}}.$$

The results of these calculations are shown in Figs. 52-56. In all these plots  $k = .99$ . The curve parameter is the  $\frac{T_0}{T_2}$  ratio and the dashed curves are for the secondary open i.e. the limiting curves as  $\frac{T_0}{T_2}$  approaches infinity.

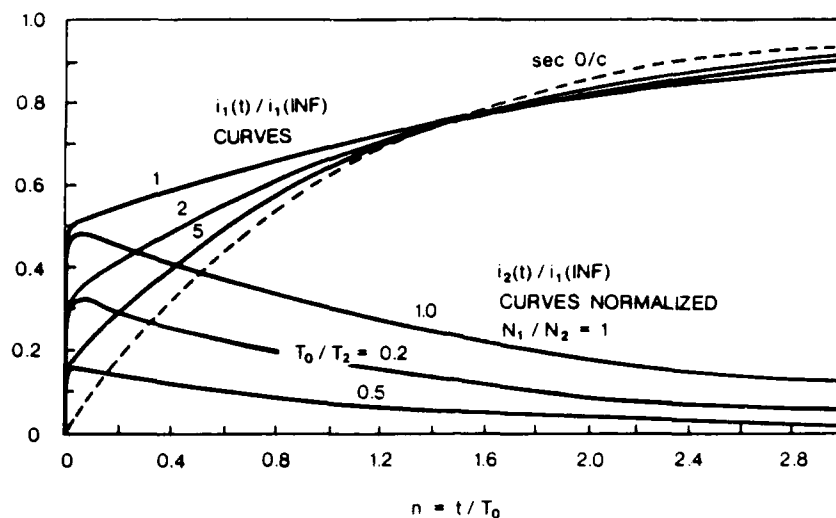


Fig. 52 Primary and secondary currents,  $i_1(t)$  and  $i_2(t)$ , during charging. To obtain actual  $i_2(t)/i_1(\text{INF})$  value, multiply value from graph by  $N_1/N_2$ .

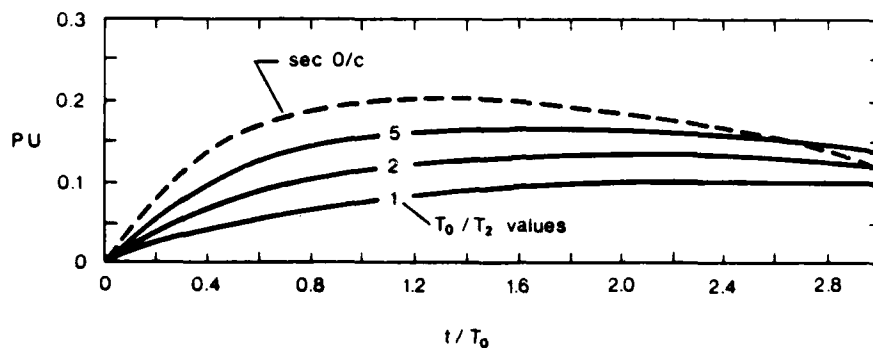


Fig. 53. Power utilization during charging.

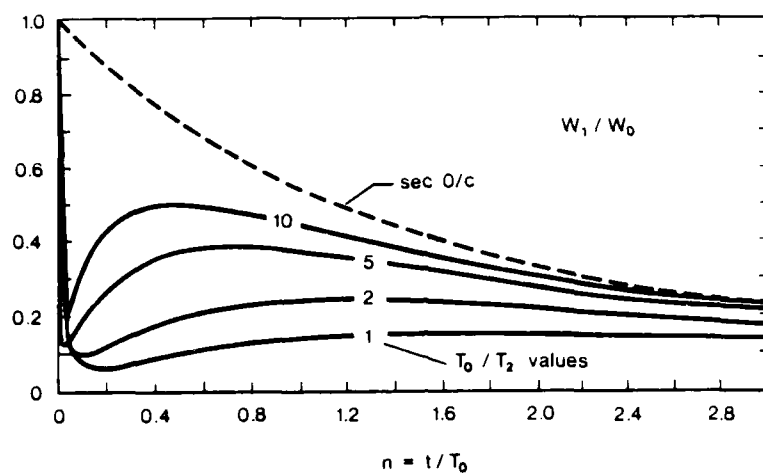


Fig. 54 Efficiency of charging.

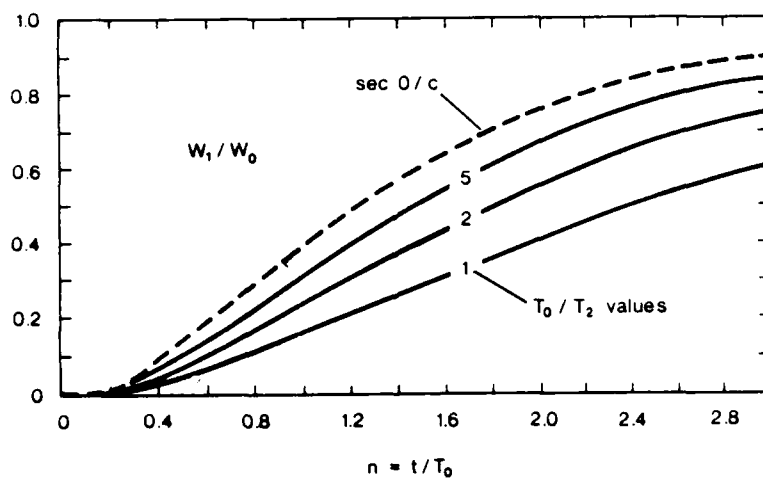


Fig. 55 Fraction of maximum possible stored energy.

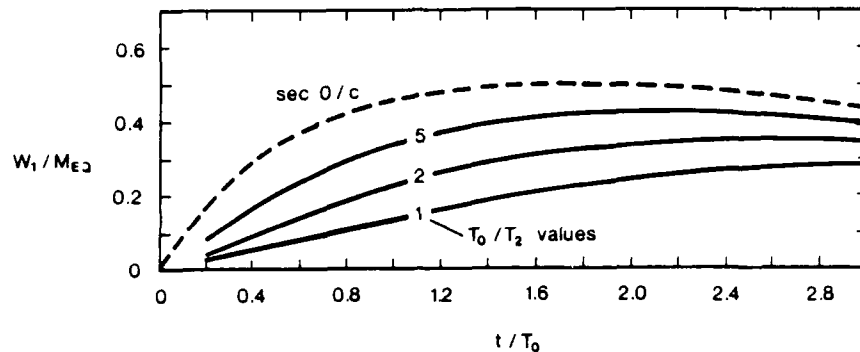


Fig. 56 Energy density factor.

The graphs of primary and secondary current (Fig. 52) show that at  $t \approx 0$ :

- (i) there is a current step, and
- (ii) the magnitude of the primary current step equals that of the secondary current step for unity turns ratio. Inspection of the approximate expressions (5.69) and (5.70) shows that this is to be expected in general, for, at  $t = 0$ :

$$i_1(t) = i_{1(INF)} \left[ 1 - \frac{1}{1 + \frac{T_0}{T_2}} \right] = i_{1(INF)} \frac{1}{1 + \frac{T_0}{T_2}}$$

i.e.  $i_1(t) = i_2(t)$  when  $N_1/N_2 = 1$ .

The factor  $\frac{1}{1 + \frac{T_0}{T_2}}$  gives the height of the initial step, approximately. For  $\frac{T_0}{T_2} = 1, 2$  and  $5$  this expression gives initial step heights of  $0.5, 0.333$  and  $0.167$ . These values are very close to the actual values in Fig. 52, which were obtained by computation using the complete current expressions.

A final point to note about the current curves is that the curve for  $\frac{T_0}{T_2} = 5$  does not differ greatly from that for the secondary open, i.e. for  $\frac{T_0}{T_2} \rightarrow \infty$ . Therefore, if  $\frac{T_0}{T_2}$  values of about 10 can be attained, as seems likely, the effect of the secondary being closed during charging will be negligible, so far as the storage of energy is concerned.

Examination of the other graphs confirms the above conclusion. In all cases, after charging the primary for about 1.2 time constants, the  $\frac{T_0}{T_2} = 5$  curve reaches at least 70% of the secondary open curve. The lowest figure is for the efficiency of charging. If the value of  $\frac{T_0}{T_2}$  is 10 then the efficiency of charging becomes about 85% of the open secondary value and all the other factors are around 90% of the open secondary values.

### 5.6 Physical explanation of closed secondary charging

There are two features of charging with a closed secondary that are quite different to charging with the secondary open. Firstly, there is a sudden step in the primary current instead of it rising gradually from zero (Fig. 52). Secondly, efficiency of energy storage is initially very small, (Fig. 54), whereas when the secondary is open it is initially at its maximum.

The initial step in the primary and secondary currents, and their magnitudes, can be explained by simple transformer theory in which the primary current is divided into two components. One component is the magnetising current and the other is the reflected load current of the secondary. The two portions are related by the requirement that the magnetising current must change continuously in such a way that the back e.m.f. of the primary is the voltage drop across the transformed resistance,  $(\frac{N_1}{N_2})^2 R_2$ , of the secondary. Initially, the magnetising current is small and primary circuit may be regarded as purely resistive. The primary current,  $i_1$ , therefore rises immediately when the primary is closed to the value given by:

$$i_1 = \frac{V_C}{R_C + (\frac{N_1}{N_2})^2 R_2} \quad (5.71)$$

where  $R_C + (\frac{N_1}{N_2})^2 R_2$  is the equivalent resistance of the primary. The above equation may be rearranged as follows, using the fact that  $(\frac{N_1}{N_2})^2 = \frac{L_1}{L_2}$  and denoting  $\frac{V_C}{R_C}$  by  $i_1(\text{INF})$ ,  $\frac{L_2}{R_2}$  by  $T_2$  and  $\frac{L_1}{R_1}$  by  $T_0$ :

$$i_1 = \frac{i_1(\text{INF})}{1 + \frac{T_0}{T_2}} = i_1(\text{INF}) \left(1 - \frac{1}{1 + \frac{T_2}{T_0}}\right) \quad (5.72)$$



Equation (5.72) is the same as (5.69) at  $t = 0$  and therefore justifies the above explanation. Furthermore, Eqn. (5.72) multiplied by  $\frac{N_1}{N_2}$  gives the secondary current, and is the same as Eqn. (5.70) at  $t = 0$ .

The second feature of closed secondary charging, viz. that the efficiency of energy storage is initially very small, follows simply from the fact that the circuit is initially virtually purely resistive and the energy is dissipated instead of stored.

To maintain the secondary voltage constant, and hence the secondary current constant, the rate of change of primary flux must remain constant. This would require the magnetizing portion of the primary current to increase linearly with time; the voltage drop across  $R_C$ , the primary resistance, though, means that the voltage across the primary inductance would diminish as the current increases. The secondary voltage and secondary current must, therefore, decrease with time. As the secondary current diminishes, so does its corresponding component in the primary current. The voltage drop across  $R_C$  therefore diminishes, allowing the voltage across the primary inductance to increase. This interaction between the secondary current and the primary current slows the rate of decrease of the secondary current, and explains why the primary and secondary time constants are the sum of those of the individual circuits in equations (5.69) and (5.70).

Since very little of the energy supplied initially is stored, the effective inductance of the primary is initially very small, when charging with the secondary closed. The magnitude of the initial inductance can be found in the same manner as in Section 5.2. In summary, a flux change  $\Delta\phi_1$  in the primary causes a secondary voltage which produces a cancelling flux change  $k_1 k_2 \Delta\phi_1$ , so that the net change in primary flux is  $(1 - k_1 k_2) \Delta\phi_1$ . Since  $\Delta\phi_1$  is the flux change which the primary self inductance produces for current change  $\Delta i_1$ , the initial equivalent primary inductance,  $L_{(EQ)}$  is:

$$L_{(EQ)} = (1 - k_1 k_2) L_1 \quad (5.73)$$

where  $L_1 = \frac{\Delta\phi_1}{\Delta i_1}$  is the primary self inductance. If the coupling factors  $k_1, k_2$  are high,  $L_{(EQ)}$  is small.

Primary resistance, as explained above, and secondary resistance cause the secondary current to diminish from its initial peak. The voltage induced back into the primary then reverses and causes primary current to rise more slowly than when the secondary is open. This can be seen in Fig. 52. If the secondary has a short time constant, such as  $\frac{Q}{T} = 10$ , as can be seen in Fig. 57, the equivalent primary inductance approaches its normal value after about one time constant. If the primary and secondary time constants are the same, about 5 time constants are required.

The variation of the equivalent primary inductance can be obtained as follows. Let the inductance of the primary at any instant during charging be  $L_{(EQ)}$ ; then the stored energy,  $W_1$ , is:

$$W_1 = \frac{1}{2} L_{(EQ)} i_1^2(t), \quad (5.74)$$

$$\therefore L_{(EQ)} = \frac{2 W_1}{i_1^2(t)}, \quad (5.75)$$

$$\text{or } \frac{L_{(EQ)}}{L_1} = \frac{W_1}{W_{(INF)}} \left( \frac{i_1(INF)}{i_1(t)} \right)^2 \quad (5.76)$$

Fig. 57 shows the results of calculations of this quantity for  $k = .99$ . Curve parameters are  $\frac{T_0}{T_2}$  ratios.

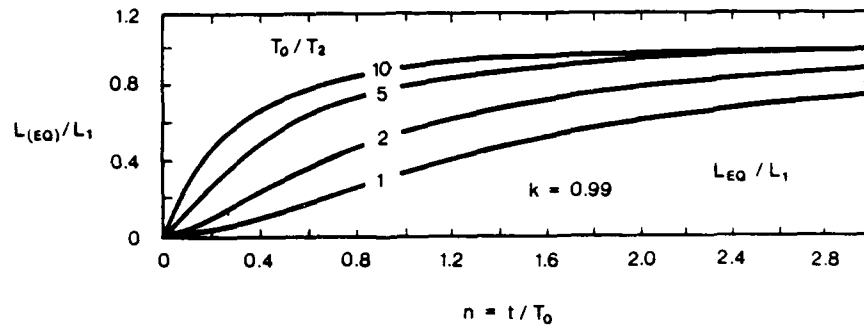


Fig. 57 Equivalent inductance of primary with secondary closed.

With  $k = \sqrt{k_1 k_2} = 0.99$ , the value of  $\frac{L_{(EQ)}}{L_1}$  at  $t = 0$  is obtained from Eqn. (5.73) as:

$$\frac{L_{(EQ)}}{L_1} = (1 - k_1 k_2) = 1 - .99^2 = .0199$$

This value is too small to show on the graphs, but the calculation print out gives .0199, i.e. equation (5.76) agrees exactly with equation (5.73).

The value of  $W_1$  in equation (5.76) is calculated from:

$$\begin{aligned}
 W_1 = \text{stored energy} = & \text{Energy supplied by voltage source, } (\int V_C i_1 dt) \\
 & - \text{Energy dissipation } R_C, (\int i_1^2(t) R_C dt) \\
 & - \text{Energy dissipated in } R_2, (\int i_2^2(t) R_2 dt).
 \end{aligned}$$

The full expressions for  $i_1(t)$  and  $i_2(t)$  were used (Eqn. (5.65), (5.66) and (5.17)). The evaluation is thus an elaborate check on Eqn. (5.73).

Other values of  $k$  were fed into the program used to evaluate Eqn. (5.76) and the results, for  $t/T_0 = .01$ ,  $\frac{T_0}{T_2} = .2$ , were:

$$k = .8, (1 - k_1 k_2) = .36, \text{ printout} = .3629$$

$$k = .4, (1 - k_1 k_2) = .84, \text{ printout} = .8400$$

These values confirm Eqn. (5.73) at  $t = 0$ .

## 5.7 Summary

In this Chapter we have studied the discharging and charging processes in depth. We have used routine circuit analysis and we have used physical insight to justify and corroborate the mathematical results.

This work leads to the following conclusions.

1. Since the three pulse transformer time constants,  $T_0$ ,  $T_1$  and  $T_2$  have ratios  $T_0/T_2 \approx 100$  and  $T_2/T_1 \approx 100$ :
  - (i) simplified expressions adequately describe the primary and secondary currents;
  - (ii) the primary can be charged while the secondary is closed, with negligible effect on efficiency of charging or on the railgun.
2. The proportion of energy transferred to the secondary is  $k_1 k_2$  times the primary stored energy.
3. The inductance of the primary during its discharge is  $(1 - k_1 k_2)$  times its self inductance. This means that the voltage across the primary is greatly reduced by a high degree of coupling.

4. The optimum time to charge the primary for reasons of energy efficiency, minimum mass and utilization of the charging source power capability is about one primary time constant.
5. The simple notion of mutual and leakage fluxes leads to correct results.
6. There is a simple and important relationship between self inductances and degrees of coupling.

## CHAPTER 6

### ASSESSMENT OF VARIOUS TRANSFORMER GEOMETRIES

The objectives of this Chapter are to compare several basic winding geometries and methods of forming the secondary in terms of their time constants relative to the conductor mass, the degree of coupling between the primary and the secondary and the mass of conductors needed to contain the stored energy.

The analysis and discussion by which the objectives are achieved takes up the first four parts of the Chapter. In the last part the actual currents, fluxes and inductances of coils with real conductors are considered, as opposed to idealized coils with current sheet distributions.

The time constant, degree of coupling and strength parameters are evaluated for three coil geometries, viz. the solenoid, the "external field" toroid and the ordinary toroid in which the magnetic field is almost entirely internal.

Degrees of coupling are evaluated for four forms of secondary applied to each of the three geometries listed above. As there appears to be no literature concerning the calculation of degree of coupling, techniques that seem appropriate to these geometries are developed.

#### **6.1 Time constant and masses**

##### **6.1.1 Relationship between battery mass and circuit resistances**

In Ch. 4 it was pointed out that battery mass is reduced by charging the primary for as long as possible. This requires the primary winding to have a correspondingly long time constant and, if the time constant is made longer by increasing the conductor size, the coil mass increases. The primary circuit time constant, however, is determined by the resistance of the battery as well as that of the winding. Before proceeding with the study of time constant in terms of coil geometry, let us determine the relative importance of battery and winding resistances upon battery mass.

The primary circuit resistance during charging, denoted as  $R_C$  in Ch. 5, is composed of the internal resistance of the battery,  $R_B$ , and the winding resistance of the primary,  $R_W$ .

The peak power,  $P_{C(INF)}$ , which the battery would eventually supply is given by:

$$P_{C(INF)} = i_1^2(INF) (R_W + R_B), \quad (6.1)$$

where  $i_1(INF) = \frac{V_C}{R_W + R_B}$  and  $V_C$  is the open circuit voltage of the battery.

Multiplying each side of Eqn. (6.1) by  $\frac{L_1}{L_1}$ , where  $L_1$  is the primary inductance, enables it to be expressed as:

$$P_{C(INF)} = \frac{2 W_{(INF)}}{L_1} (R_W + R_B) \quad (6.2)$$

where  $W_{(INF)}$  is the stored energy when the current in  $L_1$  is  $i_1(INF)$ .

$P_{C(INF)}$  may also be expressed in terms of the power density,  $p$ , of the battery, where  $p$  is the maximum power, i.e. the power delivered to a load equal in resistance to the internal resistance of the battery, divided by the battery mass, i.e.:

$$p = \frac{\left(\frac{V}{2}\right)^2}{R_B M_B} \quad (6.3)$$

where  $M_B$  is the battery mass. Note that  $p$  is a constant for a battery assembled from a given type of cell; it has the same value no matter what the arrangement of cells in parallel and series.

Expressing  $P_{C(INF)}$  as:

$$P_{C(INF)} = \frac{V_C^2}{(R_W + R_B)} \quad (6.4a)$$

and incorporating Eqn. (6.3) yields:

$$P_{C(INF)} = \frac{4pM_B R_B}{(R_W + R_B)} \quad (6.4b)$$

Combining Eqns. (6.2 and (6.4b) yields:

$$M_B = \frac{W_{(INF)}}{2L_1 p} R_W \left( \frac{R_W}{R_B} + 2 + \frac{R_B}{R_W} \right) \quad (6.5)$$

Eqn. (6.5) gives the relationship between battery mass and the primary winding resistance,  $R_W$ , and the battery internal resistance,  $R_B$ . It shows that one way to minimize battery mass is to reduce  $R_W$  and thereby to increase the circuit time constant, as we have discussed. The other way is to minimize the term  $\left(\frac{R_W}{R_B} + 2 + \frac{R_B}{R_W}\right)$ . This term, graphed as a function of  $\frac{R_B}{R_W}$  in Fig. 5a, shows that the battery mass is minimized when the battery resistance and winding resistance are equal. Eqn. (6.5) represents a family of curves,

each curve becoming shallower as  $R_W$  approaches zero.  $R_W$  clearly has the greatest control.

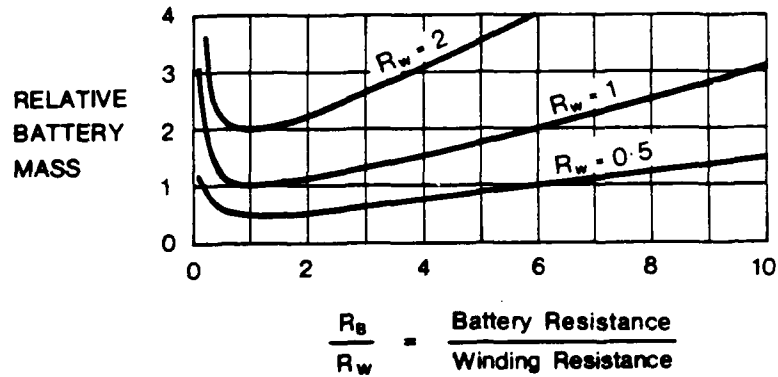


Fig. 58 Plot showing the variation of battery mass according to Eqn. (6.5). The battery mass is normalized so that when  $\frac{R_B}{R_W} = 1$  and  $R_W = 1$  battery mass has unit value.

For the condition  $R_B = R_W$ , Eqn. (6.5) may be expressed as:

$$M_B = \frac{W(\text{INF})}{\frac{L_1}{2R_W} p}, \quad (6.6)$$

which, since  $R_C = R_W + R_B$  and  $\frac{L_1}{R_C} = T_o$ , the primary circuit time constant, becomes:

$$M_B = \frac{W(\text{INF})}{T_o p}. \quad (6.7a)$$

Using the exponential relationship for the current reached after charging for  $n$  time constants (Eqn. 5.53), the battery mass may be further expressed as:

$$M_B = \frac{V_C I}{2(1 - e^{-n})p}, \quad (6.7b)$$

$$\text{or } M_B = \frac{W}{T_0 (1 - e^{-n})^2 p}, \quad (6.7c)$$

where  $I$  is the current and  $W$  is the stored energy when the primary current is interrupted after  $n$  time constants. (The derivations in this Section assume that the battery internal resistance remains constant during the charging of the primary. They do not apply if diffusion limits the current to a lesser value than  $i_1(\text{INF})$ ).

In this Section we have determined the influence of the battery resistance and the winding resistance on battery mass. The result, Eqn. 6.5, shows that the winding resistance has the most direct effect. In Ch. 4 it was calculated that to increase the time constant of a Brooks Coil from 1 second to 10 seconds by increasing the conductor size, the mass would increase from 1.6 tonnes to 50 tonnes. There is thus a large mass penalty in reducing resistance by increasing conductor size. It follows that an important measure of the geometry of the transformer primary is its resistance for a given inductance, or in other terms its time constant, for a given coil mass. Even if cooling is used to decrease the winding resistance, a coil which has a high basic  $\frac{L}{R}$  ratio is advantageous because it reduces the cooling required.

In the following Sections the  $\frac{L}{R}$  ratios and masses of three basic winding geometries are derived and compared to the Brooks Coil. The geometries selected are the solenoid, the "external field" toroid and the ordinary toroid.

### 6.1.2 The Brooks Coil

Firstly we shall find the relationship between the time constant and the mass of the Brooks Coil.

The Brooks Coil is known to be the multilayer coil which has the highest inductance for a given resistance and is a convenient basis for comparing the designs in the following Sections. Grover, [1], gives the inductance of the Brooks Coil as:

$$L = 0.01699a^2 N^2 \mu H \quad (6.8)$$

where  $a$  is the mean coil diameter (cm) and  $N$  is the number of turns. The coil geometry is shown in Fig. 59.



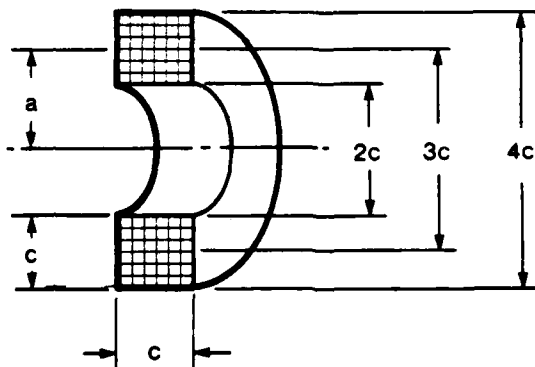


Fig. 59 Brooks Coil.

Suppose that the coil is wound from a wire of length  $l_w$  and diameter  $d$  and that the insulation is negligible. Substituting  $(\frac{c}{d})^2$  for  $N$  and  $\frac{3c}{2}$  for  $a$  and using metres instead of centimetres we obtain:

$$L = 1.6994 \times \frac{3c^5}{2d^4} \mu H \quad (6.9)$$

The resistance of the winding is:

$$R = \frac{4 \rho l_w}{\pi d^2} \quad (6.10)$$

where  $\rho$  is the resistivity of the conductor material. From these equations is obtained:

$$\frac{L}{R} = \left( \frac{1.6994 \times 3\pi}{8\rho} \right) \frac{c^5}{d^2 l_w};$$

which can be arranged as,

$$\frac{L}{R} = \frac{1.6994}{8\rho \left(\frac{3\pi}{4}\right)^{2/3}} \times (\text{Vol of conductor})^{2/3},$$

by using the fact that the volume of the wire,  $\frac{\pi d^2}{4} l_w$ , is equal to  $\frac{3\pi^2}{4} c^3$ .

Taking the conductor to be copper, for which the density is  $8.89 \times 10^3 \text{ kg/m}^3$  and the room temperature resistivity is  $1.7241 \times 10^{-8} \text{ ohm-metre}$ , we finally obtain:

$$\left(\frac{L}{R}\right)_{\text{BROOKS}} = 7.559 \times (\text{Mass of copper})^{2/3} \text{ ms}, \quad (6.11)$$

where the mass of the copper is in kg and is for a winding at room temperature. Note that (6.11) is independent of the length and diameter of the wire, and of the number of turns.

### 6.1.3 The single layer solenoid compared with Brooks Coil

The inductance of a solenoid is given by:

$$L = \frac{K \mu_0 N^2 A}{l} \quad (6.12)$$

where A is the cross sectional area,  $\frac{\pi D^2}{4}$ ; D is the diameter, l is the length, N is the number of turns and K is a correction factor for length/diameter ratio. Using the facts that, for a closely wound solenoid, the length of the conductor is  $N \cdot D$  and the conductor volume is  $\frac{N \pi d^2 D}{4}$  where d is the conductor diameter, we obtain:

$$\frac{L}{R} = \frac{K \mu_0}{4 \pi \rho} \times \text{Volume of conductor}.$$

Introducing the resistivity and density of copper yields:

$$\left(\frac{L}{R}\right)_{\text{SOL.}} = .6524K \times \frac{\text{Mass of copper}}{l} \text{ ms} \quad (6.13)$$

where l is the solenoid length in metres and the mass is in kg.

From (6.13) and (6.11) we obtain:

$$\frac{\left(\frac{L}{R}\right)_{\text{SOL}}}{\left(\frac{L}{R}\right)_{\text{BROOKS}}} = .0863 K \times \frac{(\text{Mass})^{1/3}}{l} \quad (6.14)$$

as a comparison of the solenoid and Brooks Coil time constants for coils wound with the same mass of copper. (They may have different lengths and diameters of conductors). Since the volume of copper in the Brooks Coil is given by  $\frac{3\pi^2 c^3}{4}$ , Eqn. (6.14) can be rewritten as:

$$\frac{(L/R)_{\text{SOL}}}{(L/R)_{\text{BROOKS}}} = 3.4846 \frac{Kc}{t} \quad (6.15)$$

Furthermore, it is known [2] that a single layer solenoid has its maximum L/R value when the ratio of diameter to length is 2.46, and that for this ratio,  $K = 0.48$ . Eqn. (6.15) can therefore be written as:

$$\frac{(L/R)_{\text{SH. SOL}}}{(L/R)_{\text{BROOKS}}} = 1.6726 \frac{c}{t} \quad (6.16)$$

where "SH SOL" denotes "short solenoid", and the equation refers to solenoids and Brooks Coils wound with equal masses of copper.

To evaluate (6.16) we must first determine a realistic value for the ratio  $\frac{c}{t}$ . Since the volume of wire in the solenoid equals that of the Brooks Coil, we have:

$$N_s D d^2 = 3c^3$$

where  $N_s$  is the number of turns on the solenoid. Furthermore, if the solenoid turns are touching and we neglect insulation thickness:

$$t = N_s d.$$

Combining these two expressions yields:

$$\frac{c}{t} = \left( \frac{D}{3N_s t} \right)^{1/3} \quad (6.17)$$

Substituting  $D/t = 2.46$  into (6.17) enables Eqn. (6.16) to be written as:

$$\frac{(L/R)_{\text{SH SOL}}}{(L/R)_{\text{BROOKS}}} = \frac{1.566}{N_s^{1/3}}, \quad (6.18)$$

which is the desired comparison in a convenient form.

If  $N_s = 100$  turns, as would be desirable on the primary of the pulse transformer, Eqn. (6.18) predicts that the time constant of an optimum short solenoid used for the primary would be 0.337 of that of a Brooks Coil wound with the same mass of wire.

#### 6.1.4 The external field toroid compared with Brooks Coil

In the normal toroid the turns are wound around its minor diameter and nearly all the flux is internal. If the turns are wound around the major diameter, as shown in Fig. 60, nearly all the flux is external.

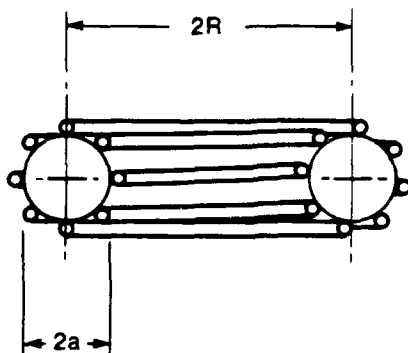


Fig. 60. External field toroid section through minor diameters.

To distinguish the above toroid from the usual toroidal winding it is referred to, in this work, as the "external field" toroid. The inner winding of the coaxial toroidal transformer discussed in Ch. 5 (Fig. 45) is an external field toroid.

An expression for the inductance of the external field toroid is obtainable from the inductance of a thin walled tube bent into a circle [3], upon which a uniformly distributed current flows, viz;

$$L = \mu_0 R \left[ \left( 1 + \left( \frac{a}{2R} \right)^2 \right) \ln \frac{8R}{a} - 2 \right], \quad (6.19)$$

where  $R$  is the major radius of the toroid and  $a$  is the minor radius.

To obtain the inductance for a toroid of  $N$  turns instead of a tube, we note that if the turns are closely packed they approximate a current sheet. If the current in the turns is  $I$ , the  $N$  turns are identical to a surface current  $NI$  upon the tube, and the magnetic field and energy stored will be the same also, i.e.

$$\frac{1}{2} L_{(N \text{ TURN COIL})} I^2 = \frac{1}{2} L_{(TUBE)} (NI)^2,$$

$$\text{or } L_{(N \text{ TURN COIL})} = N^2 L_{(\text{TUBE})}, \quad (6.20)$$

where L represents inductance. The inductance of the external field toroid with a thin layer of N turns, is therefore:

$$L_{(\text{EXT TOR})} = N^2 \mu_o R \left[ \left(1 + \left(\frac{a}{2R}\right)^2\right) \ln \frac{8R}{a} - 2 \right]. \quad (6.21)$$

To compare the external field toroid with Brooks Coil we proceed as for the solenoid. The length of the wire in the toroid is  $2\pi NR$ , and if the wire diameter is d, the resistance of the winding is:

$$\begin{aligned} & \frac{4 \rho (2\pi NR)}{\pi d^2} \\ \therefore \left(\frac{L}{R}\right)_{\text{EXT.TOR}} &= \frac{\mu_o \left[ \left(1 + \left(\frac{a}{2R}\right)^2\right) \ln \frac{8R}{a} - 2 \right] NR d^2}{2\pi \rho \cdot 4R} \end{aligned}$$

Since the volume of the wire is  $2\pi NR \left(\frac{\pi d^2}{4}\right)$  we can obtain:

$$\left(\frac{L}{R}\right)_{\text{EXT.TOR}} = \frac{\mu_o \left[ \left(1 + \left(\frac{a}{2R}\right)^2\right) \ln \frac{8R}{a} - 2 \right]}{4\pi^2 \rho} \times \frac{\text{Vol of wire}}{R}$$

Substituting for the resistivity of copper and converting the volume to mass, and also converting to milliseconds, we obtain finally:

$$\left(\frac{L}{R}\right)_{\text{EXT TOR}} = 0.2077 \left[ \left(1 + \left(\frac{a}{2R}\right)^2\right) \ln \frac{8R}{a} - 2 \right] \times \frac{\text{Mass}}{R} \text{ ms.} \quad (6.22)$$

Using Eqn. (6.11) for the Brooks Coil gives:

$$\frac{\left(\frac{L}{R}\right)_{\text{EXT TOR}}}{\left(\frac{L}{R}\right)_{\text{BROOKS}}} = 0.0275 \left[ \left(1 + \left(\frac{a}{2R}\right)^2\right) \ln \frac{8R}{a} - 2 \right] \times \frac{(\text{Mass})^{1/3}}{R} \quad (6.23)$$

as the comparison of the time constants for equal masses of copper windings.

By introducing the volume of the copper in the Brooks Coil, viz  $\frac{2\pi^2}{4} c^3$ , into (6.23), the expression is given in terms of  $\frac{c}{R}$  as:

$$\frac{(L/R)_{\text{EXT TOR}}}{(L/R)_{\text{BROOKS}}} = 1.109 \left[ \left( 1 + \left( \frac{a}{2R} \right)^2 \right) \ln \frac{8R}{a} - 2 \right] \frac{c}{R} \quad (6.24)$$

To evaluate (6.24), we must determine the ratio  $c/R$ . This can be done by equating the volume of the wire in the toroid to that of the Brooks Coil, as was done in the case of the solenoid. If there are  $N_E$  closely wound turns upon the toroid then:

$$2 N_E R d^2 = 3 c^3,$$

and, if the turns are touching and the insulation is negligible:

$$N_E = \frac{2\pi a}{d}.$$

Combining these two relationships gives:

$$\frac{c}{R} = \frac{2.975}{N_E^{1/3} (R/a)^{2/3}} \quad (6.25)$$

Substitution of (6.25) in (6.24) yields, finally:

$$\frac{(L/R)_{\text{EXT TOR}}}{(L/R)_{\text{BROOKS}}} = \frac{3.299 \left[ \left( 1 + \left( \frac{a}{2R} \right)^2 \right) \ln \frac{8R}{a} - 2 \right]}{N_E^{1/3} (R/a)^{2/3}} \quad (6.26)$$

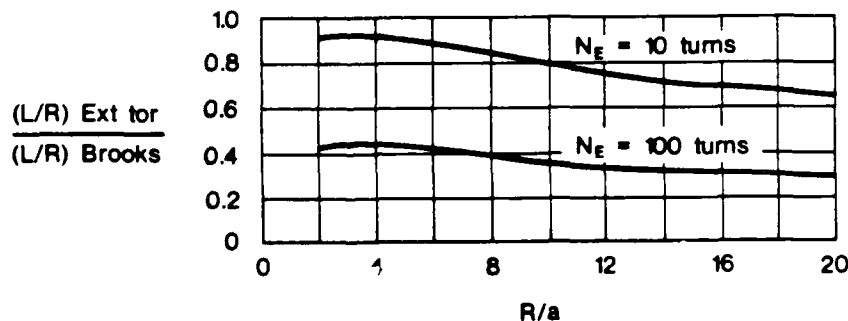


Fig. 61 Time constant of external field toroid relative to that of a Brooks Coil wound from an equal mass of conductor.

Eqn. (6.26) is plotted in Fig. 61 as a function of  $\frac{R}{a}$  and the number of turns,  $N_E$ . The maximum value occurs at about  $\frac{R}{a} = 3$ , but the peak is quite broad, especially for large numbers of turns. For 100 turns and  $\frac{R}{a}$  values of

about 5, the time constant of the external field toroid is about 40% of that of a Brooks Coil wound from the same mass of conductor, i.e. slightly more than for the short solenoid (34%). The time constant ratio increases as the number of turns decreases. Because the turns are considered to touch each other in deriving these time constant ratios, the conductor diameters increase as the number of turns decreases and the equations do not apply for low numbers of turns (e.g. 3).

#### 6.1.5 The ordinary (or internal field) toroid

A toroid which has the turns in the plane of the minor diameter may be regarded as a solenoid bent into a circle, with virtually all the flux lines forming closed circles within the winding. The inductance expression for this toroid, based upon it being a solenoid of length  $2\pi R$  (Fig. 62) with the correction factor,  $K$ , equal to unity, is:

$$L = \frac{\mu_0 N^2 a^2}{2R}, \quad (6.27)$$

where  $N$  is the number of turns and  $R$  and  $a$  are the major and minor radii, respectively.

The flux density actually varies inversely with the radius,  $r$ , (Fig. 62). When this is taken into account, the expression for the inductance is (4):

$$L = \mu_0 N^2 R \left(1 - \sqrt{1 - \left(\frac{a}{R}\right)^2}\right). \quad (6.28)$$

For  $\frac{R}{a}$  values down to 2, that is, for all practical toroids, (6.28) differs from (6.27) by, at most, 7%. Eqn. (6.28) is therefore adequate for the purpose of estimating time constant ratios.

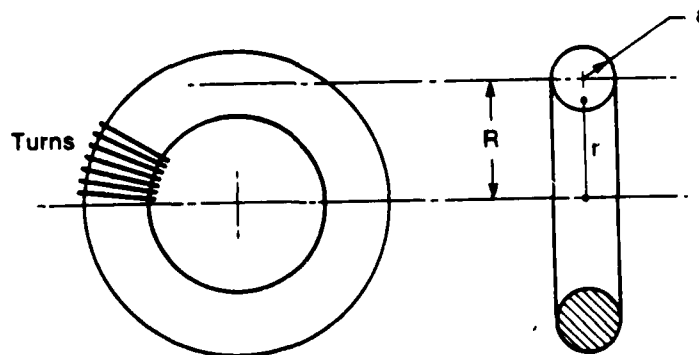


Fig. 62. The ordinary toroid in which the field is virtually all internal.

Using Eqn. (6.27) and the same methods as in the previous Sections, we obtain:

$$\left(\frac{L}{R}\right)_{\text{INT TOR}} = 0.1038 \times \frac{\text{Mass}}{R} \text{ ms,} \quad (6.29)$$

where the conductor is copper and the mass is in kg. Using Eqn. (6.11) we further obtain:

$$\frac{(L/R)_{\text{INT TOR}}}{(L/R)_{\text{BROOKS}}} = 0.555 \frac{C}{R}. \quad (6.30)$$

Assuming that the turns are tightly packed and that the insulation thickness is negligible, and equating the volume of conductor in the toroid to that of the Brooks Coil, we obtain:

$$\frac{C}{R} = \frac{2.9746}{(N_I \frac{R}{a})^{1/3}}, \quad (6.31)$$

where  $N_I$  is the number of turns on the toroid. Substituting (6.31) into (6.30) finally yields:

$$\frac{(L/R)_{\text{INT TOR}}}{(L/R)_{\text{BROOKS}}} = \frac{1.650}{(N_I \frac{R}{a})^{1/3}} \quad (6.32)$$

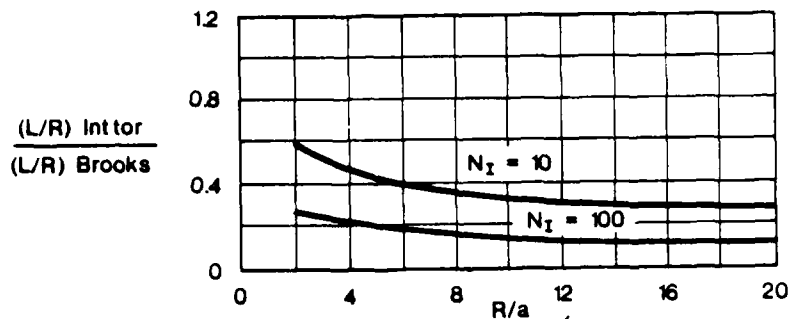


Fig. 63. Time constant of internal field toroid relative to that of Brooks Coil wound from an equal mass of conductor.



The plot of equation (6.32), Fig. 63, shows that, except for very small  $\frac{R}{a}$  values, the time constants of the internal field toroid are about half the corresponding values for the external field toroid.

## 6.2 The degree of coupling of several forms of secondary

The major problem with the secondary is how to couple it tightly to the primary. In this Section, mutual inductance calculations and the theory in Section 5.3 are used to estimate how the form and location of the secondary limit the coupling. This is done for four forms of the secondary applied to the short solenoid and the external and internal field toroids. Extremely tight coupling appears possible by using a coaxial cable form of primary and secondary with either the short solenoid or the external field toroid.

### 6.2.1 Basic theory

There is little in the literature concerning the calculation of degree of coupling. The only method would seem to be to derive the composite coupling factor,  $k_1 k_2$ , from the mutual and self inductances of the coils concerned. Mutual inductance expressions, however, appear to have been derived for only single turns and solenoid type coils. In addition, the expressions are cumbersome.

Another method, though, which particularly suits the toroidal type transformers, can be based upon the ratio relationship, Eqn. (5.49). This relationship enables  $\frac{1}{k_2}$  to be found immediately from the self inductance expressions for the windings. If one of  $k_1$  or  $k_2$  can be found, the other value and hence the product  $k_1 k_2$  can be found by means of the ratio expression. For the toroidal transformers virtually all the flux is known to be either inside or outside the winding and one of the coupling factors can be taken to be unity.

From purely physical reasoning it is evident that perfect coupling between two coils requires the flux of one coil to link every filament of current in the other coil in exactly the same manner as it links its own current. This can only come about if the two coils are physically identical and occupy the identical space. Furthermore it requires the current to be distributed over the turns so as to have no internal flux, because internal flux cannot link any other turns.

The ratio relationship, together with a knowledge of one of the coupling factors, gives a measure of the extent to which the coil geometrical requirement is met.

The distribution of current is another matter. The current in the primary of the pulse transformer is distributed uniformly over the turn cross section because of the long charging time, whereas the current in the secondary (which is to be connected so as to be effectively a single turn) has a transient distribution during the transfer of energy. For the present we shall assume that the secondary current distribution adequately matches that of primary and that the winding geometry has the major influence on degree of coupling. This assumption is justified in Section 6.5.4.

(i) Use of the ratio relationships

The ratio relationships, Eqn. (5.49) and (5.51), viz.:

$$\frac{L_2}{L_1} = \left(\frac{N_2}{N_1}\right) \frac{k_1}{k_2} \text{ and } \frac{k_1}{k_2} = \frac{B}{A},$$

and the observation that the lesser of  $\frac{k_2}{k_1}$  or  $\frac{k_1}{k_2}$  gives the maximum value of  $k_1 k_2$ , and hence of the energy that can be transferred, enable a simple assessment of the coupling between any primary and secondary to be made.

As an example of the application of the theory, consider two "long" solenoids, as shown in Fig 64(a).

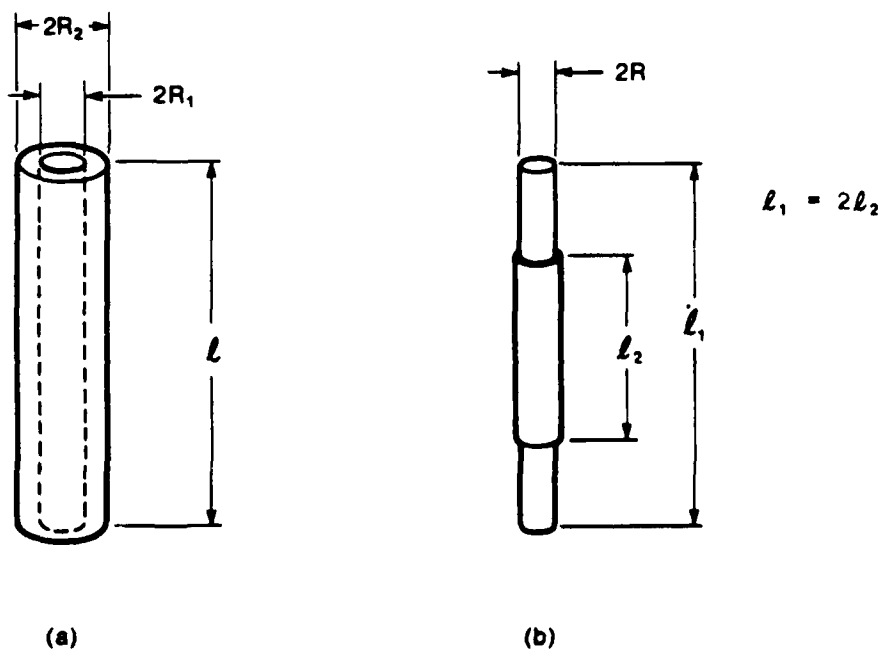


Fig. 64 Long solenoids for examples of coupling factor theory.

Since the solenoids are long, the factor "K" in the expression for solenoid inductance (Eqn. 6.12) is approximately unity. Eqns. (6.12) and (5.49) then yield:

$$\frac{k_1}{k_2} = \frac{\pi R_2^2 / \ell_2}{\pi R_1^2 / \ell_1} = \left(\frac{R_2}{R_1}\right)^2 \frac{\ell_1}{\ell_2}. \quad (6.33)$$

We can immediately state that the maximum possible fraction of stored energy which can be transferred from one coil to the other is  $\left(\frac{R_1}{R_2}\right)^2$ . This will be actually attained only if  $k_1$  or  $k_2$  is unity. If  $R_2$  is not much greater than  $R_1$ , and since the solenoids are also long, very little of the flux of the inner solenoid will return by passing through the space between the windings. Thus the inner solenoid has very little leakage flux and  $k_1$  will be very nearly 1, and we can state that the value of  $k_1 k_2$  is actually  $\left(\frac{R_1}{R_2}\right)^2$ . Obviously, a means of determining how closely  $k_1$  approaches unity is desirable. This is done later in this Section using a mutual inductance expression for solenoids.

From Eqn. (6.33) it can be seen that the "shape factors", B and A, in terms of which  $\frac{k_1}{k_2}$  may also be expressed, are the cross sectional area to length ratios of the coils, in other words, the "permeances" of their flux paths.

The above example clearly applies to the simple model of flux distribution, where the fluxes can be considered to have "mutual" and "leakage" portions. In Section 5.3 it was pointed out that the  $\frac{1}{k_2}$  relationship applies in general, though. The two solenoids shown in Fig. 64(b) are an example of a geometry in which the flux cannot be divided into mutual and leakage paths. Let us imagine that both solenoids are "long", but one is twice the length of the other, and that they are of virtually the same diameter.

Since there is no gap between the solenoids, there is no "leakage" flux. All the flux of the longer coil links the shorter one and all the flux of the shorter coil links the longer one. Applying Eqn. (5.49) to this case yields:

$$\frac{k_1}{k_2} = \frac{\pi R^2 / \ell_2}{\pi R^2 / \ell_1} = \frac{\ell_1}{\ell_2} = 2.$$

As all the flux of the long coil clearly links the turns of the short coil in the same manner as its own turns over length  $\ell_2$ , we deduce that  $k_1 = 1$  and therefore that  $k_2 = \frac{1}{2}$ . In terms of the simple equivalent average flux model,  $k_2$  is one half because the equivalent average flux of the short coil exists only over length  $\ell_2$  and has no linkage with the half of the long coil that extends beyond it.

(ii) Internal flux limitation

The internal flux of a winding limits the extent to which its coupling factor can be unity. The situation is similar to that in the railgun where the internal flux of the rails could not act upon the projectile. If the equivalent average internal flux is  $\phi_1$  and the equivalent average total flux is  $\phi$ , the maximum fraction of the flux that can couple another winding is  $\frac{\phi - \phi_1}{\phi}$ , which may also be written:

$$k_{(MAX)} = \frac{L - L_1}{L}, \quad (6.34)$$

where  $L$  is the total inductance of the winding and  $L_1$  is the internal inductance. For solid, round conductors, in which the current is uniformly distributed, the internal inductance is  $\frac{\mu_0}{8\pi}$  H/m, or approximately 50 nH/m. Eqn. (6.34) in this case becomes:

$$k_{(MAX)} = 1 - \frac{\frac{\mu_0}{8\pi} \times \text{length of conductor}}{L} \quad (6.35)$$

In the pulse transformer, the internal flux limitation applies to the primary, where the current flows for a long enough time to be uniformly distributed. The current induced into the secondary flows initially near the conductor surfaces and there is negligible internal flux.

For a solenoid, for example, the total inductance is given by  $L = \frac{KN^2 \mu_0 \pi D^2}{4l}$ , and Eqn. (6.35) becomes:

$$k_{(MAX)} = 1 - \frac{l}{2KN\pi D} \quad (6.36)$$

In the case of the optimum time constant solenoid,  $D/l = 2.46$  and  $K = 0.48$ , yielding:

$$k_{(MAX)} = 1 - \frac{0.135}{N} \quad (6.37)$$

If the short solenoid has  $N = 100$  turns as the primary of the pulse transformer,  $k_1$  has a maximum value of 0.9986 according to Eqn. (6.37).

(iii) Calculation of coupling between solenoids using mutual inductance expression

Maxwell derived a fundamental formula for the mutual inductance,  $M$ , of two equal length, coaxial solenoids, [5], viz.

$$M = 4\pi^2 a^2 n_1 n_2 [l - 2Aa] \text{ cgs units} \quad (6.38)$$

where  $a$  is the radius of the inner,  $A$  the radius of the outer,  $l$  is the common length and  $n_2$  and  $n_1$  are the turns per centimetre of the inner and outer windings respectively (Fig. 65). This expression, together with self inductance expressions, enables  $k_1 k_2$  to be directly calculated for equal length coaxial solenoids.

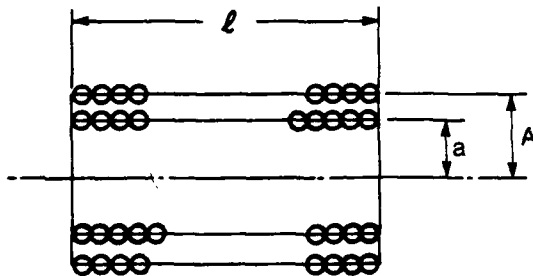


Fig. 65 Parameters for calculation of  $k_1 k_2$  from mutual inductance of equal length coaxial solenoids.

In Eqn. (6.38),  $\alpha$  is given by:

$$\begin{aligned} \alpha = & \frac{A-r+l}{2A} - \frac{a^2}{16A^2} \left(1 - \frac{A^3}{r^3}\right) - \frac{a^4}{64A^4} \left(\frac{1}{2} + 2\frac{A^5}{r^5} - \frac{5}{2}\frac{A^7}{r^7}\right) \\ & - \frac{35}{2048} \frac{a^6}{A^6} \left(\frac{1}{7} - \frac{8}{7}\frac{A^7}{r^7} + \frac{4A^9}{r^9} - \frac{3A^{11}}{r^{11}}\right) \\ & - \frac{63}{2 \times 128^2} \frac{a^8}{A^8} \left(\frac{5}{9} + \frac{64}{9}\frac{A^9}{r^9} - \frac{48}{r^{11}}\frac{A^{11}}{r^{11}} + \frac{88}{r^{13}}\frac{A^{13}}{r^{13}} - \frac{143}{3}\frac{A^{15}}{r^{15}}\right) \\ & - \frac{231}{512^2} \frac{a^{10}}{A^{10}} \left(\frac{7}{11} - \frac{128}{11}\frac{A^{11}}{r^{11}} + \frac{128}{r^{13}}\frac{A^{13}}{r^{13}} - \frac{416}{r^{15}}\frac{A^{15}}{r^{15}} + \frac{520}{r^{17}}\frac{A^{17}}{r^{17}} - \frac{221}{r^{19}}\frac{A^{19}}{r^{19}}\right), \end{aligned} \quad (6.39)$$

where  $r = \sqrt{t^2 + A^2}$ .

$$\text{Since } M = \sqrt{k_1 k_2 L_1 L_2}, \quad (6.40)$$

and, in cgs units,

$$L_1 = 4\pi^2 A^2 n_1^2 t K_1 \quad (6.41)$$

$$\text{and } L_2 = 4\pi^2 a^2 n_2^2 t K_2 \quad (6.42)$$

where  $K_1$  and  $K_2$  are the Nagaoka factors [6],  $k_1 k_2$  can be obtained from:

$$k_1 k_2 = \frac{\left(\frac{a}{A}\right)^2 \left[1 - \frac{2Aa}{t}\right]^2}{K_1 K_2} \quad (6.43)$$

The tabulation below shows the values of  $k_1 k_2$  given by Eqn. (6.43) as the radius of the inner coil varies from 0.9 to 0.999 of the radius of the outer coil. The ratio of the coupling factors, from Eqn. (5.49), is also given, enabling the individual values of  $k_1$  and  $k_2$  to be found. One tabulation is for  $A/t = 1$ , ie a short solenoid, and the other is for  $A/t = 0.1$ , ie a long solenoid.

$A/t = 1$ ; short solenoid

$a/A$	$k_1 k_2$	$k_1/k_2$	$k_2$	$k_1$
0.9	0.689924	0.849377	0.901261	0.765510
0.95	0.827280	0.946374	0.934964	0.884826
0.99	0.955707	0.984679	0.985179	0.970085
0.995	0.973098	0.992337	0.990259	0.982670
0.999	0.987473	0.998235	0.994595	0.992839

$A/\ell = 0.1$ ; long solenoid

$a/A$	$k_1 k_2$	$k_1/k_2$	$k_2$	$k_1$
0.9	0.797181	0.816643	0.988012	0.806853
0.95	0.894933	0.906189	0.993770	0.900543
0.99	0.978013	0.980896	0.998529	0.979453
0.995	0.988709	0.990427	0.999132	0.989568
0.999	0.997317	0.998082	0.999617	0.997699

Table      Coupling factors for equal length coaxial solenoids;  $a$  = inner coil radius,  $A$  = outer coil radius.

Because of the slow convergence of (6.39) as  $a$  approaches  $A$ , all the terms in (6.39) must be used.

The following points can be seen from the tabulation.

- (i) Coupling factor  $k_2$  is greater than  $k_1$ , ie the inner is more tightly coupled than the outer. This was argued to be the case previously, because the space between the windings contains the main flux of the outer, which consequently cannot link the inner, whereas only the weak external flux of the inner passes through it and does not link the outer.
- (ii) Since we desire to have  $k_1 k_2$  at least 0.99 in the pulse transformer, the radii of the two windings must be equal to within one part in a thousand, if it is a short solenoid. For long solenoids, the two radii must be equal to within one part in two hundred, which is much easier to attain.
- (iii) For solenoids the value of  $\frac{k_1}{k_2}$  is not a sufficiently accurate measure of  $k_1 k_2$  for our purpose, except in the case of long solenoids with  $a/A \geq 0.99$ .

### 6.2.2 Short solenoid with various secondaries

We shall now apply the theory of the previous Section to the short solenoid, and the external and internal field toroids with four possible types of secondary, viz:

- (a) a thin sheet;
- (b) a layer of turns identical to the primary, but each turn cut and connected in parallel to output busbars;
- (c) a bifilar winding, instead of a separate layer winding, with the turns cut and connected in parallel to busbars; and
- (d) a coil wound of coaxial cable, the inner conductor forming the primary and the cable sheaths being cut and connected in parallel to busbars to form the secondary.

Firstly, we shall deal with the short solenoid.

#### (i) Short solenoid with sheet secondary

It is natural to imagine that a thin sheet of metal, in tight contact with a primary winding, Fig. 66, would form a secondary with a high degree of coupling. In the pulse transformer application, the sheet can be thin compared to the primary, because the secondary need only have a time constant of milliseconds whereas the primary must be thick enough to have a time constant of about a second. Walker and Early (7) and others (8) used thin sheet windings. Walker and Early reported an overall coupling factor ( $\sqrt{k_1 k_2}$ ) of 0.98 and in another case, [9], 0.97 was reported.

To calculate the degree of coupling we need to know where the current in a real primary may be considered to flow as a current sheet. Inductance expressions are derived for current flowing as a sheet at the mean radius of the turns with correction factors for turn spacing and conductor size, but this does not automatically mean that the current can be considered to flow at the mean turn radius for degree of coupling purposes. Examination of this question in Section 6.5.1 suggests that when the secondary is on the inner side, as in Fig. 66, the primary current may be considered as equivalent to a sheet current approximately 1/3 the primary conductor diameter from the conductor inner surface, and when the secondary is on the outside, the primary current is effectively a sheet current at the mean radius. Thus, somewhat tighter coupling will be obtained when the thin sheet secondary is placed on the inside, because the separation of the primary and secondary is  $d/3$  compared to  $d/2$ , where  $d$  is the primary conductor diameter.



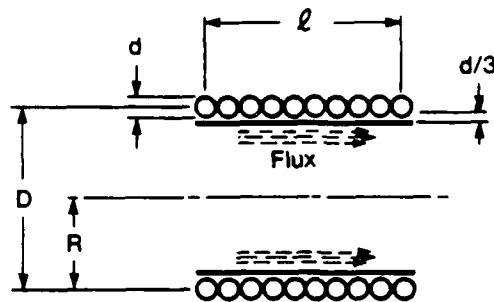


Fig. 66. Thin sheet secondary on inner side of short solenoid primary.

In the case of a short solenoid with  $D/\ell = 2.46$  and 100 turns and a separation of  $d/3$  between the primary and secondary current sheets, the ratio  $k_1 k_2$  applicable to Fig. 65 is 0.9973. The coaxial solenoid tabulation shows that  $k_1 k_2$  would be about 0.981, which is barely acceptable for high energy pulse transformer applications. If the secondary is on the outside, the separation is  $d/2$  and  $k_1 k_2 \approx 0.976$ .

The above calculation assumes that the length of the secondary is exactly the same as that of the primary. Because the effective length of a solenoid varies with its diameter (given approximately by  $\ell + 0.45D$ ), the effect of a difference in length is diminished. A difference of 1%, in the case of a short solenoid with  $D = 2.46\ell$ , limits  $k_1 k_2$  to 0.995. In order to not degrade the value calculated in the previous paragraph, the sheet secondary must match the length of the primary to within 1%. In addition to the question of the active length of the sheet secondary, the current paths are not exactly defined as with separate turns. The study of the transient current distribution of the secondary in Section 6.5.4 suggests that the secondary emfs will have the same distribution as the primary back emfs and will thus cause secondary current to flow in a duplicate pattern to that of the primary current. The degrading effect of secondary current paths will therefore be minimized, provided the sheet secondary is not shorter than the primary.

(11) Separate layer winding

The principle of a separate layer winding with its turns cut and connected to busbars to form a secondary is shown in Fig. 67.

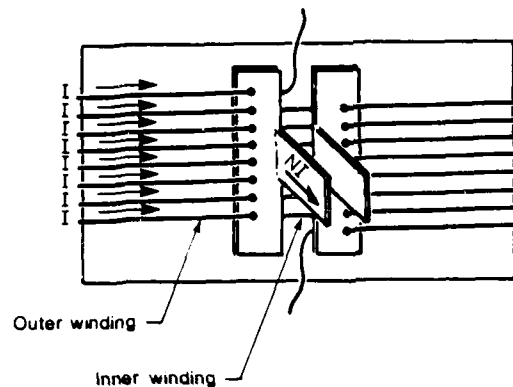


Fig. 67. Identical layer winding with outer layer turns cut and connected to busbars.

The reason for considering such a winding is that it provides each turn of the primary with a secondary turn that is identical, except that the outer radius is greater by the conductor diameter. The current in each primary turn can be imagined to transfer to its matching secondary turn, to which it is more tightly coupled than to all but the turns on either side of it in the primary winding itself.

The extent to which the energy transfers from a turn to an adjacent secondary turn can be calculated using an expression for the mutual inductance of coaxial circles, due to Maxwell [10], viz:

$$M = 4\pi a \left( \ln \frac{8a}{A-a} - 2 \right) \text{ cgs units,} \quad (6.44)$$

where  $a$  and  $A$  are the radii of the inner and outer adjacent turns. The inductance of a turn of wire of diameter  $(A-a)$  bent into a circle of radius  $A$  is accurately enough given by:

$$L_A = 4\pi A \ln \left( \frac{A}{\frac{A-a}{2}} \right) \text{ cgs units.} \quad (6.45)$$

Since  $M = \sqrt{k_1 k_2} L_A L_a$ , we obtain for the adjacent turns:

$$k_1 k_2 = \frac{a}{A} \frac{\left( \ln \frac{8a}{A-a} - 2 \right)^2}{\ln \frac{2A}{A-a} \ln \frac{2a}{A-a}} \quad (6.46)$$

If the solenoid has  $D/\epsilon = 2.46$  and 100 turns,  $\frac{a}{A} = \frac{123}{124}$ , and Eqn. (6.46) yields  $k_1 k_2 = 0.782$ . Although this indicates that the majority of the energy can be considered to transfer on a turn to turn basis, it also implies that by no means can individual turn to turn coupling reach the high values that we require.

For the windings as a whole, the coaxial short solenoid tabulation with  $\frac{a}{A} = \frac{123}{124} = 0.992$  shows that  $k_1 k_2$  is around 0.96. It makes no difference which side the secondary is on; either way the equivalent current sheets are separated by one wire diameter.

At 0.96, the coupling factor product of the identical layer windings is rather low. The uncertainties of length and path of the secondary currents present with a sheet secondary, do not exist, though. Cutting and connecting the secondary turns to busbars must be done without degrading the coupling. If the secondary conductors are identical to the primary, the secondary mass is the same as the primary mass, whereas on resistance considerations it need only be a fraction as massive. Hollow secondary conductors could be used to overcome this disadvantage.

#### (iii) Bifilar winding

By bifilar winding we mean winding a coil with a pair of identical diameter conductors, with the two conductors side by side and touching each other. The advantage of bifilar winding is that the two windings have identical diameters, lengths and number of turns and therefore, if each winding also has the same current distribution,  $k_1 = k_2$ .

However, the two windings are displaced axially by the diameter of one turn, and, if they are very long solenoids, the the simple equivalent flux model enables us to say that the degree of coupling of each winding would be  $\frac{N-1}{N}$ , where  $N$  is the number of turns. If  $N = 100$ , then  $k_1 = k_2 = 0.99$  and  $k_1 k_2 = 0.98$ . For short solenoids  $k_1 k_2$  would be less than 0.98 (but always greater than the fundamental value for two turns that touch, e.g. 0.78 if the conductor diameter is  $\frac{1}{123}$  of the turn diameter, as calculated in the previous Section). According to this reasoning, thousands of turns would be necessary on a short solenoid to obtain  $k_1 k_2 = 0.999$  using a bifilar winding.

A major disadvantage of the bifilar winding is that it doubles the length of the solenoid and to maintain a particular diameter to length ratio, the solenoid diameter must also double, resulting in double the length of winding and double the resistance. As with the layer winding there is the practical problem of cutting the secondary turns and connecting them to busbars without degrading the coupling.

(iv) Coaxial cable winding

The coaxial cable method was apparently first proposed in 1939, in Russia [11], to reduce the leakage inductance of transformers.\* Provided that the solenoid diameter is much greater than the cable diameter, all the flux of the outer is external and links the inner i.e. the coupling factor of the outer is unity (Fig. 68). The flux of the inner,  $\phi_1$ , however, has three components, viz:

$$\phi_m, \phi_2, \text{ and } \phi_1,$$

where  $\phi_m$  is the average mutual flux which links both the inner and outer,  $\phi_2$  is the portion in the space between the inner and the outer and  $\phi_1$  is the flux within the solid inner.

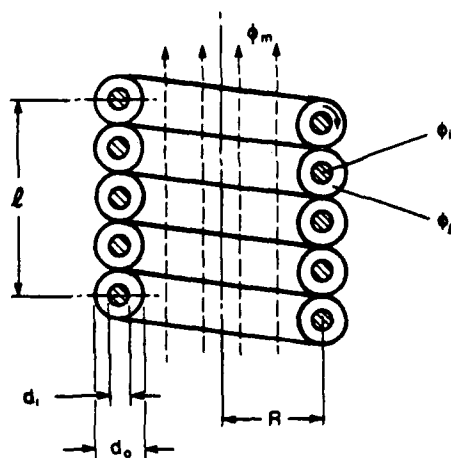


Fig. 68 Coaxial cable transformer.

In standard texts [12] the inductance of coaxial cable is shown to be:

$$\frac{\mu_0}{2\pi} \ln \frac{d_o}{d_i} \text{ H/m,}$$

---

\* The idea was first described to the author by W.H. Weldon, University of Texas.

for the component due to  $\phi_i$ , and,

$$\frac{\mu_0}{8\pi} \text{ H/m}$$

for the component corresponding to  $\phi_1$ , where  $d_o$  and  $d_i$  are the cable outer and inner diameters. Altogether, we may write for the inductance,  $L_1$ , of the inner:

$$L_1 = \frac{N\phi_m}{I} + RN\mu_0 \left( \ln \frac{d_o}{d_i} + \frac{1}{4} \right) \quad (6.47)$$

where  $N$  is the number of turns and  $R$  is the solenoid radius. When current  $I$  flows in the outer it produces only flux  $\phi_m$ , exactly equal to the flux  $\phi_m$  which the inner produces. The inductance of the outer,  $L_2$ , is therefore  $\frac{N\phi_m}{I}$ , or:

$$L_2 = L_1 - RN\mu_0 \left( \ln \frac{d_o}{d_i} + \frac{1}{4} \right) \quad (6.48)$$

The ratio of the coupling factors, by Eqn. (5.49), is thus:

$$\frac{k_1}{k_2} = 1 - \frac{RN\mu_0 \left( \ln \frac{d_o}{d_i} + \frac{1}{4} \right)}{L_1} \quad (6.49)$$

Substituting the inductance expression for the short solenoid for  $L_1$ , viz.

$L_1 = \frac{K\mu_0 N^2 \pi R^2}{l}$ , Eqn. (6.49) becomes:

$$\frac{k_1}{k_2} = 1 - \frac{2 \left( \ln \frac{d_o}{d_i} + \frac{1}{4} \right)}{K \pi N \frac{D}{l}}, \quad (6.50)$$

(assuming that the spacing of the inner turns has negligible effect on  $L_1$ ) where  $K$  is Nagaoka's factor. Since  $k_2 = 1$ , Eqn. (6.50) gives the value of  $k_1 k_2$ .

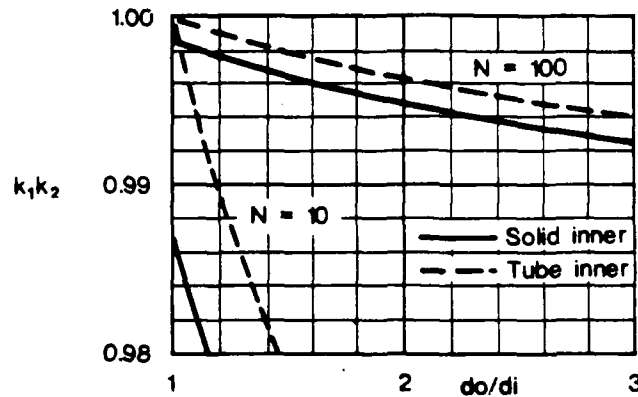


Fig. 69.  $k_1k_2$  for short solenoid wound with coaxial cable.

Eqn. (6.50) is plotted in Fig. 69, for a short solenoid with diameter to length ratio  $(D/l) = 2.46$  and  $K = 0.48$ . The broken curves are for a tubular inner and are obtained by omitting the  $1/4$  term in (6.50). With  $N = 100$  turns  $k_1k_2 = 0.996$  can be obtained with  $d_o/d_i = 1.5$  i.e. with considerable space between the outer and the inner for insulation. The coaxial cable method clearly has the highest  $k_1k_2$  values of the methods examined.

### 6.2.3 The external field toroid with various secondaries

As was discussed in Ch. 5, this form of winding with a secondary has flux distribution similar to coaxial cable, provided the ratio of the minor diameter to major diameter is not too great i.e. provided the toroid is not too "fat". All the flux of the outer winding links the inner winding, and the coupling factor of the outer winding is unity.

#### (1) Sheet secondary

A cross-section of an external field toroid with a thin sheet secondary is shown in Fig. 70. Since the flux is external, tighter coupling will be obtained with the thin sheet secondary on the outside, as shown, than on the inside by similar reasoning as in the case of solenoids.

Using the inductance expression for the external field toroid,

$$\text{viz, } L = N^2 \mu_0 R \left( 1 - \left( \frac{a}{2R} \right)^2 \right) \ln \frac{8R}{a} - 2,$$

we have for the ratio of the coupling coefficients:

$$\frac{k_1}{k_2} = \frac{(1 + (\frac{a_2}{2R})^2) \ln \frac{8R}{a_2} - 2}{(1 + (\frac{a_1}{2R})^2) \ln \frac{8R}{a_1} - 2}, \quad (6.51)$$

where  $a_1$  and  $a_2$  are the minor radii of the primary and secondary, respectively. If  $\frac{R}{a_1}$  is 5 and if the thin sheet could be located effectively

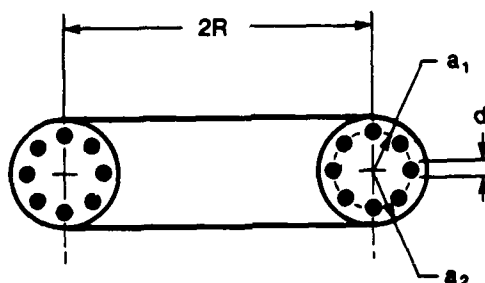


Fig. 70. External field toroid with thin sheet secondary.

within  $d/3$  of the position of the equivalent current sheet of the primary, then, assuming that the  $N$  primary conductors are tightly packed so that  $Nd \approx 2\pi a_1$  and  $a_2 = a_1(1 + \frac{2\pi}{3N})$ , Eqn. (6.51) yields  $\frac{k_1}{k_2} = 0.989$ . Since  $k_2$  will be very nearly 1, this is also the value of  $k_1 k_2$ .

The thinner the toroid, the better the coupling; for example if  $\frac{R}{a_1}$  is 20 instead of 5, Eqn. (6.51) yields  $k_1 k_2 = 0.993$ .

The internal flux of the primary conductors cannot be coupled to the secondary; Eqn. (6.35) applied to the external field toroid becomes:

$$k_1(\text{MAX}) = 1 - \frac{1}{4N[(1 + (\frac{a_1}{2R})^2) \ln \frac{8R}{a_1} - 2]}, \quad (6.52)$$

and yields  $k_1(\text{MAX}) = 0.9986$ , for  $\frac{R}{a_1} = 5$  and 0.9992 for  $\frac{R}{a_1} = 20$ . The  $d/3$  separation which results in  $k_1$  values of 0.989 and 0.993, is a much more severe limit.

An advantage of the toroid over the solenoid is that there is no length ambiguity in the toroid case. However, this is countered by the fact that the sheet secondary on the toroid must be cut somewhere to enable busbars to collect the current.

(ii) Separate layer of identical diameter conductor

The distance between the currents in this case is at least the conductor diameter, and it makes no difference which winding is considered to be the secondary. Eqn. (6.51), with  $a_2 = a_1(1 + \frac{2\pi}{N})$ , yields for  $N = 100$  turns:

$$k_1 k_2 \approx \frac{k_1}{k_2} = 0.9671 \text{ if } \frac{R}{a_1} = 5,$$

$$k_1 k_2 \approx \frac{k_1}{k_2} = 0.9803 \text{ if } \frac{R}{a_1} = 20.$$

As with the short solenoid, the coupling of a separate layer winding is relatively low, unless thousands of turns are used.

(iii) Bifilar winding

The factor which degraded the coupling of a bifilar winding in the short solenoid case, viz. the position displacement of one turn at each end, does not apply to the toroid. The bifilar windings can be identical in all respects, and, therefore can couple all but the internal flux of the primary turns. Thus, with solid conductors and  $\frac{R}{a_1} = 5$ ,  $k_1 k_2 = 0.9986$ , for example.

The very high degree of coupling will however be degraded by two practical considerations, as usual the need to cut and parallel the secondary turns to busbars, and the extent to which the two windings actually have the same major and minor radii. With a large number of turns, this last factor should be minimal, as the mean radii of the two should be very nearly the same. Noting that the external field toroid inductance, for  $\frac{R}{a} \geq 5$  can be written as  $L = \mu_0 R N^2 \ln \frac{R}{a}$  to within a few percent, we can deduce that:

$$\frac{a_2}{a_1} = \left(\frac{R}{a_1}\right)^{1 - \frac{k_1}{k_2}} \quad (6.53)$$

This equation enables the tolerance on the position of the conductors to be estimated, as in the tabulation below.



$\frac{k_1}{k_2}$	$\frac{a_2}{a_1}, \frac{R}{a_1} = 5$	$\frac{a_2}{a_1}, \frac{R}{a_1} = 20$
0.990	1.016	1.030
0.992	1.013	1.024
0.994	1.010	1.018
0.996	1.006	1.012
0.998	1.003	1.006

From the tabulation, it appears that  $\frac{k_1}{k_2} = 0.994$  could be attained if the average radii of the two windings are within 1% of each other, e.g. about 2 mm tolerance in a minor radius of 20cm.

(iv) Coaxial cable winding

To assess the coaxial cable method, we use the inductance expression for the external field toroid as  $L_1$  in equation (6.49). The result is:

$$\frac{k_1}{k_2} = 1 - \frac{\ln \frac{d_o}{d_i} + \frac{1}{4}}{N \left( 1 + \left( \frac{1}{2R} \right)^2 \right) \ln \frac{8R}{a_1} - 2}, \quad (6.54)$$

which, since  $k_2 = 1$  is also  $k_1 k_2$ .

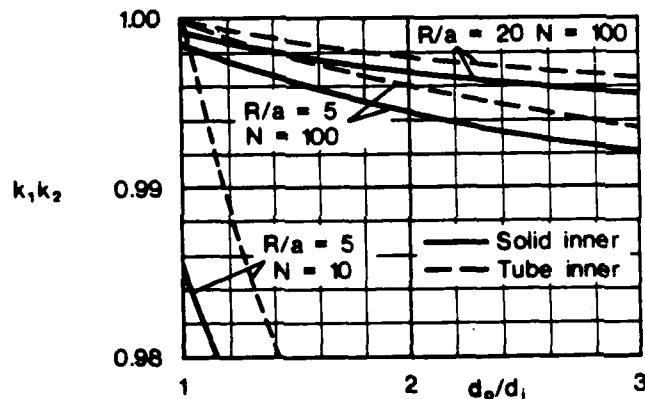


Fig. 71.  $k_1 k_2$  for external field toroid wound with coaxial cable.

Eqn. (6.54) is plotted in Fig. 71. Values of  $k_1 k_2$  greater than 0.99 appear easily attained, as in the short solenoid case, with  $N = 100$  turns. The values for tubular inner conductors are obtained by omitting the  $\frac{1}{4}$  term in the numerator of (6.54).

#### 6.2.4 The internal field toroid with various secondaries

The internal field toroid behaves as an infinitely long solenoid. The factor  $K$  in the solenoid inductance equation is unity and the external magnetic field is zero. When a secondary is placed upon it, all the flux of the inner winding links the outer; i.e. the coupling factor of the inner is unity.

##### (1) Thin sheet secondary

As with the solenoid, the tightest coupling will be obtained with the thin sheet secondary on the inside, as in Fig. 72.

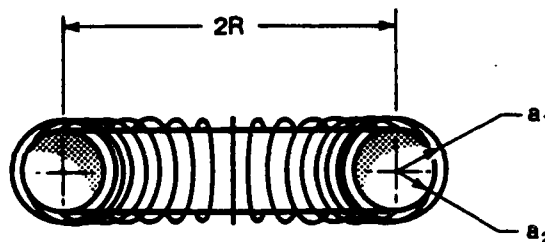


Fig. 72 Internal field toroid with thin sheet secondary on inside.

If the radius of the thin sheet secondary is  $a_2$ , and the radius of the primary is  $a_1$  (Fig. 72), then using the inductance expression (6.27) and the fact that  $k_2$  is unity, we obtain from the ratio of the inductances that:

$$k_1 k_2 = \left(\frac{a_2}{a_1}\right)^2 \quad (6.55)$$

For an internal field toroid with  $N$  tightly wound turns of diameter  $d$  and the thin sheet secondary located  $\frac{d}{3}$  away from the ideal location, Eqn. (6.55) becomes:

$$k_1 k_2 = \left(1 - \frac{2\pi R}{3N a_1}\right)^2 \quad (6.56)$$

If  $N = 100$  turns and  $\frac{R}{a_1} = 5$ , Eqn. (6.56) yields  $k_1 k_2 = 0.80$  and if  $\frac{R}{a} = 20$ ,  $k_1 k_2 = 0.34$ .

(ii) separate layer of identical diameter conductor

The separation between the currents is the conductor diameter and Eqn. (6.55) becomes:

$$k_1 k_2 = \left(1 - \frac{2\pi R}{N a_1}\right)^2, \quad (6.57)$$

which for  $N = 100$  and  $\frac{R}{a_1} = 5$ , yields  $k_1 k_2 = 0.4704$ .

(iii) Bifilar winding

As in the case of the external field toroid, the bifilar windings on the internal field toroid can be identical in all respects and all but the internal flux of the primary conductors can be coupled. Eqn. (6.35), for the maximum value of a coupling factor due to the internal flux limitation, becomes:

$$k_{1(\text{MAX})} = 1 - \frac{R}{2Na_1}, \quad (6.58)$$

which yields  $k_{1(\text{MAX})} = 0.975$ , which is also the maximum value of  $k_1 k_2$ .

(iv) Coaxial cable winding

For the coaxial cable method, we use Eqn. (6.49) with radius  $a$  instead of  $R$ , and Eqn. (6.27) for  $L_1$ , with the result:

$$\frac{k_1}{k_2} = 1 - \frac{2 \frac{R}{a_1} \left( \ln \frac{d_0}{d_1} + \frac{1}{4} \right)}{N} \quad (6.59)$$

Putting  $N = 100$  turns and  $\frac{R}{a_1} = 5$ , this equation gives:

$\frac{d_0}{d_1}$	$\frac{k_1}{k_2}$
1	0.975
1.2	.957
1.5	.934
2	.906

Since  $k_2 = 1$ , these are also the values of  $k_1 k_2$ .

Even though the internal field toroid has the benefit of one of the coupling factors being unity, it has much lower values of  $k_1 k_2$  than the solenoid and external field toroid. The secondary busbar connections to the internal field toroid would be cumbersome also, since they would have to be made around the whole major perimeter.

### 6.3 Forces and masses of windings in terms of stored energy

So far, in this Chapter, we have examined three forms of windings with regard to time constant and to their coupling to four forms of secondary. In this Section we will examine the winding forms in terms of the masses which they must have in order to have sufficient strength to contain a given amount of energy.

The need to consider winding strength can be seen from the example of an external field toroid of 1 m radius and 100 turns, carrying a current of 10,000 A. If the  $\frac{R}{a}$  ratio is 5, the field at the conductors would be about 1.4 T and would cause a force of 700 kgf/m which would bend the conductors inwards unless a supporting structure were provided.

In Ch. 3, using a simple pressure model, we determined that the minimum mass of the structure in tension,  $\sigma_s$ , that resists the forces on a coil storing energy,  $W$ , was  $M = \frac{\rho W}{\sigma}$ , where  $M$  is the mass, and  $\rho$  is the density of the structure. For the winding forms that we have studied we wish to know to what extent the minimum mass is approached and how much strength the conductors can contribute, and hence to what extent it is necessary to provide additional support structure.

#### 6.3.1 Mass of the short solenoid

According to the method of virtual work, the force,  $F_{(x)}$ , acting in direction  $x$  on a winding that carries current  $I$  is:

$$F_{(x)} = \frac{1}{2} I^2 \frac{\partial L}{\partial x} \quad (6.60)$$

Eqn. (6.12), written with an approximation due to Wheeler [13] for the factor  $K$ , gives the solenoid inductance,  $L_s$ , as:

$$L_s = \frac{\mu_0 \pi N^2 R^2}{l + 0.9R} \quad (6.61)$$

where  $N$  is the number of turns,  $l$  is the solenoid length and  $R$  is the solenoid radius. Eqn. (6.61) is in error by less than 4% for  $\frac{l}{R} \leq 2.5$ .

According to (6.60) and (6.61) the radial force,  $F_{(R)}$ , on a solenoid is:

$$F_{(R)} = \frac{1}{2} \mu_0 I^2 \pi N^2 \left[ \frac{2R}{l + 0.9R} - \frac{0.9R^2}{(l + 0.9R)^2} \right],$$

which may rearranged as:

$$F_{(R)} = \frac{W}{R} \left[ 1 + \frac{1}{1 + 0.9 \frac{R}{t}} \right] \quad (6.62)$$

where  $W = \frac{1}{2} L_s I^2$ , is the stored energy of the coil.

Eqn. (6.61) is positive; this indicates that the force acts in the direction of the radius ie is a bursting force (Fig. 73). Let us now suppose the windings to act as a thin cylinder which resists the bursting force.

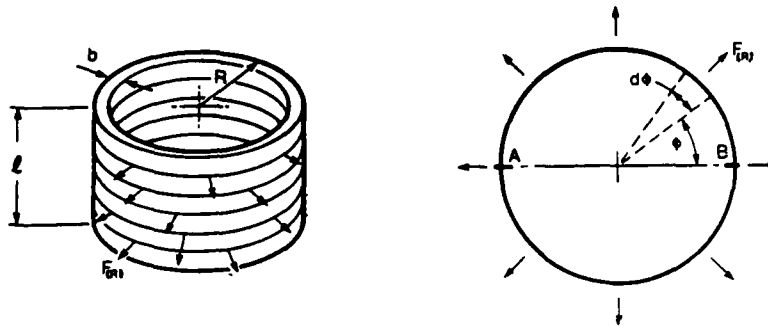


Fig. 73 Radial forces on solenoid. The force,  $F_{(R)}$  given by virtual work, is the total radial force.

To resist the bursting force, there must be a tension,  $T$ , in the cylinder. Since  $F_{(R)}$  is the total radial force on the whole coil, the force per unit length of the circumference is  $\frac{F_{(R)}}{2\pi R}$ . The vertical component of the force over a small arc,  $R d\phi$ , is  $\frac{F_{(R)}}{2\pi} \sin\phi d\phi$ . The tensile force,  $T$ , resisted at A and B is therefore:

$$T = 2 \int_0^{\pi/2} \frac{F_{(R)}}{2\pi} \sin\phi d\phi,$$

i.e.  $T = \frac{F_{(R)}}{\pi} \quad (6.63)$

If the tensile stress in the cylinder is  $\sigma_t$ , and cross section is  $t \times b$ , we have:

$$\sigma_t = \frac{T}{2tb} = \frac{F(R)}{2\pi tb}.$$

The volume of the cylinder wall is  $2\pi Rtb$ , and if the density of the cylinder material is  $w$ , the cylinder mass,  $M_s$ , is  $w2\pi Rtb$  and hence:

$$\sigma_t = \frac{wRF(R)}{M_s} \quad (6.64)$$

Substitution of (6.62) into (6.64) gives:

$$\sigma_t = \frac{wW}{M_s} \left[ 1 + \frac{1}{1 + 0.9R/t} \right]. \quad (6.65)$$

Half the flux of a long solenoid bends over and passes through the turns before reaching the end [14]. The rest curls over the end turns. The turns therefore have axial forces on them as in Fig. 74. Although the greatest forces are induced in the end turns, the centre turns have the greatest forces on them, because the accumulated forces are transmitted to the centre turns. The axial forces are well known to eventually destroy high field magnet coils because every time the magnet is pulsed the end turns receive an impulsive force which causes them to "ride over" the others and to damage insulation.

The total axial force is obtained from:

$$F(t) = \frac{1}{2} I^2 \frac{\partial L_s}{\partial t},$$

which, when applied to Eqn. (6.61), yields:

$$F(t) = - \frac{W}{t} \left[ \frac{1}{1 + .9R/t} \right]. \quad (6.66)$$

The - sign indicates that the direction of the force is opposite to that in which  $t$  increases, i.e. it indicates a compressive force. If the turns are rectangular in section and packed against each other they could resist this force (Fig. 74). Suppose that this is the case.

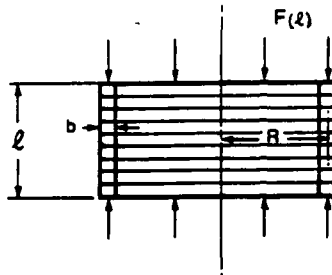


Fig. 74 Axial forces on solenoid. Rectangular section turns assumed for simple mass estimation.

The section over which the total force,  $F_{(t)}$ , acts is  $2\pi Rb$ , and hence,

$$F_{(t)} = \sigma_c 2\pi Rb,$$

where  $\sigma_c$  is the compressive stress experienced by the centre turns. Substituting  $w2\pi Rb$  for the mass,  $M_s$ , enables us to obtain:

$$\sigma_c = \frac{w}{M_s} F_{(t)} l. \quad (6.67)$$

Substituting (6.66) gives:

$$\sigma_c = \frac{w}{M_s} w \left[ \frac{1}{1 + 0.9R/l} \right] \quad (6.68)$$

We have now obtained a tensile stress and a compressive stress at right angles to each other. We need a failure theory for combined stresses. According to the maximum shearing stress theory (discussed further in Ch. 8),

the sum of  $\sigma_t$  and  $\sigma_c$  at failure is the yield stress in simple tension,  $\sigma_y$ . Adding Eqns. (6.65) and (6.68) and rearranging yields:

$$M_s \geq \frac{WW}{\sigma_y} \left[ 1 + \frac{2}{1 + 0.9R/a} \right]. \quad (6.69)$$

For the short solenoid with maximum time constant,  $\frac{R}{a} = 1.23$ , and its mass,  $M_{ss}$ , is from Eqn. (6.69):

$$M_{ss} \geq 1.95 \frac{WW}{\sigma_y}, \quad (6.70)$$

where  $\sigma_y$  is the yield stress of the conductor material.

### 6.3.2 Mass of the external field toroid

When the inductance expression for this toroid, viz.,

$$L = N^2 \mu_0 R \left[ \left( 1 + \left( \frac{a}{2R} \right)^2 \right) \ln \frac{8R}{a} - 2 \right]$$

is manipulated to obtain the forces in the major,  $R$ , and minor,  $a$ , radial directions, the results are:

$$F(R) = \frac{W}{R} \left[ 1 + \frac{1 - \left( \frac{a}{2R} \right)^2 \left( 2 \ln \frac{8R}{a} - 1 \right)}{\left( 1 + \left( \frac{a}{2R} \right)^2 \right) \ln \frac{8R}{a} - 2} \right], \quad (6.71)$$

$$\text{and} \quad F(a) = - \frac{W}{a} \left[ \frac{1 - \left( \frac{a}{2R} \right)^2 \left( 2 \ln \frac{8R}{a} - 1 \right)}{\left( 1 + \left( \frac{a}{2R} \right)^2 \right) \ln \frac{8R}{a} - 2} \right], \quad (6.72)$$

where  $W$  is the stored magnetic energy.

Eqn (6.71) is always positive, since  $R > a$ , and implies that the force in the direction of the major radius is a bursting force. To obtain the tensile stress due to this force, regard the toroid as a hoop (Fig. 75).



AD-A192 182

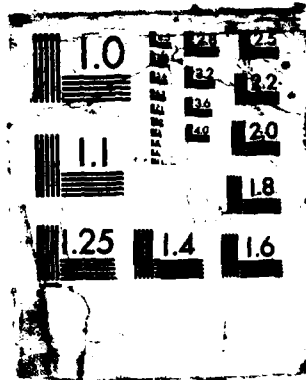
THE RAILGUN AND ITS POWER SOURCE(U) MATERIALS RESEARCH  
LABS ASCOT VALE (AUSTRALIA) D N SADEIN ET AL. JUN 87  
MRL-R-1058 DOD-AR-005-133

3/4

UNCLASSIFIED

F/G 28/3

NL



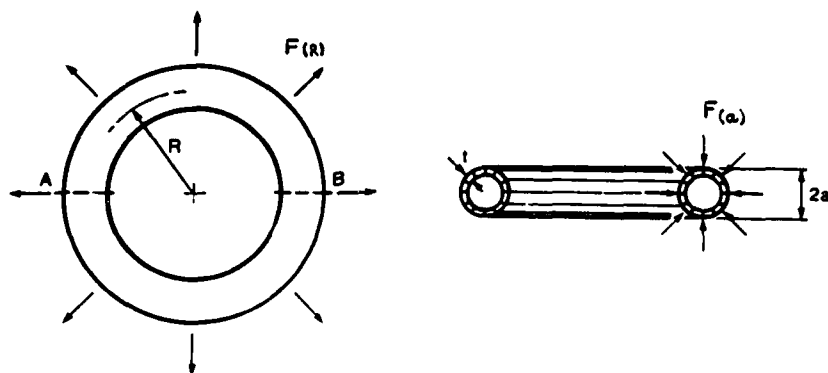


Fig. 75 External field toroid model for mass calculation.

The geometry is similar to that for the short solenoid, and, hence the tension,  $T$ , in the conductors at A and B, is:

$$T = \frac{F(R)}{w}$$

The cross sectional area of the wall (i.e. the sum of the cross sectional areas of the turns) is  $2\pi at$ , and the stress in the conductors,  $\sigma_t$ , is  $T/4\pi at$ . Since the volume of the conductors is  $4\pi^2 R at$ , we obtain  $\sigma_t$  as:

$$\sigma_t = \frac{w}{M_E} R F(R) \quad (6.73)$$

where  $w$  is the conductor density, and  $M_E$  is the conductor mass. Substitution of Eqn. (6.71) into (6.73) yields:

$$\sigma_t = \frac{wW}{M_E} \left[ 1 + \frac{1 - \left(\frac{a}{2R}\right)^2 \left(2 \ln \frac{8R}{a} - 1\right)}{\left(1 + \left(\frac{a}{2R}\right)^2\right) \ln \frac{8R}{a} - 2} \right] \quad (6.74)$$

Eqn. (6.72) is always negative; this implies that the force in the direction of the minor radius is a compressive force. As the calculation in the introduction to this section shows, it may be large. Unless the

conductors were specially shaped to form the wall of a tube, as indicated in Fig. 75, they could not resist the force and the coil would be crushed. As this is impractical, we must suppose that inner support, e.g. a tube, is provided. In either case, the force is resisted by hoop stresses, and the compressive force,  $C$ , across the wall area,  $4\pi Rt$ , is:

$$C = \frac{F(a)}{\pi}, \quad (6.75)$$

and the compressive stress  $\sigma_c$  can be written in terms of the mass of the tube as:

$$\sigma_c = \frac{W}{M_E} a F(a) \quad (6.76)$$

Substituting (6.72) into (6.76) gives:

$$\sigma_c = \frac{W}{M_E} \left[ \frac{1 - \left(\frac{a}{2R}\right)^2 (2 \ln \frac{8R}{a} - 1)}{(1 + \left(\frac{a}{2R}\right)^2) \ln \frac{8R}{a} - 2} \right] \quad (6.77)$$

Using  $\sigma_c + \sigma_t = \sigma_y$  as the failure criterion, the mass,  $M_E$ , of the external field toroid is obtained from Eqns. (6.74) and (6.77):

$$M_E \geq \frac{W}{\sigma_y} \left[ 1 + \frac{2(1 - \left(\frac{a}{2R}\right)^2 (2 \ln \frac{8R}{a} - 1))}{(1 + \left(\frac{a}{2R}\right)^2) \ln \frac{8R}{a} - 2} \right] \quad (6.78)$$

Evaluation of (6.78) gives:

$$\frac{R}{a} = 5, M_E \geq 2.08 \frac{W}{\sigma_y}$$

$$\frac{R}{a} = 20, M_E \geq 1.65 \frac{W}{\sigma_y}$$

### 6.3.3 Mass of the internal field toroid

The inductance expression for this toroid, viz.:

$$L = \mu_0 N^2 \frac{a^2}{2R},$$

gives the force components in the major and minor radial directions, in terms of the stored energy,  $W$ , as:

$$F_{(R)} = -\frac{W}{R}, \quad (6.79)$$

and  $F_{(a)} = \frac{2W}{a} \quad (6.80)$

The signs of these equations imply that the major radial force is compressive, while the minor radial force is tensile, i.e. the opposite to those of the external field toroid (Fig. 76).

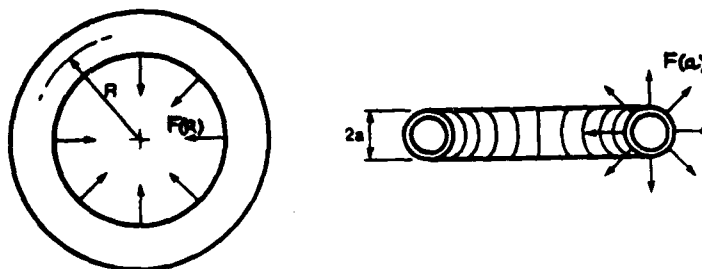


Fig. 76 Internal field toroid model for mass calculation.

The tensile forces can be resisted by the hoop shape of the conductors around the minor radius, but the compressive forces cannot, except in the impractical case in which the conductors are wedge shaped, to form a solid hoop in the major radial direction. An inner tube is therefore necessary to resist the compressive forces, in reality. The tension and compression stresses for the model in Fig. 76 are:

$$\sigma_t = \frac{2W}{M_I} \quad (6.81)$$

$$\sigma_c = \frac{W}{M_I} \quad (6.82)$$

and the mass,  $M_I$ , is:

$$M_I \geq 3 \frac{W}{\sigma_y} \quad (6.83)$$

#### 6.4 Discussion

Having studied various primary and secondary forms we are now able to choose the best geometry for the pulse transformer. The forms studied have been single layer windings, and a brief consideration of multilayer windings in this Section suggests that they are not suitable.

##### 6.4.1 Comparison of the single layer winding forms

In the Section on time constants, we obtained the following results for a winding of 100 turns.

<u>Coil type</u>		<u>Time constant, relative to Brooks Coil</u>
Short Solenoid:	$\frac{D}{t} = 2.46$	0.34
Ext Field Toroid:	$\frac{R}{a} = 5$	0.42
	$\frac{R}{a} = 20$	0.29
Int Field Toroid:	$\frac{R}{a} = 5$	0.21
	$\frac{R}{a} = 20$	0.13

In the Section on degree of coupling, the following results were obtained for a winding of 100 turns, for four types of secondary.

Degree of coupling: Maximum values of  $k_1 k_2$

Coil type	Type of secondary			
	Thin sheet	Separate layer	Bifilar	Coaxial cable ( $d_o/d_i = 1.5$ )
Short Solenoid:				
$\frac{D}{t} = 2.46$	0.981	0.96	0.98	0.996
E.F. Toroid: $\frac{R}{a} = 5$	0.989	0.967	0.999	0.996
$\frac{R}{a} = 20$	0.993	0.98	0.999	0.998
I.F. Toroid: $\frac{R}{a} = 5$	0.80	0.47	0.975	0.934

The following results were obtained for the minimum mass required to store energy,  $W$ , if the conductor shearing stress is  $\sigma_y$ , its yield stress in simple tension, and the conductor density is  $w$ .

<u>Coil type</u>	<u>Minimum mass</u>
Short solenoid:	$1.95 \frac{wW}{\sigma_y}$
E.F. Toroid, $\frac{R}{a} = 5$ :	$2.08 \frac{wW}{\sigma_y}$
$\frac{R}{a} = 20$ :	$1.65 \frac{wW}{\sigma_y}$
I.F. Toroid	$3 \frac{wW}{\sigma_y}$

In each of the above categories, the internal field toroid is a relatively poor performer. The short solenoid and the external field toroid have similar properties, except in the case of bifilar windings, where the external field toroid is much superior. Note that for the bifilar winding on the external field toroids to have the limiting  $k_1 k_2$  values shown, the conductor placement would have to be accurate to within a few parts in a thousand.

On the above figures, the short solenoid and the external field toroid, using coaxial cable windings, are equal best choices. Consideration of some more subtle points, however, favours the external field toroid.

Firstly, the forces are distributed evenly over the external field toroid, whereas both the tension and compression forces on the solenoid vary with axial distance from the centre. The compression forces of the solenoid accumulate so that the centre turns have the greatest force on them. Unless rectangular section conductors are used, these compression force may cause conductors to ride over each other, and every time the solenoid is pulsed, the insulation of the centre turns receives a blow. In addition, the last half of each end turn of the solenoid is not restrained by hoop stress and tends to unwind. A restraining structure is necessary for these turns. In the external field toroid, each turn experiences only its own compression force; not the accumulation of the forces on the conductors around it and therefore the insulation must bear only the force of one turn. There is no end turn problem because the minor radial forces hold the turns in place against their inner supports and because the beginning and end turns are adjacent to each other and may be easily coupled to a linkage to complete the "hoop" to resist the major radial forces.

The second reason for favouring the external field toroid is that its symmetry is more likely to produce high coupling during the transfer of energy. The coupling factors which have been calculated assume equal current distribution amongst the secondary conductors, but initially the current will distribute so as to produce no internal flux. The external field toroid

practically has this property with a uniformly distributed current, hence we can expect the transient distribution to naturally match the primary current distribution. Although, as discussed in Section 6.5.4, the induction process should force equal current division in the solenoid secondary, the natural transient distribution would be for current to crowd towards the end turns.

#### 6.4.2 Tension and compression components of coil mass

The expressions (6.69), (6.78) and (6.83) for winding mass,  $M$ , are all of the form:

$$M = \frac{WW}{\sigma_y} [(1 + K) + K], \quad (6.84)$$

where  $K$  is a dimensionless factor derived from the coil geometry. In the case of solenoids  $K$  is Nagaoka's factor.

Inspection of the expression in section 6.3 shows that factor  $(1 + K)$  yields the portion of the mass due to tensile forces and factor  $K$  yields the portion of the mass due to compression forces. When  $K$  becomes small compared to unity, the compression portion diminishes and the mass approaches the minimum value of  $\frac{WW}{\sigma_y}$ . This is the same value as was found in Ch. 3 from quite general considerations.

Putting  $K = 1$ , i.e. the long solenoid factor, we obtain

$M = 3 \frac{WW}{\sigma_y}$ , which is the same as the internal field toroid mass, since this toroid is effectively an infinitely long solenoid. In this case  $\frac{1}{3}$  of the coil mass is due to compressive force and  $\frac{2}{3}$  to tension force. The shorter the solenoid, the less is factor  $K$  and the less is the proportion of mass due to compressive force. For the maximum time constant solenoid,  $K = 0.48$ , and 19% of the mass is due to the compressive force. The factor  $K$  in the case of the external field toroid is approximately  $\frac{1}{\ln R_a}$  (Eqn. 6.77). The greater  $\frac{R_a}{a}$  i.e. the thinner that this toroid is, the less the proportion of the mass is due to compressive force. Note that making the toroid thinner does not eliminate the compression forces; they actually increase, but the tension forces increase at a much greater rate. Very short solenoids and very thin external field toroids approach the pure tension, minimum mass given by  $\frac{WW}{\sigma_y}$ .

#### 6.4.3 Multilayer coils

Multilayer coils, such as the Brooks Coil, are more compact and have longer time constants than the single layer coils which have been studied.

In the Section on degree of coupling it was pointed out that perfect coupling requires two coils to be physically identical and to occupy the identical space. A bifilar winding of many layers of fine wire enables two identical coils to occupy the same physical space and thus to have the geometrical basis for very tight coupling. There is a practical difficulty in cutting the turns of the secondary winding and connecting them in parallel to form a single turn secondary. More importantly, the high frequency response



of such a secondary might be poor. The resistance of multilayer coils is known to be hundreds of times the d.c. values at frequencies of about a kilohertz [15]. The secondary time constants may be so short during the transfer of energy that the efficiency would be quite low, even though the degree of coupling is basically high.

Another limitation of multilayer coils is that intense magnetic fields act upon the inner layers of, for example, solenoids and cause high stresses which determine the maximum stored energy, even though the stress in other layers may be quite low. Thus, for multilayer coils the energy stored for a given mass will be less than for single layer coils when strength is taken into account.

Although a more detailed investigation of the above limitations is necessary to rule out multilayer coils altogether, no further consideration is given to them in this work.

#### 6.5 Flux distribution and inductance of real windings

The investigations so far in this Chapter and in Ch. 5 give us a fairly detailed understanding of the pulse transformer in terms of electromagnetics and circuit theory and the physical reality of the transformer. The transformer models used have still been idealized in that inductance expressions used generally apply to current sheet distributions. In this Section the effects of using real conductors are examined in four ways, viz:

- (i) the location of an equivalent current sheet;
- (ii) the flux distribution of real conductors compared to current sheets;
- (iii) the inductance of a real coil compared to current sheets; and,
- (iv) the transient current distribution of the secondary.

##### 6.5.1 The location of an equivalent current sheet

Perfect coupling requires a winding to have the same flux linking another winding as links itself. With real conductors there is internal flux that cannot link another winding; this was dealt with for solid round conductors in Section 6.2.1. Some of the mutual flux of the turns may also not be fully linked to both windings. In effect the windings are separated and we wish to know what the separation is.

Fig. 77 shows a section of a winding of round conductors with a thin sheet secondary. There is flux on one side of the windings and none on the other, so they may be taken to represent either a toroid or a long solenoid. In Fig. 77(a) the thin sheet is on the flux side of the primary and in 77(b) it is on the other side. The distributed current in the primary causes its flux density to vary from zero to  $B_0$  across the section whereas the flux density of the secondary rises as a step function.

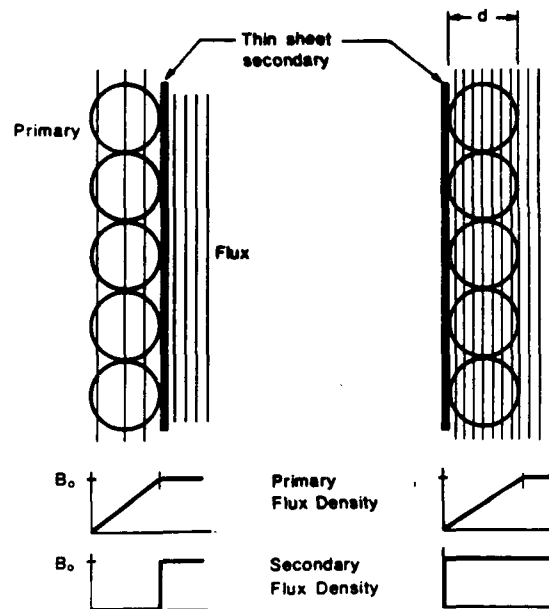


Fig. 77 Round conductor primary with thin sheet secondary. (a) secondary on flux side, (b) secondary on non flux side of primary.

When the thin sheet secondary is on the flux side of the primary, the flux within the primary cannot link it. With the simplifying assumption that the primary is rectangular in section, with thickness  $d$ , and that the flux rises from zero to  $B_0$  linearly, the flux linkage per unit width within the primary, obtained by integration, is  $B_0 \frac{d}{3}$ . The primary current can therefore be replaced by a current sheet which gives rise to flux density  $B_0$  and is positioned distance  $\frac{d}{3}$  from the flux side surface of the primary conductors. Such a current sheet will cause the same flux linkage per unit width with the secondary as the actual primary current and will also have the same uncoupled flux linkage.

When the sheet secondary is on the zero flux side of the primary, it has partial flux linkages per unit width with the distributed primary current to a value of  $B_0 \frac{d}{2}$ , instead of a full linkage of  $B_0 d$ . The linkage is therefore diminished by  $B_0 \frac{d}{2}$  and in this case an equivalent current sheet for the primary is located at  $d/2$ .

### 6.5.2 The flux distribution of $N$ conductors compared to a current sheet

One way to determine the number of conductors needed to approximate a current sheet distribution is to calculate the flux distribution of discrete conductors and compare the result with a current sheet distribution. A convenient conductor system to study is a set of  $N$  parallel wires on a long cylinder, since the internal and external current sheet flux densities are easily calculated. If the wires on a cylinder have practically the same flux distribution as a current sheet, then no matter what shape the cylinder of wires is bent into, its flux distribution will be the same as a current sheet of that shape.

Fig. 78 shows a cross section of the cylindrical arrangement. The conductors are symmetrically spaced. Since there is no current within the cylinder, there can be no complete flux lines within it. If there is flux within the cylinder, therefore, its vector sum around any path must be zero. Since the conductors are arranged symmetrically, the flux vectors along radial lines through the conductors, at equal radial distances (such as at  $X, Y$  in Fig. 78), must be identical. These considerations suggest that the flux vectors, within the cylinder of wires, must oscillate in sign and complete at least one cycle over the angular distance between conductor positions.

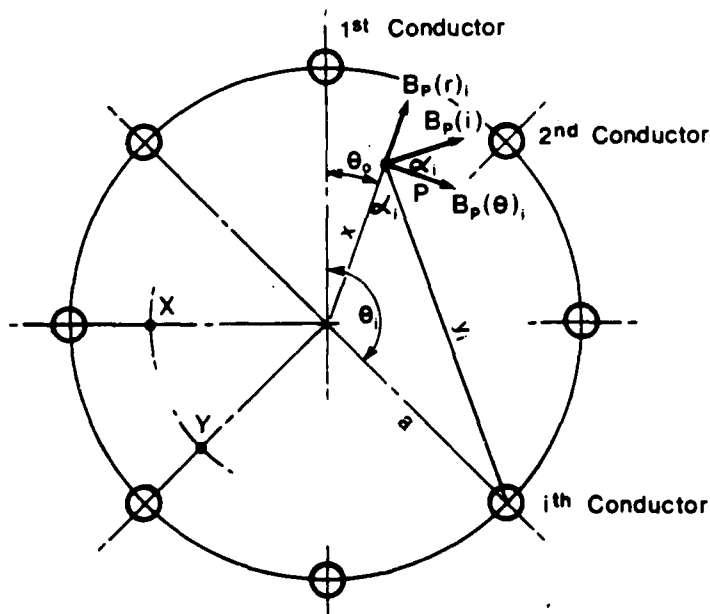


Fig. 78 Geometry for calculation of flux distribution of a cylinder of parallel conductors.

Fig. 78 shows the field components at a point P, due to the  $i$ th conductor. Each conductor carries current  $I$ . The field at P is given by:

$$B_P(i) = \frac{\mu_0 I}{2\pi} \cdot \frac{1}{y_i} \quad (6.85)$$

The radial component,  $(B_P(r)_i)$ , and the tangential component,  $(B_P(\theta)_i)$ , are:

$$B_P(r)_i = \frac{\mu_0 I}{2\pi} a \frac{\sin(\theta_i - \theta_0)}{y_i^2} \quad (6.86)$$

$$B_P(\theta)_i = \frac{\mu_0 I}{2\pi} \frac{(x - a \cos(\theta_i - \theta_0))}{y_i^2} \quad (6.87)$$

The total component values at P are therefore:

$$B_P(r) = \frac{\mu_0 I a}{2\pi} \sum_{i=1}^N \frac{\sin(\theta_i - \theta_0)}{y_i^2} \quad (6.88)$$

$$B_P(\theta) = \frac{\mu_0 I a}{2\pi} \sum_{i=1}^N \frac{(x/a - \cos(\theta_i - \theta_0))}{y_i^2} \quad (6.89)$$

where  $y_i^2 = a^2 + x^2 - 2ax \cos(\theta_i - \theta_0)$  (6.90)

and  $B_P = [B_P^2(r) + B_P^2(\theta)]^{1/2}$  (6.91)

Although the above equations are derived for point P within the circle, they also apply to points outside.

To display clearly the manner in which flux accumulates, let us select  $N = 6$ , i.e. a small number of conductors. Fig 79 shows the vector field

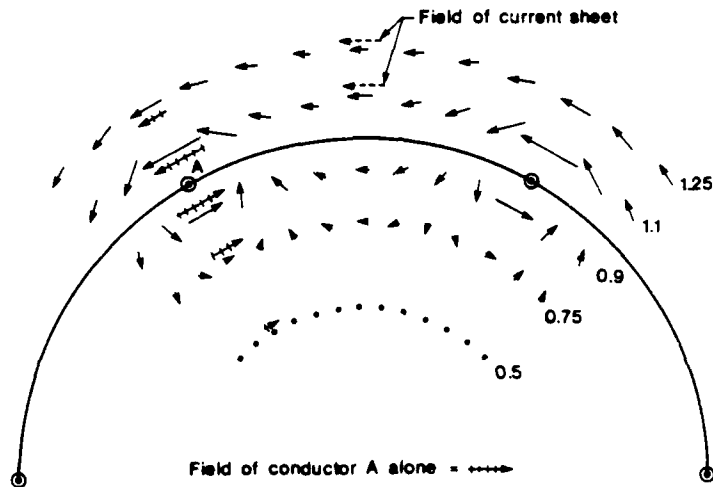


Fig. 79 Flux vectors for 6 conductors.

given by Eqn. (6.91), and Figs 80 and 81 are plots of the magnitudes of the components of the flux vectors as a function of angular position between conductors. In these plots,  $a$  is taken as unit length and  $\frac{\mu_0 I}{2\pi}$  is also taken as unity.

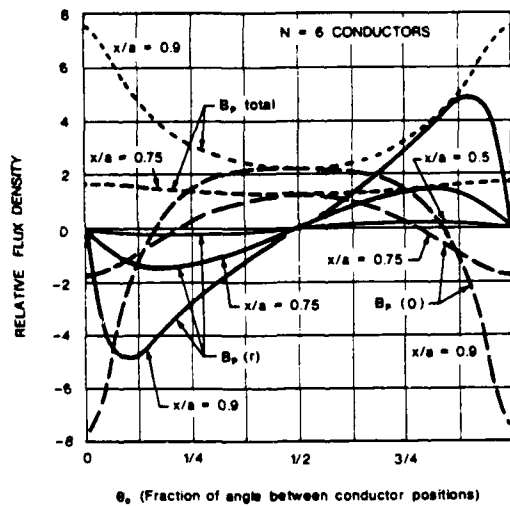


Fig. 80 Flux density vector components for internal points (i.e.  $\frac{x}{a} < 1$ )

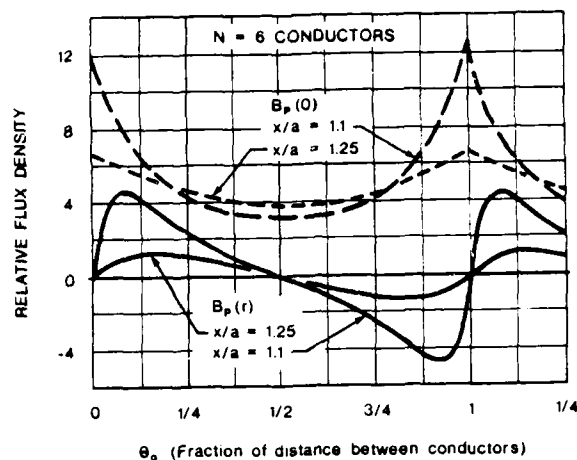


Fig. 81 Flux density vector components for external points (i.e.  $\frac{x}{a} > 1$ )

Figure 79 shows that the internal space is filled with flux vectors which are oriented at all angles between  $0^\circ$  and  $360^\circ$  and rapidly diminish in magnitude in the central region. The magnitude and orientation of these vectors must be such that no matter how a closed path is taken, their line integral is zero. Near the circumference (e.g. at  $\frac{x}{a} = 0.9$ ) the vectors in between the conductors oscillate less and point in the same general direction. The reversed vectors, necessary to make the line integral zero at a radius just within the circle, are concentrated near the conductors. The unidirectional tendency of the vectors in between the conductor positions is the same as that of the vectors just outside the circle i.e. there is no sharp distinction between the external field and the internal field. The internal/external field difference is concentrated near the conductor, where, internally, the conductor field is opposite that of the in between vectors, and, externally, the conductor field is in the same direction as that of the in between vectors. At the conductor positions the field clearly curls around the conductors as if they were isolated.

The magnitude of the internal vectors diminishes rapidly with distance from the circumference; at  $\frac{x}{a} = 0.5$  their magnitudes are only a few percent of the values at  $\frac{x}{a} = 0.9$ . Even with only 6 conductors, the field inside rapidly becomes practically zero i.e. rapidly becomes the same as if there were a uniform current sheet at the circumference.

Also shown in Fig 79 are the vectors for a conductor by itself (conductor A) at points along a radial line through its centre, and for the external field which a current sheet of magnitude  $NI$  would produce. The individual conductor fields make the dominant contribution near the

conductors. Externally, they rapidly become a smaller part of the total field and internally, they are rapidly cancelled. For example, at  $\frac{x}{a} = 0.5$ , the total internal field has a relative value of 0.191, whereas the single conductor field has a relative value of 2. The results indicate that the external field soon reaches current sheet values, also. At  $\frac{x}{a} = 1.25$ , the field varies between 6.7 units and 3.5 units, compared to a current sheet (i.e. the average) value of  $\frac{6}{1.25} = 4.8$  units.

Figures 80 and 81 show how the internal and external field components vary in between conductor positions. In both cases, the radial components oscillate in sign, and the peak values are near the conductors, so as to cause the resultant field to cross the circumference at right angles. The internal field radial components are similar in magnitude to the tangential components, near the conductor positions where they cause the field to curl around the conductor. Externally, the radial components are much less than the tangential components.

The flux distribution for only 6 conductors clearly settles down rapidly to that of a uniform current sheet. At  $\frac{x}{a} = 0.5$  and  $\frac{x}{a} = 2$ , the field is almost indistinguishable from that of a current sheet. As the number of conductors is increased, the mutual cancellation of the internal flux and the additive effect of external flux will increase. Current sheet like results will thus approach the circumference rapidly as the number of conductors is increased, e.g. to a few times as many as six. The minimum number of conductors that produces a field equivalent to a current sheet in all the space about the coil will be the number required to cause the field at the conductor surfaces to be very nearly the same as would be produced by a current sheet.

Let us now calculate the effect of increasing the number of conductors. Let us also consider only points on radial lines through the conductor positions (ie  $\theta_0 = 0$  in Fig. 78). The greatest distortion in the flux distribution occurs at these points, so when the flux density at these points is close to that of a current sheet, the flux density at all other points will be very much closer. In the case of the external field the comparison with a current sheet is given by

$$\frac{B_{P(N \text{ COND})}}{B_{P(\text{SHEET})}} = \frac{x}{N} \frac{1}{1 - \frac{x}{a}} \frac{[x/a - \cos \theta_1]}{y_1^2}, \quad (6.92)$$

in normalized units, since  $B_{P(\text{SHEET})} = \frac{\mu_0 NI}{2\pi x}$  and, through the conductor positions,  $\theta_0 = 0$ . In the case of the internal field, the current sheet value is zero, and to measure the extent of cancellation as the number of conductors is increased, let us compare the field of  $N$  conductors with that produced by an isolated conductor. For a point at distance  $x$  from the centre, along a radial line through a conductor position, the distance from the conductor to the point is  $(x-a)$ , and so the field intensity due to that conductor alone is:

$$B_{P(1 \text{ COND})} = \frac{\mu_0 I}{2\pi(x-a)}, \quad (6.93)$$

$$\text{and } \frac{B_{P(N \text{ COND})}}{B_{P(1 \text{ COND})}} = \left(1 - \frac{x}{a}\right) \sum_{i=1}^N \frac{[x/a - \cos \theta_i]}{y_i^2}. \quad (6.94)$$

Eqns. (6.92) and (6.94) are plotted in Figs 82 and 83. Both diagrams show that when the number of conductors exceeds about 48, the fields approach current sheet values quite close to the circumference i.e. as  $x/a$  approaches 1. The internal field at  $\frac{x}{a} = 0.9$  is only 3% of the field which an isolated conductor would produce at the same point, and the external field at the same distance from the other side of the circumference (i.e.  $\frac{x}{a} = 1.1$ ) is only 1% above the current sheet value. As these are the worst case flux density departures from current sheet values, we can conclude that 48 or more conductors yields a field distribution that is indistinguishable from a

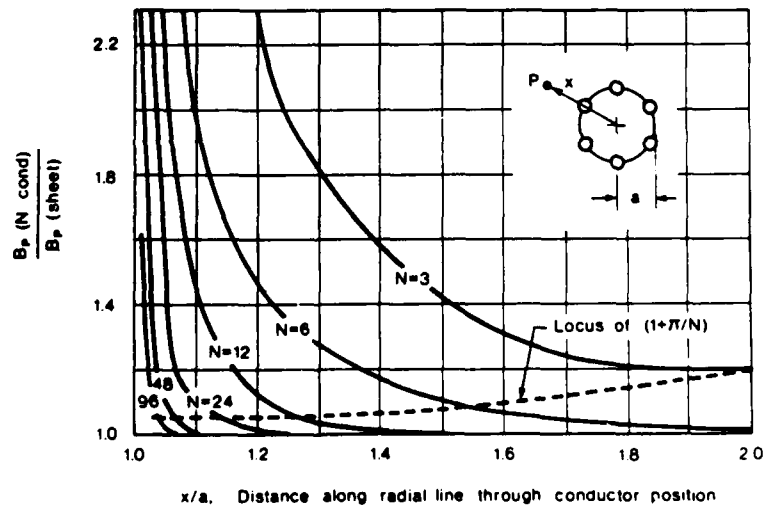


Fig. 82 Flux density outside cylinder of N conductors compared to current sheet.



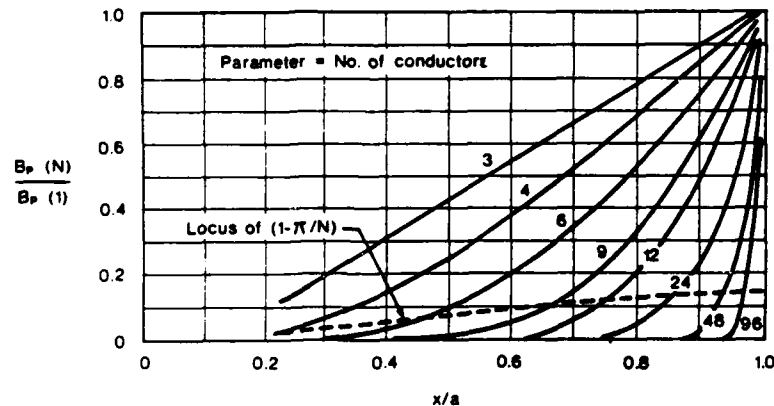


Fig. 83 Flux density within cylinder of  $N$  conductors, compared to isolated conductor.

current sheet, except within a few percent of the radius from the circumference.

Let us next take into account the conductor radius, since this determines how near to the circumference we can in practice take point  $P$ . If the conductors almost touch each other:

$$\left(\frac{x}{a}\right)_{\text{MAX}} = 1 - \frac{\pi}{N}, \text{ for internal points, and,}$$

$$\left(\frac{x}{a}\right)_{\text{MIN}} = 1 + \frac{\pi}{N}, \text{ for external points.}$$

The locus of  $(1 - \frac{\pi}{N})$  is plotted on Fig. 83; it crosses the conductor curves at  $B_p(N \text{ COND})/B_p(1 \text{ COND})$  values between 0.1 and 0.14. If the conductors almost touch each other the field intensity just outside the conductor inner surface is thus less than 0.14 of the intensity just outside the isolated

conductor surface, for all practical numbers of conductors. The locus of  $(1 + \frac{\pi}{N})$ , plotted on Fig. 82, shows that, for all practical numbers of conductors, the external flux density at the conductor surface is less than 7% greater than the current sheet value. Since Figs. 82 and 83 represent the worst case departures, we can conclude that for all practical numbers of conductors, that virtually touch each other, the flux density in the space within and without the cylinder is practically indistinguishable from that of a current sheet located at the mean diameter of the cylinder.

If there is space between the conductors the conductor diameters must be less than when the conductors touch, and the conductor surfaces become closer to the mean diameter, i.e., they are in regions where the current sheet approximation is poorer. If the conductors occupy fraction  $K$  of the circumference, the conductor diameter is  $\frac{K \cdot 2\pi a}{N}$  and the surface flux density ratios, using Eqns. (6.92) and (6.94) are:

$$\frac{B_{P(N \text{ COND})}}{B_{P(\text{SHEET})}} = \frac{(1 + \frac{\pi}{KN})}{N} \frac{N}{1 \sum_{i=1}^N} \frac{[(1 + \frac{\pi}{KN})/a - \cos \theta_1]}{y_1^2}, \quad (6.95)$$

for the external flux, and,

$$\frac{B_{P(N \text{ COND})}}{B_{P(1 \text{ COND})}} = (1 - \frac{\pi}{KN}) \frac{N}{1 \sum_{i=1}^N} \frac{[(1 - \frac{\pi}{KN})/a - \cos \theta_1]}{y_1^2}. \quad (6.96)$$

Eqns. (6.95) and (6.96) are plotted in Fig. 84, from which it can be seen that for all numbers of conductors greater than about 10 the relative flux density at the conductor surface is constant. For  $K = \frac{1}{2}$ , as in bifilar winding, the external flux density is about 27% greater than the current sheet value. Using Fig. 82, we can deduce that for as few as 12 conductors, the 27% increase drops to only 4 or 5%, one conductor diameter further away from the conductor surface.

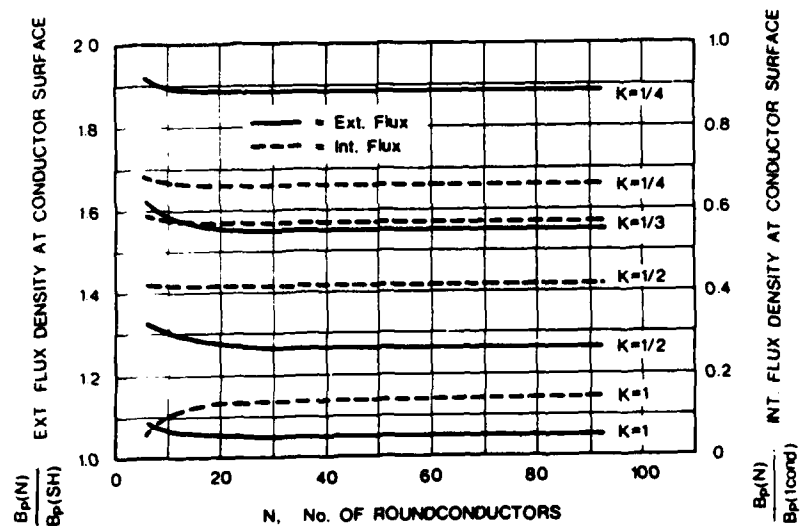


Fig. 84 Relative flux densities at conductor surfaces.  $K$  is the conductor space factor.

The flux distributions have been calculated for conductors that are exactly symmetrically placed. This may not occur in practice, although if the space factor is unity, placement errors will be reduced. Errors in placement might occur because a conductor is not exactly on the circumference, or because there are random pitch errors, causing conductors to bunch together in places and to have gaps at others, or because there is a constant pitch error, causing a gap that is too narrow or too wide.

The writer investigated the effect of pitch errors by modifying the flux density equations (e.g. by the use of random generator functions) and when the programs were run, the results were:

- (i) the internal field increases greatly with placement errors, especially in the neighbourhood of the smallest gap between conductors;
- (ii) the external field also increases, but not nearly so much, again in the neighbourhood of the smallest gap;

- (iii) overall, the increase in total flux was small, and in the case of the external field, the disturbed regions did not penetrate far from the circumference.

Altogether, it did not seem that inductance would be significantly altered (i.e. > 1%) by likely errors in conductor placement.

### 6.5.3 The inductance of an N conductor external field toroid

The calculations and graphs in the previous Section suggest that the flux of a cylinder of conductors that touch each other is practically the same as a current sheet in all the space around the conductors. We expect the same to be true for other configurations. In this Section we shall calculate the inductance of the external field toroid, which is the cylinder of parallel wires bent into a circle, from basic expressions to see how much its inductance, with N turns of round wire, differs from the current sheet expression.

The total inductance,  $L_T$ , of a winding of N turns consists of two parts;  $EM_{mn}$ , the sum of the mutual inductances of every turn with every other turn, and  $EL_s$ , the sum of the self inductances of the individual turns. Thus,

$$L_T = \sum_{m=1}^N \sum_{n=1}^N M_{mn} + \sum_{s=1}^N L_{s1}. \quad (6.97)$$

If we consider the filaments to carry current in parallel instead of in series, the current is NI instead of I, where I is the current in each conductor, and, since energy must be conserved (as was argued in Section 6.1.4), the inductance is the value given by (6.97) divided by  $N^2$ . As  $N \rightarrow \infty$  we obtain the uniform surface current condition to which Eqn. (6.19), viz.

$$L = \mu_0 R \left[ \left( 1 + \left( \frac{a}{2R} \right)^2 \right) \ln \frac{8R}{a} - 2 \right],$$

applies.

The geometry of the external field toroid for inductance calculations is given in Fig. 85. For the mutual inductance calculation we consider the turns to carry filamentary current concentrated at their centres. This will not produce quite the same flux linkages as the actual

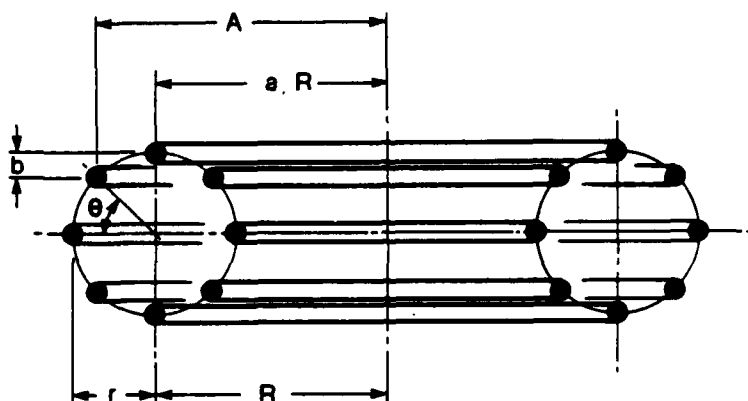


Fig. 85 External field toroid geometry for inductance calculation.

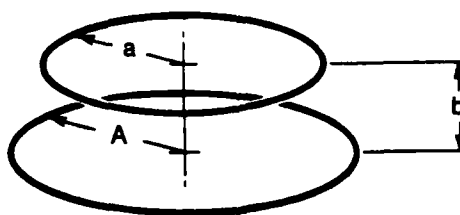


Fig. 86 Coaxial circles to which mutual inductance expression applies.

distributed current, but the error will be very small, especially for large numbers of turns. We use this model because there exists a mathematically exact expression for the mutual inductance of coaxial filamentary circles of current, [16], viz:

$$M = \frac{4\pi}{10} \sqrt{AA} \left[ \left( \frac{2}{c} - c \right) F - \frac{2}{c} E \right] \mu H, \quad (6.98)$$

where A and a are the radii of the circles (Fig. 85) and

$$c = \frac{2\sqrt{Aa}}{\sqrt{(A+a)^2 + B^2}},$$

and F and E are the complete elliptic integrals of the 1st and 2nd kinds respectively, of modulus c.

In Fig. 85, R is the major radius, r is the minor radius, A is the radius of the i-th turn and a is the radius of a turn x positions further around the minor diameter. From the figure we have:

$$A = R + r \cos i\theta, \quad (6.99)$$

$$\text{and,} \quad a = R + r \cos (i + x)\theta, \quad (6.100)$$

$$\text{and,} \quad b = r [\sin(i + x)\theta - \sin i\theta] \quad (6.101)$$

where  $\theta$  is the angle between conductor positions i.e.  $\theta = 360/N$ . Since  $M_{12} = M_{21}$  etc. it is only necessary to form the sum of half the combinations, i.e.  $\frac{N(N-1)}{2}$  combinations where N is the number of conductors (circles), and then double the answer.

The self inductance of each turn should, strictly, be calculated by Eqn. (6.98) also. However, because the conductor diameter is small compared to the circle diameter (e.g.  $\frac{1}{100}$ th) the expressions:

$$L_s = \mu_0 A \ln \frac{A}{r_w}, \quad (6.102)$$

where  $r_w$  is the conductor radius, is accurate enough. The self inductance term is small compared to the mutual inductance term and errors in it do not greatly degrade the overall result. Radius A is different for every conductor position, but calculation shows that we can in fact use the mean value, R, for A, with small error. Thus,

$$\sum_{i=1}^N L_{s1} \approx N \mu_0 R \ln \frac{R}{r_w}. \quad (6.103)$$

(Exact calculation of (6.102) for the case where  $\frac{R}{r} = 2$  and  $N = 12$  showed that (6.103) is in error by about 3%. When  $\frac{R}{r} = 5$  and  $N = 100$ , the error is about 0.2%).

The effect of conductor space factor can be simply included because it is related to the conductor radius,  $r_w$ . If the space factor is  $K$ , ie the conductors cover fraction  $K$  of the minor circumference, then:

$$r_w = \frac{Kwr}{N} \quad (6.104)$$

Eqn. (6.97), divided by  $N^2$  to yield the "single turn" inductance for comparison purposes, evaluated using Eqns. (6.98) and (6.103), is tabulated

Maj/Min Rad.		10								
K	$L_{SH}$	3.007 $\mu H$			2.169 $\mu H$			1.189 $\mu H$		
		1	0.5	0.25	1	0.5	0.25	1	0.5	0.25
$L_T$	2.911	2.965	3.020	2.072	2.126	2.181	1.087	1.142	1.196	
$L_M$	2.602	2.602	2.602	1.817	1.817	1.817	0.905	0.905	0.905	
$L_S$	0.309	0.363	0.418	0.254	0.309	0.363	0.182	0.237	0.291	

N = 36 Turns										
$L_T$	2.964	2.988	3.103	2.126	2.150	2.174	1.144	1.68	1.92	
$L_M$	2.799	2.799	2.799	1.984	1.984	1.984	1.034	1.034	1.034	
$L_S$	0.166	0.190	0.214	0.141	0.166	0.190	0.109	0.134	0.158	

N = 60 Turns										
$L_T$	2.981	2.996	3.010	2.143	2.157	2.172	1.162	1.176	1.191	
$L_M$	2.871	2.871	2.871	2.047	2.047	2.047	1.085	1.085	1.085	

N = 100 Turns										
$L_T$	2.992	3.000	3.009	2.153	2.162	2.171	1.172	1.181	1.190	
$L_M$	2.919	2.919	2.919	2.089	2.089	2.089	1.120	1.120	1.120	
$L_S$	0.072	0.081	0.090	0.064	0.072	0.081	0.052	0.061	0.070	

Tabulation of inductance (in microhenries) for 1 m major radius external field toroid, for various numbers of turns,  $N$ , and space factors,  $K$ , normalized to the single turn value.  $L_{SH}$  is the inductance given by the current sheet expression, (6.19), and  $L_T$ ,  $L_M$  and  $L_S$  are the total, mutual and self inductances for the toroids made up of turns.

below. The total, mutual, and self inductances are given for space factors,  $K$ , of 1, 0.5 and 0.25. The inductance given by the thin tube expression (6.19),  $L_{SH}$ , is also tabulated. The inductance values are for a major radius ( $R$ ) of 1 m.

Examination of the tabulation enables four statements to be made.

- (i) The total inductances agree closely with the current sheet expression. We can conclude that the current sheet expression, (6.19), is indeed accurate.
- (ii) The mutual inductance is at least 90% of the total inductance. The self inductance portion diminishes as the number of turns is increased, e.g. from about 10% to 3% as the number of turns is increased from 16 to 100.
- (iii) The total inductance is not much affected by the conductor space factor. This is because the space factor affects only the self inductance, which is much less than the mutual inductance.
- (iv) Since the inductance values agree so closely with current sheet values, the flux distributions in the space about the conductors must also be very nearly the same as those for current sheet distributions. This supports the previous conclusion that this should be so for all practicable numbers of conductors, based on the results found for a cylinder of parallel conductors.

Finally, we should note that the paths around the major circumference of the toroid do not have the same resistance. A path taken around the inner side is shorter than a path around the outer side. Unless the resistance or e.m.f. is compensated for each path, the current in each path is different, in contrast to the uniform current sheet assumption. This raises the question, considered in the next section, of whether the same current flows in each turn of a parallel connected secondary of the pulse transformer.

#### 6.3.4 The transient current distribution of the secondary

In all the preceding work we have assumed that the uniform current sheet expressions for inductance apply to the secondary as well as to the primary. In particular we have assumed that the secondary current is divided equally between the secondary parallel turns. This assumption is justified as follows.

Consider a solenoid, which is an example where the flux is distributed non uniformly through the turns, with a layer secondary, as in Fig. 87.



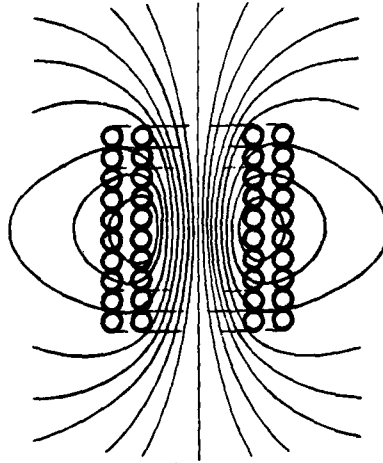


Fig. 87 Non uniform distribution of flux through the turns of a solenoid and a layer secondary.

The flux that links the central turns of the windings is more intense than near the ends; therefore the back e.m.f. per turn is greater for these turns. The same flux (practically) links the corresponding turns of the secondary (outer layer). Each portion of the primary has a different back e.m.f. and the same e.m.f. (practically) is induced into the corresponding turns of the secondary. Since the primary e.m.f. distribution is the result of equal current in each primary turn, the secondary e.m.f. distribution, being the same in a geometrically similar winding, implies the same current distribution as in the primary, i.e. equal current per turn.

The same reasoning applies to the external field toroid. The e.m.f. induced in each secondary turn matches that of its corresponding primary turn of equal length. The varying length of the turns means only that the turn resistance will cause the induced current to decay faster in the outer turns.

Let us next consider the distribution of the current upon individual turns. As with the rails of the railgun, the flux which externally links a turn induces the same e.m.f. into every filamentary path in the turn and therefore cannot affect the current distribution. The current distribution is determined almost solely by the rate of change of the internal flux of the current within the turn. As discussed in Ch. 2, this leads to the conclusion that initially the current will distribute to produce the minimum self inductance of the turn, which further implies that it produces no flux internally. (This does not mean that there is no internal flux at all, because some mutual flux passes through the turns).

Since the zero internal flux condition means that the self flux of each secondary turn is all external, and only the external flux can link the

primary, the secondary current is induced in such a way as to maximize the flux linkage with the primary, for the given boundary geometry of the secondary conductors.

Finally, let us examine the extent to which the inductance expression for the secondary is, as we have assumed, the same as for the primary. We have found that the secondary current is equally divided amongst the turns and therefore the general distribution of secondary current matches that of the primary, but that on each secondary conductor it is distributed so as to cause no internal flux, whereas the primary current, owing to the long charging time, will be uniformly distributed over the conductor cross section and will produce internal flux. The way in which the current is spread over each conductor has very little effect on the external flux though, and hence the turn self inductance and the mutual inductance with other turns are not much affected. This suggests that, since the magnitude of the current per turn matches that of the primary, the secondary transient inductance will be closely given by the same expression as for the primary steady state inductance.

An assessment of the difference between the inductance expressions for turns of round wire, under zero internal flux and uniform surface current conditions, can be made by considering each turn to be an external field toroid whose major radius is the turn radius,  $R$ , and whose minor radius is the conductor radius,  $r_w$ . For an external field toroid with  $N$  closely packed turns, the ratio of major to minor radii of a turn,  $\frac{R}{r_w}$ , is:

$$\frac{R}{r_w} = \frac{R}{a} \frac{N}{\pi}$$

where  $a$  is the toroid minor radius. If  $\frac{R}{a} = 5$  and  $N = 100$ ,  $\frac{R}{r_w} = 159$ .

The initial inductance,  $L_0$ , of an external field toroid in the form of a thin tube bent into a circle is given by Malmberg and Rosenbluth as [17]:

$$L_0 = \mu_0 R^2 \frac{(\gamma^2 - 1)^{1/2}}{\gamma} \left[ \frac{Q^1_{n+1/2}(\gamma)}{\epsilon(n+1/2)(n+3/2) P^1_{n+1/2}(\gamma)} \right]^{-1} \quad (6.105)$$

where  $L_0$  is the inductance in Henries;  $R$  is the major radius;  $\gamma$  is the ratio of major to minor radii, i.e.  $\gamma = \frac{R}{r_w}$ ;  $P^1_{n+1/2}$  and  $Q^1_{n+1/2}$  are the first order, half integral, Legendre functions of the first and second kind, respectively;  $\epsilon = 2$  for  $n = -1$ ; and  $\epsilon = 1$  for  $n > -1$ . The normalization of (6.105) agrees with that of NBS tables of functions  $P^m_{n+1/2}$  and  $Q^m_{n+1/2}$  [18].

Eqn. (6.19), viz.

$$L_{SH} = \mu_0 R \left[ \left( 1 + \left( \frac{a}{2R} \right)^2 \right) \ln \frac{8R}{a} - 2 \right],$$

gives  $L_{SH}$ , the surface current sheet inductance with which to compare Eqn. (6.105).

Eqn. (6.105) is plotted from values given by Malmberg and Rosenbluth, together with Eqn. (6.19), in Fig. 88, for  $R = 1m$ .

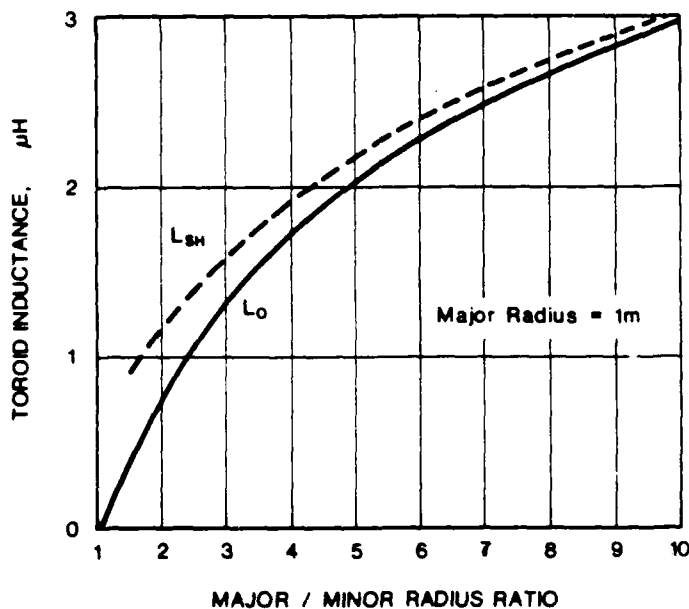


Fig. 88 Initial inductance,  $L_O$ , and uniform surface current inductance, for external field toroids.

Clearly, the two curves approach each other for  $\frac{R}{r_w}$  values as low as 10. For  $\frac{R}{r_w} = 10$ ,  $L_O$  is given as 2.960  $\mu H$ , while  $L_{SH}$  is 3.007  $\mu H$  is a difference of about 1.6%. Since the turns of the coils will have  $\frac{R}{r_w}$  values greater than 100, it is apparent from Fig. 87 that the initial and uniform surface current inductances will differ by only a fraction of a percent. (The NBS tables of Legendre functions only cover the range to  $\gamma = 10$ ; evaluation of (6.105) for  $\frac{R}{r_w}$  values of the pulse transformer turns requires the generation of these

functions. This may be done using elliptic integrals, but is a laborious task which the writer has not carried out).

Since the current sheet and initial inductance values for individual turns are so close, we can conclude that the initial secondary current distribution is practically the same as a uniform surface current. From the study of flux distribution in Section 6.5.2 we know that the field in the space about the turns will be much less distinguishable from that due to a uniform surface current than it is near the turn surface. Eqn. (6.19) is therefore applicable for the total secondary transient inductance and, multiplied by  $N^2$ , to the external flux portion of the primary steady state inductance.

In particular, the degree of coupling values calculated in Section 6.3 are much more affected by the geometrical factors discussed therein than by inaccuracy in the inductance expressions during the transfer of energy from primary to secondary.

## CHAPTER 7

### THE FORCE REDUCED TOROIDAL TRANSFORMER

#### **7.1 Problems caused by compressive forces**

In Ch. 6 the external field toroid was found to have the best combination of time constant, degree of coupling and natural strength. The forces on this toroid are mostly tension, which can be naturally resisted by the conductors without the need for additional structure. The compressive forces, however, would cause the conductors to bend because, in contrast to the conductor shape assumed in Ch. 6, the turns have no structural strength to resist them. An inner structure, such as a rigid inner tube or a series of disks, must be provided to support the conductors against the compressive forces. Eqn. (6.84) shows that for  $\frac{r}{a} = 5$  the mass of the inner support would be about a third of the mass of the conductors, if it was made from material of similar strength and density to the conductors.

Even if the inner support is provided the windings are not relieved of the compressive forces. The support will prevent the bending stresses from arising but the conductor materials must still bear the direct compressive forces while transferring them to the inner support. Each time that the coil is operated, the conductors and the insulation will impact against the support. The secondary is particularly vulnerable since it may be much thinner and hence much weaker than the primary, yet must bear the same forces as the primary when the primary energy is transferred to it. The coaxial cable construction is advantageous from this viewpoint because it couples the strength of the primary to the secondary. The risk exists, though, that the insulation between primary and secondary will be damaged and cause primary/secondary short circuits which would immediately destroy the functioning of the transformer and be extremely difficult to repair. Since compressive forces could be so disastrous, it is worthwhile examining a form of winding which reduces their effects. This concerns large coils in particular, since coil strength increases with size at a lesser rate than its ability to store magnetic energy. If large numbers of large coils were constructed, such as thousands of 100MJ coils for a space ship launcher, great attention would have to be paid to ensure that the life of the coils was of the order of a century (i.e. equivalent to that of larger civil engineering works such as dams and bridges).

#### **7.2 Magnetic force balancing**

The major radial and minor radial forces of the external and internal field toroids point in opposite directions (Figs. 75,76). By winding a toroid so that it produces both internal and external fields simultaneously, the two sets of forces will partially cancel on the same winding.

With the proper proportioning of the internal and external field strengths either the major radial or minor radial forces may be practically cancelled where they arise instead of being transmitted to other parts of the structure. This is the basis of "force reduced" coil construction. It was

explored in the 1950's [1,2] for producing "force free" regions in high field strength electromagnets wound with fragile superconductors. For multilayer coils the winding pattern is very complicated [3] and, to the writer's knowledge, the idea has not been applied in practice.

Fig. 89 shows how the external field toroid can be arranged to produce an internal field. The conductors are twisted around the minor diameter while also progressing around the major diameter, in the fashion of a multistart screw thread. The diagram shows a winding with 4 turns around the major diameter, with 4 twists around the minor diameter. The coil thus has 4 turns producing external field and 16 turns producing internal field.

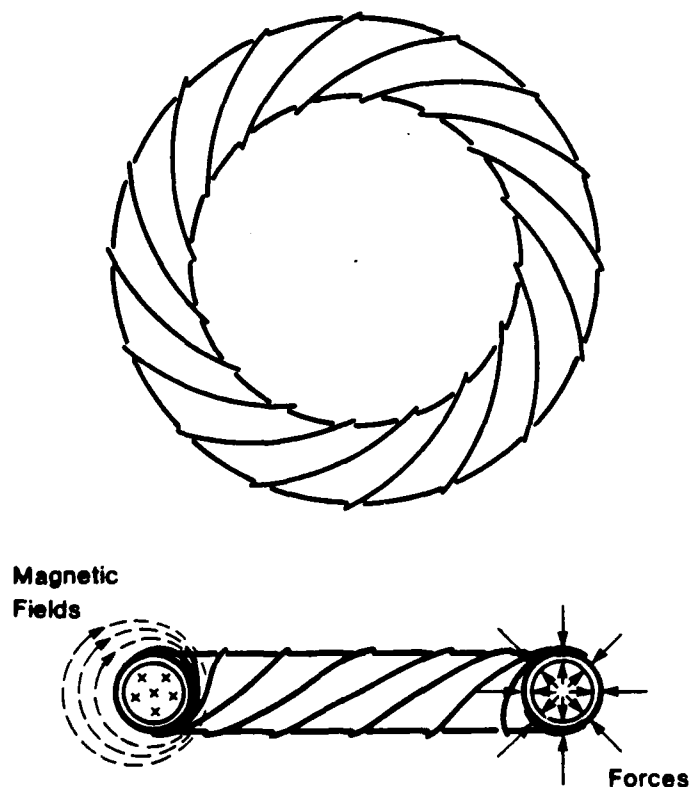


Fig. 89 Toroid with combined internal and external magnetic fields, resulting in self balancing forces. Winding shown has 4 turns around the major diameter with 4 twists around the minor diameter, giving 4 turns producing external flux and 16 turns producing internal flux.

It is impossible to have both the major and minor radial forces simultaneously balanced to zero i.e. to have a totally force free coil. This is because, as discussed in Ch. 3, where there is stored kinetic energy there must be forces at the boundaries of the container.

Let us now consider the force balance in more detail. The internal field and the current on the inner side of the conductors produce outward pointing forces and vice versa for the external field. The conductor material is "pinched" between the outward and inward pointing forces. If these forces are equal they have no resultant and no structure is required to support the winding. The internal field provides a "magnetic" former.

The compressive pressure which the conductor material must withstand is the magnetic field pressure,  $B^2/2\mu_0$ . This is much less than that due to the total compressive force acting over the thickness of the thin wall tube in Fig. 75 and in particular is much less than the local high pressure spots that may damage insulation in the external field toroid.

Reduction of the compressive stress to negligible values leaves the force reduced coil as an all tension structure. The coil mass will therefore be the minimum possible, viz  $\frac{aW}{c}$ , as discussed in Ch. 3. The mass reduction associated with force reduction has been considered an important reason for employing it [4,5] but has been criticized by others [6,7]. Although mass reduction is a valuable side effect, the important reason for considering magnetic force balancing in the present context is to eliminate the potentially damaging compressive forces.

To conclude this general discussion on force reduction, three points may be noted.

- (i) The time constant and degree of coupling properties of the external field toroid are degraded by combining it with the internal field toroid. To compensate for the resistance increase, the voltage, and hence the mass, of the battery used to charge the coil must be increased. To compensate for the degree of coupling decrease, the ratio of inner to outer diameter of the coaxial cable winding must be increased and hence the insulation must be diminished.
- (ii) The total stored magnetic energy is increased, compared to the external field toroid, owing to the internal magnetic field.
- (iii) The winding is much more difficult to construct than that of the external field toroid.

The benefit of reduced structural compressive forces and diminished mass must be weighed against the increase in battery mass, reduction in degree of coupling and increase in construction difficulty.

### 7.3 Basic force reduction relationships

#### 7.3.1 Total inductance expression

The same current causes both the internal and external fields, which is the same as if there were two windings in series. The two flux patterns are normal to each other and exist in separate spaces so that there is no mutual inductance. The total inductance is therefore the sum of the internal and external toroid inductances i.e. Eqns. (6.21) and (6.27); yielding:

$$L = \mu_0 N_E^2 R \left[ \frac{1}{2} \left( \frac{N_I}{N_E} \frac{a}{R} \right)^2 + \left( 1 + \left( \frac{a}{2R} \right)^2 \right) \ln \frac{8R}{a} - 2 \right] \quad (7.1)$$

where  $N_E$  is the number of turns around the major diameter and  $N_I$  is the number of turns around the minor diameter. If we imagine the winding to consist of the  $N_E$  turns of an external field toroid twisted around the minor diameter as they progress around the major diameter, then:

$$N_I = N_E T, \quad (7.2)$$

where  $T$  is the number of twists. Furthermore, since the pitch of the twists is  $\frac{2\pi R}{T}$  while the distance around the minor diameter is  $2\pi a$ , the helix angle of the winding,  $\alpha$ , is given by:

$$\tan \alpha = \frac{a}{R} T = \frac{a}{R} \frac{N_I}{N_E} \quad (7.3)$$

Since  $N_I$  and  $N_E$  must be whole numbers, not all helix angles are possible for a given  $\frac{a}{R}$ .

#### 7.3.2 Force reduction conditions

Differentiating the inductance expression (7.1) with respect to the minor radius,  $a$ , yields:

$$\frac{dL}{da} = \mu_0 N_E^2 \frac{R}{a} \left[ \left( \frac{N_I}{N_E} \frac{a}{R} \right)^2 - 1 + \frac{1}{2} \left( \frac{a}{R} \right)^2 \left( \frac{1}{2} + \ln \frac{8R}{a} \right) \right] \quad (7.4)$$

For zero force we require  $\frac{dL}{da} = 0$ . Eqn. (7.4) yields:



$$\frac{N_I}{N_E} = \left[ \left( \frac{R}{a} \right)^2 - \frac{1}{2} \left( \frac{1}{2} + \ln \frac{8R}{a} \right) \right]^{1/2} \quad (7.5)$$

For  $\frac{R}{a}$  values of 5 and greater  $\left( \frac{R}{a} \right)^2$  is at least 10 times the negative term, and so we have:

$$\frac{N_I}{N_E} \approx \frac{R}{a}, \quad (7.6)$$

as the condition which will yield zero net minor radial forces on the toroid. Since  $\frac{N_I}{N_E}$  is the number of twists that each turn of the external field toroid must make around the minor diameter, we have the simple rule that to make the external field toroid have zero net minor radial forces, each of its turns should be twisted  $R/a$  times about the minor diameter. From Eqn. (7.3) we see that the helix angle is then  $45^\circ$ .

Since Eqn. (7.6) is an approximation, the minor radial forces will not be exactly zero. Eqn. (7.6) represents a slight degree of overtwisting and when it is substituted in Eqn. (7.4) the result is:

$$\frac{dL}{da} = \mu_0 N_E^2 \frac{a}{2R} \left( \frac{1}{2} + \ln \frac{8R}{a} \right), \quad (7.7)$$

which is positive, indicating a small tensile force in the direction of the minor radius.

Differentiating Eqn. (7.1) with respect to the major radius,  $R$ , yields:

$$\frac{dL}{dR} = \mu_0 N_E^2 \left[ \left( 1 - \left( \frac{a}{2R} \right)^2 \right) \left( \ln \frac{8R}{a} - 1 \right) - \frac{1}{2} \left( \frac{N_I}{N_E} \frac{a}{R} \right)^2 \right] \quad (7.8)$$

Setting  $\frac{dL}{dR} = 0$  to obtain the condition for zero force in the major radial direction, yields:

$$\frac{N_I}{N_E} = \frac{R}{a} \left[ 2 \left( 1 - \left( \frac{a}{2R} \right)^2 \right) \left( \ln \frac{8R}{a} - 1 \right) \right]^{1/2}, \quad (7.9)$$

which is closely approximated by:

$$\frac{N_I}{N_E} = \frac{R}{a} \left[ 2 \left( \ln \frac{R}{a} + 1 \right) \right]^{1/2}, \quad (7.10)$$

since  $(\frac{a}{2R})^2 \ll 1$  and  $\ln 8 = 2.079 \approx 2$ .

As an example, for  $R/a = 5$  we have from Eqn. (7.6) that twisting the turns of the external field toroid 5 times about the minor diameter will reduce the net compressive forces to approximately zero, and from Eqn. (7.10) we find that if they were twisted 11 times the major radius tensile forces would be approximately reduced to zero. For numbers of twists between 5 and 11 the coil would be in tension in both the major and minor radial directions. For numbers of twists greater than 11 the minor radial forces would be tensile and the major radial forces would be compressive, i.e. the properties of the internal field toroid would outweigh those of the external field component.

We wish to retain the long time constant and high degree of coupling properties of the external field toroid as far as possible. The condition  $\frac{N_I}{N_E} = \frac{R}{a}$  achieves the objective of getting rid of the undesirable compressive forces with the least degradation of the desirable properties of the external field toroid.

### 7.3.3 Magnetic energy of the force reduced coil

The energy stored by the force reduced coil is increased because of the addition of the inductance of the internal field component. Substituting  $\frac{N_I}{N_E} = \frac{R}{a}$ , for the condition in which compressive forces are balanced, causes inductance expression (7.1) to become:

$$L = \mu_0 N_E^2 R \left( \frac{1}{2} + \left(1 + \left(\frac{a}{2R}\right)^2\right) \ln \frac{8R}{a} - 2 \right), \quad (7.11)$$

which can be arranged as:

$$L \approx L_E \left( 1 - \frac{1}{2 \ln \frac{R}{a}} \right), \quad (7.12)$$

where  $L_E = \mu_0 N_E^2 R \left( 1 + \left(\frac{a}{2R}\right)^2 \right) \ln \frac{8R}{a} - 2$ . Eqn. (7.12) is correct to within 2% for  $\frac{R}{a} \geq 5$ .

Since magnetic energy is given by  $\frac{1}{2} LI^2$ , Eqn. (7.12) can be used to obtain:

$$\frac{W_T}{W_E} = 1 + \frac{1}{2 \ln \frac{R}{a}}, \quad (7.13)$$

where  $W_T$  is the total magnetic energy of the force reduced coil and  $W_E$  is the magnetic energy of the external field toroid. Using Eqn. (7.13), the following tabulation is obtained.

$\frac{R}{a}$	$\frac{W_T}{W_E}$
5	1.311
7	1.257
10	1.217
20	1.170

The tabulation shows that the smaller the  $\frac{R}{a}$  values, i.e. the "fatter" the toroid, the greater is the increase in stored energy compared to the external field toroid. Since the force reduction requires the winding to have a  $45^\circ$  helix angle, and hence a 41% increase in resistance for given conductor size, the tabulation shows that we should choose as fat a toroid as possible to compensate for the resistance increase.

#### 7.3.4 Use of a high permeability core

If the inner of the toroid contains a magnetic material which raises the effective permeability of the internal field toroid component by a factor  $\mu_r$ , the total inductance equation becomes:

$$L = \mu_0 N_E^2 R \left( \frac{\mu_r}{2} \left( \frac{N_I}{N_E} \frac{a}{R} \right)^2 + \left( 1 - \left( \frac{a}{2R} \right)^2 \right) \ln \frac{8R}{a} - 2 \right) \quad (7.14)$$

Differentiating the above expression with respect to the minor radius,  $a$ , and setting the result to zero for balance of compressive forces, yields:

$$\frac{N_I}{N_E} \approx \frac{1}{\sqrt{\mu_r}} \frac{R}{a}, \quad (7.15)$$

$$\text{and} \quad \tan \alpha = \frac{1}{\sqrt{\mu_r}} \quad (7.16)$$

If  $\mu_r = 10$ , the number of twists,  $\frac{N_I}{N_E}$ , is reduced by a factor of 3 and the helix angle of the force reduced winding becomes  $17.5^\circ$  instead of the  $45^\circ$  angle required when  $\mu = \mu_0$ . This would mean that compressive force balance

would be achieved with a 5% increase in conductor length instead of a 41% increase and hence would overcome the disadvantage of increased resistance of the force reduced winding.

Unfortunately, it does not seem that this can actually be done. For the differentiation of Eqn. (7.14) to apply to the physical situation, the conductors must move in the medium of permeability  $\mu_r$ . If a high permeability core were provided the conductors would, however, still move in free space and hence it would still be necessary to have  $\frac{N_I}{N_E} = \frac{R}{a}$ , i.e. the 45° winding.

By providing an inner core of high permeability, though, the energy stored may be increased without increasing the forces on the conductors. This is because the extra energy is stored by the core and the core material must bear the associated forces. Eqn. (7.13) becomes, for an effective inner permeability  $\mu_r$ :

$$\frac{W_T}{W_E} = 1 + \frac{\mu_r}{2 \ln \frac{R}{a}} \quad (7.17)$$

Eqn. (7.17) shows that for  $\mu_r = 10$  the total stored energy would be about 3 times as great as for the free space condition, with  $\frac{R}{a} = 5$ .

Two points to be considered against the use of a high permeability core are (i) that it increases the total mass of the core and the material used would have to have a low density to not degrade the overall energy/mass ratio; and (ii) that the core material must have a resistivity high enough that the stored energy is released via the secondary instead of within itself.

### 7.3.5 The mass of the force reduced toroid

Each turn of the force reduced toroid is 41% longer than the direct distance around the major diameter. In principle its expansion would be resisted by twisting stresses, and not until the major diameter had increased by 41% would the stresses become simple tension. If though, the turns are held together, e.g. fastened to bands at a sufficient number of places, they will not be able to move independently and the result will be a structure that behaves like a thin walled tube. We will assume this to be the case so that we can regard the force reduced toroid as a ring upon which a uniform expansion force acts (Fig. 90).

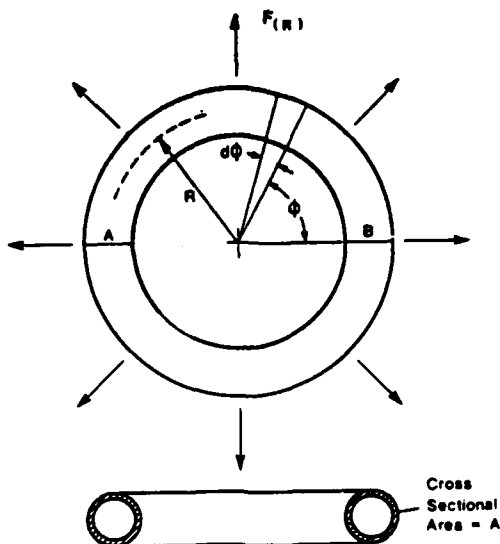


Fig. 90 Structural model for force reduced toroid.

The mass is calculated in the same manner as in Ch. 6. Let the total force in the direction of the major radius be  $F(R)$ . The force per unit length of circumference is therefore  $\frac{F(R)}{2\pi R}$ , and so the vertical component over a small angular element  $d\phi$  is  $\frac{F(R)}{2\pi} \sin \phi d\phi$ . Integrating this expression gives the total tensile force,  $T$ , being resisted at A and B, and  $T = \frac{F(R)}{2}$ . If the cross section of the tube is  $A$  and the tensile stress is  $\sigma$ , we have

$$A = \frac{T}{2\sigma} = \frac{F(R)}{2\pi\sigma},$$

and the volume of the tube is  $2\pi R A = \frac{R F(R)}{\sigma}$ . If the density of the tube material is  $w$ , we obtain the mass,  $M$ :

$$M = \frac{w}{\sigma} R F(R). \quad (7.18)$$

The force expression,  $F(R)$ , is obtained by the method of virtual work,

$$\text{i.e. } F_{(R)} = \frac{1}{2} I^2 \frac{dL}{dR}$$

where  $\frac{dL}{dR}$  is given by Eqn. (7.8). Substituting the condition for zero minor radial force, i.e.  $\frac{N_I}{N_E} = \frac{a}{R}$ , we have:

$$F_{(R)} = \frac{1}{2} I^2 \mu_0 N_E^2 \left[ \left(1 - \left(\frac{a}{2R}\right)^2\right) \ln \left(\frac{8R}{a} - 1\right) - \frac{1}{2} \right], \quad (7.19)$$

which can be rearranged as:

$$F_{(R)} = \frac{1}{2} I^2 \frac{\mu_0 N_E^2 R}{R} \left\{ \left(1 + \left(\frac{a}{2R}\right)^2\right) \ln \frac{8R}{a} - 2 + \frac{1}{2} - \left(\frac{a}{2R}\right)^2 \left(2 \ln \frac{8R}{a} + 1\right) \right\}. \quad (7.20)$$

The negative terms on the R.H.S. contribute less than 4% for  $\frac{R}{a} \geq 5$ . The remaining terms can be seen to be the same as Eqn. (7.11) i.e. they yield the total inductance,  $L$ , of the force reduced toroid, and so:

$$F_{(R)} = \frac{1}{2} \frac{I^2 L}{R} = \frac{W_T}{R}, \quad (7.21)$$

where  $W_T$  is the total stored magnetic energy.

Substituting Eqn. (7.21) into (7.18), yields:

$$M = \frac{W}{\sigma} W_T. \quad (7.22)$$

Following from the previous discussions, this is the result to be expected for a structure that confines magnetic energy by means of members in uniaxial tension.

### 7.3.6 Flux densities for force reduction

Since force per unit length on a current is given by the product of the magnitude of the current and the magnitude of the normal component of the magnetic field intensity, equal forces on a given current imply equal magnetic field intensities. That the average internal and external magnetic field intensities of the force reduced toroid are equal is shown as follows.

- (i) The average internal flux density,  $B_I$ , of the internal field is given by:

$$B_I = \frac{\mu_0 N_I I}{2\pi R} \quad (7.23)$$

- (ii) The average external flux density,  $B_E$ , of the external field, is given by:

$$B_E = \frac{\mu_0 N_E I}{2\pi a} \quad (7.24)$$

(i) and (ii) follow from the line integral relationship between magnetic intensity and current linked.

- (iii) Substitute the force balance condition  $N_I = N_E \frac{R}{a}$  into Eqn. (7.23). This yields:

$$B_I = \frac{\mu_0 N_E I}{2\pi a} \quad (7.25)$$

i.e.  $B_I = B_E$ .

### 7.3.7 Reason for major radial force

The force reduction condition apparently cancels the forces which act round the minor circumference. The demonstration that the average internal and external flux densities are equal reinforces this notion. If the forces were totally cancelled all around the minor circumference there would be no net force on the conductors at all and consequently no force in the direction of the major radius as well. From general reasoning, to do with boundary forces and stored kinetic energy, we know that this could only be the case in a system where the kinetic energy is unconfined and hence unavailable, or in a system which stored no energy, such as a non inductive coil.

The reason that there are major radial forces is that the magnetic field intensities are not in fact uniform. Referring to Fig. 91, the internal field varies from  $\frac{\mu_0 N_I I}{2\pi (R-a)}$  at A to  $\frac{\mu_0 N_I I}{2\pi (R+a)}$  at B.

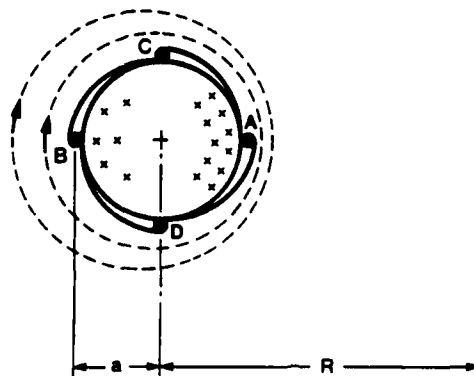


Fig. 91 Flux intensities at conductors.

The external field is given by elliptic integral functions instead of Eqn. 7.24. Only at points C and D do Eqns. (7.23) and (7.24) apply closely and practically zero force conditions pertain.

Evaluation of the elliptic integral function for the external field [8] yields, for  $R/a = 5$ :

$$\begin{aligned} B_A &= 14.18 \text{ units} \\ B_B &= 6.69 \text{ units} \end{aligned}$$

i.e. the field strength at B is 0.47 of that at A. The internal field at B compared to A is  $\frac{B-A}{B+a} = 0.67$ . The external field at A is more intense than the internal field and the nett force at A is in the direction of the major radius. The external field diminishes more rapidly at B than does the internal field and hence at B the nett force is again in the direction of the major radius.

The net force on the conductors under the force balance condition is therefore always in the direction of the major radius. It varies from approximately zero at C and D to greatest values at A and B, with the maximum force being at A. The fatter the toroid, i.e. the greater that  $a$  is compared to  $R$ , the more accentuated are these effects.

#### 7.4 Degree of coupling - coaxial cable force reduced transformer

In Ch. 6 the basic equation for the coupling coefficient ratio of the coaxial cable transformer was derived, viz.:



$$\frac{k_1}{k_2} = 1 - \frac{RN \mu_0 (\ln d_o/d_i + 1/4)}{L_1}, \quad (7.26)$$

for a cable with a solid inner, where  $N$  is the number of turns related to the primary inductance  $L_1$ ,  $d_o/d_i$  is the ratio of coaxial cable outer diameter to inner diameter and  $R$  is the radius from which the total length of the cable can be calculated.

For the force reduced winding, we have to increase the length by  $\sqrt{2}$  because of the helix angle,  $45^\circ$ , of the winding. Using Eqn. (7.11) for  $L_1$ , i.e. the force reduced inductance, Eqn. (7.26) becomes:

$$\frac{k_1}{k_2} = 1 - \frac{\sqrt{2} (\ln \frac{d_o}{d_i} + 1/4)}{N_E [1 + (\frac{a}{2R})^2 (\ln \frac{8R}{a} - 1.5)]}. \quad (7.27)$$

If the inner is tubular instead of solid, the  $1/4$  term in the numerator is omitted.

As discussed in Ch. 6, on the assumption that all the flux of the outer, i.e. all the flux of the secondary, links the inner,  $k_2 = 1$  and Eqn. (7.27) yields the maximum value of  $k_1 k_2$ , which directly determines the proportion of primary stored energy able to appear in the secondary. Eqn. (7.27) is plotted in Fig. 92 as a function of  $d_o/d_i$  for  $\frac{R}{a} = 5$  and  $\frac{R}{a} = 20$ , solid and tubular inners and  $N_E = 100$  turns. Comparison of the values in Fig. 92

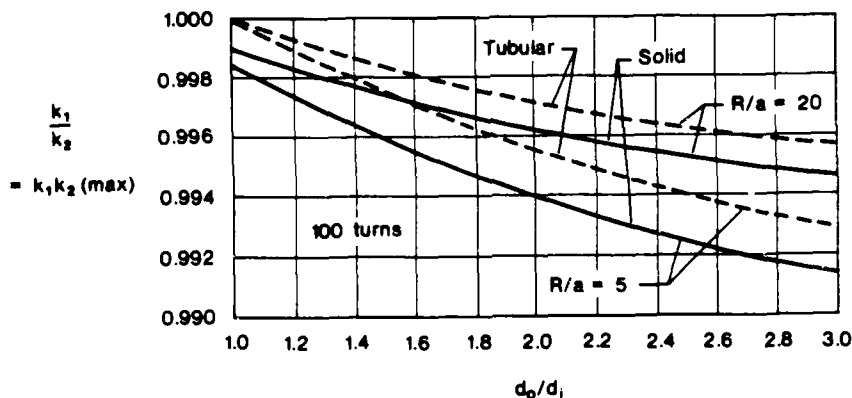


Fig. 92 Degree of coupling for force reduced toroidal transformer.

with those for the external field toroid show that the degradation in degree of coupling is not great. The increased length of cable required for the force reduced transformer increases the proportion of primary flux that is not coupled to the secondary, but this is partly compensated by the increase in primary inductance due to the internal inductance that is added.

## CHAPTER 8

### DESIGN AND PERFORMANCE OF TOROIDAL TRANSFORMER/BATTERY POWER SOURCE

In previous Chapters the charging characteristics of coils, time constants, degree of coupling and forces have been individually studied. In this Chapter the results of these studies are brought together and applied for the most advantageous coil geometry, viz. the external field toroid and its force reduced form, wound with coaxial cable.

#### 8.1 Management of the variables

Altogether, the following variables have to be amalgamated:

Stored energy	$W$
Major radius	$R$
Primary current	$I$
Battery voltage	$V_C$
Number of primary turns producing external flux	$N_E$
Ratio of major to minor radii	$\frac{R}{a}$
Resistance of the primary winding	$R_W$
Resistivity of conductors	$\rho$
Mass of primary conductors	$M_P$
Density of conductors	$w$
Stress in primary conductors	$\sigma$
Degree of coupling	$k_1 k_2$
Efficiency of charging the primary	$\eta$
Mass of the battery	$M_B$
Power density of the battery	$p$
Primary circuit time constant	$T_0$

Many relationships can be formed between the variables listed above. The problem is to separate them into suitable given and dependent variables. By setting a desirable value for one parameter, such as for the primary circuit time constant or for the number of primary turns, other parameters may become unacceptable.

In the following Sections equations which permit two design approaches are derived. Firstly, general expressions for  $M_P$ ,  $I$ ,  $V_C$ ,  $N_E$  and  $T_0$  are given in terms of  $W$ ,  $R$ ,  $\frac{R}{a}$ ,  $w$ ,  $\rho$  and  $\sigma$  for assumed values of  $k_1 k_2$  and  $\eta$ . These expressions can be plotted as families of curves as functions of  $W$  and  $R$  with values assumed for the other variables, and from these plots a design which is a broad compromise can be quickly found. Because the primary conductor stress,  $\sigma$ , is a given variable in these plots, the resulting coil designs all have a fixed energy density.

The other approach is to directly use equations to fix parameters to yield certain other desired parameters such as secondary current,  $T_0$  and  $N_E$ .

This is essentially a cut and try approach and the conductor stress, in particular, is allowed to be determined by other factors.

Another aspect to be considered in design is the support of the windings, especially the inner support of the external field toroid. Equations are given for a method using disks to support the conductors against the minor radial compressive forces of this toroid.

The plots and equations are applied to a range of example designs from which the most suitable energy range for the pulse transformer-battery system can be ascertained.

Since overall pulse energy density is the most important common measure between different types of power sources, it is discussed with the aid of an expression that shows the influence of various factors.

## 8.2 External field toroid - general relationships

The parameters of most direct concern in the design of a primary to store a given energy ( $W$ ), are the primary current required ( $I$ ), the charging voltage ( $V_C$ ), the number of primary turns ( $N_E$ ), the primary circuit time constant ( $T_0$ ) and the mass of the primary conductors ( $M_p$ ).

In this Section general expressions are obtained for these parameters in terms of  $W$ ,  $R$ ,  $\frac{R}{a}$ ,  $\rho$ ,  $\sigma$  and  $W$ .

### 8.2.1 Assumptions

The work in previous Chapters enables certain relationships to be assumed.

- (1) In Ch. 5 it was shown that the optimum charging time was about one primary circuit time constant. Let us select the charging time to be  $1.23 T_0$ , at which time (Fig. 47) the energy stored is 50% of the maximum possible and the efficiency of charging is just less than 50%.

The current,  $I$ , at this time is:

$$I = \frac{V_C}{\sqrt{2} R_C} \quad (8.1)$$

where  $R_C$  is the total primary circuit resistance and  $V_C$  is the open circuit voltage of the battery.

- (11) In Ch. 6 it was shown that the battery mass,  $M_B$ , is minimized when the battery internal resistance,  $R_B$ , equals the winding resistance,  $R_W$ , of the primary. Let us assume this condition. Since  $R_C = R_W + R_B$ , Eqn. (8.1) enables  $R_W$  to be expressed as:

$$R_W = \frac{V_C}{2\sqrt{2}I} \quad (8.2)$$

- (iii) Let us assume that coaxial cable construction is used, with a solid inner to reduce primary resistance, and that a ratio of the outer diameter to the inner diameter of 1.5 gives sufficient space for insulation between primary and secondary and a suitable value for the degree of coupling,  $k_1 k_2$ . Fig. 71 shows that  $k_1 k_2$  would be about 0.995 for  $\frac{R}{a} \geq 5$  and about 100 primary turns.
- (iv) According to the discussion in Ch. 6 the secondary current will naturally divide equally amongst the secondary turns even if there is no insulation on the outsers of the coaxial cable. Let us assume that the insulation on the outsers is negligible. Together with (iii) this implies a space factor of  $\frac{2}{3}$  for the primary conductor.

### 8.2.2 Mass of the primary in terms of resistivity, $\rho$ .

The basic expression for resistance, viz  $r = \frac{\rho l}{A}$  where  $\rho$  is the resistivity,  $l$  is the length of the conductor and  $A$  is its cross sectional area, may be rearranged as:

$$\text{Volume of conductor} = \frac{\rho l^2}{r} \quad (8.3)$$

Substituting for  $l$  the length of the external field toroid winding, viz  $2\pi R N_E$ , and using (8.2) for  $r$  and multiplying by the density,  $w$ , of the conductor yields the mass,  $M_p$ , of the primary:

$$M_p = \frac{8\sqrt{2}\pi^2 R^2 N_E^2 w \rho I}{V_C} \quad (8.4)$$

For  $N_E$  we may substitute an expression obtained by rearranging the stored energy equation  $W = \frac{1}{2} L_E I^2$ . Instead of the lengthy expression (6.21) for  $L_E$  let us use:

$$L_E = \mu_0 N_E^2 R \ln \frac{R}{a} \quad (8.5)$$

which is less than 7% in error for  $\frac{R}{a} \geq 5$ . This error is tolerable for the purposes of the equations to be derived. Using (8.5) yields:

$$N_E^2 = \frac{2W}{I^2 \mu_0 R \ln \frac{R}{a}} \quad (8.6)$$

and, substituting in (8.4) we obtain the mass of the primary as:

$$M_p = \frac{16\sqrt{2}\pi^2}{\mu_o} \frac{w_p R W}{V_C I \ln \frac{R}{a}}, \quad (8.7)$$

where  $\rho$  is in g-m.

### 8.2.3 Mass of primary conductors in terms of tensile stress of stored energy

In Ch. 6 it was shown that the mass of the conductors can also be related to the tensile stress,  $\sigma$ , due to the stored energy. The relationship, Eqn. (6.74), can be rearranged as:

$$M_p = \frac{wW}{\sigma} \left(1 + \frac{1}{\ln \frac{R}{a}}\right), \quad (8.8)$$

which slightly overestimates the mass.

### 8.2.4 Power requirement

From equations (8.7) and (8.8) we obtain:

$$V_C I = \frac{16\sqrt{2}\pi^2}{\mu_o} \frac{\sigma \rho R}{\left(1 + \ln \frac{R}{a}\right)}, \quad (8.9)$$

where  $\rho$  is in g-m,

$$\text{or} \quad V_C I = 1.777 \frac{\sigma \rho R}{1 + \ln \frac{R}{a}}, \quad (8.10)$$

where  $\rho$  is in g-cm.

Together with Eqn. (6.7b), viz.,

$$M_B = \frac{V_C I}{2(1 - e^{-n})\rho}$$

these expressions enable the mass of the battery to be obtained.

### 8.2.5 Primary Current

From the assumptions that the ratio of outer to inner diameter of the coaxial cable is 1.5 and that the secondary insulation is thin, we can write for the primary conductor diameter,  $d_1$ :

$$d_1 = \frac{2}{3} \frac{2\pi a}{N_E} \quad (8.11)$$

From the general relationship  $r = \frac{\rho l}{A}$  and Eqn. (8.2), we can further obtain:

$$\rho = \frac{V_C (\pi a)^2}{9\sqrt{2} I R N_E^3} \quad (8.12)$$

Substituting for  $N_E$  from (8.6) and then substituting the resultant expression for  $\rho$  into (8.9) yields:

$$I = \frac{9}{4\sqrt{2}} \frac{\left(1 + \frac{1}{\epsilon n \frac{R}{a}}\right) \left(\frac{R}{a}\right)^2 W^{3/2}}{\mu_o^{1/2} \pi^4 \sigma R^{7/2} \left(\epsilon n \frac{R}{a}\right)^{1/2}} \quad (8.13)$$

$$\text{or} \quad I = 14.57 \left(\frac{R}{a}\right)^2 \frac{\left(1 + \frac{1}{\epsilon n \frac{R}{a}}\right) W^{3/2}}{\sigma R^{7/2} \left(\epsilon n \frac{R}{a}\right)^{1/2}} \quad (8.14)$$

### 8.2.6 Battery Voltage

Eqns. (8.9) and (8.13) yield the battery voltage,  $V_C$ :

$$V_C = 0.1220 \times 10^8 \frac{\sigma^2 \rho R^{9/2} \left(\epsilon n \frac{R}{a}\right)^{3/2}}{\left(\frac{R}{a}\right)^2 \left(1 + \epsilon n \frac{R}{a}\right)^2 W^{3/2}} \quad (8.15)$$

where  $\rho$  is in  $\Omega\text{-m}$ .

### 8.2.7 Number of primary turns

The number of turns producing external flux,  $N_E$ , can be obtained from Eqns. (8.6) and (8.13). The result is:

$$N_E = \frac{8\pi^4}{9} \frac{\sigma R^3 \ln \frac{R}{a}}{\left(\frac{R}{a}\right)^2 \left(1 + \ln \frac{R}{a}\right) W} \quad (8.16)$$

### 8.2.8 Primary circuit time constant

The primary circuit time constant,  $T_O$ , is given by:

$$T_O = \frac{L}{R_C} \quad (8.17)$$

Since  $L = \frac{2W}{I^2}$  and  $R_C = \frac{V_C}{\sqrt{2}I}$ , (8.17) can be expressed as:

$$T_O = \frac{2\sqrt{2}W}{V_C I}, \quad (8.18)$$

which, upon substituting (8.9) for  $V_C I$ , becomes:

$$T_O = \frac{1 \times 10^{-7}}{2\pi} \frac{\left(1 + \ln \frac{R}{a}\right) W}{\sigma \rho R} \quad (8.19)$$

## 8.3 Disk supported external field toroid

It is easier to fabricate an inner support structure in the form of a series of disks on a flexible rod which can be bent into a circle (Fig. 93) instead of the rigid toroidal inner considered in Ch. 6.

Whereas the minor radial compressive forces cause only compressive stresses when a rigid toroidal inner is used for support, they cause tensile and shearing stresses in the conductors as well as compressive stresses when disks are used. In this Section we determine how closely the disks must be placed to prevent excessive tensile stress being caused in the conductors as they bend inwards (i.e. stretch) under the minor radial forces.



A schematic diagram of a ring structure, likely a tunnel or pipe, subjected to a uniformly distributed vertical load  $q/m$ . The ring is supported by two vertical supports at the top and bottom. The horizontal distance between the supports is labeled  $l$ . The ring is divided into segments by supports, with one segment highlighted in a lighter shade. A small vertical displacement  $\delta$  is indicated at the rightmost support.

The magnetic field that encircles the minor diameter causes a uniformly distributed load on each conductor. The magnitude of this loading,  $q$  N/m, is given by:

For present purposes we shall use the nominal magnetic field strength given by Eqn. (7.24), although, as has been discussed, the field strength is actually greater on the inner side and less on the outer side of the minor diameter. The variation in distance  $r$  will tend to compensate for this effect,  $r$  being shorter on the inner side and longer on the outer side. Using Eqn. (7.24), we have:

227

The situation is similar to that of a uniformly loaded suspension cable (except that in this case the loading increases as the conductor moves inwards under the loading, which we ignore). From handbooks [1] the increase,  $\delta l$ , in the length of a wire stretched between supports separated by distance  $l$  and uniformly loaded (Fig. 94) is:

$$\delta l = \frac{8}{3} \frac{f^2}{l} \quad (8.21)$$

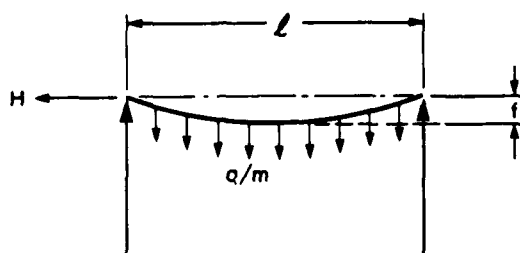


Fig. 94 Uniformly loaded suspension cable.

where  $f$  is the deflection of the mid point of the wire.

It can also be shown that the horizontal component,  $H$ , of the tension in the wire is given by [2]:

$$H = \frac{q l^2}{8 f} \quad (8.22)$$

Eqns. (8.21) and (8.22) can be combined to yield:

$$H = \frac{q l}{2\sqrt{6}} \left( \frac{E}{\sigma} \right)^{1/2} \quad (8.23)$$

where  $E = \frac{\sigma}{\epsilon}$  is Young's Modulus and  $\sigma$  is the tensile stress in the wire due to  $H$ . If the wire has cross sectional area  $A$ , the stress,  $\sigma = \frac{H}{A}$ , is:

$$\sigma = \left[ \frac{q l E}{2\sqrt{6} A} \right]^{1/2} \quad (8.24)$$

Substituting (8.20) for  $q$ , we have:

$$\sigma = \left( \frac{\mu_0 N_E I^2 t E^{1/2}}{8\sqrt{6} \pi a A} \right)^{2/3} \quad (8.25)$$

Rearranging (8.25) yields the length between supports for a given "bending" stress:

$$t = \frac{2\sqrt{6} \times 10^7 a A \sigma^{3/2}}{N_E I^2 E^{1/2}} \quad (8.26a)$$

which, using the expressions in Section 8.2 may be written as:

$$t = \frac{16\sqrt{6} \pi^4 R^4 \sigma^{3/2} \ln \frac{R}{a}}{9 \left(\frac{R}{a}\right)^3 N_E E^{1/2} W} \quad (8.26b)$$

To obtain the total stress in the wire, the "bending" stress should be combined with the direct stresses due to major radial tensile forces and minor radial shearing forces.

At the supports, the compressive force is the total load over the distance  $l$ , i.e.  $q l$ . The direct compressive stress in the conductor due to this is:

$$\sigma_c = \frac{q l}{t d} \quad (8.27)$$

where  $d$  is the conductor diameter and  $t$  is the thickness of the disk. Thickness  $t$  must be selected so that the insulation between primary and secondary of the coaxial cable winding is not damaged by repeated pulsing of the coil.

#### 8.4 Force reduced toroidal transformer

##### 8.4.1 Assumptions

Let us assume for the force reduced toroidal transformer the same charging time, battery resistance/winding resistance and coaxial cable parameters as set out in Section 8.2.1 for the external field toroid.

#### 8.4.2 Cable diameters-winding space

The inner major circumference length,  $2\pi(R-a)$ , limits the space available for turns. The turns pass through it at an angle to the vertical given by  $\arctan(\frac{R-a}{R})$ . For  $\frac{R}{a} = 5$ , this is  $38.6^\circ$ . Only on the top and bottom do the conductors have exactly  $45^\circ$  pitch angle. On the outer side the angle is  $\arctan(\frac{R+a}{R})$  and for  $\frac{R}{a} = 5$  the outside angle is  $52^\circ$  to the vertical, and the conductors are more widely spaced. If the diameter of the outer of the coaxial cable is  $d_o$  then the projected distance of  $d_o$  along the inner circumference is  $d_o \sqrt{1 + (1 - \frac{a}{R})^2}$ . Since all the turns producing internal flux must cross the inner circumference, the maximum number of such turns is

$$N_I = \frac{2\pi(R-a)}{d_o \sqrt{1 + (1 - \frac{a}{R})^2}} \quad (8.28)$$

Using the force reduction relationship  $\frac{N_I}{N_E} = \frac{R}{a}$  and the coaxial cable inner to outer diameter relationship  $d_o = \frac{3}{2} d_1$ , Eqn. (8.28) can be rearranged to yield the inner diameter:

$$d_1 = \frac{4}{3} \frac{\pi a(1 - \frac{a}{R})}{N_E \sqrt{1 + (1 - \frac{a}{R})^2}} \quad (8.29)$$

The function  $\frac{(1 - \frac{a}{R})}{\sqrt{1 + (1 - \frac{a}{R})^2}}$  yields the following values:

$\frac{R}{a}$	function
5	.625
7	.651
10	.669
20	.689
INF	.707

The tabulation shows that the function is in the range 0.6 to 0.7. Let us select a factor of 0.6, which will allow a little extra winding or insulation space for all practical  $\frac{R}{a}$  values. We then have

$$d_1 = \frac{0.8\pi a}{N_E} \quad (8.30)$$

#### 8.4.3 Mass of the primary in terms of resistivity

The derivation is the same as for the external field toroid, except that:

- (i) the length of conductor is increased by  $\sqrt{2}$
- (ii) the approximate inductance expression

$$L = \mu_0 R N_E^2 \left( n \frac{R}{a} + \frac{1}{2} \right) \quad (8.31)$$

for the force reduced toroid is used.

The expression for the mass becomes:

$$M_P = \frac{32\sqrt{2}\pi^2}{\mu_0} \frac{W \rho R W}{V_C I \left( n \frac{R}{a} + \frac{1}{2} \right)} \quad (8.32)$$

where  $W$  is the total stored energy of the internal and external fields.

#### 8.4.4 Mass of the primary in terms of tensile stress of stored energy

The mass of conductor required to resist the tensile force of the stored energy for the force reduced toroid with bands so that it behaves as a thin wall tube is:

$$M_P = \frac{WW}{\sigma}, \quad (8.33)$$

as shown in Ch. 7.

#### 8.4.5 Power requirement

Eqns. (8.32) and (8.33) yield:

$$V_C I = \frac{32\sqrt{2}\pi^2}{\mu_0} \frac{\sigma \rho R}{\left( n \frac{R}{a} + \frac{1}{2} \right)}, \quad (8.34)$$

where  $\rho$  is in  $\Omega\text{-m}$ ,

$$\text{or } V_C I = 3.554 \frac{\sigma \rho R}{\left(\ln \frac{R}{a} + \frac{1}{2}\right)}, \quad (8.35)$$

where  $\rho$  is in  $\mu\Omega\text{-cm}$ .

#### 8.4.6 Primary current

From the expressions for primary resistance, diameter of the inner (i.e. the primary) and the length of the primary conductor, we obtain:

$$\rho = \frac{0.02 V_C^2 a^2}{I R N_E^3} \quad (8.36)$$

Substituting for  $N_E$  an expression obtained by rearranging (8.31) and the stored energy expression  $W = \frac{1}{2} L I^2$ , and then substituting in (8.34), we obtain:

$$I = 28.62 \frac{\left(\frac{R}{a}\right)^2 W^{3/2}}{\sigma R^{7/2} \left(\ln \frac{R}{a} + \frac{1}{2}\right)^{1/2}} \quad (8.37)$$

#### 8.4.7 Battery voltage

Using (8.34) and (8.37) yields:

$$V_C = 1.242 \times 10^7 \frac{\sigma^2 \rho R^{9/2}}{\left(\ln \frac{R}{a} + \frac{1}{2}\right)^{1/2} \left(\frac{R}{a}\right)^2 W^{3/2}} \quad (8.38)$$

#### 8.4.8 Number of turns producing external flux

Rearranging the expression  $W = \frac{1}{2} L I^2$ , using Eqn. (8.31) for the inductance, and using (8.37) yields

$$N_E = 44.1 \frac{\sigma R^3}{\left(\frac{R}{a}\right)^2 W} \quad (8.39)$$

#### 8.4.9 Primary circuit time constant

Substitution of Eqn. (8.38) into Eqn. (8.18) yields:

$$T_0 = \frac{1 \times 10^{-7} \left( n \frac{R}{a} + \frac{1}{2} \right) W}{4\pi \sigma \rho R} \quad (8.40)$$

### 8.5 Discussion of parameters $\sigma$ , $\rho$ and $\frac{R}{a}$

#### 8.5.1 Hierarchy of parameters

The main dependent variables,  $I$ ,  $V_c$ ,  $N_E$  and  $T_0$  have been related to the stored energy,  $W$ , and the major radius,  $R$ , which are the chief independent variables, and to the tensile stress,  $\sigma$ , due to the stored energy of the primary and to  $\rho$ , the resistivity of the primary conductor and to  $\frac{R}{a}$ , the ratio of major to minor diameter. For initial design purposes it is convenient to have the equations derived in the previous sections plotted as functions of the stored energy, with families of curves to show the dependence on the major radius. This means that we must select values for the variables that remain, viz.  $\sigma$ ,  $\rho$  and  $\frac{R}{a}$ . These variables are discussed in the following Sections.

#### 8.5.2 Conductor stress theory

The stresses in the conductors are quite complicated, especially in the disk supported external field toroid. In this case the conductors experience

- (i) tensile stresses due to:
  - (a) the stored magnetic energy
  - (b) the stretching caused by minor radial forces
- (ii) compressive stresses at right angles to the above due to:
  - (a) pinch effect
  - (b) the reaction at the supporting disks
- (iii) shearing stresses due to the minor radial forces
- (iv) tension and compression where the conductors bend over the supporting disks under the action of the minor radial forces.

The region of greatest stress, and hence the most vulnerable region, is where the conductors pass over the disks because all the factors are

involved at these points. The situation is simpler in the force reduced toroid because, ideally, there are no resultant minor radial forces and hence no stretching of the conductors, bending, shear and compression that these forces cause.

The fact that the secondary can be much less massive than the primary on account of its short operating time also complicates matters. When the primary energy is transferred the tensile stress which it brings with it is directly proportional to the secondary conductor mass. If the secondary mass is one tenth that of the primary then the secondary tensile stress is ten times the primary tensile stress. In order not to over stress the secondary, the primary stress must be relatively low. This does not necessarily mean that the primary strength is under utilized because the primary should have as low a resistance as possible, which means that the copper used for the primary would have a relatively low proof stress.

In strength of materials texts [3] it is stated that for ductile materials the maximum shear stress is a satisfactory criterion of failure and that the maximum allowable shear stress,  $\sigma_s \text{ max}$ , is half the yield stress,  $\sigma_y$ , obtained in a simple tension or compression test, i.e.

$$\sigma_s \text{ max} = \frac{\sigma_y}{2} \quad (8.41)$$

When the stresses on an element consist of tension,  $\sigma_t$ , in one direction and compression,  $\sigma_c$ , at right angles, the maximum shear stress is given by:

$$\sigma_s \text{ max} = \frac{1}{2} (\sigma_t + \sigma_c) \quad (8.42)$$

Combining (8.41) and (8.42) shows that the failure criterion in the maximum shear stress theory becomes:

$$\sigma_t + \sigma_c = \sigma_y \quad (8.43)$$

Equation (8.43) applies to the region over the support disks with  $\sigma_t$  and  $\sigma_c$  the resultant stresses of the various effects listed above.

In the region between the disks the stresses on an element are tension,  $\sigma_t$ , and shear,  $\sigma_s$ , at right angles. The maximum shear stress in such an element is [4]:

$$\sigma_s \text{ max} = \sqrt{\left(\frac{\sigma_t}{2}\right)^2 + (\sigma_s)^2} \quad (8.44)$$

and hence, using (8.41), the failure criterion is:

$$\sqrt{(\sigma_t)^2 + 4\sigma_s^2} = \sigma_y \quad (8.45)$$



The maximum of (8.44) will be at the edges of the support disks because the bending and shearing stress components are greatest at these locations.

For preliminary design purposes it is convenient to suppose that the tensile stress directly due to stored energy and stretching by the minor radial forces considerably exceeds the other stresses. The failure criterion then becomes simply  $\sigma_t = \sigma_y$ . To allow for the neglected stresses we select  $\sigma_t$  as a fraction of  $\sigma_y$ . Design of the external field toroid would then require subsequent checking of neglected stresses and adjustments to the spacing and width of the supporting disks.

For the force reduced toroid we may use  $\sigma_t = \sigma_y$  where  $\sigma_t$  is due only to the stored energy, because the other stresses should be negligible.

### 8.5.3 Primary and secondary tensile stress and conductor materials

Two factors are to be remembered in the selection of conductor materials and stresses. Firstly, as mentioned before, the masses of the primary and secondary differ greatly and the tensile stress directly due to the stored energy is greatly magnified when the energy transfers to the secondary. This is because the outer of the coaxial cable is assumed to have negligible mechanical connection with the inner so far as tensile forces arising within it are concerned. Secondly, and in contrast to the above, the coaxial cable acts as a whole to resist the minor radial forces of the external field toroid because the outer cannot move inwards without transmitting force to the inner and vice versa. This means that there is no change in the tensile stresses in the primary and secondary due to minor radial forces when the energy transfers from the primary to the secondary.

From the above paragraph it follows that we may write:

- (i) for the total tensile stress in the primary conductor of the external field toroid,  $\sigma_{1t}$ ,

$$\sigma_{1t} = \sigma_{1W} + \sigma_{MR} \quad (8.46)$$

where  $\sigma_{1W}$  is the tensile stress directly due to the stored energy, W, and  $\sigma_{MR}$  is the tensile stress induced by the minor radial forces;

- (ii) for the total tensile stress in the secondary conductor of the external field toroid with a coaxial cable winding,  $\sigma_{2t}$ ,

$$\sigma_{2t} = K\sigma_{1W} + \sigma_{MR} \quad (8.47)$$

where K is the ratio of the primary to secondary mass;

(iii) for the force reduced toroid

$$\sigma_{1t} = \sigma_{1W} \quad (8.48)$$

$$\sigma_{2t} = K\sigma_{1W} \quad (8.49)$$

since the minor radial forces are negligible.

As a consequence of the magnification of tensile stress transferred to the secondary, the secondary material should be of high strength. Such materials will be alloys with relatively low conductivity (20% - 40% of that of pure copper) but this would not matter, particularly for large coils. For large coils the primary time constant would be seconds, compared to millisecond secondary discharge times. The mass ratio could therefore be hundreds even for secondary conductivities equal to 10% of that of the primary material conductivity (pure copper). An example of a high strength alloy is copper cobalt beryllium (2% - 3% Co, 0.35% - 0.7% Be), which has a 0.1% proof stress of 600 - 800 Mpa and a conductivity 45% - 55% of that of pure copper [5]. Another possibility is copper with tungsten filaments, which has a 0.1% proof stress of 1500 Mpa [5]. Iron filaments may also be used. Pure copper has a 0.1% proof stress in the range 30 to 300 Mpa, depending on the cold working to which it has been subjected after being fully annealed. (For copper we take the 0.1% proof stress to be the same as the yield stress,  $\sigma_y$ ).

The most important consideration for the primary conductor is that its conductivity be as high as possible, which means that a low strength, pure copper be used. Pure copper is desirable to ensure that the greatest benefit is obtained by cooling, e.g. with liquid nitrogen. For ease of manufacture the coaxial cable should not be too stiff, and since most of the stiffness would be due to the primary, it should be suitably low in strength on this account also. Let us assume that pure copper with a 0.1% proof stress of 100 Mpa is compatible with the foregoing requirements.

For the external field toroid we must divide the primary strength between the stress  $\sigma_{1W}$ , due directly to the primary stored energy, and the stress  $\sigma_{MR}$ , due to the minor radial forces. As an example, we might select  $\sigma_{1W} = 30$  Mpa and  $\sigma_{MR} = 50$  Mpa, leaving 20 Mpa to cover the neglected shearing and compressive stresses. If the mass ratio, K, were 10, the secondary tensile stress would be 350 Mpa according to Eqn. (8.47). In this case a cadmium copper might be selected for the secondary. If the mass ratio were 50 though, the secondary tensile stress would be 1550 Mpa and it would be necessary to use a tungsten filament copper for the secondary, or to reduce  $\sigma_{1W}$ . In the case of the external field toroid, the decrease in  $\sigma_{1W}$  could be taken up by increasing  $\sigma_{MR}$ . In the case of the force reduced toroid, the primary strength would have to be under utilized to avoid overstressing the secondary, or advantage of the situation could be taken to use a fully annealed copper to benefit ease of manufacture. Alternatively, the mass ratio could be set to suit the copper available for the secondary.

#### 8.5.4 Resistivity

The general investigation in Ch. 4 showed that to attain time constants of around 1 second and overall pulse energy densities of 1 kJ/kg it was necessary to cool copper conductors to the temperature of liquid nitrogen.

We shall therefore assume that the coils are cooled with liquid nitrogen with the result that copper conductors have resistivity,  $\rho$ , equal to  $0.25 \times 10^{-8}$   $\Omega$ -m.

#### 8.5.5 The $\frac{R}{a}$ ratio

Examination of the expressions in Sections 8.2 and 8.4 shows that  $(\frac{R}{a})$  enters directly into those for the current, the battery voltage and the number of turns. In these expressions it enters as  $(\frac{R}{a})^2$  and therefore has considerable control. In all other cases it has much reduced effect, generally only as  $\ln \frac{R}{a}$ .

The  $\frac{R}{a}$  ratio should be as small as possible to maximize the increase in stored energy of the force reduced winding and to minimize the compressive forces around the the external field toroid.

On the other hand, the  $\frac{R}{a}$  ratio should be as high as possible to increase the degree of coupling, to reduce the mass of the external field toroid for a given stored energy and to enable the force reduction principle to work as ideally as possible.

The effects in the above two paragraphs are relatively slow functions of  $\frac{R}{a}$  though and the major effect of  $\frac{R}{a}$  can be used to adjust  $I$ ,  $V_C$  and  $N_F$ .

From preliminary calculations it seems that  $\frac{R}{a}$  should be in the range 3 to 10 for the external field toroid and in the range 5 to 10 for the force reduced toroid. Because of the inductance approximations (8.5) and (8.31) the expressions in this Chapter should not be used with  $\frac{R}{a} < 5$ .

#### 8.6 Design graphs

For initial design purposes it is helpful to be able to select the major radius which yields the most desirable combination of current, voltage, number of turns and time constant for a given stored energy. This is conveniently done by graphs of the equations given in Sections 8.2 and 8.4. By plotting on logarithmic axes, straight line graphs are obtained. Other parameters of interest are the inductance of the primary and the magnetic field at the conductor surface. These parameters are plotted in Figs. 95-102 for  $\frac{R}{a} = 5$  and  $\frac{R}{a} = 10$ , for both the external field and force reduced toroids.

The graphs have been plotted from the following equations

Current, $I$	Equations (8.14) and (8.37);
Voltage, $V_C$ ,	Equations (8.15) and (8.38);
Number of turns producing external flux, $N_E$ ,	Equations (8.16) and (8.39);
Inductance of the primary, $L$ , from energy	$L = \frac{2W}{I^2}$ where $W$ is the stored energy
Primary circuit time constant, $T_0$ ,	Equations (8.19) and (8.40)
Flux density, $B$ ,	Equations (7.24) and (8.6)

The tensile stress in the primary conductor,  $\sigma$ , due directly to stored energy  $W$ , is taken as  $30 \times 10^6$  pa;  $\rho$ , the primary conductor resistivity is taken as  $0.25 \mu\Omega\text{-cm}$  (copper at  $77^\circ\text{K}$ );  $w$ , the primary conductor density =  $9 \times 10^3 \text{ kg/m}^3$  (copper).

### 8.7 Design examples

We shall now use graphs, equations and other information that we have derived to make a set of trial designs of coils for energies in the range 100 kJ to 1 GJ. From these trials the interactions of various factors can be assessed.

#### 8.7.1 100 kJ example design; external field toroid, given tensile stress

##### (1) Initial values from graphs

A 100 kJ railgun system would be a small experimental system, desirably powered from automotive type batteries. Assemblies of such batteries could supply currents of a few kA and therefore about 100 turns would be required on the primary to produce the secondary currents of a few hundred kA required by small railguns. It is also desirable that the primary voltage be as low as possible, e.g. 2 or 3 kV maximum, so that safety and insulation problems are minimal.

As was discussed in Ch. 4 the primary circuit time constant should be as long as possible in order to reduce the battery mass, a desirable value being about 1 second.

From the graphs for the external field toroid with  $\frac{R}{a} = 5$ , Figs. 95 and 96, it is found that for  $W = 10^5 \text{ J}$  a coil with a major radius of 0.5 m will have current, voltage and turn values in the desired range. The  $T_0$  graph shows that the time constant is the maximum for the radii plotted, but is only about 0.1 seconds.

Substituting  $R = 0.5$ , together with  $\frac{R}{a} = 5$ ,  $\sigma = 30 \times 10^6$  and  $\rho = 0.25 \times 10^{-8}$ , into Eqns. (8.14), (8.15), (8.16) and (8.19) yields:

$$\begin{aligned}
 I &= 5,551 \text{ A} \\
 V_C &= 460 \text{ V} \\
 N_E &= 79 \text{ Turns} \\
 T_O &= 0.111 \text{ Seconds}
 \end{aligned}$$

(ii) Mass of the transformer

The mass of the primary is given by Eqn. (8.8) in terms of the tensile stress due to the stored energy. Substituting  $\sigma = 30 \times 10^6$ , (which was suggested in Section 8.5.3 as a possible proportion of the total allowable stress) and  $w = 9 \times 10^3$  for the density of copper conductors, yields:

$$M_P = 49 \text{ kg.}$$

Allowing the secondary to have 10% of this mass and the supporting structure a further 20% yields a transformer mass of 64 kg.

(iii) Mass of the battery

Eqn. (6.7c), for the mass of the battery, viz.

$$M_B = \frac{W}{T_O(1 - e^{-n})^2 p},$$

where  $n$  is the number of time constants for which charging proceeds, and  $p$  is the battery power density, becomes:

$$M_B = \frac{2 W}{T_O p} \quad (8.50)$$

upon substituting  $n = 1.23$  (Section 8.2.1).

To evaluate Eqn. (8.50) we must select a value for  $p$ . A convenient and realistic value for lead-acid batteries constructed especially for railgun application is 1 kW/kg for a period of a few seconds (Ch. 4).

Substituting  $p = 1 \text{ kW/kg}$ , and  $T_O = 0.111 \text{ s}$ , Eqn. (8.50) yields  $M_B = 1802 \text{ kg}$ .

(iv) Overall pulse energy density

From the energy  $W = 10^5$  Joules and the total mass, 1866 kg, of the transformer and battery, the overall pulse energy density is 54 J/kg.

(v) Number of support disks

Eqn. (8.26b) enables the spacing between support disks to be calculated. In this equation  $\sigma$  is the tensile stress allowable due to stretching under the action of the minor radial forces and as suggested in Section 8.5.3 we shall set  $\sigma = 50 \times 10^6$ .

Substituting values in Eqn. (8.26b), with  $E = 10^{11}$ , yields the spacing,  $s$ , between disks to be 5 cm. Since the major circumference of the toroid with  $R = 0.5$  m is  $\pi m$ , 62 disks are required.

(vi) Consumption of liquid nitrogen

The resistivity,  $0.25 \times 10^{-8}$   $\Omega$ -m, assumes liquid nitrogen cooling. The charging of the transformer primary is approximately 50% efficient. Since the winding resistance and battery resistance are equal, half the wasted energy is dissipated in the primary. In addition the secondary will not discharge into the railgun with 100% efficiency. Assuming 50% of the secondary energy is dissipated in itself, the total energy dissipated in the transformer per shot equals the stored energy,  $W$ .

Using the latent heat of liquid nitrogen, 47.6 kcal/kg [6], the liquid nitrogen consumed per shot is 500 grams.

(vii) Number of shots from battery

Since the efficiency of charging is 50%, the battery supplies 200 kJ per shot. Assuming the battery is lead acid with an energy density of 100 kJ/kg, a battery mass of 1802 kg could supply 900 shots between charges. The 100 kJ/kg value for the energy density applies to the 2 hour rate, so the 900 shots could be fired in 2 hours.

**8.7.2 100 kJ external field toroid with improved overall energy density**

The above design consists of a small mass transformer (49 kg primary) and a large mass battery (1802 kg). The reason for these proportions is that the tensile stress in the primary conductors due to the stored energy was preset. The conductor mass and, for given  $R$  and  $\frac{R}{a}$  values, the total conductor cross section was also fixed, and a high resistance short time constant design was the eventual result.

By allowing the stress to decrease the transformer mass is increased and, as Eqn. (8.19) shows, the primary circuit time constant is increased and the battery mass is decreased.

The following design procedure allows the stress to "float" and gives flexibility in other parameters, e.g. the secondary current, as well as the primary circuit time constant.

Suppose that we desire the secondary current from the 100 kJ transformer to be 300 kA.

(i) Major radius

The major radius is fixed if a single turn secondary is specified for a certain energy and current by the relation:

$$W = \frac{1}{2} L_s I_s^2$$

where  $L_s$  is the secondary inductance and  $I_s$  is the secondary current. Since the single turn inductance is approximately given by:

$$L_s = \mu_0 R \ln \frac{R}{a},$$

the radius  $R$  is given by:

$$R \approx \frac{2W}{I_s^2 \mu_0 \ln \frac{R}{a}} \quad (8.51)$$

Substituting  $I_s = 300 \times 10^3$ ,  $W = 10^5$  and  $\frac{R}{a} = 5$  yields  $R \approx 1.099$  m.

(ii)  $T_0 N_E$  relationship

$T_0$  and  $N_E$  are parameters over which it is desirable to have control, e.g. we may wish  $T_0$  to be 1 second and  $N_E$  to be 100 turns, and hence their product should be 100. By multiplying Eqns. (8.16) and (8.19) we obtain an expression for  $T_0 N_E$  which is independent of the stress,  $\sigma$ , viz:

$$T_0 N_E = \frac{\pi^2 \mu_0 R^2 \ln \frac{R}{a}}{9 \left(\frac{R}{a}\right)^2 \rho} \quad (8.52)$$

Substituting  $R = 1.099$  together with  $\frac{R}{a} = 5$ ,  $\rho = 0.25 \times 10^{-8}$  yields:

$$T_0 N_E = 42.86.$$

Let us select  $T_0 = 0.5$  seconds and  $N_E = 86$  turns as being as good a balance of these parameters as is possible.

(iii) Stress due to stored energy

The selection of  $T_0$  and  $N_E$  fixes the remaining parameters, viz.  $\sigma$ , and the mass of the primary. The stress can be found by rearranging the equations given in Section 8.2, e.g. that for  $T_0$ . We find  $\sigma = 3.023$  Mpa, approximately 1/10 that assumed in the previous design.

(iv) Mass of the transformer

Eqn. (8.8) yields the mass of the primary as 483 kg. Applying the 1.3 factor as before yields 628 kg for the mass of the transformer.

(v) Mass of the battery

Eqn. (8.50), with  $p = 1$  kW/kg, yields  $M_B = 400$  kg.

(vi) Overall pulse energy density

The energy stored,  $10^5$  J, and the total mass of the transformer and battery, 1028 kg, yield an overall pulse energy density of 97 J/kg, about twice the value with the coil stressed with 30 Mpa by the stored energy.

(vii) Primary current

The turns ratio, 86, and the secondary current, 300 kA, yield the primary current as  $I = 3488$  A.

(viii) Primary voltage

Eqns. (8.9) or (8.15) may be used. Alternatively, an expression for  $V_C I$  in terms of  $T_0$  may be used, viz.

$$V_C I = \frac{2\sqrt{2} W}{T_0}, \quad (8.53)$$

which is obtained from the relationships in Section 6.1.1 with  $n = 1.23$ .

Using Eqn. (8.53) we obtain  $V_C = 162$  V.

(ix) Number of support disks

Since the stress due to stored energy is only 3 Mpa, we may allocate extra stress to resist the minor radial forces, e.g. 70 Mpa instead of 50 Mpa. Substituting in Eqn. (8.26b) yields  $t = 1.7$  m; i.e. very little support is needed; e.g. 16 disks might be used, simply to aid construction.



(x) Number of shots from battery

The 400 kg battery, with an energy density of 100 kJ/kg, would supply 200 shots.

(xi) Summary of 100 kJ designs

The parameters for the two 100 kJ designs are:

	(i) Stored energy stress = 30 Mpa	(ii) Stored energy stress = 3.023 Mpa
$\frac{R}{a}$	0.5	1.099 m
$\frac{a}{l}$	5	5
$\frac{I}{V_C}$	5.55	3.488 kA
$V_C$	460	162 V
$N_E$	79	86 turns
$M_P$	49	483 kg
$M_B$	1802	400 kg
Overall energy density	54	97 J/kg
No of shots	900	200
No of support disks	62	16

In the second design the transformer mass exceeds that of the battery, in contrast to the first design. The total mass though, has reduced to about half and the overall energy density has increased from 54 J/kg to 97 J/kg. These designs suggest that for an energy of  $10^5$  J, the maximum overall pulse energy density, on the basis of batteries with a power density of 1 kW/kg and liquid nitrogen cooled copper conductors, is about 100 J/kg.

**8.7.3 10MJ external field toroid transformers**

(i) Design with stress due to stored energy = 30 Mpa

Inspection of the graphs for  $\frac{R}{a} = 5$  suggests that a major radius of 3 m would yield an acceptable combination of current, voltage, number of turns and time constant.

Carrying through the calculations as in 8.7.1 yields, for  $R = 3$  m:

$I = 10,500$  A  
 $V_C = 1,456$  V  
 $N_E = 173$  Turns  
 $T_o = 1.84$  seconds  
 $M_P = 4,900$  kg

$M_B = 10,900 \text{ kg}$   
 Overall energy density = 579 J/kg  
 Number of shots from battery = 55  
 Number of support disks = 66

The current from a single turn secondary would be 1.82 MA; this is likely to be too large and suggests that the secondary should be connected so as to yield effectively 2 or 3 turns to reduce the current.

(ii)  $T_o$  and  $N_E$  selected, stress allowed to float

Following the procedure in Section 8.7.2, we first determine the major radius from the stored energy and the desired secondary current. Suppose the current is 1 MA.

Eqn. (8.51) yields  $R = 9.889 \text{ m}$ , which is much larger than the graphs suggest is necessary. Therefore we select a two turn secondary which reduces  $R$  to 2.475 m.

Eqn. (8.52) yields  $T_o N_E = 217.38$ ; let us select  $T_o = 2 \text{ seconds}$ ,  $N_E = 109 \text{ turns}$ .

Continuing as in Section 8.7.2 the design is:

$I = 18,349 \text{ A}$   
 $V_C = 771 \text{ V}$   
 $N_E = 109 \text{ Turns}$   
 $T_o = 2 \text{ Seconds}$   
 $M_P = 4,348 \text{ kg}$   
 $M_B = 10,000 \text{ kg}$   
 Stress due to stored energy = 33.56 Mpa  
 Overall energy density = 639 J/kg  
 Number of shots from battery = 50  
 Number of support disks = 74 ( $\sigma_{MR} = 50 \text{ Mpa}$ )

(iii) Summary

In both these 10 MJ designs the energy density has improved considerably compared to the 100 kJ designs. The number of shots from the battery has diminished greatly, although 50 is still probably an adequate number. The fact that the stress due to the stored energy reaches 30 Mpa together with time constants of about 2 seconds suggests that at higher energies the stress limit, rather than the time constant, will determine the coil mass.

#### 8.7.4 100 MJ and 1GJ designs

##### (1) Liquid nitrogen cooled conductors (as previously)

100 MJ and 1 GJ transformers would be useful in space launch applications, either on earth or in space.

1200 transformers, each storing 100 MJ and delivering 5 MA secondary current, distributed along a 12 km length of 2 m square bore rails upon a mountainside, could launch a 1 tonne vehicle into space at 8 km/s, assuming about 25% of the stored energy becomes kinetic energy.

Alternatively, 120 transformers, each storing 1 GJ and delivering 4 MA secondary current might be distributed along 19 km length of rails, in this case taking 5 seconds to accelerate 1 tonne to 8 km/s instead of 3 seconds for the 100 MJ system.

Using the methods in the previous examples the following design parameters were found. As in previous designs  $\rho = 0.25 \times 10^{-8}$ , but for the 1 GJ transformer  $\frac{R}{a} = 6$  instead of 5.

	<u>100 MJ, 5 MA</u>	<u>1 GJ, 4 MA</u>	
$\frac{R}{a}$	5	6	
$R_a$	3.955	13.88	m
I	50	16	kA
$V_C$	1.02	11.62	kV
$N_E$	100	500	turns
$T_o$	5.55	15.22	seconds
$M_P$	19.28	166.68	tonnes
$M_2$	36.03	131.4	tonnes
Stress, stored energy	75.7	84.1	Mpa
Overall energy density	1637	2873	J/kg
No. of shots	18	6	
No. of disks	362	1180	
No. of secondary turns	1	2	

The trend evident with the 10 MJ designs continues with these higher energy designs. Time constants of the order of ten seconds are attained with stored energy stresses that approach the 100 Mpa maximum selected in Section 8.5.3 for annealed high conductivity copper and overall energy densities are in the kilojoule per kilogram region.

The high stresses due to stored energy, as discussed in Section 8.5.3, mean that a high strength material must be used for the secondary if its mass is to be no more than about a tenth of that of the primary.

The high overall pulse power densities are the result of the long time constants and the calculation assumes that the batteries can deliver power at 1 kW/kg for these times.

The low number of shots suggests that the battery mass should be increased, even though the overall energy density would be thereby decreased. Additional batteries could be connected in series or parallel. Either way, the primary would then be charged in less than the 1.23 time constants that we have allocated and hence would be charged more efficiently. The number of shots would be increased both through the greater stored energy in the battery and the increased efficiency of charging.

(11) Room temperature operation of high energy transformers

If battery mass is to be increased, advantage can be taken of the situation to operate the transformers at room temperature instead of cooled with liquid nitrogen. Room temperature operation would increase the resistivity of copper by a factor of 7, thereby requiring 7 times the voltage, and therefore 7 times the battery mass for the same current as in the cooled conductors. The time constant would also be reduced by a factor of 7, so the primary would be charged more quickly and the system response time would be faster.

The need for liquid nitrogen is of course eliminated by operating the coils at room temperature. On the figures used in the 100 kJ example, a 1 GJ system would vaporize 5 tonnes of liquid nitrogen per shot.

The parameters affected by operating the 100 MJ and 1 GJ transformers at room temperature become:

	<u>100 MJ 5 MA</u>	<u>1 GJ 4 MA</u>	
V <sub>C</sub>	7.14	81.34	kV
T <sub>0</sub>	0.79	2.17	seconds
M <sub>B</sub>	252	920	tonnes
Overall energy density	361	879	J/kg
No. of shots	126	46	

Note the high voltage, 81 kV in the 1 GJ system, required of the battery in room temperature operation.

**8.7.5 Force reduced transformers**

The examples show that external field toroids that store greater than about 10 MJ and have suitable time constants are also highly stressed by the stored energy and require a large number of support disks.

For energies above about 100 MJ the tensile stress due to the stored energy is a large proportion of the strength of the copper (e.g. 80 Mpa compared to a proof stress of 100 Mpa for high conductivity copper). This means that higher strength copper, which has a lower conductivity, must be used to cope with the stresses due to the minor radial forces, or as in the examples, the number of support disks is so large that they practically form a solid inner.

The above results, and the potentially damaging effects of the minor radial compressive forces discussed in Ch. 7, lead us to consider force reduced windings which greatly reduce the effect of the minor radial forces and enable practically all the strength of the conductors to be used to resist the stress directly caused by the stored energy.

On the supposition that the stress due to stored energy is 80 Mpa, the 100 MJ and 1 GJ designs in Section 8.7.4 with liquid nitrogen cooled conductors have the tabulated parameters when converted to force reduced forms.

	<u>100 MJ 4.4 MA</u>	<u>1 GJ 3.7 MA</u>	
R	5	6	
a			
R	4	13	m
I	48	34	kA
V <sub>C</sub>	2.8	11.9	kV
N <sub>E</sub>	90	215	turns
T <sub>O</sub>	2.1	7.0	seconds
M <sub>P</sub>	11.25	112.5	tonnes
M <sub>B</sub>	95.33	285.14	tonnes
Stress, stored energy	80	80	Mpa
Overall energy density	919	2380	J/kg
No. of shots	48	14	
No. of secondary turns	1	2	
No. of support disks	16	16	

Examination of the tabulation shows that the transformer mass is reduced while the battery mass is increased, compared to the external field toroids. The  $V_C I$  product is more than doubled, primarily due to the increased winding resistance which is in turn brought about by the 45° winding pitch. The time constant is reduced by the increased resistance.

Apart from its main purpose of reducing potential damage to insulation, the only benefit of force reduced construction is that the inner structure is minimal. In the above tabulation 16 disks have been nominated, the number being selected simply as sufficient to aid construction.

### 8.8 Discussion - overall pulse energy density

Although different power source schemes have individual advantages which may suit one circumstance more than another, such as capacitors for low energy experimental work, they can all be compared on the basis of pulse energy delivered per kilogram of system mass. From the considerations in Ch. 3 a target figure of 1 kJ/kg was selected for the overall pulse energy density for two reasons, viz.:

- (i) for railguns to be at all comparable with powder guns,
- (ii) for alternative power sources to be comparable with HPG systems.

#### 8.8.1 Values attained by the pulse transformer-battery systems

The example designs in this Chapter yielded the following results.

<u>stored energy</u>	<u>Overall pulse energy density</u>
100 kJ	97 J/kg
10 MJ	639 J/kg
100 MJ	1637 J/kg
1 GJ	2873 J/kg

It is evident that the pulse energy density increases with the stored energy. For energies in the range 100 kJ to 1 MJ the pulse energy density of the pulse transformer system turns out to be in the range 100 to 200 J/kg, which is comparable to capacitor systems. When the energy exceeds about 10 MJ the pulse energy density approaches the 1 kJ/kg target and for very large energies, such as might be used for space launch, it becomes several kJ/kg.

The energy densities at low energies are only a fraction of 900 J/kg estimated in Ch. 4 for a 1 MJ system on the basis of the Brooks Coil. The low figures come about for two reasons, viz.:

- (i) the time constant to mass ratio of external field toroids is only a fraction of that of the Brooks Coil (e.g. 40%, Ch. 6).
- (ii) the 1.23 time constant charging time doubles the mass of the battery (Eqn. 8.50) compared to the relationship assumed in Ch. 4.

With the aid of an expression for overall pulse energy density we can assess the control that various factors have.

### 8.8.2 Expression for the overall pulse energy density

Equation (8.52) for  $T_0 N_E$  may be manipulated to give an expression for  $T_0$  that is independent of  $R$ . This expression can be used in Eqn. (8.50) for the mass of the battery,  $M_B$ , which together with Eqn. (8.8) for the mass of the primary, multiplied by 1.3 to allow for the inner support and the secondary, gives the overall pulse energy density of the external field toroid as:

$$\frac{W}{M} = \left[ \frac{28.404 \times 10^6 \rho}{W^{2/3} p} \left( \frac{N_E}{\ln \frac{R}{a}} \right)^{1/3} \left( \frac{\sigma \left( \frac{R}{a} \right)^2}{1 + \ln \frac{R}{a}} \right)^{2/3} + \frac{1.3W}{\sigma} \frac{(1 + \ln \frac{R}{a})}{\ln \frac{R}{a}} \right]^{-1} \quad (8.53)$$

where  $M$  is the total mass of the battery and transformer.

Equation (8.53) shows that the energy density increases with stored energy, as we have found. The increase is because the battery mass increases only as the cube root of  $W$ .

To maximize  $\frac{W}{M}$ , the two components in (8.53) should each be minimized. The variation with  $N_E$  and  $\sigma$  is slow. The principal variation is due to  $\left( \frac{R}{a} \right)^{4/3}$  therefore  $\frac{R}{a}$  should be selected as small as possible. The chief limitation to selecting  $\frac{R}{a}$  small is the reduction in degree of coupling. We have selected  $\frac{R}{a} = 5$  because it yields suitable accuracy in the simplified inductance expressions and acceptable degree of coupling (Section 8.2.1). The use of smaller values e.g. 3, could be explored, using equations of appropriate accuracy.

The remaining variables, resistivity,  $\rho$ , and the power density,  $p$ , directly affect the battery mass. These are discussed in the following sections.

### 8.8.3 Resistivity - cooling of conductors

Eqn. (8.53) shows that  $\rho$  should be as small as possible, and to this end we have assumed copper conductors with liquid nitrogen cooling (Section 8.5.4 and Ch. 4).

The example designs show that at the 100 kJ energy level the resistivity is not sufficiently low, and suggest that small, well stressed, low energy coils need further cooling, e.g. using liquid hydrogen. At 45 K the resistivity of copper falls by a further factor of 7 as compared to its value at 77 K (liquid nitrogen). The 100 kJ system with a stress due to stored energy at the reasonable value of 30 Mpa had a time constant of only 0.111 s and an overall pulse energy density of 54 J/kg. Further cooling to 45 K would increase the time constant to 0.777s and decrease the battery mass to 257 kg and increase the pulse energy density to 311 J/kg.

The energy needed to produce the liquid nitrogen or liquid hydrogen should be included in the efficiency statements. On thermodynamic considerations (Carnot cycle) it requires 3 to 4 Joules at room temperature to remove 1 Joule at 77 K [7]. In addition, the maximum efficiency of compressors is about 40% of the Carnot efficiency in the tens of kilowatts of cooling range [7]. Thus at least 10 Joules must be supplied to remove 1 Joule at 77 K. For liquid hydrogen cooling about ten times as much energy is required as for liquid nitrogen [7]. The I<sup>2</sup>R loss burden suggests further cooling and the use of superconductors to eliminate it altogether.

At the high energy end of the spectrum the section of the conductors needed for strength results in acceptable time constants with higher resistivity and hence with less cooling.

There is obviously a considerable saving in energy consumption and plant if cooling required is reduced or eliminated. On the figures in Section 8.7.1, 5 tonnes of liquid nitrogen would be consumed for each 1 GJ shot, or about 600 tonnes in launching a 1 tonne vehicle at 8 km/s. There would be merit in locating such a space launch facility in the polar regions to take advantage of natural cooling. For applications in space there would be no need to cool the coil, rather it would be necessary to heat the battery. The coil should face away from the sun and the earth, whereas the battery should be located so as to receive warmth from them.

#### 8.8.4 Power density of batteries

The greater the battery power density the less is the battery mass and hence the greater is the overall pulse energy density. In this Chapter we have assumed  $p = 1 \text{ kW/kg}$  because this value appears (Ch. 4) to be within the reach of modern lead-acid battery technology. It was further shown in Ch. 4 by calculation that a power density of  $2.5 \text{ kW/kg}$  for periods of a few seconds to perhaps 20 seconds is basically feasible.

Although a greater power density reduces the battery mass, the trial designs show that beyond about 10 MJ of stored energy the strength of the conductors determines that the mass of the transformer be comparable to that of the battery, when  $p = 1 \text{ kW/kg}$ . Reduction of the battery mass will therefore not be accompanied by commensurate increase in overall pulse energy density. Another important point, also evident in the example designs with  $p = 1 \text{ kW/kg}$ , is that at large stored energies the battery mass may in fact be so low that the number of shots is too few. These points are brought out clearly in the tabulation below, where the example designs are recalculated using  $p = 2.5 \text{ kW/kg}$ .

The tabulation shows that beyond 10 MJ the gains in overall energy density are rather small and the penalty in reduced number of shots is great when the battery mass is reduced. Even at the 100 kJ energy level the gain from 54 to 127 J/kg for the well stressed coil is only a small improvement upon the 97 J/kg attained by the low stress 100 kJ design. Applying the reduced battery mass to the low stress design only raises the energy density to 127 J/kg, the same as for the well stressed coil.



Comparison - Batteries with power density = 1 kW/kg and 2.5 kW/kg

<u>Stored energy</u>	100 kJ	100 kJ	10 MJ	100 MJ	1 GJ
<u>Transformer mass</u>	0.064	0.63	5.65	25.06	216.7 t
<u>Battery mass</u>					
(i) p = 1 kW/kg	1.8	0.4	10	36	131.4 t
(ii) p = 2.5 kW/kg	0.72	0.16	4	14.4	52.6 t
<u>O.E.D.</u>					
(i) p = 1 kW/kg	54	97	639	1637	2873 J/kg
(ii) p = 2.5 kW/kg	127	127	1036	2533	3714 J/kg
<u>No. of shots</u>					
(i) p = 1 kW/kg	900	200	50	18	6
(ii) p = 2.5 kW/kg	360	80	20	7	2

O.E.D. = overall pulse energy density.

Number of shots is based upon 100 kJ/kg available from battery at all discharge rates.

### 8.9 Alternative design approaches

The diminishing gain in overall energy density and the reduced number of shots in using higher values of p to minimize the battery mass give the option of trading battery mass for other advantages.

For example, Eqn. (8.53) shows that the resistivity,  $\rho$ , may be increased by the same factor as the power density without altering the battery mass. With p = 2.5 kW/kg the resistivity could be increased to  $2.5 \times 0.25 \times 10^{-8}$   $\Omega\text{-m}$ , which would require cooling to 150 K instead of 77 K. Thus, high power density permits battery mass to be traded for cooling. A power density of 7 kW/kg would enable the overall pulse energy densities obtained with liquid nitrogen cooling to be obtained at room temperature.

Other options are to alter the battery resistance/winding resistance ratio or the charging time of 1.23 time constants that were incorporated in the design equations in this Chapter. If the winding resistance is much less than the battery resistance most of the  $I^2R$  loss during charging is transferred to the battery, where it may naturally dissipate instead of evaporating the transformer coolant. If the charging is for less time than  $1.23 T_0$  the charging efficiency is increased and a greater number of shots is obtained from a given battery mass, as well as there being less evaporation of coolant.

A battery with a power density of several kW/kg, together with an energy density several times the 100 kJ/kg assumed in this Chapter, would give much greater design flexibility and would be the basis for further evaluation of the pulse transformer scheme.

#### 8.10 Conclusions

The trial designs and discussion lead to the following conclusions.

- (i) With liquid nitrogen cooling and batteries that have a power density of 1 kW/kg for several seconds, the pulse transformer - battery scheme attains overall pulse energy densities of about 1 kJ/kg when the stored energy exceeds about 10 MJ.

At low energies, e.g. 100 kJ, the energy density is about 100J/kg. The only way to increase this value is through lower resistivity, which implies further cooling, e.g. by liquid hydrogen, but such cooling would itself be a serious burden unless superconductors were used.

At large stored energies (1 GJ) energy densities of several kJ/kg may be attained.

- (ii) Beyond about 10 MJ stored energy, with liquid nitrogen cooled coils, the conductor size required for strength causes the coil mass to be the dominating factor in determining overall pulse energy density.
- (iii) Batteries with a power density exceeding 1 kW/kg do not greatly increase the overall energy density attainable, but permit valuable trade offs in other parameters, notably in the amount of cooling required.

A battery with both a power density of 3 kW/kg and an energy density of 300 kJ/kg (i.e. a factor of 3 improvement upon the values assumed for this study) would greatly increase the design options.

- (iv) Force reduced construction has no advantage other than having slightly less mass and mitigating the damaging effects of minor radial forces at large stored energies.

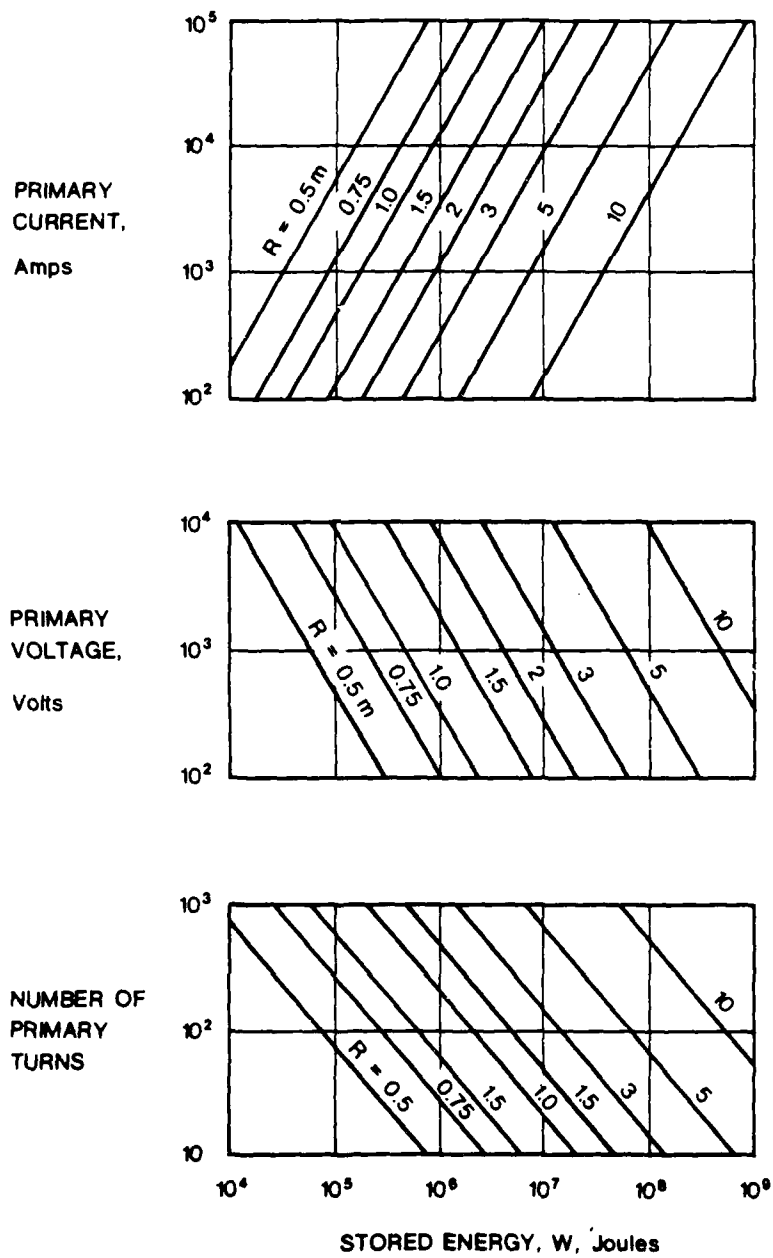


Fig. 95 Graphs, External Field toroid,  $\frac{R}{a} = 5$ .

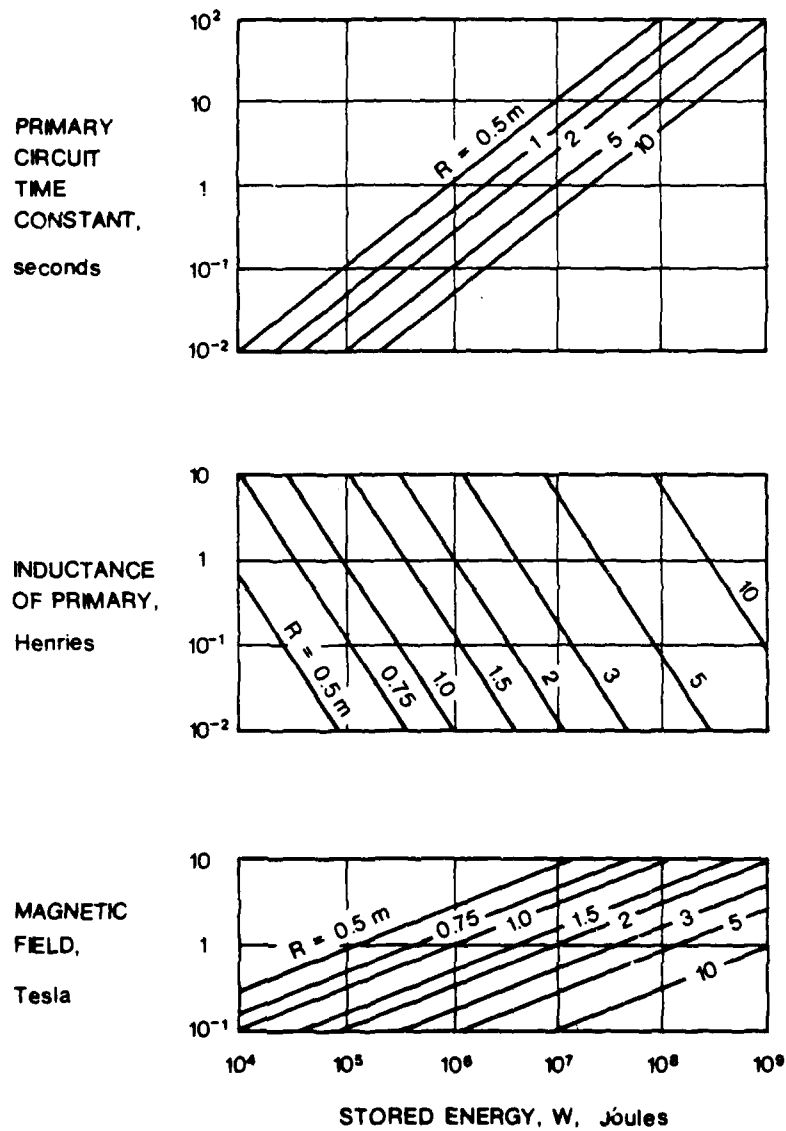


Fig. 96 Graphs, External field toroid,  $\frac{R}{a} = 5$ .

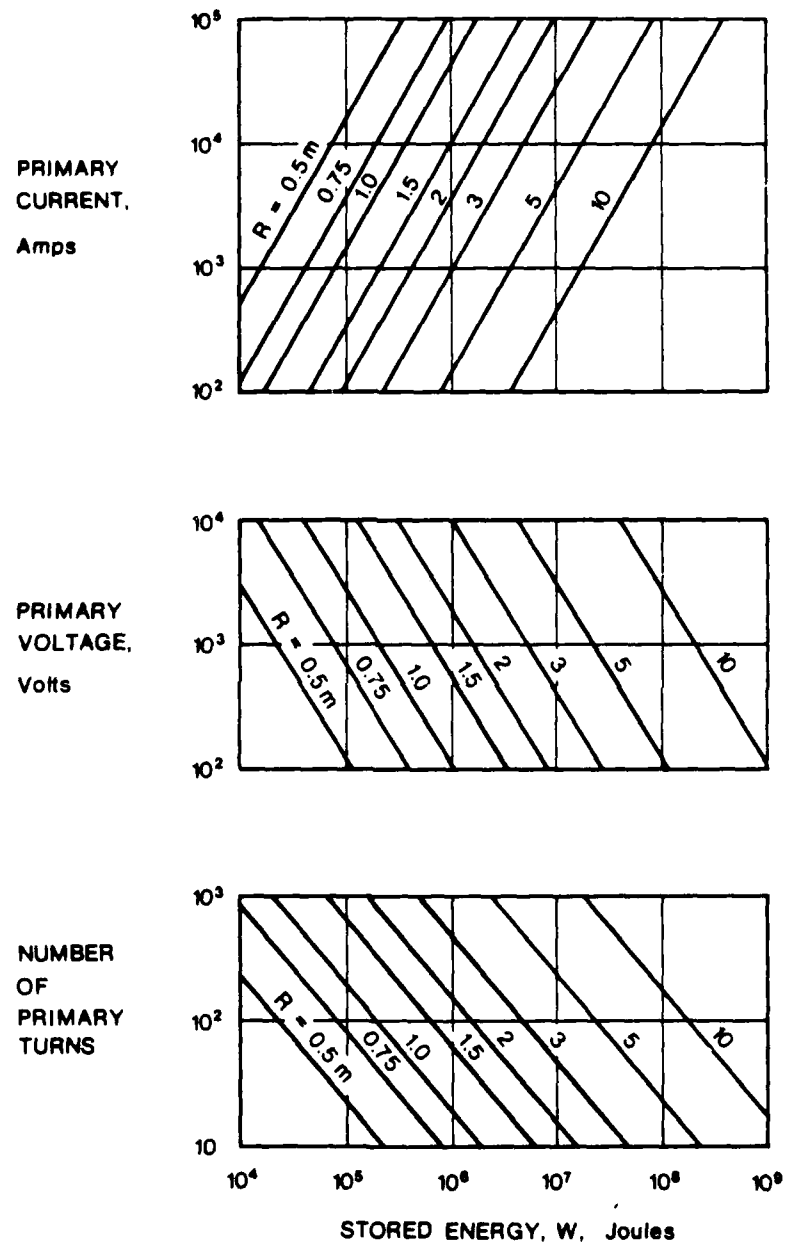


Fig. 97 Graphs, External field toroid,  $\frac{R}{a} = 10$ .

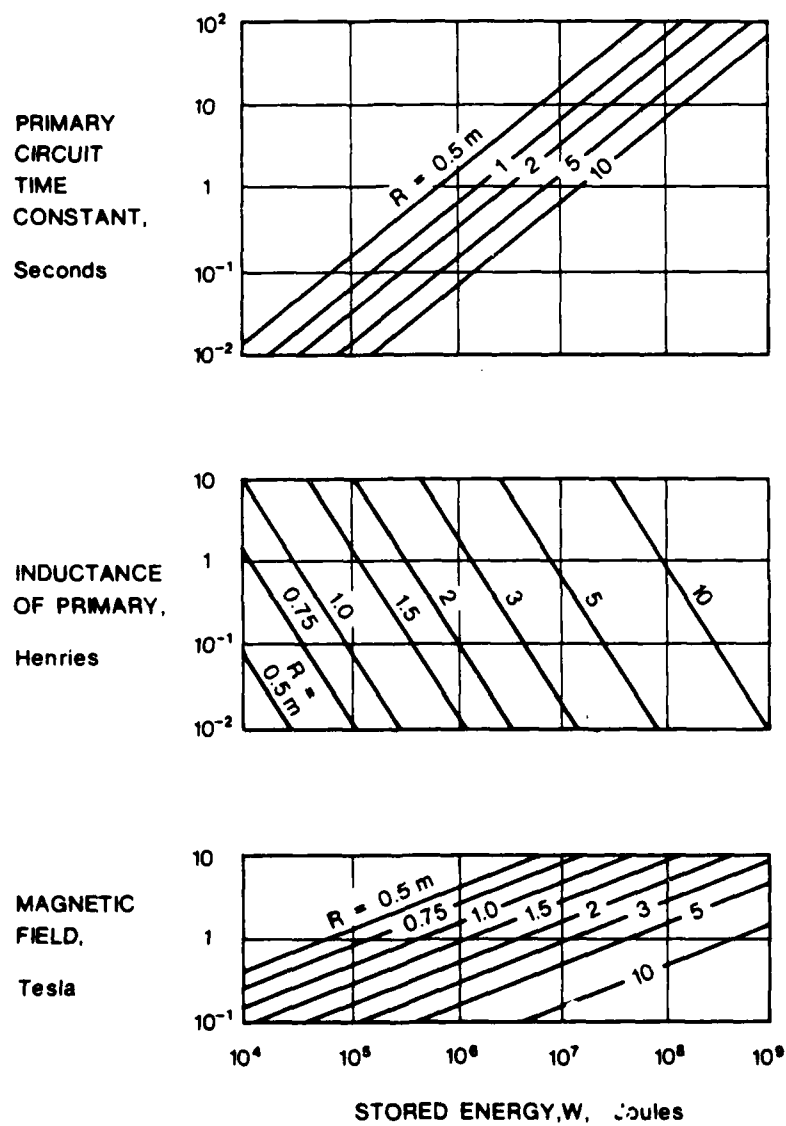


Fig. 98 Graphs, External field toroid,  $\frac{R}{a} = 10$ .

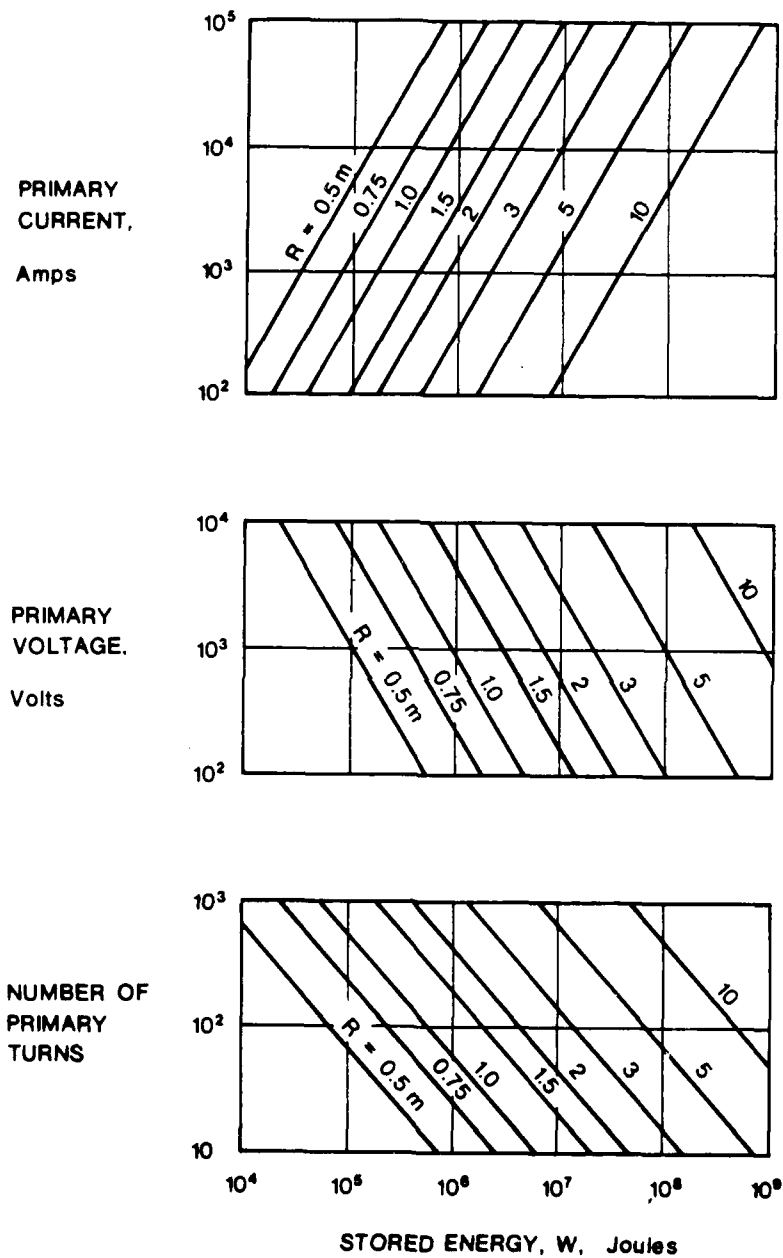


Fig. 99 Graphs, force reduced toroid,  $\frac{R}{a} = 5$ .

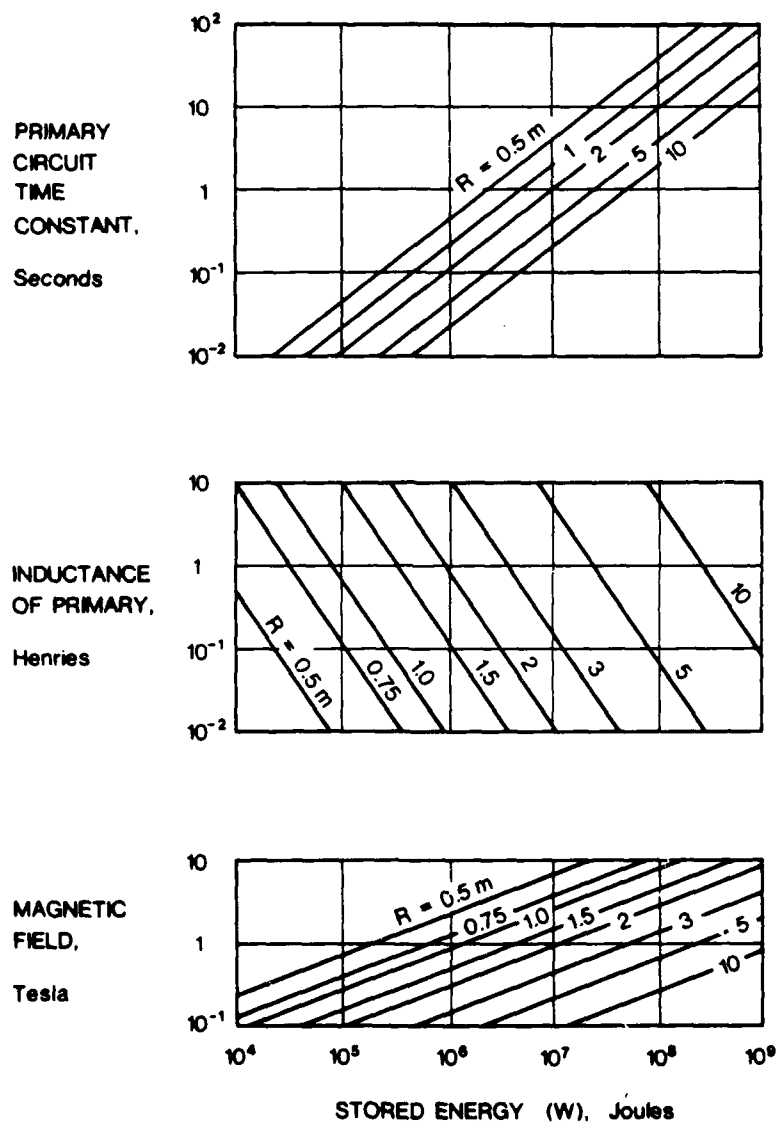


Fig. 100 Graphs, force reduced toroid,  $\frac{R}{a} = 5$ .



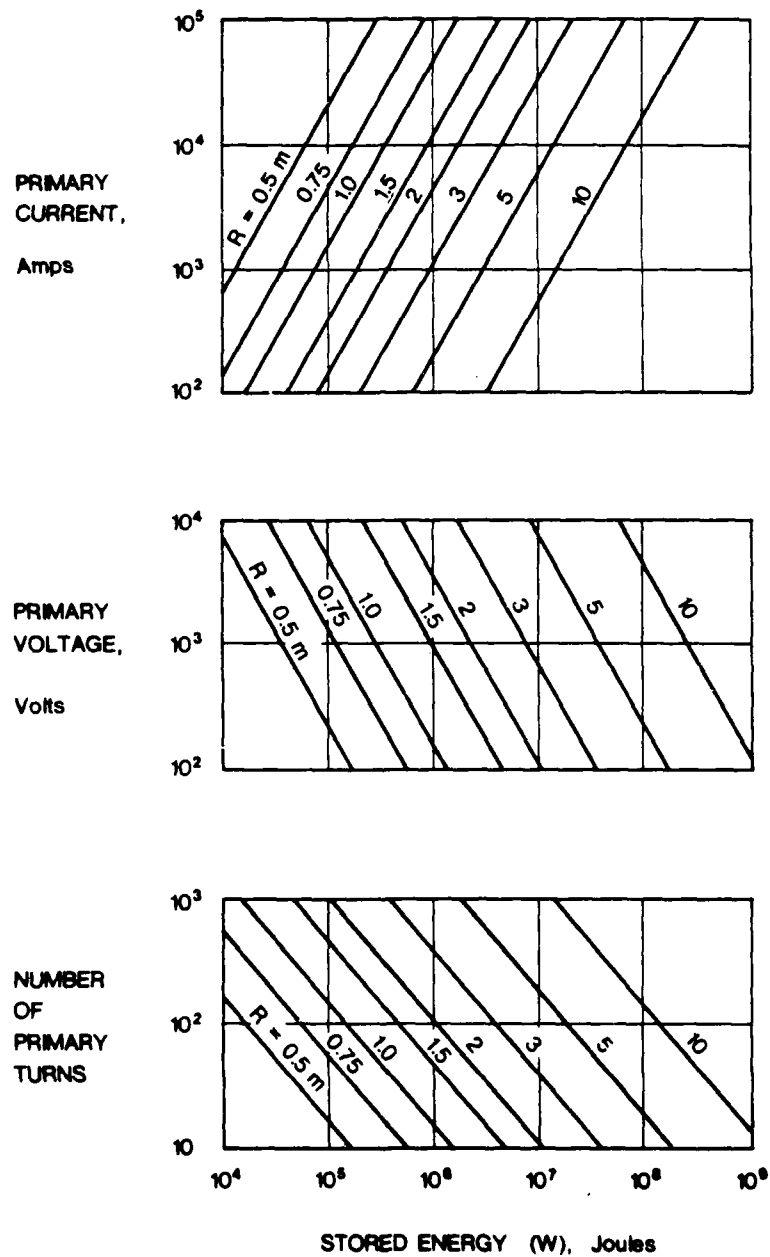


Fig. 101 Graphs, Force reduced toroid,  $\frac{R}{a} = 10$ .

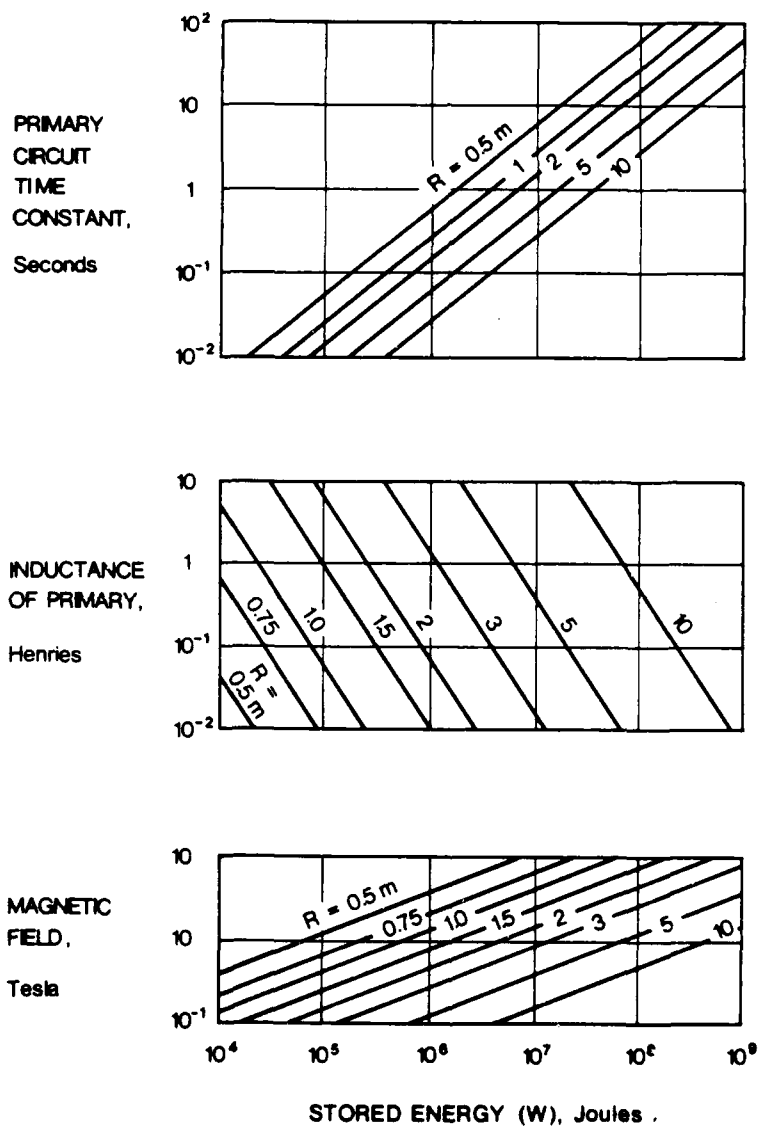


Fig. 102 Graphs, Force reduced toroid,  $\frac{R}{a} = 10$ .

## CHAPTER 9

### EXPERIMENTS - PURPOSE AND DESCRIPTION

The ideas and calculations set out in the previous Chapters were accompanied by the following practical investigations.

- (i) Inductance measurements of rectangular rails.
- (ii) Degree of coupling of primaries to various secondaries.
- (iii) Force reduction.
- (iv) Pulse power density of lead acid batteries.
- (v) Model pulse transformer systems.

#### **9.1 Inductance measurements of rectangular rails**

##### **9.1.1 Purpose**

There were two purposes for making rail inductance measurements, viz., to verify the expressions for total inductance that were derived and to infer the extent to which the current distributes initially in real conductors so as to have the minimum inductance.

##### **9.1.2 Rails measured**

Rails of copper, brass and aluminium were used, according to availability, simply to make up a size range and not to explore differences due to these materials. The rails measured were:

<u>W/H <math>\approx</math> 0</u>	<u>Material</u>	<u>H x W x Length (mm)</u>	<u>S/H</u>
(i)	Copper	25 x 0.7 x 1800	0.2, 0.5, 1, 2, 5
(ii)	Aluminium	21 x 0.58 x 890	1
(iii)	Aluminium	25 x 0.58 x 900	0.2
(iv)	20 Way ribbon cable "rail",	1" (H) x 2660	1
<u>W/H = 0.2</u>			
	Brass	1 1/4" x 1/4" x 1990	0.5, 1

W/H = 0.5

(i)	Copper	10 x 5 x 2900	0.2, 1, 2, 5
(ii)	Brass	1" x 1/2" x 1790	0.5, 1

W/H = 1

(i)	Copper	12.5 x 12.5 x 3610	0.2, 1, 2, 5
(ii)	Aluminium	25 x 25 x 1990	0.5, 1

As in Chapter 2, W is the width, H is the height and S is the separation of the rails.

The 20 way ribbon cable was used to form a thin sheet rail of parallel filaments across the height dimension instead of a uniformly conducting material. Frequencies used were 10 kHz - 20 kHz and, for the 20 way ribbon cable, 3.63 MHz.

**9.1.3 Apparatus and methods**

The inductance values for railgun geometries are small ( $\approx 0.5 \mu\text{H/m}$ ) and are thus difficult to measure accurately. The writer had access to three instruments and investigated a "phase plane" method.

(i) ESI Videobridge, automatic LRC meter, model 2100

This is an elaborate instrument with programmable current, voltage and frequency (20 Hz to 20 kHz) test conditions and a video display. Accuracy, for the conditions selected for the particular instrument, using a specially constructed test coil, was believed to be  $\pm 2\%$  of the reading.

(ii) Marconi Universal Bridge, Model TF1313A

With this instrument, the operator adjusts resistance to obtain null balance of the inductance against a standard capacitance. Frequency is selectable at 1kHz or 10kHz. Accuracy at 10 kHz is given as  $\pm 0.2\%$  of reading or  $\pm 0.025\%$  of range, whichever is the greater. In practice the difficulty in correctly finding the null is a greater cause of inaccuracy in low Q situations, such as the rails present. For the rails listed above, the writer believes the Marconi Bridge readings to be within  $\pm 2\%$  of reading.

(iii) Meguro Denpa Q Meter, Model MQ 160A

This instrument enables measurements to be made in the range 25 kHz - 50 MHz. An inbuilt air capacitor is adjusted until resonance (indicated by a maximum deflection of the Q meter) is obtained with the inductance being measured. A dial calibrated in L and C at resonance enables L to be read directly at certain frequencies and scaled therefrom at other frequencies. Stray capacitance across the inductance to be measured is a source of error in this instrument. Accuracy also depends upon that of the internal oscillator and the variable capacitor. The frequency was found to be within 1% of dial setting and the capacitance value is stated to be within 1% of dial setting.

(iv) Phase plane method

The above instruments all give the inductance for sine waves. At high frequency the sine wave inductance is the same as the initial inductance on the assumption that the high frequency "preserves" the current distribution in a condition near to the initial distribution. The fact that the initial current rise with time can be represented by a Fourier series with high frequency components is the basis of this assumption.

The "phase plane" method is an attempt to measure the actual initial inductance when a rectangular voltage pulse is applied and to demonstrate that it has the same value as the high frequency inductance. The writer (DRS) developed the method from an idea published by Huen [1]. The essential idea, stated by Huen, is that the time derivative or integral of an exponential waveform is itself an exponential. Since the current rises exponentially in a circuit with constant inductance and resistance to which a constant voltage step is applied, the plot of the current rise against its integral is a straight line. If it is not a straight line, the inductance and resistance must be changing. Due to diffusion this must occur, and the phase plane display should in theory display the process. The actual inductance can be found from the slope of the straight line display. The details of the method, including the factors that distort the display, are given in Section 9.6.

Length of rails - test frequency

In order to minimize instrument errors and end effect errors of the rails, it is desirable to use long rails. It is difficult to obtain long, straight lengths and to accurately separate them to the desired S/H values. The lengths must in any case be kept short compared to a quarter of a wavelength so that they behave as lumped inductances instead of transmission lines. Alternatively, for a given length of rail, there is an upper test

frequency for which lumped circuit measurements are applicable. From the equation given in Section 9.6 the reactance of a 2 m length of rails at 7.5 MHz is about 3% above that which its lumped inductance has.

#### Ribbon cable rail

According to theory [2] the current should distribute across thin sheet rails in the same manner, regardless of whether the rails are thin sheets of conducting metal or consist of parallel filaments as depicted in Fig. 10, Chapter 2. The 20 way ribbon cable model was constructed to test this theory.

### **9.2 Degree of coupling**

#### **9.2.1 Purpose**

The purpose of these experiments was to measure the degree of coupling attained in practice between a primary and various secondaries and to test the methods used in Chapter 6 for its estimation. It was also desired to find whether the degree of coupling improved with frequency and therefore is greatest at the moment that the primary circuit of the pulse transformer commences to open.

#### **9.2.2 Coils and secondaries used**

Five solenoids and one external field toroid were constructed, with secondaries, as follows.

##### **(1) Long solenoid with shorter layer secondaries**

This was constructed to test the simple theory set out in Chapter 6, Section 2.1, by which the value of  $k_1 k_2$  was found to be equal to the smaller of the ratios of the lengths of the windings.

The primary was wound upon a 25 mm diameter wooden mandrel with 0.86 mm diameter enamelled wire to give a winding with the length to diameter ratio equal to 10. Two secondaries were wound over the primary, using the same wire, with lengths one half and one fifth the length of the primary (Fig. 103). The half length secondary was symmetrically placed over the central portion of the primary.

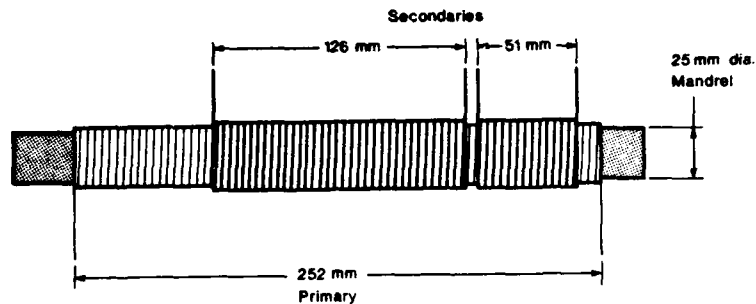


Fig. 103 Long solenoid with shorter layer secondaries

(a), construction; (b) actual model.

(ii) Short solenoid with thin sheet secondary

Two models were constructed, shown in Fig. 104.

- (a) A 160 mm diameter former was wound with 84 turns of 0.87 mm dia. enamelled wire as the primary and a 0.12 mm thick copper sheet secondary. The copper secondary was soldered to form a cylinder i.e. short circuited. Firstly the secondary was

placed on the outside, and degree of coupling was measured. Then the secondary was removed and the primary was unwound. A secondary was then fitted to the former and the primary was rewound over it to yield a primary with the secondary on the inside. The copper sheet secondary and primary were matched in length to within about one wire diameter.

- (b) The above was repeated using a 250 mm diameter former wound with 56 turns of 2.5 mm diameter enamelled wire and 0.7 mm thick copper sheet.



Fig 104 Short solenoids with thin sheet secondaries

- (a) 84 turn primary on 160mm diameter former  
(b) 56 turn primary on 250mm diameter former.

(iii) Short solenoid with separate layer winding

90 turns of 1.2 mm diameter enamelled wire were wound upon a 110 mm diameter former and a second layer of 90 turns of the same wire was then carefully wound over the first layer (Fig. 105a).

(iv) Short solenoid with bifilarly wound primary and secondary

100 turns of 1.09 mm diameter enamelled wire were bifilarly wound on a 204 mm diameter former to yield a coil with the diameter approximately equal to its length (Fig. 105b).



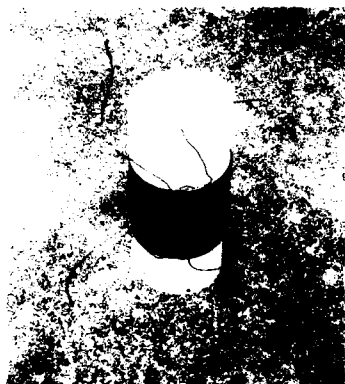


Fig. 105a Short solenoid with separate layer winding.



Fig. 105b Short solenoid with bifilar primary and secondary.

(v) Short solenoid with coaxial cable winding

The difficulty in testing this construction was to obtain a coaxial cable with the inner nearly equal in diameter to the outer, as required for high degree of coupling. In normal coaxial cable (eg. 50 ohm cable) the inner diameter is much less than that of the outer. The problem was solved by pulling the inner and its insulation out of 50 ohm coaxial cable and then sliding the outer over 2.5 mm diameter enamelled copper wire, which it fitted very closely.

40 turns were wound upon a 320 mm diameter former, to yield a winding with an overall length of 20 cm. The coaxial outers were precut to the length of one turn and their ends were bared, prior to winding the coil. The winding was done in a lathe, each turn being carefully pulled tightly into position and clamped with a clip and screw to the former, until the next turn was in place. The bared copper outers were tinned and busbars were then sweated to them. The finished coil is shown in Fig. 106.

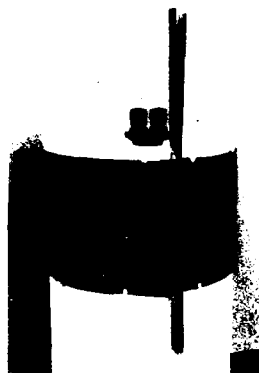


Fig. 106 Short solenoid with coaxial cable primary and secondary.

(vi) External field toroid with bifilar windings

An external field toroid with  $R = 250$  mm and  $\frac{R}{a} = 5$  was constructed with two 47 turn bifilar windings, using 2.0 mm diameter enamelled wire (Fig. 107). Due to an oversight the turns were all equally spaced instead of each primary turn being in contact with its bifilar secondary turn. Additional uncoupled flux to that considered in Ch. 6 was thus introduced. The degree of coupling was nevertheless calculable (Section 9.6).

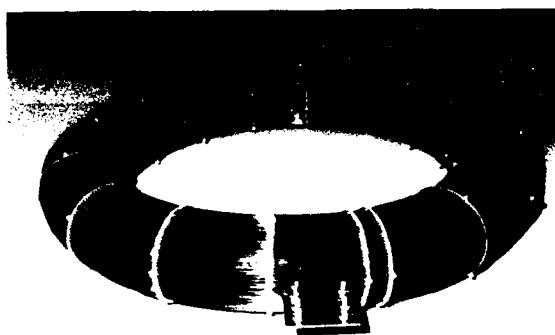


Fig. 107 External field toroid with 47 turn bifilar primary and secondary.

### 9.2.3 Method of measuring degree of coupling

The method of measuring degree of coupling was to measure the inductance of the primary with the secondary open ( $L_1$ ) and again with the secondary shorted ( $L_{1SC}$ ). The degree of coupling,  $k_1 k_2$ , was then calculated from:

$$k_1 k_2 = 1 - \frac{L_{1SC}}{L_1}$$

This equation is derived in Section 9.6.

The instruments used to measure inductance were the Marconi Bridge and the Videobridge. Frequencies used were in the range 1 kHz to 20 kHz.

## 9.3 Force reduction

### 9.3.1 Purpose

The purpose of these experiments was to demonstrate the presence of magnetic forces and force reduction in a manner which was visible as well as measurable.

### 9.3.2 Method

The method used was to set up two model sections of coils, one section being that of an external field toroid and the other being similar except that its conductors were pitched at 45° (Fig. 108).

The parallel wires model, i.e., the model of the external field toroid, was designed so that the crushing force due to the external magnetic field would cause the wires to visibly pinch inwards. The force reduced toroid model was carefully constructed with the minimum of friction and restraining structure so that it would be distorted by forces only a fraction of those present on the parallel wires model.

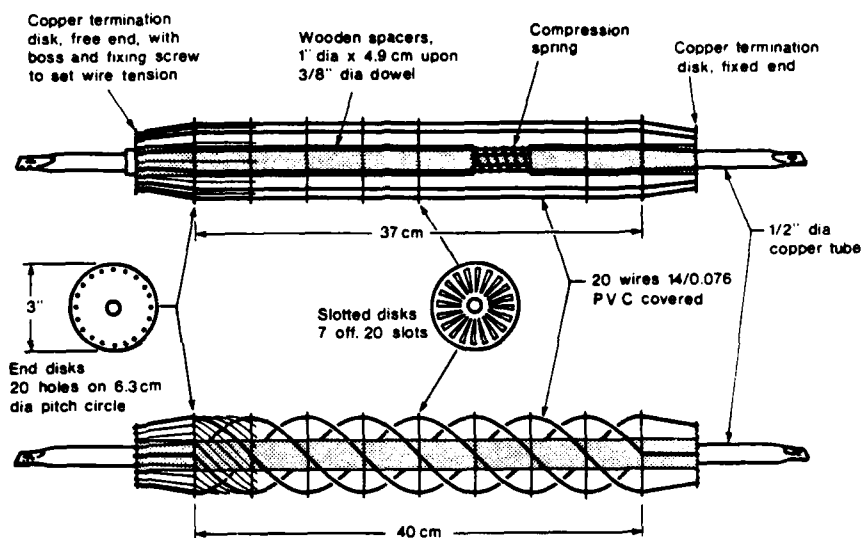


Fig. 108 Models for force reduction demonstration. The upper model represents a section of an external field toroid. The lower model is of a force reduced toroid.

The experiment was made measurable by using the catenary theory described in Chapter 8 to calculate the deflection of the wires for a given tension and current. The tension was set by adjusting the position of the free end copper terminating disk, which was free to slide on the  $\frac{1}{2}$ " copper tube, and then clamping the disk and tube by means of the fixing screw. A dial type force gauge with a lever was used to position the disk and measure the tension. (The copper termination disk at the other end was soldered to the copper tube. The  $\frac{3}{8}$ " dowel which holds the assembly together, was several centimetres shorter than the overall length, to allow other parts to slide under the action of the magnetic forces). The deflection of the wires was desired to be about 1 cm with a current of 100 A in each of the 20 wires. For these conditions, the total tension in the wires was calculated to be 2.22 kgf. The calculations are given in Section 9.6.

When the wires of the parallel wire model pinch toward the centre, the ends are also pulled inwards i.e. the overall length decreases. By fixing one end and fastening a pair of micrometer calipers to the other end, the horizontal movement can be measured. From this and the spring tension, the work done by the magnetic forces can then be calculated. This can be used to calculate the movement of the ends of the force reduced model, having measured the friction and elastic force present in the force reduced model, if the force reduction did not occur and the same energy were available.

The experiment consisted of setting up the straight wire section, with calipers attached to one end, and measuring the current required to cause approximately 1 cm deflection, and the calipers deflection. The same current was then passed through the force reduced model and movement of the wires and ends was observed.

#### **9.4 Pulse power density of lead-acid batteries**

##### **9.4.1 Purpose**

As was pointed out in Chapters 4 and 8, the pulse power density of batteries needs to be at least 1 kW/kg for the pulse transformer system to have an overall pulse energy density of about 1 kJ/kg, using liquid nitrogen cooled coils. The ohmic resistance and polarization limitations in four types of batteries were investigated to discover whether a pulse power density of 1 kW/kg for 1 second is a reasonable prospect.

##### **9.4.2 Method of measuring pulse power density**

The method used was to record the battery terminal voltage and the current, which it delivered while practically short circuited (Fig. 109), from which the internal resistance and the power delivered can be calculated.

The 400A three pole contactor, with its contacts paralleled to minimize the arcing due to contact bounce, was used to close the circuit. In most tests the fuse was used as a means of timing the test and as the opening means rather than subject the contactor to arcing. The increasing resistance of the fuse during a test also enabled the internal ohmic resistance to be gauged under heavy load without undue influence of polarization.

The fuse was not used in tests to reveal the polarization limitations, i.e. the limitation due to the diffusion of ions at the electrode/electrolyte interfaces.

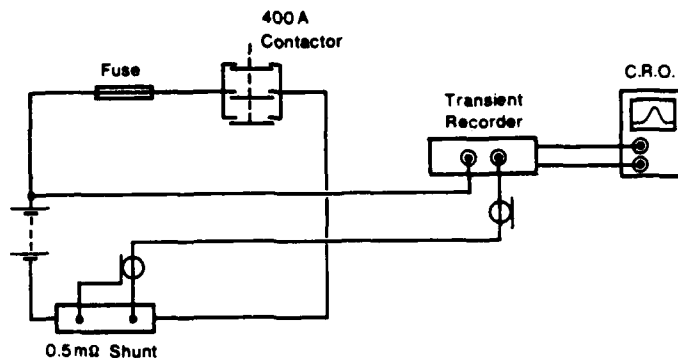


Fig. 109 System for determining battery pulse power density.

The major component of battery internal resistance, aside from the rate limitations due to diffusion, is the resistance of the acid path. The resistivity of the acid falls with temperature; at 60C it is 2/3 of the value at 20C. Some batteries were heated and their internal resistance was then measured to see if the lowered acid resistance resulted in higher short circuit current.

#### 9.4.3 Batteries tested

Four types of battery were tested (Fig. 110).

- (1) Conventionally constructed automotive starting battery, Lucas, Catalogue No 274A, 66 plates, 80AH, 12V, mass = 22.7 kg.

40 of these batteries were available, being unused stock at Materials Research Laboratories. They were a "preserved charge" type which had not been filled with acid and were still sealed, but were 7 years old. According to their manufacturer "preserved charge" meant that they had been fully charged at the factory and had then had the acid tipped out, but the plates remained wet. This meant that the battery would leap into life when refilled with acid, in contrast to dry charged batteries which require about 15 minutes for the acid to permeate the plates, and eliminated the costly drying process. They were meant to be used within a few months of manufacture.

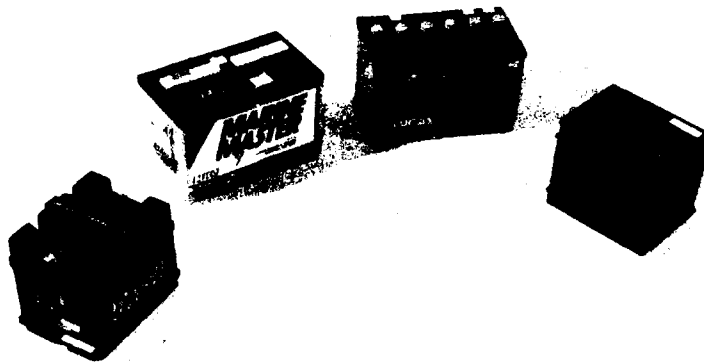


Fig. 110. Batteries tested. From left to right: Exide "Torque Starter"; Besco "Marine Master", Lucas, 274A; Dunlop "Pulsar", 15 pair prototype.

(11) Conventionally constructed automotive starting battery, low maintenance type, Besco "Marine Master", 12V, Catalogue No. 782, 90 plates. These batteries were rated at 350 A for 30 seconds to a terminal voltage of 7.6V at -18C Mass = 22.2 kg.

8 of these batteries were purchased, new.

(111) Conventionally constructed low maintenance automotive starting battery, Exide "Torque Starter", 12V, 14 kg. This is a "new technology" battery which is fully sealed and has a glass fibre mat separator which causes oxygen formed at the positive plate during charging to pass directly to the negative plate and recombine to form water, instead of bubbling up through the electrolyte and being lost, as in ordinary construction [3]

5 of these batteries were purchased, new.

(iv) Revolutionary construction automotive starting battery; the Dunlop Olympic "Pulsar" (4). This battery was invented in 1974 by Mr Bill McDowall of the Dunlop Olympic Battery Company, at Sandringham, Victoria, and was recommended by Mr John Howlett of that Company.

The construction is shown in Figs. 111 and 112. The battery is an assembly of similar shaped "frames", each divided into 6 sections. The frames which have the active materials have alternating sections of positive and negative materials. Two such frames, placed so that the positive sections of one are opposite the negative sections of the other, form a battery with 6 cells in series i.e. they form a 12V battery. The series connection between the cells is formed by the double width mesh sections shown in Fig. 111. The frame in between the active sections is a separator frame and contains a microporous plastic film. The end frames are of plastic, as are the others, and form the end walls of the battery. Assembly consists of pressing together the five frames, which seal along their edges. To increase the capacity of the battery more pairs of active frames and separator frames are used, and the tabs of the individual 12V batteries so formed are connected in parallel to output busbars (Fig. 112).

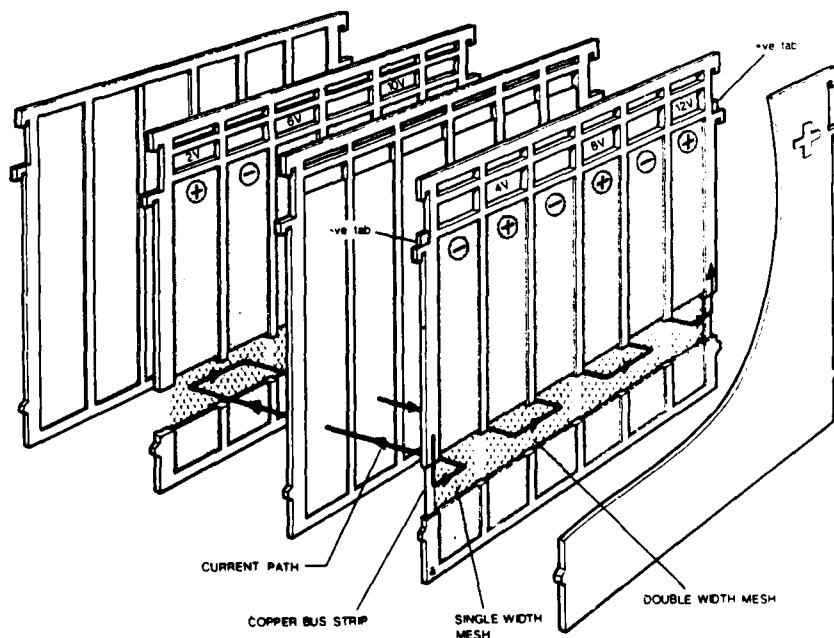


Fig. 111 Construction of the "Pulsar" Battery (Courtesy of Dunlop Olympic Australia). The construction shown is a 1 pair, 5 frame module.



The advantage which this battery has is that the current paths, from the sites at which the chemical reactions occur to the output busbars, are much shorter and more nearly equidistant from all parts of any one electrode, which means that current is more uniformly distributed over the electrode area. Ohmic resistance is thereby reduced to about half that of conventional construction, where the current must crowd to the corner of each plate and then pass via intercell connectors to the next cell, and so on. In the "Pulsar" the current can flow as a sheet from one cell to the next, via the full length of an electrode to the next electrode via the double width mesh (Fig. 111), and from the whole surface of an electrode via the acid to the opposite electrode.

The construction principle of the "Pulsar" appears to reduce ohmic resistance to the minimum and to reduce the problem of a high pulse power density to that of supplying fresh reactants to the interface regions. The construction could be applied to batteries other than lead-acid.

A prototype 15 pair "Pulsar" (mass 15 kg) was donated to the writer by Dunlop Olympic Australia. Later, 55 10 pair "Pulsar" batteries were purchased to replace the Lucas batteries, which turned out to have deteriorated too much.

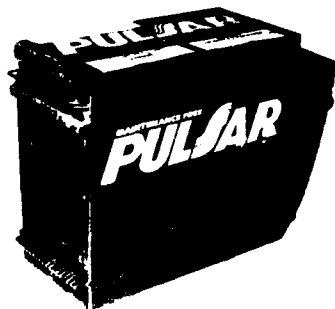


Fig. 112 10 pair "Pulsar". Mass = 10 kg. Note the busbar style output terminals on the sides of the battery.

## **9.5 Model pulse transformer systems**

### **9.5.1 Purposes of model pulse transformer systems**

Four model pulse transformers were constructed to test the overall functioning of the pulse transformer concept, and in particular:

- (i) the degree of coupling of transformers themselves;
- (ii) the practicality of using a fuse to open the primary;
- (iii) the proportion of primary energy actually transferred;
- (iv) the practicality of constructing force reduced windings.

### **9.5.2 Transformers constructed**

Two of the transformers constructed were external field toroids and two were force reduced toroids. Both external field toroids had 24 turn primaries with major diameters of 1 metre and minor diameters of 50 mm. The secondaries were, in one case, a 25 mm diameter aluminium bar on the inside of the primary, and in the other case a 75 mm diameter copper pipe fitted over the outside of the primary. The construction of the transformer with the internal secondary is shown in Fig. 113. The primary of the transformer with the external secondary was constructed in the same manner. The external secondary was formed by bending the 75 mm, 16 gauge copper pipe into a circle and then slitting it into halves. The primary was laid into one half and the other half was then placed on and the two halves were banded together with hose clips (Fig. 114). The D.C. inductances and resistances of the primaries of these transformers were:

transformer with internal solid secondary: 1.1 mH, 130 mΩ.  
transformer with external sheet secondary: 1.1 mH, 90 mΩ.

AD-A192 102

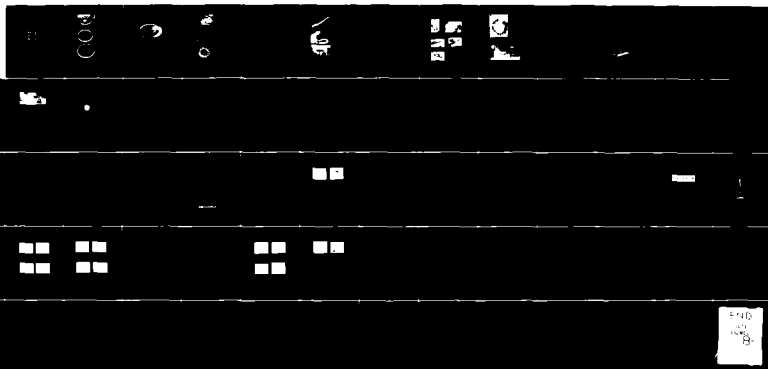
THE RAILGUN AND ITS POWER SOURCE(U) MATERIALS RESEARCH  
LABS ASCOT VALE (AUSTRALIA) D R SADEIN ET AL. JUN 87  
MRL-R-1038 DOD-AR-805-133

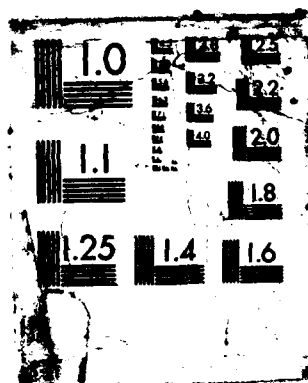
4/4

UNCLASSIFIED

F/G 20/3

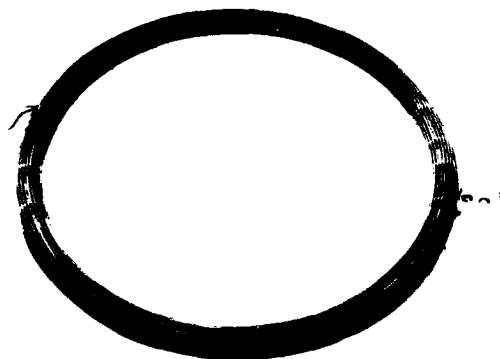
ML



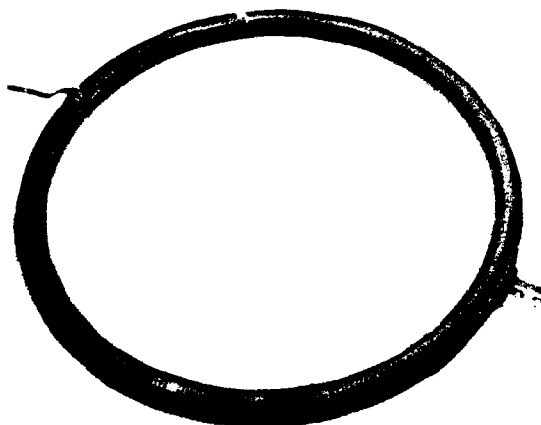




(a)  
Primary turns being laid  
into notched disks which  
have been cemented to the  
25mm dia aluminium bar used  
for the secondary.



(b)  
Primary, 24 turns of 7/0.052  
electrical wire, completed.  
Secondary output bus is on  
right.



(c)  
Completed transformer,  
wrapped and lacquered.

Fig. 113 External field toroid with secondary internal

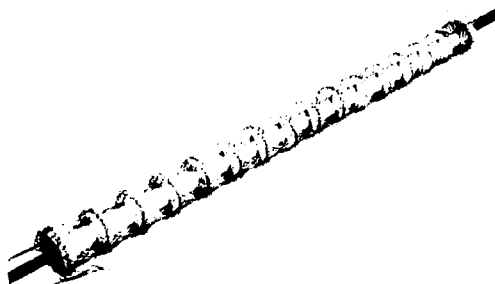


Fig. 114 External field toroid with external sheet secondary upon 24 turn primary.

The force reduced transformer requires each primary turn to progress around the periphery with a 45° helix angle and the turns must all be in series. It might be possible to construct such a transformer in small sizes by passing a reel of wire through the toroid, but in large sizes, using copper rod, this would be difficult. The construction method which was devised was to lay separate wires at a 45° helix angle around a straight, but flexible, former and then to bend the assembly into a circle and to then join the ends of the wires to form the series connected turns. The construction sequence is shown in Fig. 115.



(a)  
Components of a flexible  
former. PVC tube, spacers  
(cut from suction hose) and  
wooden disks with 32 nails.  
Ruler = 15".



(b)  
Former assembled on pipe  
( $\frac{1}{4}$ " dia rod through small  
holes in disks to prevent  
rotation) and 32 wires laid  
at 45° helix angle.



(c)  
Pipe and rod removed from  
former and assembly bent  
into circle. Note the  
circular shape which is  
taken up naturally when the  
ends are brought together.

Fig. 115 Manufacture of force reduced toroids.

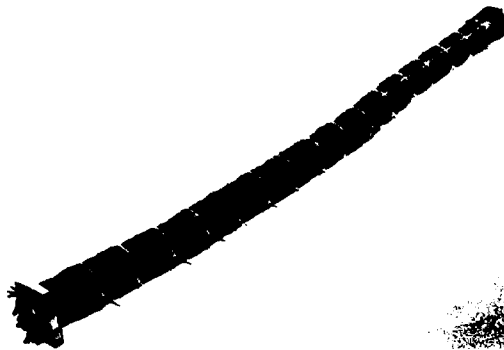
A small force reduced transformer was constructed as above using 2.5 mm diameter enamelled copper wire (Fig. 116). The secondary was "partly" bifilar. The details of the coil were:

major diameter:	460 mm
minor diameter:	90 mm
conductor diameter:	2.5 mm
no. of primary turns:	47
no. of secondary turns:	16
calculated primary inductance:	1.43 mH (D.C.)
primary resistance:	0.32 $\Omega$ (D.C.)
estimated value of $k_1 k_2$ :	0.91
mass:	7 kg

The flexibility of the winding and the ease with which it was bent into a circle can be seen in Fig. 116.

Instead of 47 bifilar turns, only 16 secondary turns were used, i.e. one secondary turn to every three primary turns. This was done to enable a larger diameter wire to be used, and so reduce the primary resistance at the expense of the secondary, which need have a time constant only a fraction of that required for the primary. This of course reduces the degree of coupling, which can be estimated from the mutual inductance components tabulated in Ch. 6, Section 5.3. For 16 turns we obtained a mutual inductance of 1.817  $\mu$ H and for 47 turns we can estimate from the tabulation a mutual inductance of 2.0  $\mu$ H. Using Eqn. 5.49 we then find  $k_1 k_2$  has a maximum value of 0.91. (This is an estimate only, since the tabulation refers to external field toroids, not the force reduced geometry).





(a) Wires laid upon flexible former. Note the flexibility.



(b) Bending the assembly into a circle.



(c) Completed transformer 47 primary turns connected in series, 16 secondary turns connected in parallel to gapped copper collecting bands.

Fig. 116 Manufacture of 47 turn primary, 0.5 m dia force reduced toroid.

Initially, the primary of this transformer was constructed with 48 turns, but when the coil was completed it was found that many sections of the primary were short circuited. This came about because of the difficulty of identifying the correct ends with which to commence joining the turns in series. Study of the problem showed that if the number of turns is a prime number, it does not matter which ends are picked initially, so long as they do not form a shorted turn. A practical rule for construction, therefore, is that the number of primary turns should be a prime number. This is proven in Section 9.6.

Following the ease of construction and success of the small force reduced transformer, a larger version was constructed, using 6.4 mm diameter copper rod. This transformer was vastly more difficult to construct. Whereas the small version took about 2 man weeks, this one took about 3 man months\*. Its details were:

major diameter:	1 m
minor diameter:	200 mm
conductor diameter:	6.4 mm
no. of primary turns:	43
no. of secondary turn:	16
calculated primary inductance:	2.59 mH (D.C.)
primary resistance:	0.10 $\Omega$ (D.C)
estimated value of $k_1 k_2$ :	0.91
mass:	100 kg

The coil was constructed from 59 copper rods, each 4.8 metres long. As these were quite hard when received, they were annealed. Finding a furnace of adequate size was a problem. It was also necessary to insulate the rods. This was done by winding on teflon tape in a lathe with a specially constructed wrapping attachment. Handling of the long, very flexible rods and wrapping them around the former was a tedious and laborious task. The rods were carried inside a long plastic pipe when it was necessary to move them. Although the coil was massive, it bent into a circle with the same ease as the small version. The primary turns were joined in series by fitting tinned copper sleeves on one set of tinned ends and pushing the other ends into them, plug and socket fashion. The secondary turns were clamped between cast copper gapped rings that were tightly bolted together to minimize stray secondary inductance\*\*. The construction and the transformer are shown in Figs. 117 and 118.

---

\* The construction of this transformer succeeded only due to the ingenuity and determination of Mr H. Wenzel of the Electrical Workshop.

\*\* The authors are grateful to Dr G.K. Cambrell for the design of the secondary termination.



(a)



(b)



(c)



(d)



(e)

- Fig. 117 Manufacture of large force reduced toroidal transformer
- (a) Rolling copper rods straight.
  - (b) Winding teflon tape onto rods.
  - (c) The former. Plywood slats were used to define the position of the 16 secondary turns, which were put on first.
  - (d) Secondary turns and some primary turns laid on. Slats removed as primary turns laid on.
  - (e) Bending assembly into a circle.

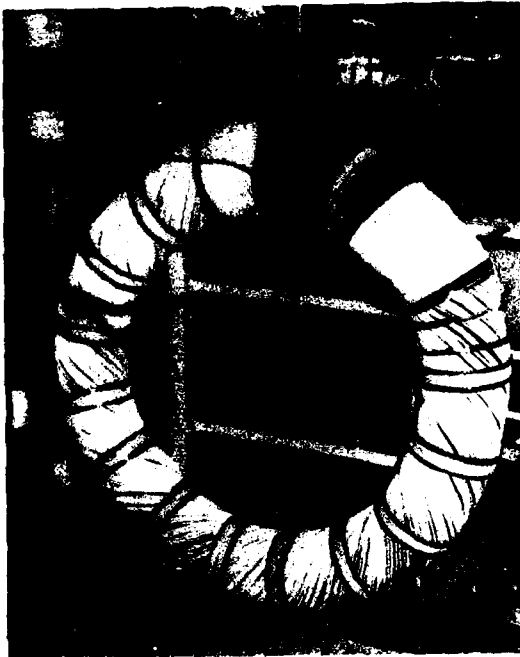


Fig. 118 Large force reduced transformer

Left: After being bent into a circle and joining of most of the primary turns.

Below: Completed transformer under test. Note the secondary termination consisting of two pairs of cast copper rings, between which ends of secondary turns were clamped and sweated.



### 9.5.3 Fuses

As was discussed in Chapters 4 and 5, the important function of the fuse is to cause the time constant of the primary circuit to suddenly change from being long compared to that of the secondary to short (e.g.  $1/10$ ). It is not desirable that the fuse resistance becomes extremely high because the high voltage that arises across it might cause it to restrike to a low resistance before the energy transfer is completed, or it might cause breakdown elsewhere.

There is extensive literature on fuses, both as conventional electrical protection devices and as exploding wires in physics experiments [5-8]. The following is a digest of the theory that is relevant to the pulse transformer application.

The operation of a fuse has three stages. Firstly it is heated to its melting point. During this stage its resistance increases several times (approximately a factor of 10 for iron wires). In the next stage the molten metal is heated to its boiling point and the resistance increases much more rapidly than in the first stage. These first two stages take up most of the time, but it is the third stage which is most important in determining whether the fuse interrupts the primary current successfully. Exactly what happens during the third stage depends on the rate of deposition of energy in the fuse and upon its confinement. Frungel [9] summarizes the dependence on rate of deposition of energy as follows. If the time to vapourize the entire fuse is greater than about  $100 \mu s$ , gravitational and surface tension forces are able to move portions of the fuse and to cause it to separate into globules before significant vapourization occurs. Droplets may also form and arcing, via cumulative breakdown of vapour, will have time to develop. If the time to vapourization is in the region 5 to  $20 \mu s$ , the fuse will not have time to form into droplets but will distort under mechanical and magnetic forces. "Unduloids" form, and as the unduloids part, arcs are formed to carry the current. If the time to vapourization is less than about  $2 \mu s$ , the fuse "explodes". There is insufficient time for any shape changes and it becomes a superheated fluid. Its temperature goes far above the normal boiling point. Bubbles form and the superheated liquid expands violently, i.e. explodes, into the gaseous state. There is no arcing in this rapid process because there is no discontinuity until the violent separation of the atoms. Arcing does not occur initially after the explosion because cumulative breakdown is inhibited by the density of the vapour and the explosion forces. The resistance is thus very high, and if current must be carried, as it must in an inductive circuit, the voltage across the fuse is very high. As the vapour expands, though, the length of path between colliding electrons and atoms increases and the electrons can gain sufficient energy to ionize the atoms that they strike, and so arcing can be established. The high resistance period is called the "dwell time".

The confining structure affects the final behaviour of the fuse. The shock waves from the vapour generation are reflected from the boundaries and hollow tubes [10] may be utilized to blow out or suppress arcs. Sand is

commonly used to slow down the rate of expansion of the vapour and to disperse it so that when it cools the resultant metal is dissipated in a non conducting matrix, and also to cool and obstruct arcs that do form and so cause them to be higher in resistance than if they were unconfined (in particular, preventing arcs from joining and forming one long, low resistance arc).

A simple concept for the design of a fuse, mentioned in Ch. 4, is to select the fuse mass such that the fuse vapourization energy is the same as the energy necessarily dissipated in the pulse transformer primary during the transfer of energy. If the mass is too little, the excess circuit energy will maintain conduction until it is disposed of, either at very high voltage or by arcing due to cumulative breakdown of the metal vapour. If the mass is too great, not all the fuse will disappear and conducting traces may maintain a low resistance for too long. From the previous discussion we can appreciate that this simple concept is most applicable when the deposition of energy is very fast, otherwise vapourization and arcing will develop at individual sections of the fuse instead of rapid vapourization causing all the atoms to separate virtually instantly.

Maisonnier and others [11] applied this concept to calculate the dimensions of fuses in a capacitor-inductor oscillatory circuit. The writer adapted the method to the pulse transformer circuit, (Section 9.6), and calculated the dimensions of foil fuses. The energies in the pulse transformer experiments were so small though, that the fuses were too short ( $\approx 10$  mm) to withstand the arc voltages, and arcs which could not be quenched until all the primary energy had dissipated, were established.

By experiment it was found that fine copper wires in parallel, and tightly bound, worked well [8] (Fig. 119).

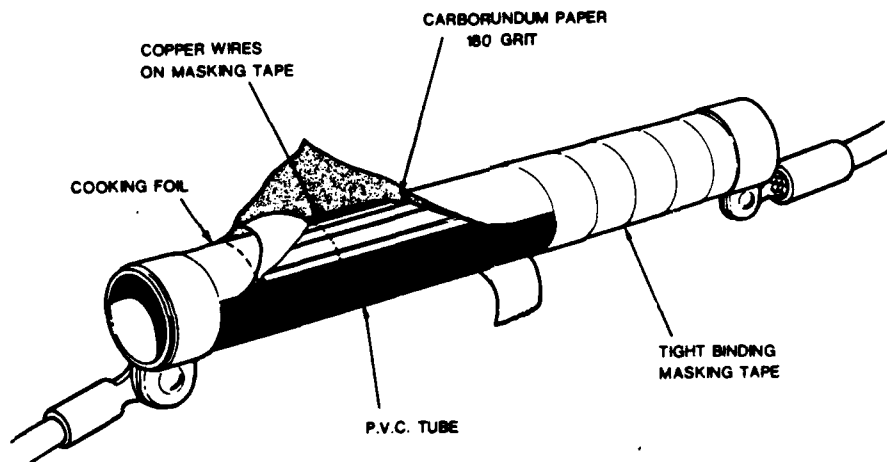


Fig. 119 Fuse used successfully in pulse transformer experiments.

The idea of using parallel wires is that one wire will rupture before the others, causing its current to be transferred to the remaining wires which will successively rupture with greater rapidity. An important advantage of parallel wires is that it enables the fuse resistance to be kept low enough to not affect the charging of the primary, except when it is near to rupture. The number of wires can be selected so that the last wire to break does so at an energy density which produces a high density, high resistance vapour.

The purpose of the carborundum paper was to provide a sand like matrix into which the vapour would disperse, while the tight binding was to eliminate air and to maintain the vapour in a high pressure state. That the tight binding was necessary was demonstrated when sometimes the binding over the terminations of the wires was not tight enough. A large flame would appear and burn through the bindings at that spot and the transformer current transfer was markedly degraded.

The writers used 2 to 4 bare copper wires, 0.0076" diameter, spaced about 5 mm apart and with an exposed length of 40 to 70 mm, in most experiments. The active part of each wire (the wires were actually 150 mm long, but the ends were covered with aluminium foil to control the active length) had a mass of 10 to 20 mg. Since the energy necessarily dissipated in the primaries was around 20J, the energy density in the final wire could be as much as 2kJ/gm, which is in the region of that necessary to cause a wire to "explode".

#### 9.5.4 Battery

The 40 Lucas batteries, which were intended as the battery pack for pulse transformer experiments, had deteriorated too much. After several weeks of effort to rejuvenate them by giving them the "water treatment" [12] it was clear that a new set was required. Fifty five 10 pair "Pulsar" batteries were accordingly purchased. Prior to obtaining these, the 8 Besco Marine Master batteries were used for pulse transformer tests.

The Pulsar battery pack can be seen in Fig. 118. The batteries were connected in series.

80 special connectors were devised and manufactured to suit the busbar terminals of the "Pulsar" batteries and to enable them to be easily connected in series and parallel. All exposed parts of these connectors were of plastic and covered the entire terminal, thus ensuring that the pack could not be accidentally shorted or cause electric shock by accidental contact. The connectors also functioned as switches.

#### 9.5.5 Current shunts

The primary current rises relatively slowly, then falls rapidly when the fuse operates. A 1 m $\Omega$  shunt, simply made from a 500 mm length of 8 B&S copper wire, folded into 4 sections and held closely together to minimize inductance, was initially used to measure primary currents (Fig. 120 (a)). Later a commercial parallel strip shunt was used.

The secondary current rises rapidly while the fuse operates and then falls slowly, with the time constant of the secondary circuit. More care was taken to design the secondary shunts so that the secondary current rise was properly recorded. Two 0.1 m $\Omega$  parallel strip shunts and a 0.5 m $\Omega$  disk shunt were constructed, (Fig. 120 (b), (c), for secondary current measurements.

The 0.1 m $\Omega$  parallel strip shunts were constructed from 0.25 mm thick copper sheet and the 0.5 m $\Omega$  disk shunt consisted of two disks of 22 SWG (0.7 mm thick) stainless steel, 3.1" diameter, with a 3/4" centre hole, in series. 47 ohm resistors were used to match the shunts to coaxial cable. Fig. 120 (c) shows the disk shunt with coaxial copper tubes as leads. The inner tube is shorted to the outer at one end to form a loop in a calibration check with a Rogowski belt.

As was discussed in Ch. 2, current is not distributed uniformly throughout the available metal if it arises sufficiently quickly, and the impedance of the path is different from the D.C. resistance. It was suggested, however, that the current actually flows at all times such that the total opposition, i.e. the impedance, is least. Then, if the geometry is such that at a certain frequency the inductive reactance is much less than the resistance no matter how the current is distributed, the minimum opposition must be controlled mostly by the resistance component. In this case the minimum will occur when the current is uniformly distributed. This situation will be enhanced by the fact that it is actually the internal inductance, which is less than the total inductance, that is connected with current distribution.

A simple rule for shunt design, therefore, is to ensure that its D.C. resistance is much greater than its inductive reactance at the highest frequency component of interest. Knoepfel [13] indicates this, but without the above justification.

The parallel strip shunt has virtually no space between the strips. There is therefore virtually no external flux and the only flux is internal flux. A simple estimate of the maximum inductance of the strip shunt in Fig. 120 is 0.5 nH. The frequency at which the inductive reactance is 0.1 m $\Omega$  is 32 kHz. On the basis of the above theory, the shunt impedance is its D.C. resistance to within about 5% up to 3.2 kHz, or for pulses with about 100  $\mu$ s rise time.



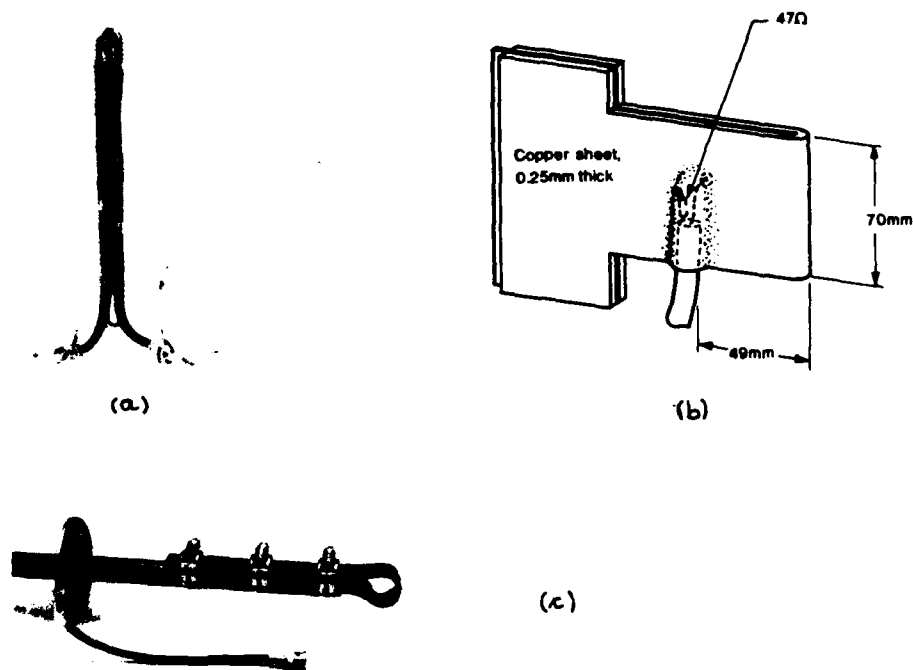


Fig. 120 Current Shunts

- (a) 1 mΩ, primary currents
- (b) 0.1 mΩ, parallel strip shunt, secondary currents
- (c) 0.5 mΩ, disk shunt, secondary currents.

The shunts were calibrated at D.C. by passing a current of 10A through them, in series with standard 1 mΩ and 0.1 mΩ shunts and finding points on the shunts being calibrated that gave the same voltage as across the standards (Fig. 121). The shunts were accurate at D.C. to within  $\pm 1/2\%$ .

The parallel strip shunts were clamped and bound to withstand magnetic forces. (The secondary current of the large transformer blew its shunt into a balloon shape when this was not done.)



Fig. 121 Calibration of shunts by comparison with voltage across standard shunt.

## 9.6 Calculations and derivations

### 9.6.1 1.5 $\mu$ H test inductor

A known inductor of around 1  $\mu$ H was constructed to readily verify the accuracy of the various inductance measuring means. The coil, shown in Fig. 122, had the following geometry:

Overall length (l):	24 mm
Mean diameter (D):	29 mm
Wire diameter (d):	2.5 mm
No. of turns (N):	9

The inductance was calculated using Nagaoka's equation with corrections to take account of wires instead of uniform surface current, as set out by Rosa and Grover [14].

From Table XXI of Rosa and Grover, Nagaoka's factor, K, for a diameter to length ratio of  $\frac{29}{24} = 1.208$ , is .64601772. The uniform surface current inductance is given by:

$$L_s = \frac{KN^2 \mu_0 \pi D^2}{4l} = 1.8097 \mu\text{H}$$

The low frequency inductance for the coil of solid round wires is

$$L = L_g - \Delta L,$$

where  $\Delta L = 4\pi n^2(A + B)$  nH where A and B are given in terms of  $d/D$  by Rosa and Grover, p 122 and Tables VII and VIII, yielding  $\Delta L = 246.9$  nH and hence  $L = 1.5628 \mu\text{H}$ .

Finally, we correct for the internal inductance of the wire to obtain the high frequency inductance, at the rate of  $\frac{\mu_0}{8\pi} = 50$  nH/m. Since the wire is 0.82 m long, the internal inductance of uniformly distributed current is 41.0 nH, yielding the calculated high frequency inductance of the test coil to be  $1.522 \mu\text{H}$ .

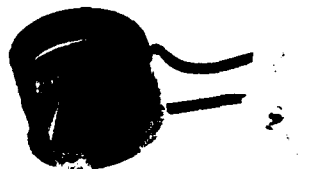


Fig. 122 9 turn calculated test inductor.

### 9.6.2 Phase plane plotting

The circuit for phase plane plotting is given in Fig. 123.

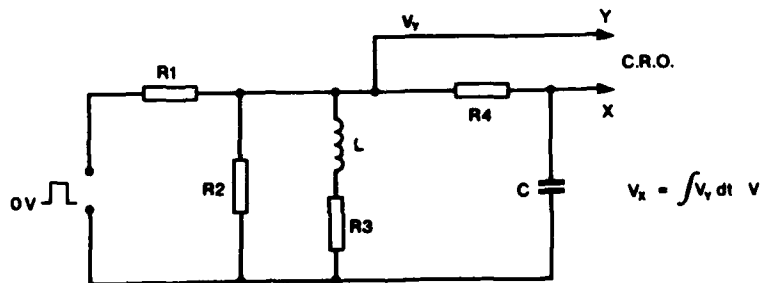


Fig. 123 Phase plane plotting circuit.

The inductor under test is  $L$  and  $R_3$  is its resistance.  $R_1$  and  $R_2$  form a low internal resistance voltage source and  $R_4$  and  $C$  form an integrator. Assuming that the inductor resistance,  $R_3$ , is negligible, the voltage across the inductor,  $V_Y$ , is:

$$V_Y = V \frac{R_2}{R_1 + R_2} e^{-\frac{R_1 R_2}{R_1 + R_2} \frac{t}{L}} \quad (9.1)$$

Assuming that the simple integrator places no load on the inductor circuit and that its time constant is sufficiently long,

$$V_X = \frac{r_L}{r_I} V \frac{R_2}{R_1 + R_2} - \frac{r_L}{r_I} V_Y, \quad (9.2)$$

where  $r_L = L \frac{R_1 + R_2}{R_1 R_2}$  and  $r_I = R_4 C$ .  $R_1$  includes the internal resistance of the pulse source.

A plot of  $V_Y$  against  $V_X$  is a straight line graph (Fig 124).

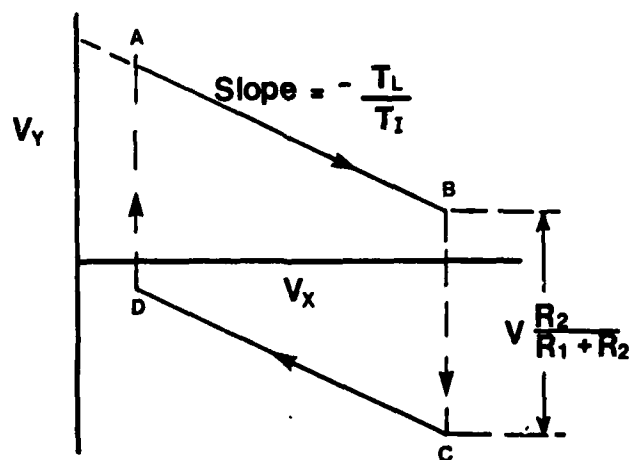


Fig 124 Phase plane plot from circuit of Fig. 123.

Line AB is drawn during the pulse "on" period and line CD is drawn during the "off" period. The horizontal and vertical displacements from the X and Y axes depend on the "on" and "off" periods relative to  $\tau_L$ . If these periods are several time constants long,  $V_Y$  and  $V_X$  become zero and point B is on the X axis and point D is at 0,0. The arrows indicate the direction in which the lines are plotted.

Since the slope of lines AB, CD is  $\frac{\tau_L}{\tau_I}$ , we have:

$$\tau_L = \tau_I \frac{\Delta V_X}{\Delta V_Y} \quad (9.3)$$

or 
$$L = \frac{R_1 R_2}{R_1 + R_2} \cdot R_4 C \frac{\Delta V_X}{\Delta V_Y} \quad (9.4)$$

where  $\frac{\Delta V_X}{\Delta V_Y}$  is measured from AB or CD.

Five factors that need to be ensured to obtain good measurements of microhenry inductors by this method are as follows.

- (i) The phase plane plot is substantially plotted in one inductor time constant. Since resistor  $R_2$  has to be of the order of ohms, the time constant using microhenry inductors is less than a microsecond. To obtain displays several centimetres long, the oscilloscope must have X and Y bandwidths of many megahertz.
- (ii) The pulse generator must be capable of high pulse current to enable  $R_2$  to be as low as possible while still presenting to the circuit a voltage that will produce several millivolts at the integrator output. The rise time of the pulse generator must be fast compared to the inductor circuit time constant.
- (iii) It is necessary to accurately know the values of  $R_1, R_2, R_4$  and C at the frequency representative of the test.
- (iv) For sub microhenry inductors the circuit must be mounted on a ground plane with great care given to attaching CRO leads. Since the voltage V is necessarily selected as high as possible, a ground plane shield must be used to isolate the integrator from direct feed through of pulse generator signal.
- (v) The resistance,  $R_3$ , of the inductor itself must be negligible, otherwise  $V_Y$  and  $V_X$  will contain components due to the voltage across it as well due to the inductor. The effect of  $R_3$  is found by the following analysis.

If  $V_Y'$  and  $V_X'$  are the values of  $V_Y$  and  $V_X$  when  $R_3$  is included, circuit analysis yields:

$$V_Y' = \frac{V}{1+k} \frac{R_2}{R_1 + R_2} [k + e^{-(1+k)n}], \quad (9.5)$$

$$\text{and } V_X' = \frac{V}{1+k} \frac{L}{R_1 R_4 C} [nk + \frac{1}{1+k} (1 - e^{-(1+k)n})] \quad (9.6)$$

where  $k = \frac{R_3}{\frac{R_1 R_2}{R_1 + R_2}}$  i.e. the ratio of  $R_3$  to the Thevenin resistance of the voltage source viewed from the inductor, and

$$n = \frac{t}{\tau_L} \text{ where } \tau_L = \frac{R_1 + R_2}{R_1 R_2},$$

and  $t$  is the pulse "on" time, i.e.  $n$  is the number of inductor circuit time constants neglecting  $R_3$ .

Putting  $k = 0$ , i.e.  $R_3 = 0$ , in Eqns. (9.5) and (9.6) yields  $V_Y$  and  $V_X$ , equivalent to Eqns. (9.1) and (9.2). By means of the ratios  $\frac{V_Y'}{V_Y}$  and  $\frac{V_X'}{V_X}$  the error due to  $k$  can be calculated in terms of  $n$ . The ratios are:

$$\frac{V_Y'}{V_Y} = \frac{1}{1+k} \left[ \frac{k + e^{-(1+k)n}}{e^{-n}} \right] \quad (9.7)$$

$$\frac{V_X'}{V_X} = \frac{1}{1+k} \left[ \frac{nk + \frac{1}{1+k} (1 - e^{-(1+k)n})}{1 - e^{-n}} \right] \quad (9.8)$$

Evaluation of Eqns. (9.7) and (9.8) for some values of  $k$  and  $n$  is shown below. From the tabulation it can be seen that the integral ( $V_X'$ ) values are

k	n	$\frac{V'_Y}{V_Y}$	$\frac{V'_X}{V_X}$
0.1	3	2.5	1.125
	1	1.07	1.016
0.05	3	1.776	1.064
	1	1.035	1.008
0.02	3	1.317	1.026
	1	1.014	1.003
0.01	3	1.160	1.013
	1	1.007	1.002

affected much less than the  $V'_Y$  values and that the pulse "on" period, measured by  $n$ , should not exceed about one inductor circuit time constant and that  $R_3$ , measured by  $k$ , should not be greater than about 0.02 of  $R_2$ , for  $V'_Y$  and  $V'_X$  errors to be only a few percent.

### 9.6.3 Maximum length and frequency for rail measurements

We wish to calculate the error, due to transmission line behaviour, of taking the impedance of a shorted pair of rails to be due to lumped inductance.

In texts [15] it is shown that the impedance,  $Z$ , of a shorted transmission line is:

$$Z = Z_0 \tanh \gamma l \quad (9.9a)$$

where  $Z_0 = \sqrt{\frac{L}{C}}$  is the characteristic impedance,  $\gamma = j\omega\sqrt{LC}$ ,  $L$  and  $C$  are the inductance and capacitance per unit length and  $l$  is the length of the line.

Since  $\tanh x = j \tan x$ , and  $\omega\sqrt{LC} = \frac{\pi/2}{\lambda/4}$ , where  $\lambda$  is the wavelength, Eqn. (9.9a) may be written:

$$Z = j \sqrt{\frac{L}{C}} \tan \left[ \left( \frac{l}{\lambda/4} \right) \frac{\pi}{2} \right] \quad (9.9b)$$

If the rails behave as a lumped inductance we may also write:

$$X = j\omega L = j\sqrt{\frac{L}{C}} \omega \sqrt{LC} \ell = j\sqrt{\frac{L}{C}} \frac{\ell}{\lambda/4} \frac{\pi}{2}, \quad (9.10)$$

where X is the inductive reactance. The ratio of the impedance Z to the reactance X is:

$$\frac{Z}{X} = \frac{\tan \left[ \frac{\ell}{\lambda/4} \frac{\pi}{2} \right]}{\frac{\ell}{\lambda/4} \frac{\pi}{2}} \quad (9.11)$$

Evaluating Eqn. (9.11) yields the following:

$\frac{\ell}{\lambda/4}$	$\frac{Z}{X}$
0.01	1.00008
0.05	1.00206
0.10	1.008
0.20	1.034
0.25	1.055
0.333	1.103
0.50	1.273

The tabulation shows that the rails should not be more than about a fifth of a quarter of a wavelength long for the difference between Z and X to be 3% or less.

For 2 m long rails, the test frequency wavelength should not be less than 40 metres, which means that the test frequency should not be greater than 7.5 MHz.

#### 9.6.4 Degree of coupling of external field toroid with bifilar winding

The external field toroid described in Section 9.2.2 was wound with the primary and secondary conductors equally spaced, as in Fig. 125(b) instead of touching as in Fig. 125(a).



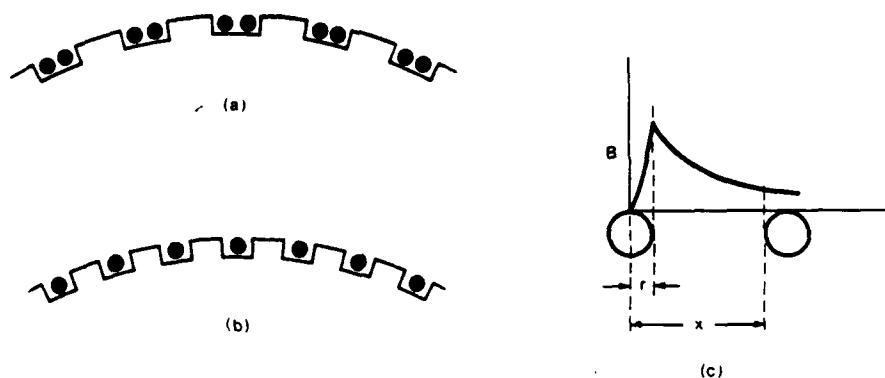


Fig. 125 Effect of conductor spacing, bifilar external field toroid

- (a) correctly placed bifilar conductors
- (b) equispaced conductors
- (c) uncoupled flux between conductors.

When the primary and secondary conductors touch, the uncoupled flux is virtually only the internal flux, as assumed in Section 6.2.3. When the conductors are spaced as in Fig. 125(b) the flux between them i.e. between distances  $r$  and  $x$ , Fig. 125(c) links only its own conductor and effectively increases its internal flux.

The uncoupled flux in the region from  $r$  to  $x$ ,  $\Delta\phi$  is:

$$\Delta\phi = \int_r^x \frac{\mu_0 I}{2\pi x} dx = \frac{\mu_0 I}{2\pi} \ln \frac{x}{r} \quad (9.12a)$$

where  $I$  is the conductor current. The increment in uncoupled inductance,  $\Delta L_u$ , is:

$$\Delta L_u = 0.2 \ln \frac{x}{r} \text{ H/m} \quad (9.12b)$$

The 94 turns of 2 mm dia wire were equispaced in accurately milled slots upon 100 mm dia. disks, yielding  $r = 1$  mm and  $x = 2.3$  mm and Eqn. (9.12b) yields  $\Delta L_u = 167$  nH/m.

To this must be added the internal flux of the conductor, ( $\frac{\mu_0}{8\pi} = 50$  nH/m), yielding a total uncoupled inductance of 217 nH/m. This value should be used in Eqn. (6.35) instead of  $\frac{\mu_0}{8\pi}$ . The result is  $k_{\max} = 0.9857$ . At high frequency there is no self inductance and the 167 nH/m value applies and  $k_{\max} = 0.9890$ .

In the tests the coils were excited with sine waves, therefore each winding has the same penetration and degree of coupling. The calculated coupling factors for the 47 turn windings as constructed are therefore, with sine wave excitation:

$$\begin{aligned} k_1 k_2 &= (0.9857)^2 = 0.9715 \text{ (full penetration)} \\ k_1 k_2 &= (0.989)^2 = 0.978 \text{ (zero penetration)} \end{aligned}$$

#### 9.6.5 Derivation of degree of coupling expression

Let  $L_1$  and  $L_2$  be the primary and secondary self inductances of a transformer, and let  $M$  be the mutual inductance. Let the secondary be shorted and the primary and secondary currents be  $i_1$  and  $i_2$  while the primary is connected to voltage  $V$  (Fig. 126).

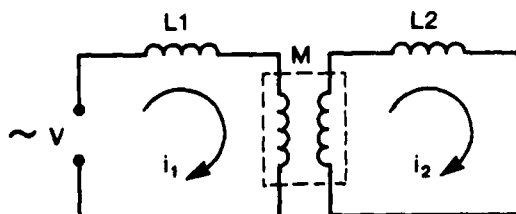


Fig. 126 Degree of coupling of windings.

Let the inductance as measured on the primary side with the secondary shorted be  $L_{1SC}$ . Then:

$$V = L_{1SC} \frac{di_1}{dt} = L_1 \frac{di_1}{dt} - M \frac{di_2}{dt}, \quad (9.13)$$

for the primary, and,

$$0 = L_2 \frac{di_2}{dt} - M \frac{di_1}{dt} \quad (9.14)$$

for the secondary. Substituting  $\frac{di_2}{dt} = \frac{M}{L_2} \frac{di_1}{dt}$  into Eqn. (9.13) yields:

$$L_{1SC} = L_1 - \frac{M^2}{L_2}, \quad (9.15)$$

$$\text{or} \quad L_{1SC} = L_1 (1 - k_1 k_2), \quad (9.16)$$

since  $M^2 = k_1 k_2 L_1 L_2$ . Rearranging (9.16) yields

$$k_1 k_2 = 1 - \frac{L_{1SC}}{L_1} \quad (9.17)$$

(Eqn. (9.16) was also obtained as the initial inductance during switching or charging with a closed secondary, in Ch. 5, where the effect of resistance was also included).

#### 9.6.6 Force reduction models

Firstly let us calculate the horizontal force caused by a sag of 1 cm in the wires of the straight wire model. With reference to Fig. 94, Ch. 8, the horizontal force,  $H$ , in a wire that sags distance  $f$  is

$$H = \frac{q l^2}{8f}. \quad (8.22)$$

where  $q$  is the load per unit length of the wire and  $l$  is the distance between its supports. The load  $q$  is the pinch force i.e.

$$q = \frac{\mu_0 N I^2}{4\pi a} \quad (8.20)$$

where  $N$  is the number of wires,  $I$  is the current in each wire and  $a$  is the radius of the cylinder of wires. Substituting in (8.22) we have:

$$H_T = \frac{\mu_0 N^2 I^2 \epsilon}{32 \pi a f} \quad (9.13)$$

For the model we have  $N = 20$  wires,  $\epsilon = 37$  cm and  $a = \frac{6.3}{2}$  cm. Let us select  $I = 100$  A in each wire and sag  $f = 1$  cm. Equation (9.13) yields  $H_T = 2.22$  kgf.

With the spring compressed to 2.22 kgf, so as to produce a tension force of this magnitude in the wires, and a current of 100 A per wire, we expect the sag to be 1 cm.

Secondly, let us check that the model with the 45° pitch, which results in each wire having 2 turns around the diameter, is force balanced.

The internal field is due to the total current that links the axis, i.e.  $NTI$ , where  $T$  is the number turns that each of the  $N$  wires makes about the axis. Over the central region this field has the value

$$B_I = \frac{\mu_0 NTI}{\epsilon}$$

and the force on a wire,  $F_I$ , is  $F_I = \frac{\mu_0 NTI^2}{2 \epsilon}$  N/m, radially outwards.

The external field is the same as that of the straight wire model (because a path taken around the outside links the same total current), hence the force given by Eqn. (8.20) acts radially inwards.

For zero net force we require

$$\frac{\mu_0 NI^2}{2} \left( \frac{1}{2 \pi a} - \frac{T}{\epsilon} \right) = 0$$

$$\text{i.e.} \quad T = \frac{1}{2 \pi a} \quad (9.19)$$

We have  $\epsilon = 40$  cm,  $a = \frac{6.3}{2}$  cm, and Eqn. (9.19) yields  $T = 2$  i.e. two turns are required, i.e. as constructed.

#### 9.6.7 Prime number of turns for primary of force reduced transformer

The problem with manufacturing a force reduced primary by joining the ends of wires laid on a straight former which is then bent into a circle is the same as the following.

Suppose we have a piece of flexible round rod upon which we rule  $Z$  equally spaced parallel lines (Fig. 127). Firstly, let us twist the rod so that the lines spiral around the rod an arbitrary number of times, including fractions of a revolution. Secondly, let us bend the rod into a circular shape so that the ends touch each other. Finally, we join the lines on one end to their nearest neighbour on the other end until only two free ends remain. What are the conditions under which the lines will always connect in series, so that if the lines were pipes, water could flow in at one end and not come out of another end until it has passed through all the pipes?

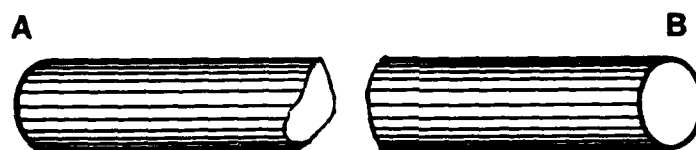


Fig. 127 Rod upon which  $Z$  lines are ruled.

Even though the twisting of the rod preserves the cyclic order of the lines, we cannot join them starting from any arbitrary combination. In general closed loops will arise before all the ends are joined. Consider say 8 lines as in Fig. 128(a) where the lines have a displacement of 6 positions after the twisting (drawn "opened out" for convenience). If we commence by joining 1 to 7 then we find 7 will join to 5, 5 to 3 and 3 back to line 1; thus we will have a closed loop before all lines have been joined. In Fig. 128(b) the displacement is 3 lines. If we now commence by joining 1 to 4 etc. we will have to join all the ends before forming a closed loop. In the following paragraphs we will show that only if the number of lines is a prime number can the lines be joined with any initial arbitrary displacement and result in all loops being connected in series.

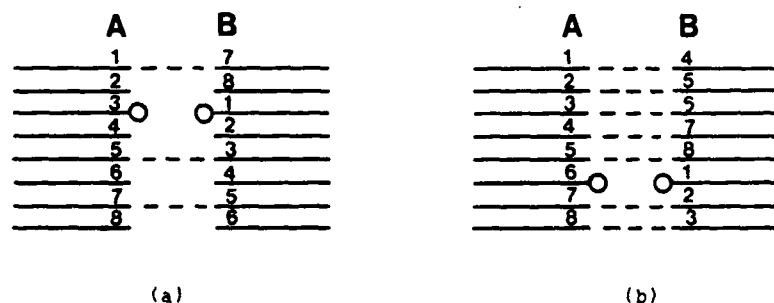


Fig. 128 Ends joined with displacements of (a), 6 and (b), 3.

Let the  $Z$  lines have their opposite ends displaced  $T$  positions where  $1 \leq T \leq Z - 1$ . The positions that the lines occupy are thus:

END A	END B
1	$1 + T$
2	$2 + T$
3	$3 + T$
$Z - T$	$Z$
$Z$	$Z + T$

Let  $N$  equal the number of joins we can make, in the fashion described in the previous section, before meeting the first line again. If all the ends except the last two are series connected we have:

$$N_{\max} = Z - 1 \quad (9.20)$$

After making the  $N$  joins we will be connected at end B, and hence also at end A, to line  $X$ , where:

$$X = 1 + NT. \quad (9.21)$$

Since the next join would be to line 1 at end B, which is displaced  $T$  positions from end A, we have:

$$X + T - KZ = 1, \quad (9.22)$$

where  $K$  is the number of times that we have skipped line  $Z$  in the joining process.

From (9.21) and (9.22) we obtain:

$$N = \frac{KZ}{T} - 1 \quad (9.23)$$

in order to form a closed loop after  $N$  joins.

Since  $N$  must be an integer it follows that closed loops will occur whenever  $\frac{KZ}{T}$  is an integer. If  $Z$  and  $T$  have a common factor, say  $M$ , then for:

$$K = T/M, 2T/M, 3T/M \quad (9.24)$$

there will be closed loops.

If  $Z$  has no common factor with  $T$  in the range  $1 \leq T \leq Z - 1$  i.e. if  $Z$  is a prime number, then in order that  $\frac{KZ}{T}$  be an integer we must have:

$$K = T \text{ for } 1 \leq T \leq Z - 1 \quad (9.25)$$

Substituting this in (9.23) we obtain:

$$\begin{aligned} N &= Z - 1 \\ \text{i.e. } N &= N_{\max} \end{aligned} \quad (9.26)$$

i.e. the condition for all loops to be joined in one series connection, (Eqn. (9.20)) for any displacement, is that the number of lines be a prime number.

For the original example, with  $Z = 8$ , displacements of 2, 4 and 6 have common factors with 8, and so the theory predicts closed loops for:

$$K = 1, 1, 3 \text{ passes of line } 8$$

and for  $N = 3, 1, 3$  joins before producing a closed loop.

We can check these by writing out the connection sequences.

$$\begin{aligned} T = 2; & \quad 1, 3, 5, 7, 1 \text{ i.e. } K = 1, N = 3 \\ T = 4; & \quad 1, 5, 1 \text{ i.e. } K = 1, N = 1 \\ T = 6; & \quad 1, 7, 5, 3, 1 \text{ i.e. } K = 3, N = 3 \end{aligned}$$

i.e.  $K$  and  $N$  are as predicted.

For displacement of 1, 3, 5 and 6 we expect that all conductors will be joined before a closed loop is produced, i.e.  $N = 7$ , and that  $K = 1, 3, 5, 7$  also. Writing out the actual connection sequences we find

$$\begin{aligned} T = 1; & \quad 1, 3, 4, 5, 6, 7, 1 \text{ i.e. } K = 1, N = 7 \\ T = 3; & \quad 1, 4, 7, 2, 5, 8, 3, 6, 1 \text{ i.e. } K = 3, N = 7 \\ T = 5; & \quad 1, 6, 3, 8, 5, 2, 7, 4, 1 \text{ i.e. } K = 5, N = 7 \\ T = 7; & \quad 1, 8, 7, 6, 5, 4, 3, 2, 1 \text{ i.e. } K = 7, N = 7 \end{aligned}$$

Again  $K$  and  $N$  are as predicted.

### 9.6.8 Fuse dimensions

We use the same principles as Maisonnier et al [11], that were referred to previously, but for the current waveform of the transformer primary while it is being charged, instead of that of an LC circuit.

The heating of the fuse to boiling point is to be due to the charging current and the vapourization energy is to be the part of the stored energy which cannot be transferred to the secondary. Since the time to raise the fuse temperature to boiling point depends on its cross section and not its length and the energy needed to vapourize it depends on its mass i.e. its length as well as cross section, the two stages can be separated, in principle. Note that we assume that the current is uniformly distributed through the fuse cross section.

The transformer charging current,  $I$ , is:

$$I = \frac{V_C}{R_C} \left( 1 - e^{-\frac{t}{T_0}} \right) \quad (9.27)$$

where  $V_C$  is the battery voltage,  $R_C$  is the circuit resistance and  $T_0$  is the circuit time constant, assuming that the fuse resistance is negligible up to the boiling point.

The energy supplied to the fuse in time  $\Delta t$  equals its heat energy increase, assuming the heating is sufficiently fast, i.e.:

$$I^2 \rho \left( \frac{l}{A} \right) \Delta t = mc \Delta T \quad (9.28)$$

where  $\rho$  is the resistivity,  $m$  is the mass,  $c$  is the specific heat,  $\Delta T$  is the temperature increment,  $l$  is the length and  $A$  is the cross section of the fuse. The mass  $m$  may be written as  $l A \gamma$ , where  $\gamma$  is the density of the fuse material, yielding:

$$\left( \frac{V_C}{AR_C} \right)^2 \left[ 1 - 2e^{-\frac{t}{T_0}} + e^{-\frac{2t}{T_0}} \right] dt = \frac{lC}{\rho} dT, \quad (9.29)$$

where  $\rho$  has been placed on the right hand side since it is a function of temperature.

We have found that the primary should be charged for about 1 time constant, i.e.  $t = T_0$ . Eqn. (9.29) then becomes, after integrating:



$$0.169 \left( \frac{V_C}{AR_C} \right)^2 T_0 = \gamma \int_{\text{Room Temp}}^{\text{Boiling Temp}} \frac{C}{\rho} dT \quad (9.30)$$

The value of the right hand side has been empirically calculated. For aluminium, its value is approximately  $1 \times 10^{17}$  MKS units [11]. Substituting into Eqn. (9.30) yields, for the cross section of an aluminium fuse:

$$A = 1.3 \times 10^{-9} \frac{V_C}{R_C} \sqrt{T_0} \text{ m}^2 \quad (9.31)$$

As an example, the first transformer circuit constructed had a primary circuit resistance of 189 mΩ, a primary circuit time constant of 5.9 ms and was used with a battery of 100V. Eqn. (9.31) yields a fuse cross section of about 0.05 sq mm. Aluminium cooking foil has a thickness of about  $\frac{1}{40}$  mm, so the width of a foil fuse should be 2.1 mm.

The stored energy of the primary after one time constant was approximately 100 joules and the calculated value of  $k_1 k_2$  was 0.82, hence the energy allocated to vapourize the fuse is 18 joules.

If  $W$  is the energy available for the vapourization and  $E_V$  is the vapourization energy per kilogram under the given conditions,

$$W = l A \gamma E_V$$

$$\text{or } l = \frac{W}{A(\gamma E_V)} \quad (9.32)$$

For aluminium, the value of  $\frac{1}{\gamma E_V}$  is given as  $3.5 \times 10^{-11}$  MKS units [11].

Substituting the values  $W$  and  $A$  for the example into equation (9.32), we obtain 12 mm for the length of the aluminium foil fuse.

## CHAPTER 10

### EXPERIMENT RESULTS

#### 10.1 Rail inductance measurements

##### 10.1.1 Rectangular rails results

The results of measurements made upon the rectangular rails listed in Section 9.1.2 at 10 KHZ are tabulated below.

W/H	S/H	L, Measured ( $\pm 2\%$ )	L, Calculated Kerrisk eqns.	L, Calculated Unif. Surf. Curr.
Approx	0.2	0.21 $\mu\text{H/m}$	0.195 $\mu\text{H/m}$	0.202 $\mu\text{H/m}$
zero	0.5	0.39	0.382	0.407
(0.028)	1.0	0.59	0.583	0.628
	2.0	0.84	0.825	0.885
	5.0	1.20	1.185	1.245
0.2	0.5	0.39	0.358	0.376
	1.0	0.56	0.536	0.556
0.5	0.2	0.22	0.170	0.253
	0.5	0.35	0.327	0.371
	1.0	0.53	0.500	0.517
	2.0	0.72	0.699	0.712
	5.0	1.04	1.007	1.023
1.0	0.5	0.32	0.303	0.380
	1.0	0.47	0.456	0.494
	2.0	0.65	0.640	0.656
	5.0	0.93	0.921	0.933

The calculated values were obtained using Eqns. (2.52) for the minimum inductance (Kerrisk's equations) and Eqn. (2.50) for the total inductance due to a uniform surface current (derived in Ch. 2).

The measured values generally fall between the two calculated values, which is to be expected as the current penetration is about 0.7 mm at 10 kHz. The general agreement between the measured and calculated values suggests that Eqns. (2.52) and (2.50) are correct.

The results for  $W/H \approx 0$  are particularly interesting. At 10 kHz the nominal penetration depth is 0.7 mm, and since the copper sheet used for the rails was 0.7 mm thick (i.e.  $W = 0.7$  mm) it might be concluded that the current was virtually uniformly distributed, particularly at the surface. The inductance values measured though are much closer to the minimum values than to the uniform surface current values. This suggests that diffusion normal to the surface occurs in preference to sideways diffusion, and that the current distribution remains similar to the initial distribution.

In the cases of the wider rails and with  $S/H \geq 1$ , the inductance values are closer to the uniform surface current values, which suggests that sideways diffusion played a more significant role.

The conditions of the above measurements are different to those in the railgun (e.g. the test current had a maximum value of 100 mA). As discussed in Ch. 2 the high current and arcing may affect the current distribution.

The ribbon cable rails (Fig. 129) approximate the model in Fig. 10, Ch. 2, with 20 filaments. The measured inductance was:

(i)	10 kHz	0.63 $\mu$ H/m	(Videobridge, Marconi)
(ii)	3.5 MHz	0.64 $\mu$ H/m	(Meguro Denpa)
(iii)	0.5 $\mu$ s pulse	0.66 $\mu$ H/m.	(Phase plane method)

The theoretical values with which to compare the results are 0.58  $\mu$ H/m for the minimum inductance distribution and 0.628  $\mu$ H/m for equal current in each filament. The results suggest the latter distribution. In Ref. 2 Ch. 9 it is clearly demonstrated that alternating currents in parallel filaments should not be equal. The outer filaments should carry more current as in the minimum inductance distribution. The only explanation that the writer can offer for the above result is that the space between the filaments reduces the interaction between them. This result is an indication that it may be possible to increase the propelling inductance by using parallel filamentary rails in practice.



Fig. 129 Ribbon cable rails

### 10.1.3 Test inductor

The 9 turn test inductor (Fig. 122) had calculated inductances of 1.56  $\mu$ H and 1.52  $\mu$ H at low and high frequencies respectively. At 10 kHz the measured values were:

Videobridge: 1.54  $\mu$ H  
Marconi Bridge: 1.56  $\mu$ H

At 10 kHz the depth of penetration, 0.7 mm, means that the current occupies about 3/4 of the wire area (wire dia = 2.5 mm), and we could therefore expect a measured value of 1.55  $\mu$ H. The Videobridge has given a slightly low value while Marconi Bridge has given a slightly high value.

### 10.1.4 Phase plane method

The phase plane circuit (Fig. 123) was constructed with the following values:

$R_1 = 50 \Omega$  (plus output resistance of pulse generator)  
 $R_2 = 2.5 \Omega$   
 $R_4 = 470 \Omega$   
 $C = 10 \text{ nF}$ .

These values yield a design that is suitable for measuring inductances in the range 20 nH to 2  $\mu$ H. A Hewlett Packard pulse generator (Model 8012 B), set to 50  $\Omega$  output resistance, was used to supply pulses, typically 0.5  $\mu$ s wide with 5 ns rise and fall times and 10 V open circuit amplitude. A Tektronix Model 2215 60 MHz oscilloscope was used for the X-Y display.

The circuit was calibrated using the test coil, which, during the 0.5  $\mu$ s wide pulse, should have an inductance of 1.52  $\mu$ H. The calibration yielded the inductance expression to be:

$$L = 12.023 \frac{\Delta V_X}{\Delta V_Y} - .048 \mu\text{H}.$$

Various rails were connected to the circuit and the above expression yielded values that were always within a few percent of those in tabulated in Section 10.1.1. Figs. 130 (a) and (b) show the phase plane plots obtained for the thin sheet rails ( $W/H \approx 0$ ) set to  $S/H = 1$ . The entire plot is shown in Fig. 130(a) and an expanded portion is shown in Fig. 130(b).



Fig. 130. Phase plane plot from thin sheet rails

- (a) whole plot,  $X = 2 \text{ mV/Div}$ ,  $Y = 50 \text{ mV/Div}$   
 (b) upper slope expanded,  $X = 2 \text{ mV/Div}$ ,  $Y = 10 \text{ mV/Div}$ .

From the expanded plot we obtain:

$$\Delta V_X = 6 \text{ mV}, \Delta V_Y = 63 \text{ mV}.$$

Substituting in the inductance expression yields  $L = 1.097 \mu\text{H}$ . The rails were 1.80 m long, so we obtain  $0.61 \mu\text{H/m}$ , which compares quite well with  $0.59 \mu\text{H/m}$  obtained using 10 kHz sine waves.

As indicated in Ch. 9, the major reason for developing the method was to verify that the inductance measured by high frequency sine wave methods is the same as that when a voltage pulse is suddenly applied. The lines plotted were always perfectly straight during the time that the pulse was flat topped (i.e. once the slight initial overshoot had subsided). From the results it was evident that the inductance values were constant and close to those given by Kerrisk's equation and were attained within 20 ns of the application of the voltage pulse.

## 10.2 Degree of coupling

### 10.2.1 Long solenoid with shorter layer secondaries

The theory in Section 6.2.1 enables ratio of the coupling factors to be written as:

$$\frac{k_2}{k_1} = \frac{K_1}{K_2} \frac{l_2}{l_1} \frac{A_1}{A_2},$$

where  $k$  is the coupling factor,  $K$  is Nagaoka's factor,  $l$  is the length of the winding,  $A$  is the cross-sectional area and subscripts 1 and 2 refer to the primary and secondary respectively.

If  $k_1$  is unity, as suggested in Ch. 6 for a long solenoid, the above expression also gives the value of  $k_1 k_2$ . The model (Fig. 103) enables 3 tests to be made, viz. for  $\frac{l_2}{l_1} = 0.2, 0.5$  and  $0.7$ .

The mean diameters of the windings were 26 mm and 27 mm and hence  $\frac{A_1}{A_2} = \left(\frac{26}{27}\right)^2 = 0.9273$ . Using the tabulation in Rosa and Grover (Ref. 14 Ch. 9),  $K_1^2$  and  $K_2$  were found to be

Primary, 252 mm, dia/length = 0.1,	$K_1 = 0.959$
Secondary, 51 mm,	0.54, $K_2 = 0.818$
126 mm,	0.216, 0.920
177 mm,	0.153, 0.942

The 177 mm secondary = 51 mm + 126 mm windings in series.

Using the above values in the expression for  $\frac{k_2}{k_1}$  yields:

$\frac{l_2}{l_1}$	$\frac{k_2}{k_1}$
0.2	0.217
0.5	0.483
0.7	0.661

#### Measured values of $k_1 k_2$

The open circuit/short circuit method described in Section 9.6.4 gave the following results at 10 kHz.

$\frac{t_2}{t_1}$	$L_1$	$L_{1SC}$	$k_1 k_2 = 1 - \frac{L_1}{L_{1SC}}$
0.2	207 $\mu$ H	161 $\mu$ H	0.22
0.5	207	108	0.48
0.7	207	71	0.66

The agreement between the calculated and measured values of  $k_1 k_2$  is remarkably good and indicates that  $k_1 = 1$  very closely, as was suggested in Ch. 6. It can also be seen that the  $k_1 k_2$  values are close to the  $t_2/t_1$  values, which confirms the example in Ch. 6 where both windings were considered to be long, so that  $K_1 = K_2 = 1$ , and of virtually the same diameter, so that  $A_1 = A_2$ .

At lower frequencies the agreement was poor; e.g. at 1 kHz  $k_1 k_2 = 0.34$  for  $t_2/t_1 = 0.5$ . The low Q of the secondary at 1 kHz is assumed to be the cause.

#### 10.2.2 Short solenoids with thin sheet secondaries

It was postulated in Ch. 6 that, when the secondary is a sheet of negligible thickness compared to the diameter of the primary conductors, the current in the primary effectively flows as a sheet located 1/3 of the wire diameter from the inside when the secondary is on the inside and as a sheet located at the middle of the conductor diameter when the secondary is on the outside.

From the data for the two test solenoids, viz.

- (i) 160 mm dia former, 84 turns of 0.87 mm dia. wire, thin sheet secondary of 0.12 mm thick copper; and
- (ii) 250 mm dia. former, 56 turns of 2.5 mm dia. wire, thin sheet secondary of 0.7 mm thick copper,

the calculated values of  $\frac{k_2}{k_1}$  and  $\frac{k_1}{k_2}$  are:

<u>Coil</u>	<u>Secondary on inside</u>	<u>Secondary on outside</u>
160 mm	$\frac{k_1}{k_2} = \left(\frac{160.24}{160.82}\right)^2 = 0.993$	$\frac{k_2}{k_1} = \left(\frac{160.87}{161.74}\right)^2 = 0.989$
250 mm	$\frac{k_1}{k_2} = \left(\frac{251.4}{253.1}\right)^2 = 0.987$	$\frac{k_2}{k_1} = \left(\frac{252.5}{255}\right)^2 = 0.980$

The results of  $k_1 k_2$  measurements at 20 kHz were:

<u>Coil</u>	<u>Secondary on inside</u>	<u>Secondary on outside</u>
	$k_1 k_2$	$k_1 k_2$
160 mm	0.991	0.977
250 mm	0.979	0.972

The measured values of  $k_1 k_2$  are generally about 1% less than the  $k_1/k_2$  or  $k_2/k_1$  values. This is to be expected because the solenoids are short and the coupling of the inner to outer will not be sufficiently close to unity. Furthermore, the thickness of the copper sheets, particularly the 0.7 mm sheet, may not be negligible. Nevertheless, the results show that the simple ratio calculation is a useful guide to the value of  $k_1 k_2$ .

#### 10.2.3 Short solenoid with separate layer winding

The value of  $k_1 k_2$  to be expected in this case can be estimated using the tabulations based on Maxwell's mutual inductance expression for equal length coaxial solenoids in Section 6.2.1. The mean diameter of the inner winding was 111 mm and its overall length was 112 mm and hence the radius to length ratio ( $a/l$ ) was 0.5, and as the wire diameter was 1.2 mm the radius ratio ( $a/A$ ) was 0.99. Referring to the tabulations in Ch. 6 we find:

$$A/l = 1, k_1 k_2 = 0.9557$$

$$A/l = 0.1, k_1 k_2 = 0.9780.$$

Since we have  $A/l = 0.5$  we expect the measured value of  $k_1 k_2$  to be between the above values.

Measurement yielded the following results at 10 kHz and 20 kHz.

<u>Freq</u>	<u><math>L_1</math></u>	<u><math>L_{1SC}</math></u>	<u><math>k_1 k_2</math></u>
10 kHz	598 $\mu$ H	23.1 $\mu$ H	0.961
20 kHz	598 $\mu$ H	20.4 $\mu$ H	0.966

The results are clearly compatible with the values obtained from the tabulation.



#### 10.2.4 Short solenoid with 100 turn bifilar windings

In Ch. 6 it was anticipated that the axial displacement by one turn of the two windings would cause each coupling factor to have the value  $(\frac{N-1}{N})$ , where  $N$  is the number of turns, and hence  $k_1 k_2 = (\frac{N-1}{N})^2$ . For 100 turns we therefore anticipate  $k_1 k_2 = (0.99)^2 = 0.98$ .

The actual measured values for the 100 turn model at various frequencies are tabulated below.

Freq	$L_1$	$L_{1SC}$	$k_1 k_2$
100 Hz	1.363 mH	1026 $\mu$ H	0.247
200 Hz	1.363	589	0.568
500 Hz	1.363	162	0.881
1 kHz	1.363	57.8	0.958
10 kHz	1.357	19.6	0.986
20 kHz	1.346	16.8	0.988

The high frequency limit appears to be 0.99 rather than 0.98 and suggests that the bifilar solenoids are effectively displaced by half a turn instead of a full turn and that  $k_1 k_2$  is given by  $k_1 k_2 = (\frac{N-1/2}{N})^2$ .

The low values of  $k_1 k_2$  at low frequencies are considered to be due to energy dissipated in the secondary resistance because its time constant is too short compared to the sine wave period. In other terms, the  $Q$  is too low at low frequencies.

#### 10.2.5 Short solenoid with co-axial cable winding

The calculated value of  $\frac{k_1}{k_2}$  for this model is given by Eqn. 6.49 using the following measurements.

Dia. of inner, $d_1$	= 2.5 mm
Dia. of braid, $d_o$	= 4.0 mm
No of turns, $N$	= 40
Primary inductance, $L$	= 454 $\mu$ H
Radius of windings, $R$	= 162.5 mm

The value calculated is  $\frac{k_1}{k_2} = 0.987$  at low frequencies and 0.992 at high frequencies (no internal flux in primary). Since  $k_2$  is expected to be very nearly unity these values are also the expected values of  $k_1 k_2$ .

The measured values were as follows:

Freq	$L_1$	$L_{1SC}$	$k_1 k_2$
1 kHz	454 $\mu$ H	19 $\mu$ H	0.958
3 kHz	446 $\mu$ H	7.5 $\mu$ H	0.983
10 kHz	441 $\mu$ H	5.16 $\mu$ H	0.988
20 kHz	441 $\mu$ H	4.46 $\mu$ H	0.990

The measured values of  $k_1 k_2$  at high frequencies approach the calculated value of 0.992, confirming the proposition that  $k_2 = 1$ . The inductance and resistance of the braid were measured as 360 nH at 1 kHz and 330  $\mu\Omega$  at D.C. The secondary time constant was therefore about 1 ms and shows that a frequency of several kHz is necessary to ensure that resistive losses during each cycle are a small portion of the stored energy.

#### 10.2.6 Bifilar external field toroid

The calculated values of  $k_1 k_2$  for this model, set out in Ch. 9, were 0.9725 at low frequencies and 0.978 at high frequencies.

Measurement yielded the following values.

Freq	$L_1$	$L_{1SC}$	$k_1 k_2$
200 Hz	1.250 mH	120 $\mu$ H	0.904
1 kHz	1.246 mH	32.8 $\mu$ H	0.974
10 kHz	1.237 mH	29.5 $\mu$ H	0.976
20 kHz	1.235 mH	28.2 $\mu$ H	0.977

The high frequency values clearly approach the calculated value of 0.978 and confirm the calculation method. The low frequency discrepancy is again assumed to be due to resistance.

#### 10.2.7 Conclusions regarding degree of coupling experiments

The measured values of  $k_1 k_2$  confirm that the simple models used in Ch. 6 give useful estimates. They also show that in these models a frequency of 10 kHz is necessary to approach the calculated values.

#### 10.3 Force experiments

In Ch. 9 it was calculated that a current of 100 A in each of the wires of the external field toroid model should cause a deflection of about 1 cm with the spring set to produce a total tension of 2.22 kgf in the wires. The 45° pitch of the force reduced model should balance the magnetic forces so that when the same current is passed through it there is no deflection of the wires.

(i) External field toroid (parallel wires) model

The total tension was set to 2.2 kg.f (21.58 N) and a total current of 2,250 A was passed through the wires for about 1 second. The current was applied only briefly because the wires heated rapidly. The wires pinched inwards (Fig. 131). By closely observing the wires it was estimated that the deflection at the centre was to about 0.5 cm from the wooden spacers.

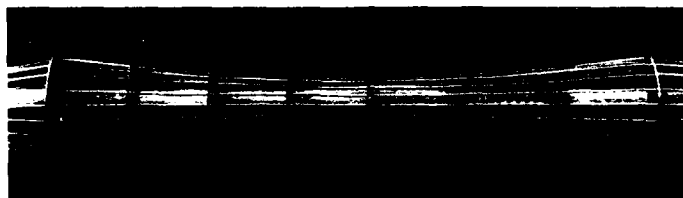


Fig. 131 Pinching of external field toroid model.

Since the pitch circle diameter of the wires was 6.3 cm and the spacers were 1" (2.54 cm) diameter (Fig. 108), the sag,  $f$ , was:

$$f = \frac{6.3}{2} - \frac{2.54}{2} - 0.5 = 1.38 \text{ cm}$$

Calculation, using Eqn. (9.18) with

$$H_T = 21.58 \text{ N}, \quad r = 0.37 \text{ m}, \quad NI = 2250 \text{ A}, \quad a = 3.15 \times 10^{-2} \text{ m},$$

yields  $f = 1.27 \text{ cm}$ , which confirms the observed sag and shows that the calculation methods in Ch. 8 are correct and adequate.

The calipers attached to one end of the model registered a movement of 1.7 mm against the compression spring when the wires pinched. Since the force was 2.2 kg.f the work done during the pinching was 3.74 kg.f. mm.

(ii) Force reduced model

The force reduced model used in the experiment is shown in Fig. 132. Figure 132(a) shows the construction in progress. The wires were pre-cut to the exact length and curled into  $2\frac{1}{2}$  turns. Each wire was threaded through the slots in the disks and naturally formed a  $45^\circ$  helix.

A force of about 100g could move the free end of the model about 3 cm. Since the work done by the magnetic forces on the straight model was 3.74 kg.f mm, the  $45^\circ$  winding should extend  $3.74/0.1 = 37$  mm if the same energy is available.

When the coil was pulsed with the same current as the straight wire model the end was observed to lengthen by only about 5 mm and to twist slightly. Virtually no radial movement of the wires was observed anywhere.

Since the 2.2 kg.f proven to be present in the straight wire model could easily deform the delicate structure of the force reduced model, it is concluded that such a force was not present, i.e. force balance was achieved by the  $45^\circ$  pitch winding.

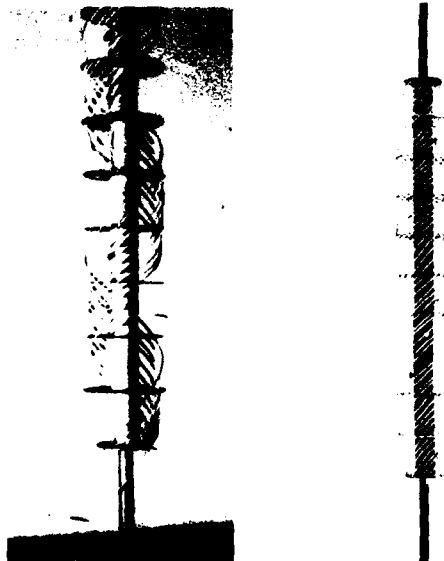


Fig. 132 Force reduced model: (a) during construction; (b) finished model.

#### 10.4 Internal resistance of batteries

Example recordings from the battery tests are given in Figs. 133 and 134. The voltage traces show the terminal voltage of the batteries during the tests. The fall in voltage from the initial value (12.5 V) divided by the current gives the effective internal resistance of the battery.

The recordings in Fig. 133 are from tests where a fuse was used. The fuse was a 15 cm length of 16 B & S tinned copper wire. These tests enable the internal ohmic resistance to be found under a heavy load condition, without the interference of polarization, since they are of short duration (< 1 second) and the fuse resistance increases rapidly from its initial low value.

The results of tests with the fuse replaced by a copper bar are shown in Fig. 134. These tests, up to 9 seconds duration, show the effect of polarization. According to the theory in Ch. 4 the decline of the current in such tests is due mainly to the generation of water at the positive electrode.

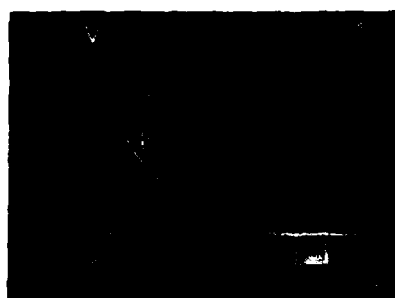
The batteries were probably between half and fully charged when tested, having been standing for periods of days to many months between charging and testing.

Using the fuse test oscillograms in Fig. 133 the following results are obtained.

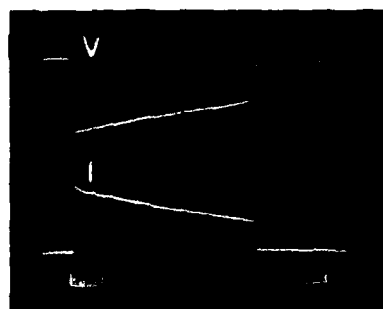
Battery	Mass	Current	Volt. Drop	Int Res	Initial Power Density
Pulsar	10 kg	1600 A	8 V	5 mΩ	720 W/kg
Torque Starter	14 kg	1600 A	8 V	5 mΩ	514 W/kg
Besco	22.2 kg	1100 A	9 V	8.2 mΩ	198 W/kg
Lucas	22.7 kg	1100 A	9 V	8.2 mΩ	193 W/kg

The superiority of the Pulsar and Torque Starter over the conventional batteries is evident. The internal resistance of these new style batteries increased during the discharge, though, whereas that of the Besco actually decreased.

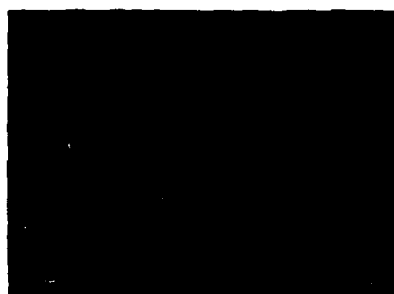
The short circuit tests using the copper bar give an idea of the time for which the batteries can supply maximum power. The Pulsar and the Torque Starter have the shortest time, about 1 second, while the more massive



(a) 10 pair Pulsar  
 $V = 4V/Div$ ;  $I = 400 A/Div$   
 $t = 0.4 \text{ sec}/Div$



(b) Torque Starter  
 $V = 4 V/Div$ ;  $I = 800 A/Div$   
 $t = 0.1 \text{ sec}/Div$

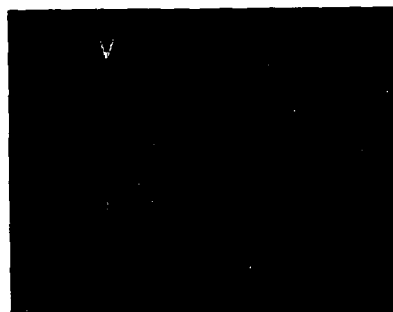


(c) Besco Marine Master  
 $V = 2 V/Div$ ;  $I = 400 A/Div$   
 $t = 0.2 \text{ sec}/Div$

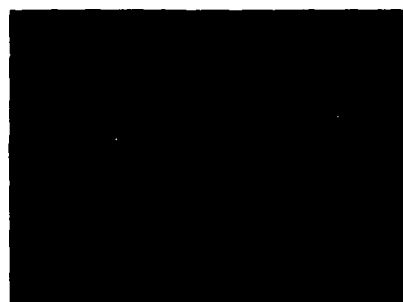


(d) Lucas 274 A  
 $V = 2 V/Div$ ;  $I = 400 A/Div$   
 $t = 0.2 \text{ sec}/Div$

Fig. 133 Battery voltage and current when short circuited through fuse consisting of 15 cm 16 B & S tinned copper wire.



(a) 10 pair Pulsar  
Recently charged  
 $t = 1 \text{ sec/Div}$



(b) 10 pair Pulsar  
Standing for 8 months  
 $t = 0.5 \text{ sec/Div}$



(c) Torque Starter  
Standing for 18 months  
 $t = 1 \text{ sec/Div}$



(d) Besco  
Recently charged  
 $t = 1 \text{ sec/Div}$

Fig. 134 Battery voltage and current when short circuited through copper bar.

Voltage = 4 V/Div, Current = 800 A/Div.

conventional batteries can maintain their lower maximum power for at least ten seconds.

Although the above results are typical, there was a wide variation in the results from batteries of the same type. The highest power density measured was 960 W/kg for about 1 second from a Pulsar 5 plate experimental battery supplied to the writer by the Dunlop-Olympic Company.

#### Hot battery tests

The results were, on the whole, inconclusive. Increases in short circuit current up to 50% were recorded at 60 C over the 20 C values, but the voltage drops across the batteries also increased, with the result that the internal resistance did not decrease to 2/3 of the value at 20 C. The best result was about 3/4 of the value of 20 C.

#### 10.5 Pulse transformer tests

The circuit for the model pulse transformer tests is shown in Fig. 135.

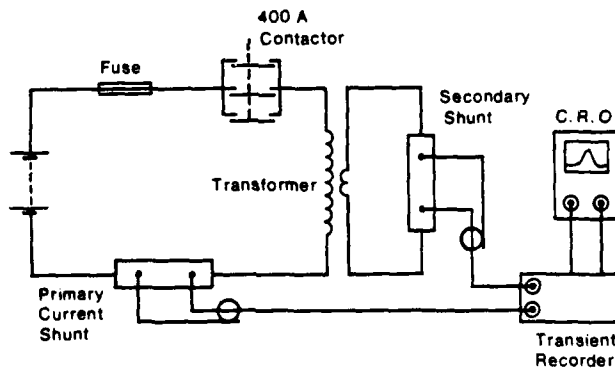


Fig. 135 Pulse transformer test circuit.

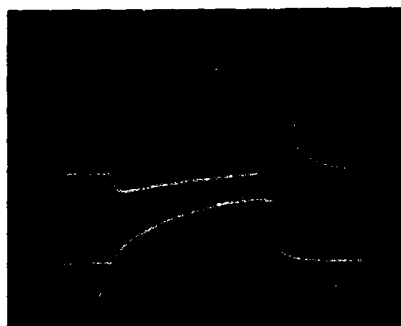
The experiments were conducted at room temperature. The secondaries of the transformers were short circuited directly via the current measuring shunts so as to reduce the uncoupled inductance of the transformers as much as possible. The transient recorders were either Datalab DL912 or Iwatsu Digital Memory DM-7100 systems according to availability. A Tektronix Model 466 oscilloscope was used for the displays.



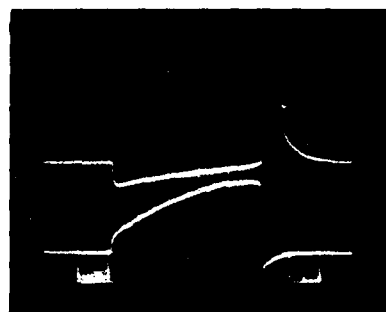
The open circuit/short circuit method was used to measure  $k_1 k_2$  of the transformers at 10 kHz.

The primary and secondary current traces from each of the four transformers are shown in Figs. 136 and 137. The performance of the transformers is summarized below.

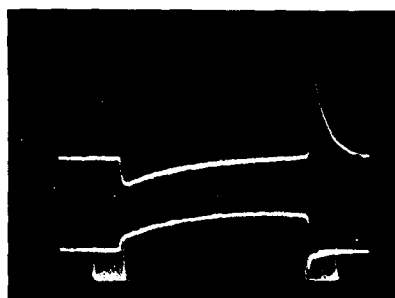
Transformer	Primary Turns	$k_1 k_2$ 10 kHz	Primary Current	Secondary Current	Effective $k_1 k_2$
Ext. F. Tor. R/a = 20 Int. solid secondary	24	0.76	400 A	5.2 kA	0.29
Ext. F. Tor. R/a = 20 Ext. sheet secondary	24	0.90	440 A	8 kA	0.57
Force reduced, bifilar, R/a = 5, R = 0.25 m.	47	0.87	200 A	7 kA	0.55
Force reduced, bifilar R/a = 5, R = 0.5 m.	43	0.89	900 A	30 kA	0.60



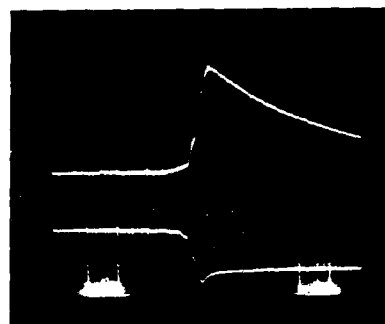
(a) Ext. F. Tor.  $R/a = 20$ ,  
24 Turns, Internal  
solid secondary.  $R = 0.5$  m



(b) Ext. F. Tor.,  $R/a = 20$ ,  
24 Turns, External  
sheet secondary.  $R = 0.5$  m



(c) Force reduced,  $R/a = 5$   
47 Turns, Bifilar  
secondary.  $R = 0.25$  m



(d) As for (c), traces  
expanded  $\times 10$ .

Fig. 136. Current waveforms - three small pulse transformers. Upper traces, secondary currents, 2 kA/Div; lower traces, primary currents, 200 A/Div. Time = 2 ms/Div., (a), (b), & (c); 0.2 ms/Div, (d). Battery = 98V.



(a) Complete wave forms.



(b) Current transfer detail.

Fig. 137 Current waveforms - 43 turn force reduced bifilar transformer,  $R/a = 5$ ,  $R = 0.5$  m. (a) Upper trace, secondary current, 10 kA/Div; lower trace, primary current 400 A/Div; time, 8 ms/Div. (b) Primary current fall (left), 200 A/Div; secondary current rise (right), 5 kA/Div; time, 0.5 ms/Div. Battery = 392 V.

The oscilloscope displays show that the transformers and fuses worked in general as expected. The coupling factors  $k_1 k_2$  however are considerably less than the values measured at 10 kHz. This is most probably because the fuse rupture times of 100-200  $\mu$ s were not fast enough. It must also be noted that these rise times are at the limit of the ability of the current shunts to record them properly.

The negative current in the secondary is due to transformer induction while the primary is being charged, as discussed in Ch. 5. In the three small transformers it becomes negligible by the time the fuse blows. The initial step in primary current during short circuit charging, also discussed in Ch. 5, can be clearly seen in Figs. 136 (b) and (c) and in Fig. 137 (a).

## CHAPTER 11

### SUMMARY, CONCLUSIONS AND FURTHER WORK

#### 11.1 Summary and conclusions

This Report has dealt with the "railgun" method of propelling masses, and the associated power source. This is a relatively new technology and, in order to define the important relationships among the many factors that interact, the investigations have been broadly based and exploratory.

Firstly, the railgun propulsion mechanism and its efficiency were studied. A quantity of energy, analogous to the "free energy" of a chemical reaction, was found to be released when the projectile movement changed the circuit inductance. Some or all of this "associated energy" becomes the kinetic energy of the projectile depending on the current distribution and the properties of the plasma or arc that carries the current. A factor, "f", was introduced to account for the loss of associated energy and the consequent reduction in force on the projectile. The effect of current distributions was studied by comparing the force on the projectile for minimum inductance, uniform surface and fully penetrated current distribution. In the final part of the railgun study efficiency expressions were developed and evaluated for three versions of the railgun, viz. breech supplied, segmented and distributed energy store railguns.

The main conclusions from the railgun study are as follows.

- (i) The plasma arc may be very inefficient in transmitting the electromagnetic forces to the projectile.
- (ii) The rails should be as thin as possible to minimize the energy loss due to current distribution, which, for example, could otherwise limit the railgun efficiency to 80%.
- (iii) The reduction in power source size achieved by segmented and distributed energy store railguns may not justify their complexity.
- (iv) Maximum railgun efficiencies are likely to be in the range 10% to 30%.

The second broad topic was a review of power sources for railguns. By considering the ratio of the muzzle energy to mass for powder guns a minimum energy density of 1 kJ/kg was set for railgun power sources. Capacitors, flywheel machines and explosive magnetic flux compression were critically reviewed with regard to the pulse energy delivered per unit mass and system complexity. A simple application of mechanics was used to obtain the minimum mass of any system that stores energy in kinetic form. Finally, in this review, the possibility of using batteries and a pulse transformer to charge the railgun inductor was described.

The main conclusions of the power source review are as follows.

- (i) Capacitors are unlikely to result in power sources with overall energy densities exceeding a few hundred J/kg unless dramatic breakthroughs are made in dielectric materials and construction methods.

Advanced homopolar generator systems may attain the target figure of 1 kJ/kg but cannot realize more than a small fraction of the energy density of the flywheels upon which they are based.

Single shot self destructing explosives based systems may attain several kJ/kg.

- (ii) The maximum pulse energy density of any system is not likely to exceed 10 kJ/kg.
- (iii) The battery and pulse transformer scheme is worth investigation because it appears to incorporate a prime energy store, and therefore give a multishot capability, with the same overall mass as single shot capacitor and homopolar generator systems.

The third broad topic was the detailed investigation of the battery and pulse transformer scheme. This was done in four main subsections:

- (i) general considerations,
- (ii) circuit analysis,
- (iii) transformer geometry,
- (iv) design and performance.

The general consideration included the pros and cons of the system, particularly in comparison with the essentially equivalent battery-inductor scheme. The maximum possible pulse energy densities of battery-coil systems were estimated on the basis of the coils being Brooks Coils. The battery and coil interact in determining the overall mass; the mass of the battery being reduced by taking longer to charge the coil, but the mass of the coil being increased to obtain correspondingly long time constants. System mass is dependent on the power available from the battery and this led to a detailed investigation of the power density of lead-acid batteries.

The main conclusions from this part of the work are as follows.

- (i) The low current of the pulse transformer is probably a major advantage as compared to the battery-inductor scheme.
- (ii) The pulse transformer must have a degree of coupling,  $k$ , of at least 0.995 on account of opening switch limitations.
- (iii) To obtain an overall pulse energy density of 1 kJ/kg from the pulse transformer system, liquid nitrogen cooled coils and batteries with a power density of at least 1 kW/kg are necessary.

- (iv) Existing lead-acid battery technology appears capable of extension to yield power densities of 1 kW/kg for 1 second. Power densities to 2.5 kW/kg for 20 seconds appear feasible from specially constructed lead-acid batteries.

Circuit analysis consisted of obtaining the primary and secondary currents during discharge and charge by simple and rigorous methods with physical interpretations. The charging analysis enabled two important questions to be answered, viz. what is the optimum time for which to charge the primary and what is the effect of the short circuited secondary. Since the degree of coupling during discharge is a most important parameter, the applicability of the simple flux models was examined.

The main conclusions from the above analyses are as follows.

- (i) The optimum time to charge the primary is about one primary circuit time constant.
- (ii) The primary can be charged while the secondary is closed via the railgun with negligible effect on efficiency of charging or on the railgun.
- (iii) The simple notion of mutual and leakage fluxes leads to correct results in real coils, particularly those forms eventually considered for the pulse transformer.
- (iv) There is a simple and important relationship between self inductances of coils and their degrees of coupling.

Transformer geometry was investigated next, from three viewpoints, viz. time constant compared to that of a Brooks Coil, degree of coupling with various forms of secondary, and the forces and masses of the windings. Three forms of windings were studied; the solenoid, the "external field" toroid and the ordinary internal field toroid. In the discussion leading to time constant evaluations, the battery mass was obtained in terms of the battery resistance, the primary winding resistance and the power density of the battery. Degree of coupling was estimated for thin sheet, identical layer, bifilar and coaxial cable secondaries. Compressive forces were considered to be particularly damaging and the possibility of reducing their effects by magnetic force balancing was investigated.

The main conclusions in regard to transformer geometry are as follows.

- (i) The external field toroid with coaxial cable windings has the best performance from each of the time constant, degree of coupling and force viewpoints.

- (ii) Magnetic force balancing of the external field toroid reduces the high compressive stress to the uniformly distributed and much lower stress  $B^2/2\mu_0$ . The winding is much more complicated and degrades the time constant and degree of coupling of the external field toroid.

The final phase of the theoretical study of the pulse transformer system was to bring the preceding work together in the form of design equations and to use these equations in example designs. The example designs ranged from 100 kJ to 1 GJ in stored energy and enabled the battery-pulse transformer system to be assessed as a function of stored energy, conductor stress, cooling and the power density of the batteries.

The main conclusions from the example designs are as follows.

- (i) Using liquid nitrogen cooled windings and batteries with a power density of 1 kW/kg, the pulse transformer system attains the target overall pulse energy density of 1 kJ/kg only when the stored energy exceeds 10 MJ.
- (ii) Using liquid nitrogen cooled windings, the conductor cross-section, and hence the system mass, is determined by strength requirements at energies greater than about 10 MJ.
- (iii) Batteries with a power density exceeding 1 kW/kg enable advantages other than reduced mass to be realized. In particular, the number of shots desired may mean that the benefit from more powerful batteries is that less cooling is needed,
- (iv) In comparison with capacitor and homopolar generator systems, the battery and pulse transformer system is comparable in terms of mass with capacitor systems at energies below about 1 MJ and with homopolar generator systems at higher energies. It has the advantage of being multishot, particularly at energies below about 10 MJ/shot, and in comparison with capacitor systems, has the disadvantage of requiring liquid nitrogen cooling.

## 11.2 Applicability to the battery-inductor scheme

Although the work in this Report has been directed at the battery and pulse transformer scheme, it should be noted that much of it relates directly to the battery and inductor scheme.

## 11.3 Further work

The exploratory work in this Report requires further experimental support.

For example, railguns with thin and wide rails might be compared to determine current distribution effects. The composition of the plasma could be varied to assess the gas pressure and electrostatic force contributions.

The practicability of high power density batteries, such as the lead-acid battery design described in Ch. 4, needs confirming since a power density of several kW/kg is one of the most important requirements for obtaining a pulse energy density of at least 1 kJ/kg and in reducing the cooling required for the windings.

Larger pulse transformers and higher energy tests (e.g. 100 kJ), with faster and probably more elaborate fuses and with current shunts that have a corresponding transient measurement ability, are necessary to properly gauge the pulse transformer as a means of obtaining high current pulses.

Actual stress measurements using strain gauges are necessary to determine the extent to which force balanced windings are effective, particularly at low  $R/a$  values.

Finally, it yet remains to connect the pulse transformer to a railgun.

On the theoretical side three areas of further work are suggested.

Firstly, the degree of coupling between various types of primaries and secondaries needs to be calculated by more exact methods and presented in the form of tables, graphs or simplified fitted equations.

Secondly, a new set of design equations and exploratory designs could be based upon batteries with power densities of several kW/kg and transformers with  $R/a$  values less than 5.

Thirdly, the extent of the problems due to the field of the external field toroid, and the ways of minimizing them with a shield structure, needs investigation. In this connection it should be noted that short solenoids of gigantic proportions, which also have large external fields, have been proposed as alternatives to hydroelectric storage by the University of Wisconsin Engineering Experiment Station.



#### ACKNOWLEDGEMENTS

The authors are grateful to the people who made possible the Research Agreement with Monash University and to those who assisted in the many theoretical and practical matters that the work entailed.

Drs M.E.C. Biffin, G.J. Jenks, Y.C. Thio and D.W. Williams are to be thanked for their valuable support when the program with Monash University was proposed. Dr H.L. Wain, former Chief Superintendent of Materials Research Laboratories, and Professor D.G. Lampard, Professor of Electrical Engineering at Monash University, are particularly to be thanked for their concurrence with the proposal. The authors would also like to record their thanks to Drs A.J. Bedford and C.I. Sach for their continued support when the project came under their control.

Dr R.A. Marshall was an invaluable resource during his stay at Materials Research Laboratories in 1983 and 1984 because of his first-hand knowledge of modern railguns and homopolar generators, and of the people working on these in the US.

Dr G.K. Cambrell of Monash provided assistance in various aspects of electromagnetism. Mr P.M. Hart, also of Monash, checked the force balance concept in Chapter 7 by computing the forces at every point of the helical winding using the vector form of the magnetic force law. Mr J. Howlett of the Dunlop-Olympic Company spent many hours discussing the practical and theoretical details of lead-acid batteries. Dr R.J. Taylor and Mr B.S. Smith of the Electrochemistry Group at MRL were also greatly appreciated for their readiness to answer questions.

For their help in the construction of the test coils we wish to thank Mr N. Strong, Mr H. Wenzel, Mr E. Conod, Mr J. McLeod, Mr G. Pearce and Mr D. Homewood of Monash and Mr B. Jones and Mr L. de Paolo of MRL. The Hargrave Library, which provided a huge number of references, was much appreciated, especially the help of Miss L. Harding.

For their help in the production of the thesis and this Report we wish to say thankyou to Mr M. Butler and Mr J. Ferrett (illustrations and photography) and to Mrs J. Marasco for typing and for making many alterations as we became aware of the errors and other shortcomings in what had been written.

## REFERENCES

## INTRODUCTION

1. Rashleigh, S.C. and Marshall, R.A. Electromagnetic Acceleration of Macroparticles to High Velocities. J. Appl. Phys. 49 (4), 2540, 1978.
2. Barber, J.P. The Acceleration of Macroparticles and a Hypervelocity Electromagnetic Accelerator. Ph. D. Thesis, The Australian National University, 1972.
3. Brooks, A.L. and Hawke, R.S. The Electromagnetic Launcher - A New Weapon? 6th International Symposium on Ballistics, Orlando, Florida, Oct. 22-24, 1981.
4. Miller, Lisa A., Rice Eric E., Earhart, Richard W. and Conlon, Robert J. Final Technical Report on Preliminary Analysis of Space Mission Applications for Electromagnetic Launchers. Battelle Columbus Laboratories. NASA CR-174748 Aug. 30, 1984.
5. Peaslee, A.T. Jr. (Compiler). Proceedings of the Impact Fusion Workshop, July 10-12 1979. LA 8000 C. Los Alamos Scientific Laboratory, Los Alamos, New Mexico.
6. Clark, G.A. and Bedford, A.J. Performance Results of a Small Calibre Electromagnetic Launcher. IEEE Transactions on Magnetics, Vol. Mag-20, 276, 1984.
7. MacLaren, F.B. Electric Gun, Patent No 1,384,769 United States Patent Office, July 19, 1921.
8. Fauchon-Villeplee, A.L.O. Electric Gun or Apparatus for Propelling Projectiles. Patent No 1,370,200 United States Patent Office, Mar 1 1921.
9. Birkeland, K. Swedish Patent No. 16147, 1 Aug 1903.
10. Liebhafsky, H.A. Gesellschaft Fur Geratebau. (A report of the work of J. Hansler). Combined Intelligence Objectives Sub-Committee, 14 June 1945.

## CHAPTER 1

1. Seely, S. Electromechanical Energy Conversion McGraw-Hill Book Company Inc. 1962. Ch. 2.
2. Plesset, M.S. and Venezian, G. Free Energy in Magnetostatic or Electrostatic Fields. Am. J. Phys. Vol. 32 1964 pp 860-864.

3. Lindvall, F.C. The Educational Value of the Theorem of Constant Linkages. Gen. Elec. Rev. Vol. 33 1930 pp 273-278.
4. English, A.C. Force on a Wire in a Magnetic Field. Am. J. Phys. Vol. 35 1967 pp 326-327.

## CHAPTER 2

1. Marshall, R.A. Current Flow Patterns in Railguns. IEEE Transactions on Magnetics, Vol. Mag-20, No. 2, March 1984 pp 243-244.
2. Seely, S. Introduction to Electromagnetic Fields McGraw-Hill Book Company Inc. 1958. Ch. 10.
3. Knoepfel, H. Pulsed High Magnetic Fields. North Holland Publishing Company, Amsterdam. 1970 Ch. 3.
4. Seely, S. and Poularikas, Electromagnetics, Classical and Modern Theory and Applications. Marcel Dekker, Inc. N.Y. 1979 Ch. 9.
5. Steinberg, M.S. Electromagnetic waves without Maxwell's equations. Am. J. Phys. Vol. 51 Dec 1983 pp 1081-1086.
6. Feynman, R.P., Leighton, R.B. and Sands, M. The Feynman Lectures on Physics. Vol. 2 Addison-Wesley Publishing Company 1964 Ch. 19.
7. See Ref. 3, Ch. 4.
8. Deeley, E.M. and Okon, E.E. An Integral Method for Computing the Inductance and the A.C. Resistance of Parallel Conductors. International Journal for Numerical Methods in Engineering, Vol. 12, 1978 pp 625-634.
9. Higgins, T.J. Formulas for Calculation of the Inductance of Linear Conductors of Structural Shape. AIEE Transactions, Vol. 62, 1943 pp 53-57.
10. Russell, A. The Inductance Coefficients of a Part of a Circuit, and their Applications. Journal IEE, Vol. 69, 1931, pp 270-280.
11. Kerrisk, J.F. Current Distribution and Inductance Calculations for Rail-Gun Conductors. LA 9092-MS Los Alamos National Laboratory, New Mexico, 1981.
12. Bauer, D.P., Barber, J.P., Swift, H.F. and Vahlberg, C.J. Electric Rail Gun Propulsion Study. Final Technical Report AFRPL-TR-81-02 Edwards Air Force Base, California, May 1981. Appendix A, Section 2.
13. Arnold, A.H.M. The Inductance of Linear Conductors of Rectangular Section. Journal IEE, Vol. 70, 1932, pp 579-586.

14. Silvester, P. Modern Electromagnetic Fields. Prentice-Hall, 1968. Ch. 5, Sec. 6.
15. Rosa, E.B. and Grover, F.W. Bulletin of the Bureau of Standards, Vol. 8 No. 1, Jan 1912. (Formulas and Tables for the Calculation of Mutual and Self Inductance) Ch. 9.
16. Gray, A. The Theory and Practice of Absolute Measurements in Electricity and Magnetism. Macmillan and Co. London 1893. Vol. II Part 1 Chapter VI Section II.
17. Hawke, R.S. Devices for Launching 0.1 g projectiles to 150 km/s or more to Initiate Fusion, Part 2, Railgun Accelerators. UCRL-52778 Part 2. Lawrence Livermore Laboratory, University of California, July 6, 1979.
18. Marshall, R.A. and Weldon, W.F. Analysis and Performance of Railgun Accelerators Powered by Distributed Energy Stores. 14th Pulse Power Modulator Symposium, Orlando, Florida, June 3-5, 1980, IEEE Conference Record.
19. Deadrick, F.J., Hawke, R.S. and Scudder, J.D. Magrac- A Railgun Simulation Program. IEEE Transactions on Magnetics, Vol. Mag 18 No. 1, Jan 1982. pp 94-104.
20. Grover, F.W. Inductance Calculations. D. Van Nostrand Company Inc. N.Y. 1946. Ch. 3.
21. Higgins, T.J. Formulas for the Geometric Mean Distances of Rectangular Areas and of Line Segments. J. App. Phys. Vol. 14, April 1943 pp 188-195.
22. Barber, J.P. The Acceleration of Macroparticles and a Hypervelocity Electromagnetic Accelerator. Ph D Thesis, The Australian National University, 1972. Appendix A.

#### CHAPTER 3

1. McFarland, E. Textbook of Ordnance and Gunnery. John Wiley & Sons Inc. N.Y. 1929.
2. Hatcher, J.S., Harrison, E.H., Waite, M.D., and Olson, L.E. NRA Firearms and Ammunition Fact Book. National Rifle Association of America, Washington, D.C. 1970.
3. Hayworth, B.R. Specifying a flashlamp capacitor. Tech. Note No 115, CSI Capacitors, P.O. Box 2052, Escondido, California.
4. Hayworth, B.R. Effect of D.C. Life on the Discharge Life of Pulse Capacitors. Tech Note No 112, CSI Capacitors, P.O. Box 2052, Escondido, California.

5. Maxwell Laboratories, Inc. Bulletin 301-1, 1977. Series C Pulse Discharge Capacitors.
6. Hayworth, B.R. Composite High Voltage Capacitors Challenge Paper Capacitors. Unnumbered technical note, Capacitor Specialists Inc. Escondido, California.
7. Brotherton, M. Paper Capacitors under Direct Voltages. Proc. IRE, Vol. 32, Mar. 1944 pp 139-143.
8. Parker, R.D. High Power Capacitor Technology. IEEE 1980 14th Pulse Power Modulator Symposium Conference Record 80 CH 1573-5 ED pp 137-143.
9. Maudlin, G.H., Nunnally, W.C. and Thompson, M.C. The Performance of the Perfluorocarbon Liquid/Plastic Film Capacitor Technology in Repetitive Discharge Pulse Power Service. 4th IEEE Pulsed Power Conference, June 6-8, 1983, Albuquerque, New Mexico pp 695-697.
10. Brotherton, M. Capacitors, Their Use in Electronic Circuits D. Van Nostrand Company Inc., 1946. p73.
11. Ennis, J.B. Dielectric Materials for Airborne Energy Storage Systems. See Ref. 9 pp 698-701.
12. Kulkarni, S.V. Composite Laminate Flywheel-Rotor Development Program. Conf. 790854. Proceedings of the 1979 Mechanical and Magnetic Energy Storage Contractors Review Meeting. Department of Energy, Washington, D.C., Dec. 1979, pp 388-398.
13. Robson, A.E. Inertial-Inductive Energy Storage Systems. Reported in High Power High Energy Pulse Production and Application, Ed. E.K. Inall, ANU Press, Canberra, Australia, 1978, pp 113-128.
14. Mole, C.J. and Mullan, E. Design Trends in Homopolar Machines since the Mid 1960's and Weldon, E.F., Rylander, H.G. and Woodson, H.H. Homopolar Generator Development at the University of Texas. See Ref. 13, pp 96-112 and pp 86-95.
15. Knoepfel, H. Pulsed High Magnetic Fields. North Holland Publishing Company, Amsterdam, 1970, Ch. 6.
16. See Ref. 13, Newstead, p 85 and Mole and Mullan, p 109 and Satkowski and Seng, p 177.
17. Marshall, R.A. Copper Graphite Brushes for Very High Current Density. See Ref. 13 pp 196-200.
18. Mole, C.J. and Mullan, E. Design of a 10 MJ Fast Discharging Homopolar Machine. See Ref. 13 pp 157-168.
19. Lupton, W.H. et al. Use of Transformers in Producing High Power Output From Homopolar Generators. 2nd IEEE International Pulsed Power Conference, Lubbock, Texas, June 12-14 1979 pp 83-86.
20. See Ref 18.

21. Inall, E.K. Homopolar Generator Rotor Configuration and Designs. See Ref. 13 pp 251-257.
22. Bullion, T.M. et al. Five Megajoule Homopolar Upgrade. 3rd IEEE International Pulsed Power Conference, Albuquerque, New Mexico, June 1-3 1981. pp 126-129.
23. Gully, J.H. et al. Compact Homopolar Generator Developed at CEM-UT. IEEE Transactions on Magnetics, Vol. Mag 20 No. 2 March 1984 pp 203-206.
24. Walls, W.A. and Estes, E.G. Continued Development of High Energy Density, Higher Current Rated Homopolar Generators at CEM-UT. See Ref. 9 pp 419-422.
25. Spann, M.L. et al. Fabrication of a Compact Storage Inductor for Railguns. See Ref. 23 pp 215-218.
26. Mole, C.J. The Westinghouse 3GVA Short Circuit Generator. See Ref. 13 pp 129-134.
27. Weldon, W.F. et al. Fundamental Limitations and Design Considerations for Compensated Pulsed Alternators. See Ref 19 pp 76-82.
28. Pratap, S.B. et. al. A Compulsator Driven Rapid Fire EM Gun. See Ref 23 pp 211-214.
29. Bird, W.L. et al. Applying a Compensated Pulsed Alternator to a Flashlamp Load for Nova-Part II. See Ref. 19 pp 463-466.
30. Fowler, C.M. et al. Explosive Flux Compression Generators for Rail Gun Power Sources. IEEE Transactions on Magnetics Vol. Mag 18 No. 1, Jan 1982 pp 64-67.
31. Cowan, M. Pulsed Power for Electromagnetic Launching. See Ref. 30 pp 145-150.
32. Fowler, C.M., Caird, R.S. and Garn, W.B. An Introduction to Explosive Magnetic Flux Compression Generators. LA-5890-MS Los Alamos Scientific Laboratory, University of California, Los Alamos, New Mexico.
33. See Ref. 15, pp 199-202.
34. Herlach, F. Explosive-driven energy generators with transformer coupling. J. Phys. E.: Sci. Instrum., Vol. 12, 1979. pp 421-429.
35. See Ref. 15, p 191.
36. Herlach, F. and Knoepfel, H. Megagauss Fields Generated in Explosive-Driven Flux Compression Devices. Rev. Sci. Instrum. Vol. 36, 1965. pp 1088-1095.
37. Frankenthal, S., Manley, O.P. and Treve, Y.M. Design of Efficient Explosively Driven Electromechanical Energy Converters. J. App. Phys. Vol. 36 No. 7, 1965, pp 2137-2139.

38. Marshall, R.A. A Reusable Inverse Railgun Magnetic Flux Compression Generator to Suit the Earth to Space Rail Launcher. See Ref. 23 pp 223-226.
39. Semon, M.D. Note on the analogy between inertial and electromagnetic forces. Am. J. Phys. Vol. 49, July 1981, pp 689-690.
40. Eyssa, Y.M. and Boom, R.W. Considerations of a Large Force Balanced Magnetic Energy Storage System. IEEE Transactions on Magnetics, Vol. Mag. 17, No. 1, Jan 1981. pp 460-462.
41. Boom, R.W., Peterson, H.A. and Young, W.C. Wisconsin Superconductive Energy Storage Project, NSF-RA-N-74-065 Wisconsin University, 1974. Ch. 3.
42. See Ref. 40 or Ref. 41 Ch. 5.
43. Moses, R.W. Flywheel Energy Storage. Physics Today, Oct. 1975, p15.
44. Whitehead, S. Dielectric Breakdown of Solids Oxford, Clarendon Press, 1951. Ch. 2.

#### CHAPTER 4

1. Parkman, N. Advances in insulating materials. IEE Electronics and Power Nov. 1972 pp 421-425.
2. Haarman, R.A., Dike, R.S. and Hollen, M.J. Exploding Foil Development for Inductive Energy Circuit. LA-UR-73-1610, Los Alamos Scientific Laboratory, University of California, Los Alamos, New Mexico.
3. Barber, J.P. and Bauer, D.P. Switching for Electric Rail Guns. IEEE Transactions on Magnetics, Vol. Mag. 20, No. 2, March 1984, pp 304-307.
4. Grover, F.W. Inductance Calculations D. Van Nostrand Company Inc. N.Y. 1946. p 101.
5. Glazebrook, R.W. Efficiencies of Heat Engines and Fuel Cells: The Methanol Engine as a Competitor to Otto and Diesel Engines. Journal of Power Sources, Vol. 7, 1982, pp 215-256.
6. Teno, J. and Sonju, O.K. Explosively Driven MHD Generator Power Systems for Pulse Power Applications. International Conf. Energy Storage, Compression and Switching, Nov 5-7, 1974 Torino, Italy. pp 151-156.
7. Jasinski, R. High Energy Batteries Plenum Press, New York, 1967.
8. Barak, M. Batteries and Fuel cells. IEE Reviews, Vol. 117, August 1970, pp 1561-1583.
9. Rand, D.A.J. Battery Systems for Electric Vehicles - A State of the Art Review. Journal of Power Sources, Vol. 4, 1979. pp 101-143.

10. Hammel, R.O. Ch. 15, Handbook of Batteries and Fuel Cells Ed. D. Linden. McGraw-Hill, New York, 1984.
11. Bagshaw, N.E. Optimizing Lead Acid Cell Design for Differing Applications. Proceedings of the Symposium on Battery Design and Optimization. Ed. S. Gross. The Electrochemical Society, Princeton, N.J. 1979. pp 1-11.
12. Takagaki, T., Ando, K. and Yonezu, K. Improving lead battery performance - what practical possibilities? Lead 74, Proceedings of the fifth International Conference on Lead, 1976. Lead Development Association, London. pp 113-122.
13. Vinal, G.W. Storage Batteries John Wiley and Sons, New York. 4th Ed. 1951, Ch. 4.
14. Metzendorf, H. The Capacity Limiting Role of the Electronic Conductivity of the Active Material in Lead-Acid Batteries During Discharge. Journal of Power Sources, Vol. 7, 1982. pp 281-291.
15. Winsel, A., Hullmeine, U. and Voss, E. Passivation Reactions on the Electrodes of a Lead-Acid Cell. Journal of Power Sources. Vol. 2, 1977/78 pp 369-385.
16. See Ref. 13 Ch. 5.
17. Electric Gun and Power Source, Armour Research Foundation, Project No 15-391E, 1946. p. 203.
18. Private Communication - Department of Mechanical Engineering, Monash University.
19. Henman, R. Engineering Development Establishment, Dept of Defence, Maribyrnong. Private Communication.
20. Gilmour, A.S. and Marshall, J.D. Liquid Nitrogen Cooled Wires as Switchable High-Power Direct Current Limiting Elements. Proceedings, IEEE International Pulsed Power Conference, Nov 9-11, 1976, Lubbock, Texas. Paper IC3.
21. Doljack, F.A. Poly Switch PTC Devices - A New Low Resistance Conductive Polymer Based PTC Device for Overcurrent Protection. IEEE Transactions on Components, Hybrids and Manufacturing Technology, Vol. CHMT-4, No. 4, Dec. 1981, pp 372-378.
22. Maisonnier, Ch., Linhart, J.G. and Gurlan, C. Rapid Transfer of magnetic Energy by Means of Exploding Foils. Rev. Sci. Instrum. Vol. 37, 1966, pp 1380-1384.
23. Henderson, R.P. Smith, D.L. and Reinovsky, R.E. Preliminary Inductive Energy Transfer Experiments 2nd IEEE International Pulsed Power Conference Lubbock, Texas, June 12-14, 1979 pp 347-349.
24. Salge, J., Braunsberger, U. and Schwarz, V. Circuit Breaking by Exploding Wires in Magnetic Energy Storage Systems. See Ref. 6. pp 477-480.



25. Vitkovitsky, I.M. et al. Explosively Driven Switches and Fuses for Inductive Storage. In High Power High Energy Pulse Production and Application, Ed. E.K. Inall, ANU Press, Canberra, Australia, 1978. See Fig. 4 p. 421.
26. Gilmour, S.J. and Lockwood, D.L. The Interruption of Vacuum Arcs at High D.C. Voltages. IEEE Transactions on Electron Devices, Vol. ED-22, No 4, April 1975 pp 173-180.
27. Kapitza, P.L. A Method of Producing Strong Magnetic Fields. Proceedings of the Royal Society of London, Series A, Vol 105, 1924, pp 691-710.
28. Walker, R.C. and Early, H.C. Half Megampere Magnetic-Energy-Storage Pulse Generator. Rev. Sci. Instrum. Vol. 29 No. 11, 1958, pp 1020-1022.
29. Early, H.C. and Walker, R.C. Economics of Multimillion-Joule Inductive Energy Storage. AIEE Commun. Electronics, Vol. 31, 1957, pp 320-325.
30. Lupton, W.H. et al. Use of Transformers in Producing High Power Output From Homopolar Generators. See Ref. 23 pp 83-86.

#### CHAPTER 5

1. Fitzgerald, A.E. and Kingsley, C. Electric Machinery McGraw Hill Book Company, New York, 2nd Ed. 1961 Ch. 1.
2. Carter, W.G. The Electromagnetic Field in its Engineering Aspects. Longmans, London. 2nd Ed 1967, pp 177,178.

#### CHAPTER 6

1. Grover, F.W. Inductance Calculations D. Van Nostrand Company, Inc. N.Y. 1946, p 98.
2. Pender, H. and McIlwain, K. Electrical Engineers' Handbook. Electric Communication and Electronics. Third Edition 1941, John Wiley. Section 4-16.
3. Grover, F.W. The Inductance of a Metal Tube Bent into the Form of a Ring. Phys. Rev. Vol. 30 1910. pp 787,788.
4. Seely, S. Introduction to Electromagnetic Fields McGraw-Hill Book Company Inc. 1958. p 183.

5. Rosa, E.B. and Grover, F.W. Bulletin of the Bureau of Standards, Vol. 8 No. 1, Jan 1912. (Formulas and Tables for the Calculation of Mutual and Self Inductance) p. 53.
6. See Ref. 5, pp 223-225.
7. Walker, R.C. and Early, H.C. Half Megampere Magnetic Energy-Energy-Storage Pulse Generator. Rev. Sci. Instrum. Vol. 29 No. 11, 1958 pp 1020-1022.
8. Clark, W.H. and Myerberg, J.E. Megampere Pulse Transformer for Coaxial Load. Rev. Sci. Instrum. Vol. 37, No. 7, 1966. pp 883-885.
9. Bar-Avraham, E. and Ginzburg, A. Energy Transfer from a low-voltage capacitor bank to a high inductance with the aid of an air pulse transformer. J. Phys E: Sci. Instrum. Vol. 11, 1978 pp 320-322.
10. See Ref. 5, p 13. Eqn. (11) adapted for adjacent turns.
11. Gaaze, V.G. and Shneerson, G.A. A High Voltage Cable Transformer For Producing Strong Currents. Translation in Instruments and Experimental Techniques, No. 6, Nov-Dec 1965 pp 1413-1418.
12. See Ref. 4 pp 180, 181.
13. Wheeler, H.A. Simple Inductance Formulas for Radio Coils. Proc. IRE Vol. 16, 1928 pp 1398-1400.
14. See Ref. 4 p 161.
15. Early, H.C. and Walker, R.C. Economics of Multimillion Joule Inductive Energy Storage. AIEE Commun. Electronics, Vol. 31 1957. pp 320-325.
16. See Ref. 5 p 6.
17. Malmberg, J.H. and Rosenbluth, M.N. High Frequency Inductance of a Torus. Rev. Sci. Instrum. Vol. 36, 1965 pp 1886, 1887.
18. Tables of Associated Legendre Functions Columbia University Press, New York, 1945.

#### CHAPTER 7

1. Furth, H.P., Levine, M.A. and Wanlek, R.W. Production and Use of High Transient Magnetic Fields. II Rev. Sci. Instrum. Vol. 28 No. 11 1957 pp 949-958.
2. Wakefield, K.E. Ch. 4. High Magnetic Fields, Eds. H. Kolm, B. Lax, F. Bitter and R. Mills. MIT Press and Wiley, New York, 1962.
3. Wells, D.R. and Mills, R.G., Ch. 5 Ref. 2.

4. Willinski, M.I. Comment on "Radiation Shielding of Space Vehicles by Means of Superconducting Coils". American Rocket Society Journal, Vol. 32 1962. p 787.
5. Mawardi, O.K. Design of a Force Free Inductive Storage Coil. LA-5953-MS Los Alamos Scientific Laboratory, University of California, Los Alamos, New Mexico, 1975.
6. Levy, R.H. Authors Reply to Willinski's Comment on "Radiation Shielding of Space Vehicles by Means of Superconducting Coils". See Ref. 4, p 787.
7. Eyssa, Y.M. and Boom, R.W. Considerations of a Large Force Balanced Magnetic Energy Storage System. IEEE Transactions on Magnetics, Vol. Mag. 17, Jan 1981. pp 460-462.
8. Blewett, J.P. Magnetic Field Configurations Due to Air Core Coils. J. App. Phys. Vol. 18, 1947. pp 968-976.

#### CHAPTER 8

1. Pender, H. and Del Mar, W.A. Electrical Engineers' Handbook 4th Ed. John Wiley and Sons, New York 1949. Ch. 14 p 67.
2. Timoshenko, S. and Young, D.H. Engineering Mechanics Third Edition, McGraw-Hill Book Company Inc. 1951 p. 150.
3. Seely, F.B. and Smith, J.O. Advanced Mechanics of Materials, John Wiley and Sons, New York, 2nd Ed 1952 pp 79,80.
4. See Ref. 3 p 57.
5. Burns, R.L. Recent Developments in the use of Copper and Copper Alloys in Electrical Engineering. Conference paper presented to Conference on Recent Developments with Copper in Electrical Engineering, Sydney, 24th Sept. 1969. Copper and Brass Information Centre.
6. CRC Handbook of Chemistry and Physics. Ed Robert C. Weast. 55th Ed. 1974-75 p. B-416.
7. Strobbridge, T.R. Refrigeration for Superconducting and Cryogenic Systems. IEEE Trans Nuc. Sci. NS16 No. 3 1969 pp 1104-1108.

#### CHAPTER 9

1. Huen, T. Phase-Plane Method of Exponential Waveform Measurement. Rev. Sci. Instrum. Vol. 40 No. 8 1969 pp 1067-1069.

2. Casimir, H.B.G. and Ubbink, J. The Skin Effect. Philips Technical Review Vol. 28 No. 9 1967. p 273-275.
3. Watson, P. A true maintenance free battery. Electronics Australia Vol. 44 No. 1 Jan. 1982 pp. 16-21.
4. Howlett, J. High Power Lead/Acid Batteries. Journal of Power Sources. Vol. 11 1984 pp. 43-45.
5. Baxter, H.W. Electric Fuses E. Arnold and Co. London, 1950.
6. Guile, A.E. The Calculation of the Complete Time/Current Characteristics of Cartridge Fuses with Single Wire Element. IEEE Transactions on Power Apparatus and Systems, Dec 1955 pp 1108-1115.
7. Chase, W.G. and Moore, H.K. (Eds.) Exploding Wires, Vols. 1-4. Proceedings of Conferences on the Exploding Wire Phenomenon, 1959-1967. Plenum Press, New York, 1959-1968.
8. Janes, G.S. and Koritz, H. High Power Pulse Steepening by Means of Exploding Wires. Rev. Sci. Instrum. Vol. 30, No. 11 1959. pp 1032-1037.
9. Frungel, F.B. High Speed Pulse Technology, Vol. 1 Academic Press, New York, 1965 pp 390, 391.
10. McFarlane, H.B. A High Voltage Quick Acting Fuse to Protect Capacitor Banks. In Exploding Wires, Eds. W.G. Chase and H.K. Moore, Plenum Press Inc. New York, 1959, pp 324-344.
11. Maisonnier, Ch., Linhart, J.G. and Gouylan, C. Rapid Transfer of Magnetic Energy by Means of Exploding Foils. Rev. Sci. Instrum. Vol. 37 1966 pp 1380-1384.
12. Vinal, G.W. Storage Batteries John Wiley and Sons, New York. 4th Ed 1951 p 155.
13. Knoepfel, H. Pulsed High Magnetic Fields. North Holland Publishing Company, Amsterdam, 1970 p. 307.
14. Rosa, E.B. and Grover, F.W. Bulletin of the Bureau of Standards, Vol. 8 No. 1, Jan. 1912. (Formulas and Tables for the Calculation of Mutual and Self Inductance).
15. Johnson, W.C. Transmission Lines and Networks McGraw-Hill Book Company, Inc. 1950 p. 115.

# PRINCIPAL SYMBOLS

Symbol	Principal meaning
a	Minor radius of toroid
B	Magnetic flux density
c	Velocity of light, dimension of Brooks Coil
d	Conductor diameter
D	Solenoid diameter
e	Base of natural logarithms, induced e.m.f.
E	E.m.f.
f	Fraction of associated energy that becomes projectile energy, or deflection of loaded wire.
H	Magnetic intensity, height of rail, horizontal force
i, I	Current
k	Degree of coupling, resistance ratio in phase plane circuit
K	Nagaoka factor for solenoid inductance, space factor.
l	Length of winding, distance between support disks
L	Inductance
M	Mass of projectile, winding or battery; mutual inductance.
n	Number of time constants, number of railgun segment.
N	Number of turns or conductors, total number of railgun segments.
p	Power density of battery.
P	Permeance of flux path.
q	Force per unit length.
R	Resistance, major radius of toroid, geometric mean distance.
S	Separation between rails, Laplace Transform operator.
T	Time constant.
v	Velocity of projectile.

V	Voltage, voltage drop.
w	Density of conductor material.
W	Energy, width of rails.
$\Phi$	Magnetic flux.
$\rho$	Density, resistivity.
$\sigma$	Conductivity, stress.
$\mu, \mu_0$	Magnetic permeability.

Note the unfortunate reproduction of script l throughout the text,

viz  $e$ .

For example, the natural logarithm appears as ' $ln$ '.

SECURITY CLASSIFICATION OF THIS PAGE

UNCLASSIFIED

## DOCUMENT CONTROL DATA SHEET

REPORT NO.  
MRL-R-1058AR NO.  
AR-005-133REPORT SECURITY CLASSIFICATION  
Unclassified

## TITLE

The railgun and its power source

## AUTHOR(S)

D.R. Sadedin and  
W.J. Bonwick\*\* Monash University  
Clayton, Victoria

## CORPORATE AUTHOR

Materials Research Laboratories  
PO Box 50,  
Ascot Vale, Victoria 3032REPORT DATE  
June 1987TASK NO.  
DST 82/212SPONSOR  
DSTOFILE NO.  
G6/4/8-3169REFERENCES  
150PAGES  
XXX

## CLASSIFICATION/LIMITATION REVIEW DATE

CLASSIFICATION/RELEASE AUTHORITY  
Superintendent, MRL  
Physics Division

## SECONDARY DISTRIBUTION

Approved for Public Release

## ANNOUNCEMENT

Announcement of this report is unlimited.

## KEYWORDS

Railgun accelerators  
Railgun power supplies  
Electromagnetic launchers

## SUBJECT GROUPS

0097I

0046G

0079G

## ABSTRACT

Investigations into the propulsion mechanisms of railguns and into the power source requirements of railguns are reported. Power sources based upon rotating machines, capacitors and explosives are reviewed and a new method based upon batteries and pulse transformers is identified. The battery and pulse transformer method is studied in detail.

SECURITY CLASSIFICATION OF THIS PAGE

UNCLASSIFIED

END

DATE  
FILMED

6 88